Transient Lightning Impulse Performance Analysis of a Fully Composite Pylon with an External-grounding Down-lead

Zhang, Hanchi

DOI (link to publication from Publisher):
10.54337/aau510563268

Publication date:
2022

Document Version
Publisher's PDF, also known as Version of record

TRANSIENT LIGHTNING IMPULSE PERFORMANCE ANALYSIS OF A FULLY COMPOSITE PYLON WITH AN EXTERNAL-GROUNDING DOWN-LEAD

BY
HANCHI ZHANG

DISSERTATION SUBMITTED 2022

AALBORG UNIVERSITY
DENMARK

Transient Lightning Impulse Performance Analysis of a Fully Composite Pylon with an External-grounding Down-lead

Ph.D. Dissertation

Hanchi Zhang

Dissertation submitted October, 2022

Dissertation submitted: October, 2022

PhD supervisor: Prof. Claus Leth Bak
Aalborg University

Assistant PhD supervisor: Assoc. Prof. Filipe Miguel Faria da Silva
Aalborg University

PhD committee: Professor Birgitte Bak-Jensen
Aalborg University, Denmark
Professor Stephan Pack
Graz University of Technology, Austria
Professor Ivo Uglešić
University of Zagreb, Croatia

PhD Series: Faculty of Engineering and Science, Aalborg University

Department: AAU Energy

ISSN (online): 2446-1636
ISBN (online): 978-87-7573-804-5

Published by:
Aalborg University Press
Kroghstræde 3
DK – 9220 Aalborg Ø
Phone: +45 99407140
aauf@forlag.aau.dk
forlag.aau.dk

Printed in Denmark by Stibo Complete, 2022

Abstract

A large number of renewable power plants have been established to meet the increasing demand for decarbonizing energy to alternative fossil energy. These power plants are typically located geographically far away from the load centers. Overhead lines appear as the most economic and practical way to transmit plenty of electric power over long distances. However, nowadays, public opinion is opposed to the erection of more conventional steel lattice towers, because of their negative visual impact. A fully composite pylon has been proposed to meet the requirements of compact structure and elegant appearance for new-generation transmission towers, together with two down-leads installed externally from shield wires downward to ground, to bring ground potential to shield wires. The composite pylons will serve in the open air, thus, a crucial problem impacting the safety and reliability of the power grid is backflashover. Some challenges in evaluating the transient lightning impulse performance of this specific tower convincingly and precisely should be properly addressed.

Looking through the backflashover phenomenon, a lightning flash hits one shield wire of a composite pylon, its current passes through the down-lead to the pylon footing and it is partly reflected, causing a high overvoltage at the top of the down-lead, which exceeds the electrical strength of air clearance. Some components, such as overhead lines, pylon footing electrodes, grounding down-leads, and cross-arm insulation, are determined, while some environmental factors, such as lightning current and footing soil, are not. Therefore, the challenging issues can be summarized into "how to represent determined components of the composite pylon accurately in lightning transient studies" and "how to estimate environmental factors properly with mathematical tools."

To tackle these issues, this Ph.D. project presents a backflashover rate evaluation procedure for overhead lines supported by composite pylons. The project improves transient models for some components of composite pylons, implements them in PSCAD to analyze the overvoltage level and backflashover performance, and discusses engineering applications for composite pylons to be cast into service.

Firstly, a backflashover rate evaluation procedure based on the Monte Carlo method is proposed. In the Monte Carlo method, the parameters which control the outcome of each lightning incident, are randomly selected from probabilistic distributions. In this project, the sampling parameters do not only include lightning current amplitude and front time but also include their correlation and soil resistivity. The adequacy of sampling size is verified based on the Central Limit Theorem.

Secondly, the pylon footing model and down-lead surge impedance model are improved. The current-dependent footing model is optimized. The soil resistivity in the current-dependent footing model can be processed by the Monte Carlo method, considering variant soil resistivity distribution under large-scale overhead lines supported by composite pylons. It is found that applying the Monte Carlo method to soil resistivity provides a lower backflashover rate than selecting constant soil resistivity for a high soil resistivity region. A frequency-dependent footing model is also applied in some cases and discussed as a comparison. Besides, a simplified dynamic surge impedance model for thin-wire conductors considering voltage-dependent surge corona is proposed. Because the extent of corona in a lightning surge is small in comparison to the size of a steel lattice tower, but large in comparison to the size of the down-lead, the corona effect is commonly ignored in tower surge impedance models, but it should not be ignored when modeling down-lead. After applying the dynamic surge impedance model to represent down-leads on composite pylons, the backflashover rate decreases by 7.7% in the low-resistivity soil region and by 21.4% in the high-resistivity soil region in contrast to adopting the constant surge impedance model without considering corona effect. The disregard of corona effect overstates the severity of backflashover, which emphasizes the importance of considering corona effect for thin-wire grounding devices in lightning studies.

Finally, two engineering applications of overhead lines supported by composite pylons are investigated. The backflashover performance of composite pylons should be assessed in comparison with traditional steel lattice towers. Although the backflashover rate of composite pylons is a little higher than that of traditional transmission towers, it eliminates the danger of simultaneous outages of double circuits. Besides, a unique feature of composite pylons is that the fully insulated pylon body makes it desirable not to ground every pylon in transmission lines. It is found that if partially grounding transmission lines is applied, a longer traveling distance for lightning current to ground will cause an overvoltage with higher amplitude and a rather longer wave front. Then, the amplitude of the overvoltage is mainly dependent on the distance to the nearest grounded pylon. As for countermeasures, improving pylon footing conditions is not effective anymore, and increasing insulation distance has a limited effect to some extent. Future emphasis may lie in the application and coordination of surge arresters. After that, the back-

flashover performance and the overall lightning protection performance of OHLs supported by fully composite pylons with external grounding down-leads are summarized.

Resumé

Et stort antal vedvarende kraftværker er blevet etableret for at imødekomme den stigende efterspørgsel efter dekarbonisering og alternativer til fossil energi. Disse kraftværker er typisk placeret geografisk langt væk fra belastningscentrene. Luftledninger fremstår som den mest økonomiske og praktiske måde at overføre store mængder af elektrisk strøm over lange afstande. I dag er den offentlige mening imod opførelsen af mere konventionelle stålgittermaster på grund af deres negative visuelle indvirkning. En fuldt sammensat pylon er blevet foreslået for at opfylde kravene til kompakt struktur og elegant udseende for den nye generation af transmissionsmaster sammen med to nedadgående ledninger installeret eksternt fra skærmledninger ned til jorden for at bringe jordpotentiale til jordtråde. De sammensatte pyloner vil tjene i det fri, og derfor er et afgørende problem, der påvirker sikkerheden og pålideligheden af elnettet, backflashover . Udfordringerne med at evaluere påvirkningen af den forbigående lynimpuls for denne specifikke tårntype bør adresseres overbevisende og præcist.

Når man ser på overslagsfænomenet, hvor et lyn rammer en jordtråd på kompositmasten, passerer strømmen gennem nedlederen til mastefoden, og reflekteres delvist, hvilket forårsager en høj overspænding i toppen af nedlederen, som overstiger luftens elektriske feltstyrke . For nogle komponenter, såsom luftledninger, masteelektroder, nedledernes jordforbindelser og traverser, er deres isoleringsevne kendte, mens nogle miljøfaktorer, såsom lynstrøm og jordens impedans, ikke kendes. Derfor kan de udfordrende spørgsmål opsummeres til "hvordan kan man repræsentere bestemte komponenter for kompositmasten nøjagtigt i undersøgelser af lyntransienter " og "hvordan kan man vurdere miljøfaktorer korrekt med matematiske værktøjer."

For at løse disse problemstillinger, vil dette ph.d. projekt præsentere en procedure til evaluering af backflashover-raten for luftledninger, der etableres med kompositmaster. Projektet forbedrer transiente modeller for nogle komponenter af kompositmasten, implementerer dem i PSCAD med henblik på at analysere overspændingsniveauet og backflashover, samt diskuterer de tekniske applikationer for kompositmaster, der skal tages i brug.

For det første foreslås en evalueringsprocedure for backflashover-rate baseret på Monte Carlo-metoden. I Monte Carlo-metoden vælges parametrene, der styrer udfaldet af hvert lynnedslag, tilfældigt ud fra sandsynlighedsfordelinger. I dette projekt inkluderer prøveudtagningsparametrene ikke kun lynstrømmens amplitude og fronttid, men også dennes korrelation og jordresistivitet. Tilstrækkeligheden af stikprøvestørrelsen verificeres baseret på "Central Limit Theorem ".

For det andet forbedres modellerne for mastefod og nedlederens bølgeimpedans. Den strømafhængige model af mastefoden er optimeret. Jordresistiviteten i den strømafhængige model kan behandles ved hjælp af Monte Carlo-metoden, idet der tages hensyn til varierende fordeling af jordresistiviteten for luftledninger på kompositmaster. Det konstateres, at anvendelsen af Monte Carlo-metoden til bestemmelse af jordresistiviteten giver en lavere backflashover-rate i forhold til at vælge en konstant jordresistivitet for områder med en høj jordresistivitet. En frekvensafhængig model for mastefoden anvendes også i nogle tilfælde og diskuteres til en sammenligning. Desuden foreslås en forenklet dynamisk model af bølgeimpedansen for vertikale tyndtrådsledere , der tager hensyn til spændingsafhængig overspændingskorona. Fordi andelen af korona i et lyn er lille i forhold til størrelsen af en gittermast i stål, men stor i forhold til størrelsen af nedlederne, ignoreres koronaeffekten almindeligvis i modeller for mastens bølgeimpedans, men den bør ikke ignoreres ved modellering af nedledere. Efter at have anvendt den dynamiske model for bølgeimpedansen til at repræsentere nedlederne på en kompositmast, falder backflashover-raten med 7,7 % i områder med lav jordresistivitet og 21,4 % i områder med høj jordresistivitet i modsætning til en model med konstant bølgeimpedans uden at tage højde for koronaeffekten. Ignoreres koronaeffekten overvurderes størrelsen af backflashover, hvilket understreger vigtigheden af at overveje koronaeffekten for tyndtrådsjordingsenheder i lynstudier.

Til sidst undersøges to tekniske anvendelser af luftledninger ophængt på kompositmaster. Kompositmastens evne til at modstå backflashover bør vurderes i sammenligning med traditionelle stålgittermaster. Selvom backflashoverraten for kompositmaster er lidt højere end for traditionelle transmissionsmaster, eliminerer kompositmasten faren for samtidige udfald af dobbelte systemer og dens backflashover-hastighed kan reduceres til et sammenligneligt niveau efter installation af overspændingsafledere . Derudover er et unikt træk ved kompositmasten, at den fuldt isolerede mastekrop gør det ønskeligt ikke at jordforbinde hver enkelt mast i et transmissionsnet. Det har vist sig, at ved ikke at jordforbinde alle master på en linje, vil den længere rejseafstand for lynstrømmen til jord forårsage en overspænding med en højere amplitude og en længere bølgefront. Derfor afhænger amplituden af overspændingen hovedsageligt af afstanden til den nærmeste jordforbundne mast. Hvad angår modforanstaltninger overfor dette, er det ikke længere ef-

fektivt at forbedre mastens overgang til jord, og øget isoleringsafstand har til en vis grad begrænset effekt. I fremtiden kan der lægges vægt på anvendelse af overspændingsafledere og isolationskoordination. Derefter opsummeres mastens evne til at modstå backflashover og den overordnede lynbeskyttelse for OHL ophængt på kompositmaster med eksterne nedledere.

Contents

Thesis Details

Thesis Title:	Transient Lightning Impulse Performance Analysis of a Fully Composite Pylon with an External-grounding Down-lead
Ph.D. Student:	Hanchi Zhang
Supervisors:	Prof. Claus Leth Bak, Aalborg University
	Assoc. Prof. Filipe Miguel Faria da Silva, Aalborg University

The main body of this thesis consists of the following papers:

Publications in Refereed Journals

J1. **H. Zhang**, Q. Wang, F. Faria da Silva, C. L. Bak, K. Yin, and H. Skouboe, "Backflashover Performance Evaluation of the Partially Grounded Scheme of Overhead Lines with fully Composite Pylons," *IEEE Trans. Power Delivery.*, vol. 37, no. 2, pp. 823-832, Apr. 2021.

J2. **H. Zhang**, M. Ghomi, Q. Wang, F. Faria da Silva, C. L. Bak, K. Yin, and H. Skouboe, "Comparison of Backflashover performance between a novel composite pylon and metallic towers," *Electric Power Systems Research.*, vol. 196, pp. 107263, July. 2021.

J3. **H. Zhang**, M. Ghomi, Q. Wang, F. Faria da Silva, C. L. Bak, and K. Yin, "Backflashover performance of a novel composite pylon with external grounding down-lead modeled in dynamic surge impedance considering corona effect," *IEEE Trans. Power Delivery.*, 2022, Status: Under review.

O1. M. Ghomi, **H. Zhang**, C. L. Bak, F. Faria da Silva, and K. Yin, "Integrated model of transmission tower surge impedance and multilayer grounding system based on full-wave approach," *Electric Power Systems Research.*, vol. 198, pp. 107355, Sept. 2021.

Publications in Refereed Conferences

C1. **H. Zhang**, Q. Wang, K. Yin, C. L. Bak, and F. Faria da Silva, "Transient modelling and backflashover rate analysis of a fully composite pylon," *Proc. of IET ACDC*,

Xi'an, China, 2020, pp. 460-466

C2. **H. Zhang**, M. Ghomi, K. Yin, Q. Wang, F. Faria da Silva, and C. L. Bak, "Evaluation of Lightning Backflashover Rate of a Fully Composite Pylon using Monte Carlo Method on Environmental Factors," *Proc. of IEEE PES GM*, Denver, Colorado, 2022, Status: Accepted

C3. **H. Zhang**, K. Yin, Q. Wang, K. Y. See, F. Faria da Silva, and C. L. Bak, "A Simplified Dynamic Surge Impedance Model with Corona Effect for Grounding Down-Leads of Composite Pylons under Lightning Surges," *Proc. of ICLP*, Cape Town, South Africa, 2022, Status: Accepted

O2. K. Yin, M. Ghomi, F. Faria da Silva, C. L. Bak, **H. Zhang**, and Q. Wang, "Lightning performance and formula description of a Y-shaped composite pylon considering the effect of tower-footing impedance," *Proc. of ICLP*, Colombo, Sri Lanka, 2021, pp. 1-6

This dissertation has been submitted for assessment in partial fulfilment of the Ph.D. degree. The thesis is a summary of the outcome from the Ph.D. project, which is documented based on the above publications. Parts of the results are used directly or indirectly in the extended summary of the thesis. The co-author statements have been made available to the assessment committee and are also available at the Faculty of Engineering and Science, Aalborg University.

Preface

The work presented in this dissertation is a summary of the outcome from the Ph.D. project *"Transient Lightning Impulse Performance Analysis of a Fully Composite Pylon with an External-grounding Down-lead"*, which was carried out at AAU Energy, Aalborg University, Denmark.

First of all, I would like to express my sincere gratitude towards my supervisor Professor Claus Leth Bak for his valuable guidance, patience, and encouragement during my entire Ph.D. period. It has been such a precious experience to work under your supervision. I would like to thank my co-supervisors Associate Professor Filipe Faria da Silva and Assistant Professor Qian Wang for their guidance, kindness, and help. I can learn how to become an excellent researcher by your examples. I will treasure every meeting with you as my lighthouse in future research stage.

I am also grateful to Associate Professor See Kye Yak for providing me an opportunity to visit Nanyang Technological University during my study abroad and broadening my knowledge in the field of EMC in power electronics. I would also like to thank my colleagues at NTU, Minghai Dong, Huamin Jie, Zhenyu Zhao, Fei Fan, and Zhenning Yang for their fruitful discussion and great hospitality during my stay. I will keep in memory this wonderful and perhaps the longest summer in my life.

Special thanks go to my master supervisor, Professor Chengrong Li, Professor Guoming Ma in North China Electric Power University, and my senior and lifelong friend, Dr. Hongyang Zhou for their valuable suggestions and help. It is my honor to be educated in Advanced Sensing Laboratory.

I would like to thank my best friend, Wei Fan. I treasure all our shared memories in Europe and Singapore. The same thanks go to my colleague, roommate, and lifelong friend, Kai Yin. Fortunately, I can finally finish my Ph.D. study owing to our support to each other both in research and life. I would like to thank my colleague Ghomi Mohammad for his help and cooperation. I would also like to thank Zhengfa Zhang, Changjiang Zheng, Zhaoxin Wang, Bjarne Søndergaard Bukn, Felipe Camara, and all my colleagues from Modern Power Transmssion Grids. It is my pleasure to work with all of you for three years. I would also like to thank all my colleagues

and secretaries at AAU Energy for their selfless help. I would like to thank all my friends here, Tianbao Gu, Shiyi Liu, Cheng Chi, Wei Xu, Xiangting Ren, Luyao Gao, Min Liu, and Weiheng Zhang for our shared overseas experiences during these three years.

Last but not least, I would like to express my greatest gratitude and love to my parents and family for encouraging me to find my own life track. Deepest miss goes to my beloved grandpa who left me last autumn. As a pioneer in electrical engineering in New China, he is the origin of today's me. All their love and support have been, and will always be my confidence and strength in my whole life.

Hanchi Zhang
Aalborg University, October 10, 2022

Part I

Report

Chapter 1

Introduction

1.1 Background

The demand for energy in the worldwide economic development has been rising yearly. In terms of energy, the rising prices and shortages emphasize the continued significance of energy "security" and "affordability" with "lower carbon" when tackling the energy trilemma [1].

The growth of significant new renewable power plants, like offshore wind and solar power, is essential and is already occurring in order to meet the demand for growing the amount of electricity annually without excessive carbon emission. Those renewable power resources are generally located far away from the existed power grid. It is inevitable to expand power transmission systems [2]. Considering the plans of the construction of new long-distance transmission systems, underground power cables are much more expensive than overhead lines, which drives up the cost of energy transmission invisibly. Thus, overhead lines appear as the most economic and practical way to transmit plenty of electric power over long distances.

However, the conflict between such demand and limited land at the same time. Another concern is expressed in the environmental impact of overhead lines, which is the growing opposition of the public to the construction of new lattice towers, whose structures are considered to be unsightly to the surrounding landscape. As a result, more aesthetically-designed pylons have emerged in many areas. These pylons also have compactness and simplicity to save lines corridors. Since their introduction in the 1960s, composite-based pylons have been viewed as a possible alternative for the next generation of pylons due to their excellent insulating features, decreased weight-to-strength ratio, and comparable cost [3]. Because of their elegant aesthetic appearance and compact structure, the novel pylons may also promote to be a possible alternative for the conventional steel lattice towers where reducing visual

impact is required [4].

The T-pylon design by Bystrup architects was chosen in a competition for the new design of the following generation of power pylons held in the UK in 2011. In order to keep up with the trend of installing new environmentally friendly OHLs, a novel pylon design concept based on entirely composite material has been presented as the next generation of the T-pylon concept in 2013. The appearance of the fully composite pylon is depicted in Fig. 1.1. It is clear that the totally composite pylon design does not have suspension insulators; instead, they are a part of the composite cross-arm design, specifically the unibody cross-arm. Conductor clamps will be used to secure the conductors to the unibody cross-arm. For the insulation of the unibody crossarm, shed profiles are taken into consideration.

Fig. 1.1: Appearance of the fully composite pylon

The fully composite pylon has exceptional qualities from the following angles. The pylon's span is intended to be 250 meters, and it can support two circuits of 400 kV AC lines. The pylon is shaped like a "Y" and has an integrated cross-arm without insulator strings. It also has an axially symmetric structure. The height of the fully composite pylon is just 22.5 m, which is significantly less than the height of traditional lattice pylons for the same power level. The cross-arm is comprised of a hollow FRP (fiberglass reinforced plastic) tube, polymeric weather sheds, and metallic end fittings. Phase conductors are attached to the cross-arm directly by specially designed cable clamps. In order to protect the phase conductors from lightning strokes, two shield wires will be attached to the tips of the cross-arm. As a result, the shielding angle for the pylon is negative. Since the cross-arm is no longer conductive as it is in traditional steel towers, an initial idea of external down-lead has been proposed to bring ground potential to the shield wires as marked in red lines in Fig. 1.2, which needs further research and discussion.

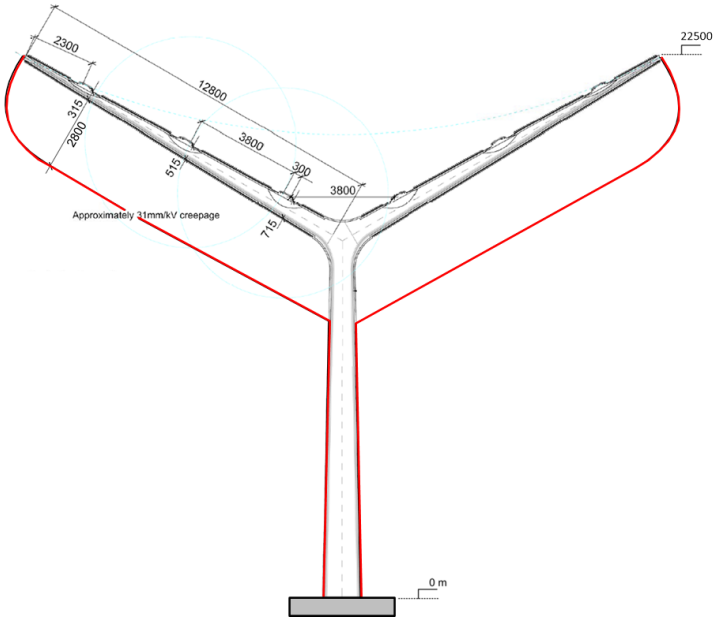

Fig. 1.2: Demonstration of the external grounding down-leads installed on composite pylon

1.1.1 Research Foundation and Research Motivation of Fully-Composite Pylon

A fully composite pylon has been designed and developed of fiberglass composite material [5]. Using this new material, it will be possible to integrate the insulators in the cross-arms, thereby reducing the height of the pylon significantly. The pylon will be able to carry 2x400kV. Since the initial design, the 'Y' shape of the fully-composite pylon was proposed, several aspects to test and optimize the electric performance of the pylon have been studied in different fields [6–8].

Firstly, the minimum required air clearances and the insulated distance of the cross-arm were calculated based on a deterministic approach of insulation coordination [6]. The dimension of the cross-arm and the insulating distance between phases and phase to shield wire were decided. Secondly, the electric field distribution of the unibody cross-arm was calculated. The shed housing and conductive clamps were recommended to reduce the flashover and enhance the insulated performance [9], what's more, the design of the inner grounding cable was discarded if the cross-arm is hollow within air because of the electric field calculated exceeding the air breakdown strength [7]. Thirdly, a review of the literature gave guidelines for verifying the novel pylon by summarizing the experience and significant advancements in testing

methodologies to evaluate the electrical performance of composite cross-arms and composite-based pylons [10]. Finally and mostly, the lightning shielding performance has been studied comprehensively. Based on theoretical analysis and the electro-geometric model (EGM) [11], the effectiveness of the pylon's lightning shielding was examined. It was discovered that the central span of the pylon was not shielded from lightning. When the effectiveness of the pylon's lightning shielding was further examined using the scale model test method [12], it was established that shielding failure might occur in the centre of a pylon. The electro-geometric model (EGM) and scale model tests were used to evaluate two distinct shielding angles, -60 ° and -70 °, in order to optimize the lightning shielding performance [13]. It was determined that shielding performance can be improved at -60 °. Based on the aforementioned experience, the potential for lightning shielding failure was thoroughly explored using scale model testing and the revised electro-geometric model (EGM) [8], which was proved to be practically negligible. Operating experience points out that for the OHLs over 500 kV, lightning outages are mainly caused by the shielding failure of lightning hitting phase conductors directly. However, for the OHLs below 500 kV, lightning outages are mainly caused by backflashover (BF) when lightning hits towers and shield wires, increasing the electric potential, and provoking a flashover [14]. The rate of BF per 100-km transmission line each year is termed as backflashover rate (BFR). Therefore, the research on BF of the 400 kV fully composite pylon is of significance.

Previous research has achieved some outcomes, but is still limited in the following aspects. Firstly, in the previous research, the means to provide ground potential to shield wires is not decided. In this project, two thin-wire bare conductors act as grounding down-leads externally. Secondly, the lightning shielding performance has been investigated, but BFR of the pylon with external grounding down-lead is still beyond discussion. Even though the phase conductors are shielded successfully by shield wires, there are still possibilities that the lightning overvoltage is strong enough to cause backflashover to impair security and reliability of power system.

Looking through the backflashover phenomenon, a lightning flash terminates one shield wire on a composite pylon, the surge current passes through the downlead to the pylon footing and it is partly reflected, causing a high overvoltage at the top of the down-lead, which exceeds the electrical strength of air clearance. Some components, such as overhead lines, pylon footing electrodes, grounding down-leads, and cross-arm insulation, are determined, while some environmental factors, such as lightning current and footing soil, are not. Therefore, the challenging issues can be summarized into "how to represent determined components of the composite pylon accurately in lightning transient studies" and "how to estimate environmental factors properly with mathematical tools." The solutions to answer the above two questions

lead to the final answer to the basic question of this project "how many back-flashover cases probably occur on the overhead lines supported by fully composite pylons with external grounding down-leads".

1.1.2 Transmission Tower with Composite Components and Its Grounding Method

In order to meet different demands for insulating levels, the composite materials, especially FRP, are used partially or fully in the design of transmission towers. If the composite materials are used partially and the body of the tower is still metallic, the connection between shielding wires and the ground can be achieved by the metallic tower body. As for fully composite poles or pylons, extra grounding down-leads are installed. There are several designs of transmission towers with composite components.

The composite cross-arms were developed and installed on the conventional metal lattice tower to omit the insulators, so as to reduce the conductor swinging, save line corridors and decrease tower weight [15]. In this design, because the tower body is still made of steel, the grounding function connecting shielding wires and ground potential can be accomplished by the tower itself. This type of tower is a modified conventional UHV or EHV transmission tower, thus it is more convincing to be used in the same voltage class to become a possible alternative for conventional ones. The voltage class of the composite cross-arm in theoretical research has risen to 1000 kV [16], and the 750 kV towers with composite cross-arms have passed through the field tests and been cast into installation and operation in China [17], as shown in Fig. 1.3.

Fig. 1.3: Metallic lattice tower with composite cross-arm [17]

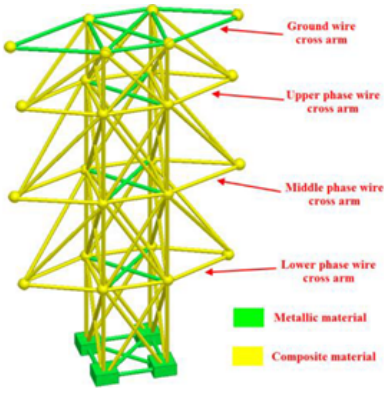

Fig. 1.4: Sketch of a composite-metal hybrid lattice tower [18]

Besides the cross-arms, if the material of other supports in the body of

metallic lattice towers is replaced from steel to FRP, the insulating performance can be improved more and the dimension of the tower can be reduced. This is the design principle of another type of composite-based lattice. This type of composite tower was initially developed and installed in the USA in 1996. Among the composite body, they installed two or more steel ladders to connect the shielding wires to ground. This type of composite tower of 330 kV is under research in China before testing and operating, as shown in Fig. 1.4 [18]. In this design, BF might occur between the ground wire and upper phase wire along the surface of the composite supports. Because of the complicated and compact lattice structure, it was difficult to avoid the flashover by adding sheds. Increasing insulating distance was the only choice.

Furthermore, if the whole tower is made of composite material, the structure will be more compact with the same insulation strength. For a typical example, one kind of tubular structure composite tower made of polyurethane resin has been successfully applied in a few 132 kV voltage level single-circuit transmission lines in Canada since 1995, as shown in Fig. 1.5 [19]. And two kinds of composite-based towers, whose tower body is made from glass fiber reinforced polyurethane, were designed for 110kV double circuits for the first time in China in 2010. as shown in Fig. 1.6, the structure of which was similar to that in Canada [20]. In the composite poles, there were several grounding methods taken into consideration. 1) Grounding down lead vertically along the external surface of the tower body, 2) Grounding down lead vertically along the internal surface of the tower body 3) Grounding down lead vertically suspending outside with its ends fixed on the tower body, and 4) Grounding down lead vertically suspending inside with its ends fixed on the tower body [21]. However, only a pollution flashover test was carried out to test the feasibility of the composite tower and down-lead design, instead of the lightning impulse voltage test, thus, the insulating performance and conducting capability of this method under lightning striking were not clear. Besides, the test voltage is relevantly lower.

Fig. 1.5: 132 kV composite pole in Canada [20]

Fig. 1.6: 110 kV semi-composite I-pole and full composite II-pole in China [21]

An interesting engineering phenomenon can be seen from the development of composite-based towers obviously, the towers with more composite components or even fully composite towers are commonly used in the transmission lines of relatively lower voltage levels. The main reason is that towers used at lower voltage levels need smaller heights, and the probability of lightning striking will be lower, thus the request for the down-lead to conduct lightning current will not be so strict. As for this project, the 'Y' shape fully composite pylons used in such high as 400 kV double-circuit lines put forward higher requirements for the performance of down-lead under lightning striking.

1.1.3 Lightning Transient Evaluation Based on Traveling Wave Theory

The operating voltage of the power system will surge sharply when the power system is subjected to large internal or external disturbances like switching actions or lightning strokes. The system might change from one operational state to another, or it might sustain partial or whole damage due to operating parameters that have significantly varied from their typical range. Transient processes of the power system are a transition because changes in operation states cannot be made immediately. According to the duration, the transient processes can be namely classified into traveling wave process [22], electromagnetic transient process, electromechanical transient process. The emphasis of this project is pylons and the transmission lines, thus the transient wave process and electromagnetic transient process are the main focuses, which will be specified in this section and the next.

The duration of the wave process is about microseconds while the amplitude changing rate is about decades kilo ampere per microsecond. The measurement and observation of the whole wave process for the overvoltage in experiments are difficult. Some simplified mathematical methods were recommended by CIGRE and IEEE, based on observational and experimental data. Along with the development and advancement of electromagnetic transient analysis software, simulation research becomes an excellent method to study the lightning traveling wave process of the transmission systems. Some simulating tools utilize the nodal analysis method to solve the differential equations based on circuit theory, such as EMTP and PSCAD. Some simulating methods solve Maxwell's equations based on the electromagnetic theory using different methods to discretize space, such as the Finite Different Time Domain (FDTD) method, the Finite Element Method (FEM), the Hybrid Electromagnetic Model (HEM), and the Method of Moments (MoM). The advantages and disadvantages of the above tools are clear. Methods based the circuit theory can solve equations rapidly, and thus are good at dealing with large-scale power systems. Methods based on electromagnetic theory can

solve specific problems in arbitrary geometries, which is time-consuming, however. Thus, they are good at dealing with relatively small-size devices, such as the transmission pylon and its components. As a result, a clear research path rises that the modeling of every component on composite pylons concerning transient is studied based on electromagnetic theory, then BF performance of the OHLs supported by composite pylons is evaluated using PSCAD/EMTP.

1.1.4 Models of Components in Lightning Transient Evaluation

In order to study BF of the novel pylon when lightning flashes terminating on shielding wires via simulation, the whole-wave progress needs to be analyzed to reflect transient wave characteristics of the pylon and the transmission lines [23]. The different parameters of lightning impulse, the revised model of grounding down-leads, the time-varying and frequency-varying impedance model of grounding devices [24] and the flashover models of BF [25] were needed to describe the transient wave process after lightning striking.

When modeling conventional metallic towers, the tower body is the main conductor of lightning current, and the tower body is modeled by constant-parameter circuit representing the tower as a single vertical lossless line, a multiconductor vertical line or a multistory model [26]. However, the fully composite pylon body is insulated, which can be neglected in the wave process analysis, the down-lead will conduct all the lightning current. Therefore, the modeling of grounding down-lead deserves more concern. When a lightning flash strikes at the shield wires of the OHLs, the lightning current passing through either the metallic tower or the down-leads of the composite tower will cause corona discharges. The tower models all neglect surge corona because of the relatively small corona radius compared with tower size [27]. However, the grounding down-leads are very thin with a cross-section radius of several centimeters, which is comparable to the corona developing distance during a lightning surge. Corona discharge around the down-leads decreases the surge impedance of the down-leads, distorts the wavefronts of overvoltage, and enhances the coupling effect between down-leads to phase conductors [28]. Thus, the modeling of down-leads needs to consider the impact of surge corona effect.

The modeling of the pylon footing using electrodes has been improved for years. During a lightning surge, grounding electrodes exhibit two different dynamic behaviors. To begin with, the nonlinear effect brought on by soil ionization may enhance the performance of grounding by lowering the grounding impedance during high current discharge and essentially increasing the equivalent size of the electrode. Since it takes time for the soil

to ionize, there are significant delays in both the ionization and deionization processes [29]. This means the minimum value of electrode resistance, occur after the peak injected current. Meanwhile, with rapid front lightning currents, the frequency-dependent inductive effects may worsen grounding performance by raising the grounding impedance [30]. To specify the ionization of soil when spark discharge, the PI-circuit with standard dynamic resistance was proposed [31]. Simplified methods of estimating the impulse resistance of concentrated ground electrodes to reduce the footing resistance have been summarized and compared in CIGRE Technical Brochure No. 839 [25]. Proposing pylon footing models exhibiting frequency-dependent effects are generally via two approaches. The first one is to establish equivalent circuit or transmission-line models based on data measured from experiments [24, 32, 33]. The other one is to establish electromagnetic models based on simulations [34, 35]. When frequency-dependent effects of the pylon footing model are considered, generally two physical factors are studied, the electrical parameters of soil and the inductive effect of electrodes.

According to different demands of the modeling precision, there are also several available models to simulate the characteristics of flashover which can be selected at present. Firstly, the switch model takes the 50% flashover voltage as the criterion [36]. Then considering the volt-time characteristics of the flashover on the insulators as the criterion, the volt-time model and the integration model can be established [37, 38]. Comprehensive physical analyses have confirmed that there are three different phases in the development of flashover, namely corona inception, streamer propagation, and leader propagation [39]. Thus, the leader progression model can be described into three steps along with the time. It was shown that compared with the other models, the use of the leader progression model was better in BF analysis as a good agreement to published results [40]. The occurrence of the flashover is also statistical, thus the Monte Carlo method (MCM) can be used to calculate BFR [41].

1.2 Project Objectives and Limitations

1.2.1 Project Objectives

Under the guidance of the project motivation above, the final goal of this Ph.D. project is to evaluate the lightning transient performance of the OHLs supported by the fully composite pylons with external grounding downleads. Faced with solving specific engineering problems, the objectives can be divided into scientific objectives and engineering objectives. The former one is to make contributions to the research of lightning protection of transmission systems and power system transients. The latter one is to utilize the

general outcomes to solve the practical engineering problems for the future operation of the fully composite pylons.

The scientific objectives are listed as follows:

- Improvement of Monte Carlo method used to evaluate the statistical result of backflashover performance considering environmental factors
- Development of a dynamic surge impedance model considering corona effect for thin-wire grounding devices

The engineering objectives are listed as follows:

- Calculation of back-flashover rate of the overhead lines supported by composite pylons
- Comparison of lightning transient performance of composite pylons to conventional metallic lattice towers
- Validation of the partially-grounded scheme that not all pylons in the transmission lines supported by composite pylons are grounded

1.2.2 Projects Limitations

The achievements of the above objectives are all based on theoretical derivation and simulation. Lacking experimental validation is the main limitation of the project.

As for simulating models of composite pylon components, the flashover model is selected as the leader progression model in the present project. Flashover has statistical characteristics, which are related to the materials of surface and electrodes' geometry. The cross-arm is made of FRP which is different from the common material of insulators, such as glass, ceramic or, silicone rubber. If the impulse flashover test can be carried out on the real cross-arm to obtain the specific volt-time curve, the establishment of a flashover model for the cross-arms on the composite pylons can be more convincing.

There are some assumptions during the development of the dynamic surge impedance model considering the corona effect for grounding down-leads. It is quite difficult to observe the micro plasma dynamics in surge corona on a large scale. However, if the macro parameters can be observed and measured, such as corona expansion radius and dynamic capacitance, the difference between experimental results and simulating results offered by the novel model can be compared to validate and revise the present model.

Further real-scale tests for this type of fully composite pylons are not realistic to be carried out and accomplished in the near future. Firstly, a real-scale composite pylon is challenging to be installed inside high voltage testing

laboratory. Besides, how to identify simulation results with realistic situation in transmission pylons is another challenging issue. Factors influencing the testing results like switching impulses polarities and wave head time and grounding conditions should be taken into consideration. Even though, the research outcomes achieved in this project are given fully expectations to be validated by lightning impulse withstand tests.

1.3 Project Outlines

The summary of the outcome of the Ph.D. project is documented in the Ph.D. thesis based on the collection of papers published during the Ph.D. study. The document is structured in two main parts: Report and Selected Publications. The thesis structure is illustrated in Fig. 1.7, providing a guideline on how the content in the Report is connected to the Selected Publications.

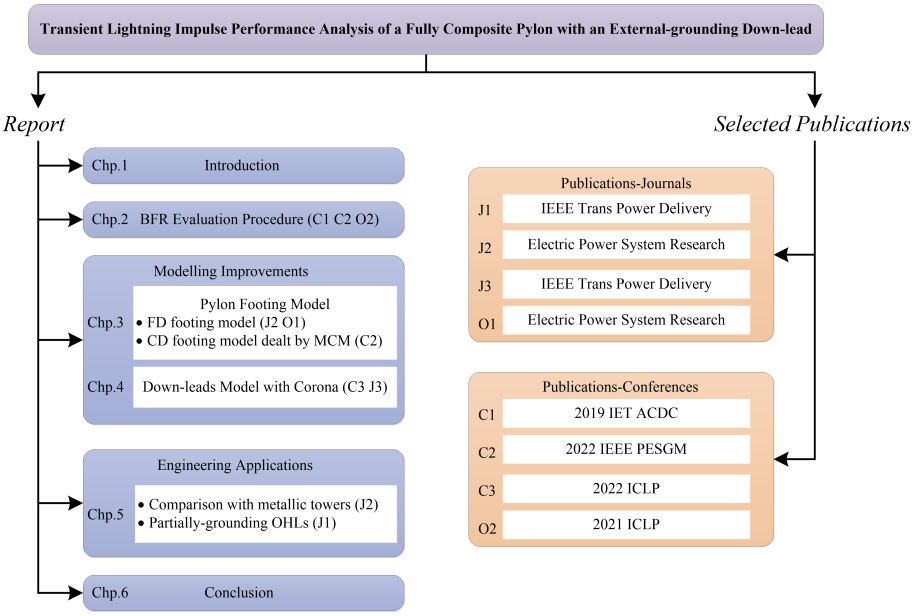

Fig. 1.7: Thesis structure and related topic of each part

In the Report, a brief summary of research conducted during the Ph.D. study is presented, where the main results are based on the Selected Publications. The Report is organized into six chapters. In *Chapter 1*, the introduction of the Ph.D. thesis is presented, where the background of the research topic is described and the motivation, objectives, and limitations of the Ph.D. study are discussed. In *Chapter 2*, the procedure to evaluate

the backflashover performance of the transmission lines supported by fully composite pylons is introduced. Then the following two chapters present the improvements in the modeling of the components on composite pylons. In *Chapter 3*, two pylon footing models are proposed and revised. One of them is the frequency-dependent model based on MoM. The other one is the current-dependent model dealt with by MCM. In *Chapter 4*, a dynamic surge impedance model considering the corona effect for grounding down-leads is proposed and introduced. Then, *Chapter 5* focuses on the research on the engineering application of the transmission lines supported by composite pylons. Firstly, the backflashover performance of composite pylon is compared to two conventional steel lattice towers, and several improving approaches are analyzed. Secondly, the feasibility of a partially-grounded scheme of the transmission lines supported by composite pylons is studied. After that, the BFR and the lightning protection performance of OHLs supported by fully composite pylons are summarized. Finally, concluding remarks and the main contributions in this Ph.D. thesis are summarized in *Chapter 6* and the future research perspectives are outlined.

1.4 List of Publications

The research outcomes during the Ph.D. study have been disseminated in several forms of publications: journal papers, conference publications, as listed in the following. Parts of them are used in the Ph.D. thesis as previously listed.

Publications in Refereed Journals

J1. **H. Zhang**, Q. Wang, F. Faria da Silva, C. L. Bak, K. Yin, and H. Skouboe, "Backflashover Performance Evaluation of the Partially Grounded Scheme of Overhead Lines with fully Composite Pylons," *IEEE Trans. Power Delivery.*, vol. 37, no. 2, pp. 823-832, Apr. 2021.

J2. **H. Zhang**, M. Ghomi, Q. Wang, F. Faria da Silva, C. L. Bak, K. Yin, and H. Skouboe, "Comparison of Backflashover performance between a novel composite pylon and metallic towers," *Electric Power Systems Research.*, vol. 196, pp. 107263, July. 2021.

J3. **H. Zhang**, M. Ghomi, Q. Wang, F. Faria da Silva, C. L. Bak, and K. Yin, "Backflashover performance of a novel composite pylon with external grounding down-lead modeled in dynamic surge impedance considering corona effect," *IEEE Trans. Power Delivery.*, 2022, Status: Under review.

O1. M. Ghomi, **H. Zhang**, C. L. Bak, F. Faria da Silva, and K. Yin, "Integrated model of transmission tower surge impedance and multilayer grounding system based on full-wave approach," *Electric Power Systems Research.*, vol. 198, pp. 107355, Sept. 2021.

- K. Yin, M. Ghomi, **H. Zhang**, F. Faria da Silva, C. L. Bak, Q. Wang, and H. Skouboe, "The design and optimization of the down-lead system for a novel 400 kV composite pylon," *IEEE Trans. Power Delivery.*, 2022, Status: Under review.

Publications in Refereed Conferences

C1. **H. Zhang**, Q. Wang, K. Yin, C. L. Bak, and F. Faria da Silva, "Transient modelling and backflashover rate analysis of a fully composite pylon," *Proc. of IET ACDC*, Xi'an, China, 2020, pp. 460-466

C2. **H. Zhang**, M. Ghomi, K. Yin, Q. Wang, F. Faria da Silva, and C. L. Bak, "Evaluation of Lightning Backflashover Rate of a Fully Composite Pylon using Monte Carlo Method on Environmental Factors," *Proc. of IEEE PES GM*, Denver, Colorado, 2022, Status: Accepted

C3. **H. Zhang**, K. Yin, Q. Wang, K. Y. See, F. Faria da Silva, and C. L. Bak, "A Simplified Dynamic Surge Impedance Model with Corona Effect for Grounding Down-Leads of Composite Pylons under Lightning Surges," *Proc. of ICLP*, Cape Town, South Africa, 2022, Status: Accepted

O2. K. Yin, M. Ghomi, F. Faria da Silva, C. L. Bak, **H. Zhang**, and Q. Wang, "Lightning performance and formula description of a Y-shaped composite pylon considering the effect of tower-footing impedance," *Proc. of ICLP*, Colombo, Sri Lanka, 2021, pp. 1-6

- K. Yin, M. Ghomi, F. Faria da Silva, C. L. Bak, **H. Zhang**, and Q. Wang, "The Effect of Frequency-Dependent Soil Electrical Parameters on the Lightning Response of a 'Y' Shaped Composite Pylon for 400 kV Transmission Lines," *Proc. of ISH*, Xi'an, China, 2021

- K. Yin, F. Faria da Silva, C. L. Bak, **H. Zhang**, Q. Wang, and H. Skouboe "Electric Field Computation and Optimization for A 400 kV Y-shaped Composite Cross-arm," *Proc. of ICEMPE*, Chongqing, China, 2021, pp. 1-4

Chapter 2

Backflashover Evaluation Procedure based Monte Carlo Method

2.1 Background

The basic question for insulation coordination and lightning protection of transmission lines supported by novel fully composite pylons is how many lightning flashes originated flashovers the transmission line may experience per year, and the answer is referred to as BFR [42]. In terms of incoming overvoltage emerging from backflashovers on nearby transmission pylons incident to the substation, it is very significant in the design of substation overvoltage protection. Furthermore, it is required in the planning phase for surge arrester protection on OHLs.

Many researchers and experts have looked at how to analyze BFR using analytical and numerical methodologies. The most common-used analytical methods are proposed by CIGRE [25] and IEEE [43], because of their convenience of application. However, some simplifications and approximations assumed in the methodologies are dubious. Nowadays, it is prevalent to deal with BF problems by numerical simulations, which are carried out using electromagnetic transients simulation software (EMTSS) [44]. By means of the numerical technique to analyze the transient performance, some sophisticated models of transmission line components can be established, some of which exhibit non-linear behaviors, electromagnetic coupling effects, and frequency dependence. Furthermore, some factors with uncertainties and statistical randomness can be taken into consideration via EMTSS like PSCAD. For instance, to begin with, natural circumstances for BF performance eval-

uation are generally in wide-range variation, such as lightning current amplitude and shape, and soil resistivity distribution. Secondly, the electrical stress induced by lightning and the electrical strength of insulation both have probabilistic nature. Thirdly, BFR is not linear to the change of lightning current, grounding conditions, and insulation level. Under these circumstances, EMTSS simulation combined with the Monte Carlo method (MCM) appears as an optimal strategy to investigate the statistical probability of BF of OHLs [45–47].

In this chapter, the analytical methods recommended by IEEE and CIGRE, and the numerical methods based on the MCM to evaluate BFR has been presented first. The adequacy of MCM sampling size and accuracy of MCM results are verified.

2.2 Analytical Methods on Backflashover Rate Evaluation Proposed by CIGRE and IEEE

Some simplified mathematical methods are advocated by CIGRE [25] and IEEE [43], respectively, based on observational and experimental data. Both methods intend to compute the lightning withstand level, then estimate BFR based on the probability that the level is exceeded by the lightning current. Some modeling details are described and compared as follows.

In both methods, the transmission tower is treated as a uniform surge impedance, and tower footing is treated as a resistance. The soil ionization effect can be considered inclusively, while the frequency-dependent characteristics of soil electrical parameters are ignored. As for the flashover determination for insulators, CIGRE method employs a withstand voltage level termed as non-standard critical flashover overvoltage for insulators. IEEE adopts the volt–time curve as the withstand voltage level to determine the flashover of insulators. The lightning current that causes overvoltage to exceed withstand voltage level is termed lightning withstand level. As for the estimation of backflashover rate, both methods follow equation (2.1),

$$BFR = 0.6 \cdot N_d \cdot P(I_c) \tag{2.1}$$

where N_d is the estimated number of lightning strikes that terminate on the transmission lines, constant coefficient 0.6 is used to account for the fact that overvoltage at the shield wire caused by lightning flashes striking within the span is lower than that caused by lightning striking at the pylon head. I_c is the minimum lightning current inducing BF, and $P(I_c)$ is the probability of the lightning current larger than I_c. IEEE and CIGRE propose different equations to calculate $P(I_c)$. CIGRE employs the integration of the probability density function of lightning current based on the statistical data from observation.

IEEE reproduces the equation into the following equation (2.2). P_I calculated by the two different models along with lightning current is compared and shown in Fig. 2.1.

$$P(I_c) = \frac{1}{1 + (\frac{I}{31})^{2.6}} \tag{2.2}$$

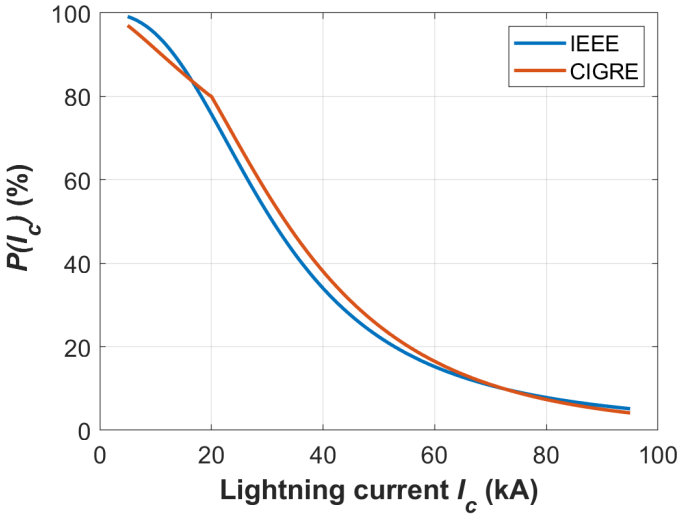

Fig. 2.1: Comparison of $P(I_c)$ between IEEE and CIGRE

The simplifications and approximations in analytical methods truly make the calculation process of BFR fast, but raise doubts on the accuracy at the same time, for instance, among the aspects of the representation of lightning current, the transient performance of grounding device, and the criterion on flashover occurrence [48]. The analytical approach to evaluate BFR of the composite pylon based CIGRE model is revised and compared with simulating results by PSCAD in **O2** [49].

2.3 Description of MCM-based Procedure for Backflashover Performance Evaluation

In order to simulate the statistical uncertainties of lightning incidences, MCM is generally used to address such problems and it has an excellent consistency with observed data [50]. A standard MCM for lightning performance evaluation of transmission lines requires a sufficient number of

lightning events, which are characterized by different lightning current waveshape parameters and different lightning stroke locations [47]. For evaluation of BFR, lightning stroke location is generally omitted, while lightning current crest and lightning front time are selected as key parameters for MCM, which are implemented in EMTSS [44].

The procedure to evaluate BF performance of the transmission lines supported by fully composite pylons is based on the application of MCM, within which the computation of transient overvoltages is implemented in the PSCAD. Such a procedure consists of three steps: pre-processing step, numerical simulation step, and post-processing step [51].

2.3.1 Pre-Processing Step

The pre-processing step aims to randomly generate data pools for the environmental factors with wide-range variation according to their probability distribution. Lightning current parameters are paid main concentration in the past research. The environmental factors can include lightning current parameters and soil conditions.

For lightning current parameters, each lightning event is characterized by polarity and current waveform parameters. Positive and negative lightning flashes take 10% and 90% of the total number of lightning data pool. Four variables are utilized to shape the lightning current waveshape of the first stroke of the downward flash as recommended by CIGRE, namely, the lightning current amplitude I_c, the maximum steepness S_m, the front time (from 30% to 90%) t_f, and the tail time t_f. The probability of the four parameters follows log-normal distribution [42]. Table 2.1 displays the median M of the variables as well as their log standard deviation β.

Table 2.1: The median and log standard deviation of the lightning current parameters. Source: **C1** [52],**C2**

Variable	M, median	β, log std. deviation
I_c [>20 kA, kA]	33.3	0.605
S_m [kA/μs]	24.3	0.599
t_f [μs]	3.83	0.553
t_h [μs]	77.5	0.577

Because the front time of lightning current follows a log normal distribution, inverse transform sampling is employed to generate a pool of front times [53]. There is a correlation between front time t_f and current amplitude I_c. The median of log-normal distribution of I_c can be obtained according to

the value of t_f in equation (2.3) [42],

$$M_I = 19.5 \cdot {t_f}^{0.39} \tag{2.3}$$

Then, based on every front time, a pool of lightning current amplitudes can be generated. In this project, the number of different front times is 100 and the number of different lightning current amplitudes corresponding to every front time is also 100, thus, the number of lightning currents N_{total} is 10000. The adequacy of the sampling pool size is discussed in the following section.

2.3.2 Numerical Simulation Step

In the numerical simulation step, all lightning currents produced from the previous step were imported into the OHLs model established in PSCAD to serve as the lightning impulse current source. The overvoltages between down-leads and closest phase conductors are measured.

Then, taking into account the operating voltage of phase conductors, the BF probability for every lightning current *P(I)* was estimated. The occurrence of BF depends on the difference between the overvoltages on the down-leads which are negative and the AC voltage V on the phase conductors. The AC voltage can be treated as a constant because of the comparatively extremely short period of overvoltage. There is a minimum value of AC voltage, V_i, and the voltage difference between overvoltage and V_i is the minimum voltage to result in flashover. The voltage difference between overvoltage and the AC voltage larger than V_i can definitely result in flashover. The BF probability can be estimated as the ratio of the period in one AC cycle when the AC voltage exceeds V_i for the entire AC cycle.

The leader progression mechanism determines the flashover (LPM). The insulating surface flashover is defined by LPM as the physical process of air gap discharge, which has two major stages: the streamer progression stage T_s and the leader progression stage T_l [54].

The streamer progression time can be calculated by equation (2.4) [55],

$$T_s = \frac{1}{k_1(E/E_{50\%}) - k_2} \tag{2.4}$$

where, E is the maximum electric field before insulation flashover and $E_{50\%}$ is the electric field under the 50% flashover voltage. k_1 and k_2 are the factors of streamer progression time, which are advised to be 1.25 and 0.95 respectively [56].

The leader progression duration can be calculated related to its developing speed suggested by CIGRE in equation (2.5) [25],

$$\frac{dx}{dt} = ku(t)(\frac{u(t)}{D-x} - E_l) \tag{2.5}$$

where, x is the length of the leader, $u(t)$ is the voltage at the air gap, D is the length of insulation, E_l is the threshold electric field of leader progression and k is the factor of leader progression speed. E_l and k are related to the type of the insulators and the polarity of lightning impulse voltage, as determined in experiments and presented in Table 2.2.

Table 2.2: Recommended values for leader progression method of lightning impulse flashover. Source: **C2**

Configuration	Polarity	k [$m^2/(kV^2 \cdot \mu s)$]	E_l [kV/m]
Air gaps, post insulators,	Positive	0.8	600
long-rod polymer insulators	Negative	1.0	670
Cap-and-pin porcelain insulators,	Positive	1.2	520
glass insualtors	Negative	1.3	600

The parameters of a long-rod polymer insulator are used instead of a cap-and-pin insulator with metallic connecting hardware, because the flashover characteristics between the shield wire and upper phase conductor along the crossarm are more similar to those of a long-rod polymer insulator.

2.3.3 Post-Processing Step

In the post-processing step, BFR is computed after processing the results of BF probability *P(I)* of all lightning flashes.

The total BF probability P_{BF} can be computed by adding $P(I)$ of all lightning flashes together in the following equation (2.6),

$$P_{BF} = \frac{\sum P(I)}{N_{total}} \tag{2.6}$$

where $\sum P(I)$ is the sum of BF probability of every lightning flash and N_{total} is the total number of lightning flashes. Their ratio means the probability that the lightning flashes terminating at the shield wires can result in BF.

The BFR is expressed in equation (2.7) [42],

$$BFR = 0.6 \cdot N_d \cdot P_{BF} \tag{2.7}$$

where the numerical multiplicative coefficient 0.6 takes it into consideration that lightning flashes hitting within the span cause lower overvoltage at the shield wire than those hitting at the pylon head. Consequently, if lightning flashes hitting within the span are considered, the BFR decreases by 40%. N_d

can be computed by the ground flash density N_g and the shadow region of OHLs, where if the lightning terminates within, it will be attracted to the shield wires. The shadow area is shown as the red area in Fig 2.2. Therefore, the estimated number of lightning flashes terminating on a 100-km OHL supported by composite pylons can be calculated into equation (2.8)

$$N_d = N_g \cdot (D + 28 \cdot H^{0.6}) \cdot 10^{-1} \tag{2.8}$$

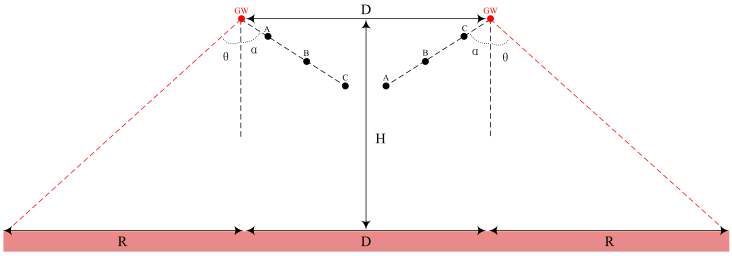

Fig. 2.2: The demonstration of shielding shadow area of OHLs supported bu composite pylons. Source: **C1** [52]

2.4 Precision Verification on the Uncertainties in Backflashover Performance Evaluation

MCM is highly efficient and highly accurate by approaching the "real" results after large amounts of sampling. There automatically raises the question that how large sampling amount is enough to obtain a result with high accuracy.

An intuitive way is to show BF probability changing trend along with the increasing lightning incidences, as illustrated in Fig. 2.3 [44]. At the initial stage of importing lightning incidences to determine whether BF occurs and calculate BFR, the results fluctuate dramatically because of insufficient sampling amount. Along with the increase of lightning incidences imported in, in another word, the increase of N_{total}, BF probability P_{BF} converge to stability gradually. When N_{total}>5000, the convergence error can be calculated to be less than 5%. When N_{total}>8000, the convergence error can be calculated to be less than 1%.

Another statistical approach to verify the adequacy of sample size is to calculate the estimation precision level reversely based on the 90% confidence interval. According to the *Central Limit Theorem*, the confidence interval can be calculated as follows,

$$CI = (\bar{x} - z^* \times \frac{s}{\sqrt{n}}, \bar{x} + z^* \times \frac{s}{\sqrt{n}}) \tag{2.9}$$

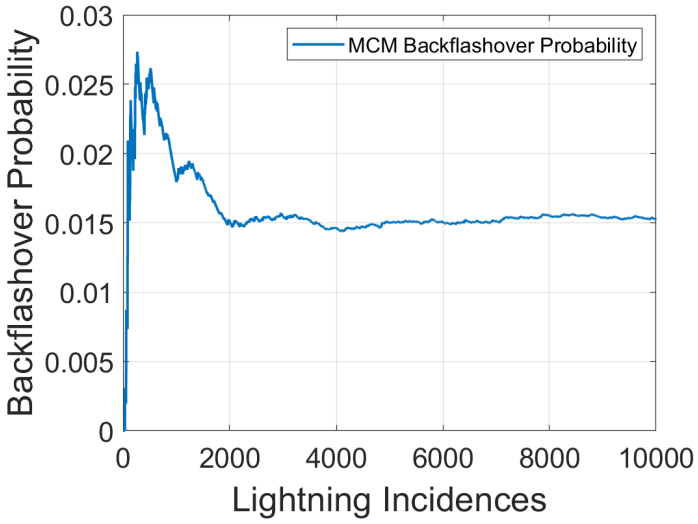

Fig. 2.3: Backflashover probability converges to stability along with increasing lightning incidences using MCM

where $\bar{x}$ is the sample mean and z^* is the statistic associated with a certain confidence interval. In the case of a 90% confidence interval z^* equals 1.64, approximately, s is the sample standard deviation, and n is the sample size. Thus, the estimation precision level can be described in the following equation,

$$\phi = z^* \times \frac{s}{\sqrt{n}} \tag{2.10}$$

For example, if the sample sizes of lightning front time and lightning current amplitude are both 100, their median M and standard deviation β are as listed in Table 2.1. The estimation precision levels of front time and lightning current amplitude are computed as 0.0907 and 0.1095, and take 2.37% and 0.33% of their medians. At a 90% confidence interval, the sample size with a precision level lower than 5% is enough to provide reliable results using MCM [57]. Thus, the sample size of 100 for lightning front time and lightning current can provide trustful results.

2.5 Summary

In this chapter, the procedures to evaluate BF performance for transmission lines, as well as transmission pylons have been introduced. Firstly, two analytical methods recommended by CIGRE and IEEE have been introduced

and compared. Analytical methods have advantages of simplicity in estimation, while some factors cannot be considered comprehensively, especially the uncertainties of some parameters with randomness like lightning current waveform parameters. MCM is generally used to solve such problems and it has an excellent consistency in observation data. Then, a standard procedure based on MCM to evaluate BFR has been presented. The MCM-based procedure is utilized throughout this research with improvement and revision. Finally, the adequacy of the sample size used in MCM to obtain results with high precision has been discussed and verified.

Related Publications

O2. K. Yin, M. Ghomi, F. Faria da Silva, C. L. Bak, **H. Zhang**, and Q. Wang, "Lightning performance and formula description of a Y-shaped composite pylon considering the effect of tower-footing impedance," *Proc. of ICLP*, Colombo, Sri Lanka, 2021, pp. 1-6

Main contribution:

Analytical approach to evaluate BFR recommended by CIGRE is revised to be applied on composite pylons.

C1. **H. Zhang**, Q. Wang, K. Yin, C. L. Bak, and F. Faria da Silva, "Transient modelling and backflashover rate analysis of a fully composite pylon," *Proc. of IET ACDC*, Xi'an, China, 2020, pp. 460-466

Main contribution:

The procedure applied MCM to evaluate BF performance of the composite pylon has formed and several modeling details have been calculated or simulated.

C2. **H. Zhang**, M. Ghomi, K. Yin, Q. Wang, F. Faria da Silva, and C. L. Bak, "Evaluation of Lightning Backflashover Rate of a Fully Composite Pylon using Monte Carlo Method on Environmental Factors," *Proc. of IEEE PES GM*, Denver, Colorado, 2022, Status: Accepted

Main contribution:

The procedure applied MCM has been revised by considering lightning current parameters and soil resistivity together.

Chapter 3

Analysis on Modeling of Composite Pylon Footing

3.1 Background

The grounding device is one of several variables that affect how well transmission towers or pylons protect against lightning. It must have "sufficiently low impedance and current-carrying capability to prevent the development of voltages that may result in unacceptable hazard to connected equipment and to individuals" [58]. It is of great significance to reduce BF probability and avoid tripping faults of OHLs [59]. For evaluating the BF performance of transmission towers and OHLs, establishing the simulating model of the grounding device in the electromagnetic transient analysis program such as PSCAD, EMTP-RV or ATP-EMTP is crucial to the protection of towers and transmission lines against lightning strokes.

In this chapter, models to describe the transient response of transmission tower footing are presented. Current-dependent impedance model and frequency-dependent impedance model are paid more attention to and compared in detail. A revised current-dependent impedance model processed by MCM has also been presented to deal with variant soil resistivity.

3.2 Models of Tower Grounding Impedance

In general, there are three models which are frequently applied to describe the transient performance of the grounding device.

3.2.1 Constant Resistance (CR) Model

The constant resistance model is the simplest one in the lightning protection evaluation. In this model, a lumped resistance serves as the impedance of the grounding system, which is described by equation (3.1) [60],

$$R_{CR} = \frac{max[v(t)]}{max[i(t)]} \tag{3.1}$$

where *max*[*v(t)*] is the peak of the voltage injected into the ground and *max*[*i(t)*] is the peak of the current passing through the pylon footing.

The modeling accuracy is generally positively correlated to the computational workload and negatively correlated to the computational speed. CR model is commonly used because it is simple and time-saving. However, the pylon grounding impedance is not constant during lightning current injecting into the ground, neither in time domain nor frequency domain. Firstly, while impulse current energizes the grounding electrodes, the soil around will ionize, thus the grounding impedance will change along with the impulse current [61, 62]. Moreover, the soil parameters and the conductor parameters are both frequency-dependent, which also results in frequency-dependent grounding impedance [63].

3.2.2 Current-Dependent Impedance (CDI) Model

In order to consider the time-variant grounding impedance caused by soil ionization, CIGRE recommends a current-dependent impedance model, described as equation (3.2) [25],

$$R_{CDI}(t) = \frac{R_0}{\sqrt{1 + (I(t)/I_g)}} \tag{3.2}$$

where R_0 is low-current footing resistance, *I(t)* is the function of lightning current injecting into ground and I_g is the critical current to ionize the surrounding soil described by equation (3.3) [64],

$$I_g = \frac{\rho E_0}{2\pi {R_0}^2} \tag{3.3}$$

where E_0 is the electric field gradient for soil ionization and ρ is the soil resistivity. The relationship of them can be described in the equation (3.4),

$$E_0 = 241 \cdot \rho^{0.215} \tag{3.4}$$

If the footing device is a cylindrical conducting electrode buried in the soil vertically, R_0 can be calculated in equation (3.5),

$$R_0 = \frac{\rho}{2\pi L}(\ln \frac{4L}{r} - 1) \tag{3.5}$$

where L is the length of the electrode and r is the radius of cross-section of the electrode.

From the above equations, it can be deduced that the impedance model of a cylindrical conducting electrode buried in the soil vertically is dependent on the injected impulse current, and only restricted by its geometry dimension and soil resistivity.

3.2.3 Frequency-Dependent Impedance (FDI) Model

The lightning current passing through down-leads and injecting into soil via pylon footing has are of high frequency. The soil electrical parameters, especially relative permittivity and resistivity, are frequency-dependent. Therefore, the soil electrical parameters cannot be simply considered as constant as the values recorded at power frequency [65]. It will help improve lightning protection and transient analysis of power systems by using a precise soil model considering its frequency-dependence.

R. L. Smith-Rose first presented comprehensive measurements of the electrical conductivity and permittivity of various soil samples at frequencies ranging from 1 kHz to 10 MHz [66]. After that, the frequency-dependence of soil electrical parameters has been investigated in the past decades, and summarized into analytical formulas by many scholars [32, 67–69]. A comparison of these common-used frequency-dependent soil models is performed in [70]. The frequency-dependent relative permittivity and resistivity of soil shown respectively in equation (3.6) and equation (3.7) are used in the presented research because they are fitted from experiments of wide-bandwidth frequency [32],

$$\epsilon_r(f) = 1.3 + (7.6 \times 10^3 \cdot f^{-0.4}) \tag{3.6}$$

$$\rho(f) = \frac{\rho_0}{1 + (1.2 \times 10^{-6} \cdot \rho_0^{0.73}) \cdot (f - 100)^{0.65}} \tag{3.7}$$

where ρ_0 is the soil resistivity at 100 Hz, f is the frequency.

Based on frequency-dependent soil electrical parameters, the current research utilizes a frequency-dependent impedance model for the composite pylon footing model, which is well-matched with actual measurements of soil with varied frequencies ranging from 1 kHz to 10 MHz by applying the full-wave approach MoM solution to Maxwell's equations in **O1** [71, 72]. The MoM, which provides the current distribution along the grounding segments, is used in this method to build the governing electric field integral equation for the induced currents along the grounding conductor segments. The grounding system admittance matrix is then approximated rationally using vector fitting methods in the frequency domain. In order to create a model of the grounding system described as statespace equations, which can be simulated and expressed in the time-domain blocks in EMTSS, such as EMTP-RV and PSCAD/EMTDC, the derived rational approximation is used.

3.3 Comparison between CDI Model and FDI Model

From last section, it can be known that CR model sacrifice modeling accuracy for simplicity. The other two models, CDI model and FDI model focus on soil ionization effect and electrode inductive effect respectively. A detailed comparison between CDI model and FDI model is carried out from the aspects of modeling simplicity, dynamic impedance, and overvoltage level at the tower top.

3.3.1 Analysis on Modeling Simplicity

Compared to CR model, both CDI model and FDI model are more complicated. From the derivation process, CDI model is more convenient to obtain and revise. CDI model is simply described by concise analytic formulations. Thus, it is convenient to be implemented into EMTSS, and to replace relevant parameters according to different soil conditions and different geometrical dimensions of electrodes. The derivation of FDI model depends on MoM to solve Maxwell's differential equations. It still needs to be transferred from frequency-domain solutions into time-domain solutions, which can be implemented into EMTSS. Any change in the modeling initial stage demands the derivation process again. Therefore, CDI model is of advantages in the case of variant modeling parameters.

3.3.2 Comparison on Dynamic Impedance

The dynamic impedance under a lightning surge of the two models is compared. The waveform of the example lightning surge is 1.2/50 μs, 80 kA. The geometry dimension of the pylon footing is set as a cylindrical electrode buried vertically in the soil. The cross-section radius of the electrode is 12.5 mm. The length of the electrode is set as 3 m, 9 m, and 12 m. Two soil conditions are selected, 10 Ωm and 100 Ωm. The dynamic impedance curves are demonstrated in Fig. 3.1 for electrodes of different lengths and two soil resistivity.

If the geometrical dimension of the electrode and soil resistivity is the same, both models have the same power frequency resistance R_0. However, the dynamic impedance curves of the two models present totally different changing trends. The impedance of CDI model varies along with the current magnitude passing through the electrode, thus it reaches the lowest while the current reaches its peak because of the soil ionization effect, and increases gradually to equal to R_0. The impedance of FDI model varies along with the current frequency, thus it rises up dramatically at the beginning because of the inductive effect of the electrode and decreases to R_0 afterward. Therefore,

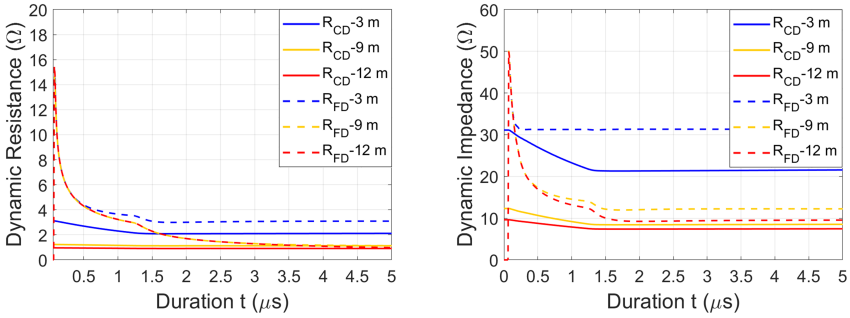

(a) ρ=10 Ωm (b) ρ=100 Ωm

Fig. 3.1: The dynamic impedance of CDI model and FDI model with different electrode length

the dynamic impedance of CDI model is always smaller than that of FDI model.

Longer electrodes and higher soil resistivity both cause larger R_0. Besides, if the electrode is longer, the inductive effect presents more significant while the soil ionization effect does not, thus the dynamic impedance of FDI models need a longer time to reach R_0 and the impedance reduction in CDI model caused by soil ionization becomes smaller.

3.3.3 Comparison on Overvoltage Level at Tower Top

A tower model with the surge impedance of 200 Ω and a height of 20 m is established for example. The overvoltage curves at the top of the tower are demonstrated in Fig. 3.2 for electrodes of different lengths and two soil resistivity.

For the same electrode and soil resistivity, the footing impedance at power frequency R_0 is also the same. The soil ionization reduces footing impedance at wave front with high current, while the inductive effect of the electrode increases the footing impedance at wave front with high steepness. Therefore, the dynamic impedance of CDI model is always smaller than that of FDI model, and the overvoltage at the tower top provided by CDI model is always lower than FDI model in the same condition. When soil resistivity is large and the electrode is short, in another word, when grounding condition is poor, the difference in overvoltage given by CDI model and FDI model is very large. This is pointed out by other scholars that CDI model overestimates the beneficial influence of soil ionization on reducing lightning overvoltage in high-resistivity soil [73]. Therefore, under such circumstances, FDI model is more appropriate to describe the transient performance of pylon footing.

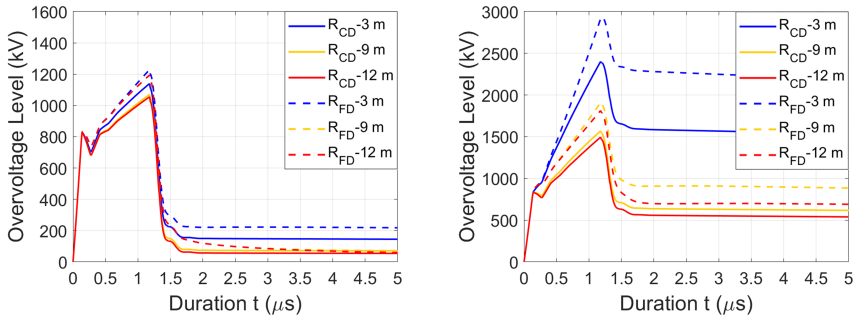

(a) ρ=10 Ωm (b) ρ=100 Ωm

Fig. 3.2: The overvoltage provided CDI model and FDI model with different electrode length

3.4 Application of MCM on CDI Model

As mentioned above, the CDI model can describe the time-varying grounding impedance caused by soil ionization. The CDI model of a cylindrical conducting electrode with a particular geometry dimension is only restricted by the soil resistivity where it is buried.

An OHL generally covers several to even hundreds of kilometers. BFR is also termed in the unit of the amount of BF cases per 100 km lines each year. Thus, the soil resistivity of the earth where the pylons stand and their footing electrodes are buried is variant from pylon to pylon. Besides, BFR is not linear to soil resistivity. In order to take these unpredictabilities into consideration, MCM is applied to process both lightning parameters and soil resistivity.

A standard MCM for lightning protection performance evaluation of transmission lines needs a large amount of lightning incidents, which are characterized by different lightning current waveshape parameters and different lightning stroke locations [47]. For evaluation of BFR, lightning stroke location is generally ignored, while lightning current crest and lightning front time are selected as key parameters for MCM, which are implemented in EMT software [41, 44]. Aside from the lightning parameters, tower footing resistance also affects BF performance of the towers significantly. However, at present, MCM is only applied on the pre-ionization footing impedance at power frequency R_0 of the tower in equation 3.2 [45, 74]. It has been overlooked that R_0 is closely related to soil resistivity, which also varies in a wide range from tower to tower randomly.

3.4.1 Probability Distribution of Soil Resistivity

The soil types are ranked into three levels: low-resistivity soil (fills-ashes, cinders, brine wastes), median-resistivity soil (clay, shale, gumbo, loam), and high-resistivity soil (gravel, sand, stones, with little clay and loam). Reference [75] provides the soil resistivities of different soil types with their average, minimum and maximum values. The distribution of soil resistivity follows log normal distribution approximately. The average is regarded as μ, the median of log normal distribution. The minimum and maximum are regarded as $\mu \pm 3\sigma$, the confidential interval of 99.7%. As a result, σ, the deviation of distribution can be obtained. The statistics parameters are shown in Table 3.1 and the probability distributions of the three types of soil are drawn and shown in Fig. 3.3.

Table 3.1: The statistics parameters of different soil classifications. Source: **C2**

Soil classification	Soil resistivity [Ωm]			
	Min.	Ave. μ	Max.	Dev. σ
Low resistivity	5.9	23.7	70	0.41
Median resistivity	10.2	158	1350	0.81
High resistivity	590	940	4580	0.34

3.4.2 Comparison of BF Probability of CDI Model with Constant Soil Resistivity and Soil Resistivity Processed by MCM

The sampling of soil resistivity for MCM follows the log normal distribution, which is restricted by median and deviation. Therefore, the BF probability of composite pylon is evaluated with the pylon footing model of constant soil resistivity and the pylon footing model of soil resistivity processed by MCM respectively, the results are shown and compared in the following Fig. 3.4.

The black dot-line depicts the relationship between BF probability and constant soil resistivity. The red dots represent the BF probability where the soil resistivity equals the medians of soil resistivity distribution of different types, as listed in Table 3.1. The blue lines show the levels of BF probability when MCM is applied to soil resistivity distribution of different types. It can be found that when soil resistivity is lower than around 500 Ωm, BF probability is almost linear to the log of soil resistivity. When soil resistivity is higher than 500 Ωm, BF probability is not closely sensitive to the change in soil resistivity. For low-resistivity soil and medium-resistivity soil, the MCM BF

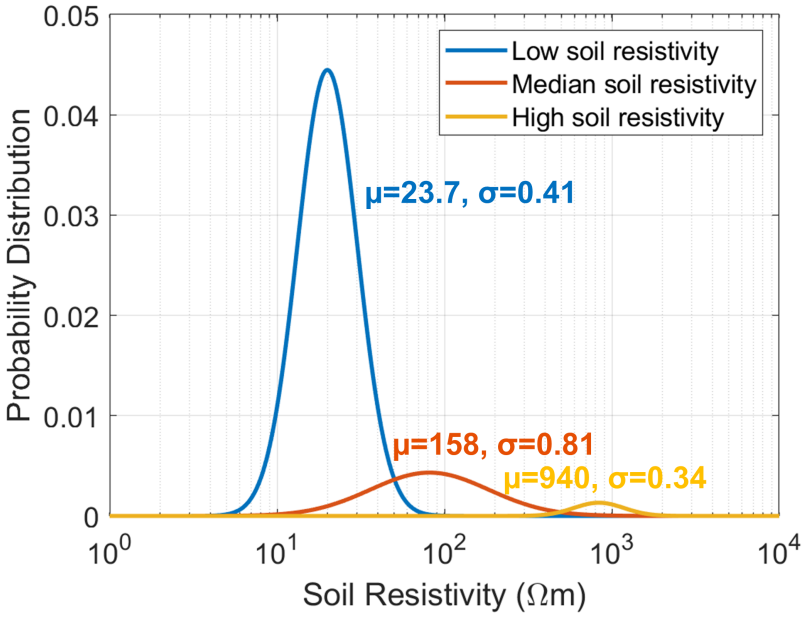

Fig. 3.3: The probability distributions of the three types of soil. Source: **C2**

probability is close to the BF probability of the median soil resistivity. However, for high-resistivity soil, the MCM BF probability has a larger deviation, roughly 10% smaller than the BF probability of the median soil resistivity.

3.4.3 Discussion on Application of MCM on Soil Resistivity in Backflashover Evaluation for Composite Pylons

The discrepancy between MCM result and the constant median result is due to the non-linearity of the relationship between BF probability and the log of soil resistivity.

For low-resistivity soil and medium-resistivity soil, the values of soil resistivity in the sample are lower than 500 Ωm, BF probability is approximately linear to the log of soil resistivity. Because soil resistivity yields to log-normal distribution, the linearity between BF probability and the log of soil resistivity results in the small discrepancy between the MCM BF probability and the BF probability of the median soil resistivity. However, for high-resistivity soil, most values of which are larger than around 500 Ωm, the relationship of BF probability is not linear to the log of soil resistivity and presents an increasing and concave trend. Thus, it can be inferred that the MCM BF probability is much lower than the BF probability of the median soil resistivity.

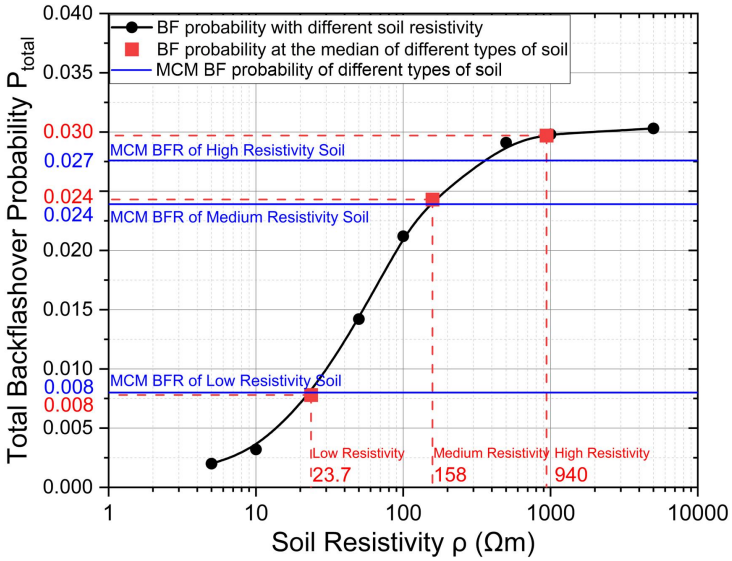

Fig. 3.4: Backflashover probability of CDI model with constant soil resistivity v.s. backflashover rate of CDI model with MCM soil resistivity. Source: **C2**

The turning point of the linearity between BF probability and the log of soil resistivity is related to the insulation level of the transmission pylon. If the insulation strength is higher, the slope of the BF probability-to-log of soil resistivity relationship will be smaller, which means the turning point will locate at higher soil resistivity and vice versa.

In summary, if CDI model with constant soil resistivity is adopted in BF study for a transmission tower installed in high resistivity region, the BFR is probably overestimated because of the non-linearity between BF probability and the log of soil resistivity, and the dispersion of soil resistivity.

3.5 Summary

In this chapter, the transient footing model of the composite pylon has been discussed. Three common-used models are introduced, namely constant resistance (CR) model, current-dependent impedance (CDI) model and frequency-dependent impedance (FDI) model. Compared to constant resistance model, the other two models, CDI model and FDI model focus on the soil ionization effect and the electrode inductive effect respectively, which

provide dynamic impedance during lightning injecting into ground. During a lightning surge, the dynamic impedance of CDI model is always smaller than that of FDI model, thus the overvoltage provided by CDI model is always smaller than that of FDI model. Under poor footing conditions, CDI model overestimates the beneficial influence of soil ionization on reducing lightning overvoltage, while FDI model is more appropriate to describe the transient performance of pylon footing. However, the derivation of FDI model for implementing in EMTSS with given parameters is pretty complicated and time-consuming. One of the advantages of CDI model is that it is convenient to be implemented in EMTPSS, which can import and change relevant parameters such as soil resistivity. Therefore, MCM can be applied to process both lightning parameters and soil resistivity, considering that the soil resistivity of the ground where the pylons stand and their footing electrodes are buried is variant from pylon to pylon in large-scale transmission lines. If CDI model with constant soil resistivity is adopted in BF study for a transmission tower installed in high resistivity region, the BFR is probably overestimated because of the non-linearity between BF probability and the log of soil resistivity, and the dispersion of soil resistivity.

Related Publications

O1. M. Ghomi, **H. Zhang**, C. L. Bak, F. Faria da Silva, and K. Yin, "Integrated model of transmission tower surge impedance and multilayer grounding system based on full-wave approach," *Electric Power Systems Research.*, vol. 198, pp. 107355, Sept. 2021.

Main contribution:

A full-wave approach based on the method of moment (MoM) is proposed to investigate the frequency-dependence of grounding electrode surge impedance considering multilayer soil.

J2. **H. Zhang**, M. Ghomi, Q. Wang, F. Faria da Silva, C. L. Bak, K. Yin, and H. Skouboe, "Comparison of Backflashover performance between a novel composite pylon and metallic towers," *Electric Power Systems Research.*, vol. 196, pp. 107263, July. 2021.

Main contribution:

The frequency-dependent impedance footing model is applied to simulate the lightning surge response of three transmission towers. Application of frequency-dependent impedance footing model can increase the simulation accuracy in high-frequency domain to compare the lightning overvoltage level of three transmission towers better.

C2. **H. Zhang**, M. Ghomi, K. Yin, Q. Wang, F. Faria da Silva, and C. L. Bak, "Evaluation of Lightning Backflashover Rate of a Fully Composite

Pylon using Monte Carlo Method on Environmental Factors," *Proc. of IEEE PES GM*, Denver, Colorado, 2022, Status: Accepted

Main contribution:

MCM has been used on current-dependent impedance model to process variant soil resistivity, because the soil resistivity where composite pylons stand may have a wide distribution in large-scale region.

Chapter 4

Analysis on Modelling of External Grounding Down-lead Considering Corona Effect

4.1 Background

Because the pylon is fully made of composite materials, the pylon body and the crossarms are insulated. There rises a problem that a method is needed to bring the ground potential to shield wires when lightning strikes. A direct method is installing grounding down-leads to conduct lightning current to ground, acting as the function of a conventional metallic tower. In the studies of the transient behavior of the power system, the accurate representation of the transmission tower is an essential part. Thus, in the lightning transient studies of composite pylons, it is necessary to propose an accurate model for the external grounding down-leads.

When a lightning flash strikes at the shield wires of OHLs, the lightning current passing through both the metallic tower and the down-leads of the composite tower will cause corona discharge. In lightning electromagnetic transient studies, the tower is represented by means of one or several line/surge impedance sections that are assembled taking into account the tower structure [27]. The tower models all neglect surge corona because of the relatively small corona radius compared with tower size. However, the grounding down-leads are very thin with a cross-section radius of a few centimeters, which is comparable to the corona developing distance during a

lightning surge. Corona discharge around the down-leads increases the coupling effect between down-leads to phase conductors, distorts overvoltage wavefronts, and lowers the down-leads' surge impedance. Therefore, it is important to consider how surge corona may affect the grounding down-leads' transient performance.

This chapter will review the constant surge impedance models of traditional metallic towers and surge corona dynamics, propose a dynamic surge impedance model for thin-wire grounding devices, and present the corona developing process and its effect on overvoltage and BFR of composite pylons.

4.2 Surge Impedance of Grounding Down-leads

4.2.1 Definition of Surge Impedance of Conventional Transmission Towers

Three definitions are adopted to describe the time-domain surge impedance of a transmission tower. The first one is defined by the instantaneous values of the voltage-to-ground at top of the tower *v(t)* and the current through the tower *i(t)* [76], as shown in equation (4.1),

$$z(t) = \frac{v(t)}{i(t)} \tag{4.1}$$

This description only applies to circuits that are completely resistive, where the voltage and current have identical waveforms. If the injected current is of a step or ramp waveform, then the surge impedance of the tower is defined as equation (4.2) [77],

$$z(t) = \frac{v(t)}{max[i(t)]} \tag{4.2}$$

Another commonly-used definition adopts the maximum values of tower top voltage and injected current, described as equation (4.2) [78],

$$Z = \frac{max[v(t)]}{I} \tag{4.3}$$

where *max[v(t)]* is the peak of tower top voltage and I is the value of *i(t)* when the voltage *v(t)* is maximum. Obviously, this definition of the surge impedance is not a function of time.

4.2.2 Methods to Model Transmission Tower

Corresponding to the definition of surge impedance, the basic principle to model a transmission tower is to derive an equivalent surge impedance or

equivalent circuit with the same surge response as the real waveforms under lightning transient. The current methods can be classified into three categories, theoretical representation, experimental measurement, and numerical computation.

In the theoretical representation, the structure of conventional metallic towers is generally complicated, thus some of the tower details, such as its crossarms or bracings, are usually neglected. The tower body is approximated as a cylinder [79] or cone [80]. The cylindrical shape is in good consistency with a thin-wire grounding down-lead.

Generally speaking for specific towers, experimental measurement is the most accurate method to obtain the lightning response, but this is actually where the restriction of this method lies. There are only a few experimental studies on several types of in-service towers [81–83]. Experimental results lack justifications for the transmission towers of different structures and dimensions.

Numerical computation is paid increasing attention to acquiring an accurate lightning response of transmission towers owing to the development of computational electromagnetic techniques. Commonly-used approaches include MoM [27, 84], FEM [85, 86], HEM [87], and FDTD [88, 89].

4.2.3 Overview of Present Transmission Tower Models

Based on the above method to obtain tower models with equivalent surge impedance, there exist many expressions proposed by different scholars with different assumptions, which can be seen in the following Table 4.1.

Among the above models, the applicable situation for grounding down-leads deserve discussion. Firstly, only equation (4.7) ignores the radius of the tower. One main difference between grounding down-leads and the metallic tower is that down-lead is quite thin in cross-section radius compared with the approximate shape of transmission towers. Secondly, equation (4.6) and equation (4.8) are derived by approximating towers into conical shapes instead of cylindrical shapes like down-leads. Besides, in some models, the current injected into the tower is assumed with a specific shape, such as a ramp in equations (4.6), (4.9), and (4.11), a double exponential in equations (4.6), (4.7), and (4.8), or a rectangular wave shape in equation (4.5) and equation (4.10), which restricts the applicability of such equations to other waveshapes. Equation (4.6) is derived via the revision and extension of equation (4.4) and is validated by experimental data and a hybrid electromagnetic model. Thus, equation (4.6) is adopted and revised to model the dynamic surge impedance of the down-lead.

Table 4.1: Formulations to calculate surge impedance for transmission towers

Scholar & year	Equation	Numbering
Jordan 1934 [90]	$60\ln(\frac{h}{r}) - 60$	(4.4)
Wagner & Hileman 1960 [76]	$60\ln(\sqrt{2}\cdot\frac{2h}{r})$	(4.5)
Sargent & Daverniza 1969 [78]	$60\ln(\sqrt{2}\cdot\frac{\sqrt{h^2+r^2}}{r})$	(4.6)
Menemenlis & Chun 1982 [91]	$50 + 35\sqrt{h}$	(4.7)
Chisholm et al. 1983 [80]	$60\ln(\cot(\frac{\tan^{-1}(r/h)}{2}))$	(4.8)
CIGRE WG 1991 [25]	$60\ln(\frac{h}{r})$	(4.9)
Takahashi 1994 [92]	$60(\ln(\sqrt{2}\cdot\frac{2h}{r}) - 1.54)$	(4.10)
Hara & Yamamoto 1996 [93]	$60(\ln(\sqrt{2}\cdot\frac{2h}{r}) - 120$	(4.11)
IEEE Std. 1997 [94]	$60\sqrt{\frac{\pi}{4}}\ln(\frac{1}{\sqrt{2}}\cot(\frac{\tan^{-1}(2r/h)}{2}))$	(4.12)
De Conti et al. 2006 [95]	$60\ln(\frac{4h}{r}) - 60$	(4.13)

4.3 Representation for Surge Corona on the Grounding Down-leads

4.3.1 Review on Methods to Model Surge Corona

The surge corona modeling for OHLs has been developed a lot. There are two main ways to model corona. One is to obtain $q - v$ curve by experiments first and then to reproduce the specific $q - v$ curve by constructing linear, piece-wise linear, or nonlinear circuits. Moreover, it is practical for simulation to reproduce the $q - v$ curve without field test.

Therefore, the other way is to attempt to reproduce the $q - v$ curve from the geometrical configuration of the conductor and physical process. Some FEM simulating tools are used, but the modeling of plasma dynamics inside corona makes the calculation quite time-consuming [96]. Recent research has proposed a simplified model to consider the corona developing process on OHLs by FDTD in the simulation of large-scale transmission lines [97–99]. Another model considering the physical process of corona is corona shell model, which points out that space charges generated by corona form a shell around the conductor [100]. This concept makes the modeling simple considerably. The corona shell model is proposed for the calculation of steady-state

corona for the first time and recently it was applied to surge corona afterwards [101, 102]. There is little modeling research to be referred for the surge corona on grounding down-leads in the lightning study of composite pylons. The main difference lies in the vertical position in space of down-leads whereas OHLs are horizontal. The corona modeling of trigger-wire can be referred to because the lightning trigger-wires and down-leads can be regarded as vertical cylinders and the presence of corona is regarded as the increasing radius of the cylinders [103, 104].

4.3.2 Overview on Corona Dynamics

Corona is the partial breakdown of the air in the vicinity of a conductor applied high electric stress. The physical properties of impulse corona effect in air are introduced at first.

One of the necessary conditions for corona to initiate is that the electric field around the stressed conductor exceeds a critical threshold, namely corona inception electric field E_{cr}. Correspondingly, the overvoltage causing E_{cr} is termed as critical overvoltage V_{cr}.

Another one is that there exist free electrons in a high electric field area to induce a self-sustained electron avalanche. It takes a certain time for a specific electron to initialize electron avalanche, namely statistical time lag, t_s.

The expansion of the corona sheath is governed by the guiding electric field E_g, which is the sum of the electric field created by conductor potential and the electric field created by space charges in the corona. The expansion velocity equals the streamer velocity v_{cr}.

Corona effect only occurs when the applied voltage is increasing. Thus, the corona only expands and develops during wave front of impulse overvoltage instead of wave tail. A critical background electric field E_{bg} is necessary for streamer propagation, which determines the maximum expansion radius of the corona sheath.

In summary, once the impulse overvoltage on the conductor rises and exceeds V_{cr}, the corona will initiate after t_s. Then, corona expands at the velocity of v_{cr} until the overvoltage starts decreasing. The total time from overvoltage rising to decreasing is the front time of overvoltage t_f.

4.3.3 Review on the Corona Parameters

The corona inception electric field E_{cr} (kV/mm) of cylindrical conductors was investigated experimentally many years ago by Peek [105] and summarized in the following equation (4.14),

$$E_{cr} = 2.98e6 \cdot m\delta(1 + \frac{0.301}{\sqrt{r\delta}}) \tag{4.14}$$

where m is the roughness coefficient of the conductor surface, δ is the relative density of the air, r is the conductor radius in mm. After that, A. M. Zalesski [106], M. Robinson [107], R. T. Waters et al [108], and G. Hartmann [109] reproduced some more practical equations to evaluate E_{cr} based on Peek's law, from equation (4.15) to equation (4.18).

$$E_{cr} = 2.45e6 \cdot (1 + \frac{0.613}{r^{0.4}}) \tag{4.15}$$

$$E_{cr} = 3.22e6 \cdot (1 + \frac{0.846}{\sqrt{r}}) \tag{4.16}$$

$$E_{cr} = 2.38e6 \cdot (1 + \frac{0.67}{r^{0.4}}) \tag{4.17}$$

$$E_{cr} = 2.594e6 \cdot (1 + \frac{0.1269}{r^{0.4346}}) \tag{4.18}$$

Statistic time lag t_s is generally irrelative to the electric field and other electrostatic parameters, while is related to air pressure, temperature, humidity, and other air conditions. Thus, it can be directly referred to the experimental results of other scholars. In [96], t_s varies from 0.4 μs to 0.7 μs. In [110][19], t_s varies from 0.45 μs to 0.88 μs.

After the electric field on the surface of the conductor exceeds E_{cr}, corona effect initials. The expansion speed of corona concluded in [96] ranges from 0.3 m/μs to 2 m/μs under the voltage ranging from 300 kV to 500 kV. Besides, [111] reported the radial speed of negative corona streamer from conductor surface in coaxial cylindrical electric field equals around 0.1 m/μs. Corona expansion velocity v_{cr} is generally related to the electric field. A 1-D air corona discharge model is established in *COMSOL Plasma Module*. Corona developing process under different voltage is shown in Fig. 4.1. By this means, v_{cr} can be estimated more precisely. On the other side, when the overvoltage meets its peak value, it will decrease and the corona will shrink and extinct. Because corona starts shrinking when applied voltage decreases, corona shrinking stage hardly affects overvoltage level which is a most concern in lightning transient studies. It is simply assumed that the corona shrinking velocity is equal to the expansion velocity.

The critical background electric field is necessary for streamer propagation and determines the maximum extent of the radially expanding corona region. The corona sheath is assumed as an ideal conductor with a conductivity of 40 μS/m [99]. Electric field is the sum of the electric field created by conductor potential and the electric field created by space charges in the corona. The space charge density distribution related to electric field can be described by equation (4.19),

$$E(r) = \frac{Q}{2\pi\epsilon_0 r} + \frac{Q}{2\pi\epsilon_0(2h - r)} \tag{4.19}$$

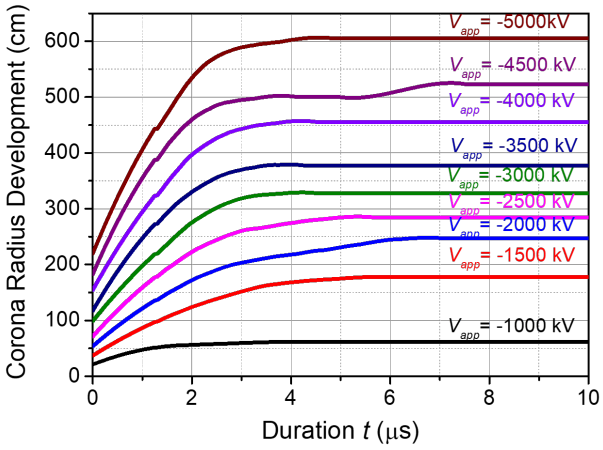

Fig. 4.1: Corona radius development process under different applied voltage. Source: **J3**

where *E(r)* is the radial electric field, Q is the space charge per meter, h is the height from ground flat to the top of vertical conductor, and r is the radial distance from the center. For $h \gg r$, equation (4.19) can be simplified into equation 4.20, then the space charge density distribution can be expressed by equation (4.21),

$$E(r) = \frac{Q}{2\pi\epsilon_0 r} \tag{4.20}$$

$$\rho(r) = \frac{Q}{\pi r^2} = \frac{E(r)\cdot\epsilon_0}{r} \tag{4.21}$$

Then equation (4.21) is given to the domain of corona in *COMSOL Plasma Module*, together with electric potential on the conductor to calculate the total electric field at the surface of corona. In *COMSOL Plasma Module*, electron is assumed to be diffuse in the direction of electric field [112]. A simplified set of reactions that describes correctly the creation and destruction of electrons, ions and molecules of nitrogen in a background of dry air is used [113].

Based on the above analysis and assumptions, the time-dependent corona radius $r_{cr}(t)$ is restricted by both the expansion velocity and the maximum expansion radius. Thus, it can be described as equation (4.22), where t_0 is the time when $r_{cr}(t_0)$ equals to 0.

$$r_{cr}(t) = \begin{cases} min\{v_{cr}\cdot(t - t_s - t_{cr}), r_{max}(t)\}, & 0 < t \le t_f \\ r_{cr}(t_f) - v_{cr}\cdot(t - t_f), & t_f < t < t_0 \end{cases} \tag{4.22}$$

4.4 Corona Development and Overvoltage of a Single Conductor Represented by the Dynamic Surge Impedance Model

A single vertical thin-wire conductor is set as a demonstration to present the corona development clearly. The down-lead is in the configuration of a vertical cylindrical conductor with a height of 20 m from ground flat and a cross-section radius of 0.01 m.

4.4.1 Influence of Corona Developing on Surge Impedance and Overvoltage

The overvoltage, surge impedance, and corona radius influence each other every time step. The surge impedance is in negative correlation with corona radius, and overvoltage is impacted by surge impedance. Then overvoltage induces the development of corona radius. When overvoltage meets the maximum, surge impedance is the lowest, and corona radius is the largest, then corona starts shrinking.

Fig. 4.2 shows an example of the mutual influence among overvoltage, surge impedance, and corona radius. The lightning current is 80 kA/2 μs. When overvoltage exceeds V_{cr}, after a delay of t_s, corona starts developing at the velocity of v_{cr}. The stage that corona develops at v_{cr} is marked in the red shadow. When the electric field of the streamer's tip reaches E_{bn}, the electric field keeps constant as E_{bn} and limits the corona radius to change with the curve in Fig. 4.2. The stage that corona develops limited by E_{bn} is marked in the orange shadow. When overvoltage meets crest and starts decreasing, surge impedance is the lowest, and corona radius is the largest, then corona starts shrinking. The stage when corona shrinks is marked in the yellow shadow.

4.4.2 Corona Development with Different Lightning Current Peaks

Fig. 4.3 shows the corona radius developing processes under the lightning currents of the same front time (2 μs) and different peaks, from 50 kA to 200 kA at the increment of 10 kA. As a result, the maximum radius that the corona can reach ranges from 0.14 m to 0.79 m. Because the front times of the lightning current keep the same, the corona radius also reaches the maximum at the same time. Looking through into the corona initial stage, a higher lightning current peak will exceed V_{cr} earlier, so the corona onsets at an earlier time.

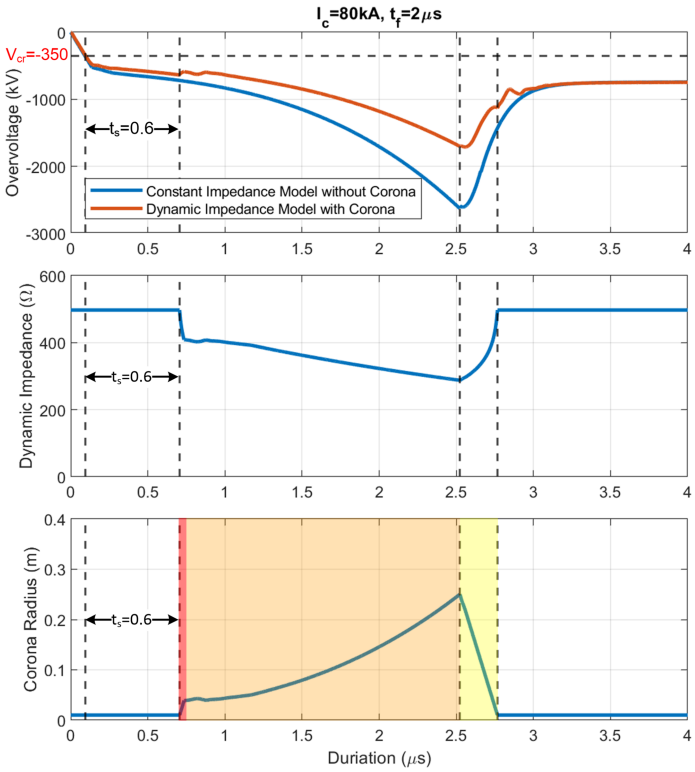

Fig. 4.2: Relationship among overvoltage at the top of conductor, surge impedance, and corona radius during one lightning impulse case. Source: **C3**

4.4.3 Corona Development with Different Lightning Current Front Times

Fig. 4.4(a) shows the corona radius developing processes under the lightning currents of the same peak amplitude (80 kA) and different front times, from 0.5 μs to 4 μs. Firstly, if the front time is even shorter than 0.5 μs, there is not adequate time for corona to onset and develop because ts is 0.6 μs. Then the corona developing processes can be classified into two cases. The first case is shown in Fig.4.4(b). The front time increases from 0.5 μs to 0.9 μs, and the maximum corona radius increases from 0.10 m to 0.47 m. In this case, the front time is short, thus, the overvoltage as well as the electric field can reach quite high magnitudes, but the electric field at the streamer-tip is always lower than E_{bn}. Therefore, the corona radius only depends on v_{cr}, and a longer front time leads to developing a longer corona radius. The other case is shown in Fig.4.4(c). The front time increases from 1 μs to 4 μs, and the maximum corona radius decreases from 0.43 m to 0.16 m. Along

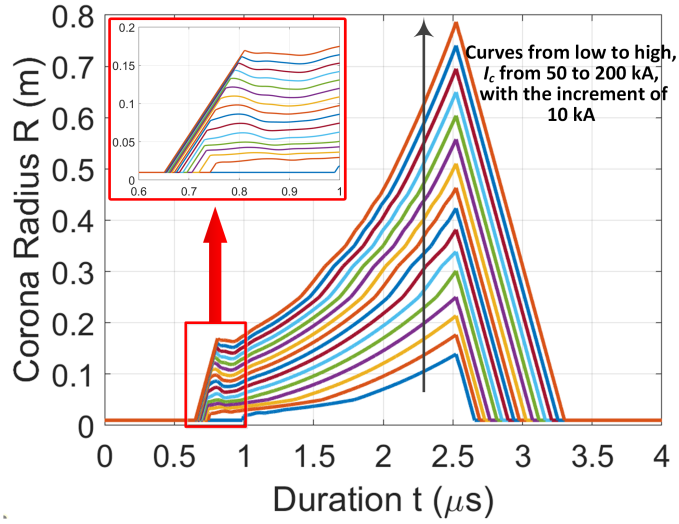

Fig. 4.3: Corona radius developing processes under different lightning current peaks from 50 kA to 200 kA at an increment of 10 kA. Source: **C3**

with the increasing front time, the corona developing process is limited by E_{bn} gradually. Therefore, longer front time causes shorter maximum corona radius.

4.5 Corona Development and Backflashover Performance of Grounding Down-leads Represented by the Dynamic Surge Impedance Model

After analyzing the corona development on an ideal vertical conductor, the dynamic surge impedance model is employed in the grounding down-leads. Because the configuration of the down-lead is special, and the electric field distribution is different at the surface of down-lead at different heights, the down-lead is divided into seven segments to get a more accurate simulation of corona sheath development. The dimension of every segment is shown in Fig. 4.5 on the left side. The bending and inclining segments are approximated into vertical and horizontal segments as shown in Fig. 4.5 on the right side.

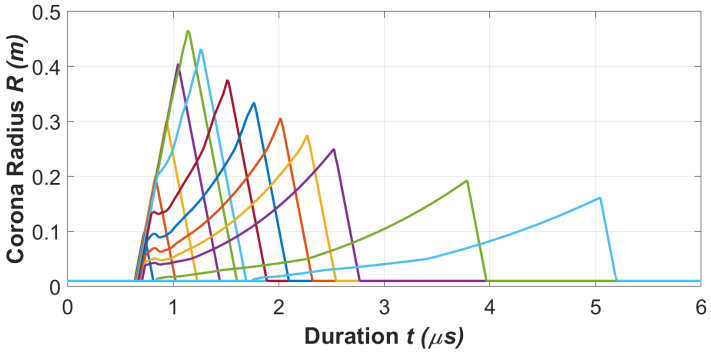

(a) Corona radius developing processes under different lightning current front times from 0.5 μs to 4 μs

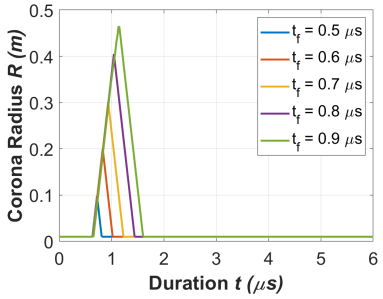

(b) Front time from 0.5 μs to 0.9 μs at an increment of 0.1 μs

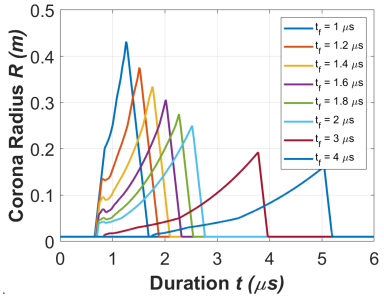

(c) Front time from 1 μs to 2 μs at an increment of 0.2 μs and to 4 μs

Fig. 4.4: Corona radius developing processes under different lightning current front times. Source: **C3**

4.5.1 Corona Development of Segments at Different Heights

The height where every segment locates from ground influences the electric distribution, and the corona developing process.

Corona developing processes of every down-lead segment are shown in Fig. 4.6. If the lightning front time is short around 1 μs, as shown in Fig. 4.6(a), corona development is mainly dominated by expansion velocity. Segment 7 is the nearest to ground, thus the voltage applied on it is the smallest, it is the last one to reach E_{cr}. In the v_{cr}-dominant stage, the maximum extent that corona on Segment 7 can reach is the shortest one, and the maximum corona radius of the other segments from low to high also ranges from short to long. To be noted, Segment 1 in this case has come into the E_{bn}-dominant stage, thus its maximum corona radius is shorter than that of Segment 2. In Fig. 4.6 (b), (c), and (d), the lightning front time is long enough for the

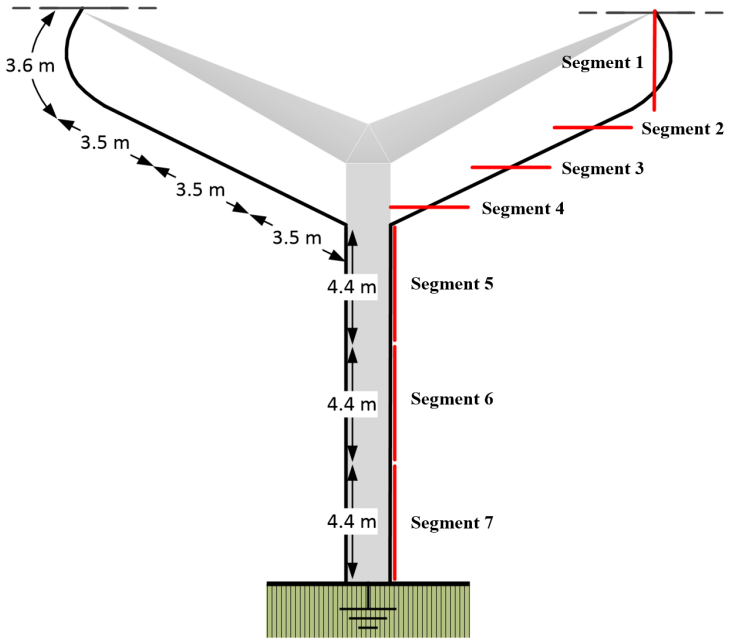

Fig. 4.5: The demonstration of down-lead segments and dimension. Source: **J3**

corona on all segments to come into the E_{bn}-dominant stage. Although the segments at low height initial corona later, the relatively low voltage makes their v_{cr}-dominant stage longer. As a result, the maximum corona radius of the segments from low to high ranges from long to short.

4.5.2 Influence on Overvoltage Crest by Considering Corona on the Down-leads

The surge impedance of the model considering corona is dynamic to the overvoltage. A constant surge impedance model without considering corona is established for comparison.

Fig. 4.7 shows the overvoltage crests of the two models under the lightning current of the same front time (2 μs) and different peaks and their differences. Along with the increasing lightning current peak, the overvoltage of the model with corona is always smaller than the overvoltage of the model without corona and the difference of the overvoltage crests increases from 8.97 % to 23.41 %. It results from the decreasing surge impedance, which is due to the increasing corona radius. Fig. 4.8 shows the overvoltage crests of the two models under the lightning current of the same peak amplitude (80 kA) and different front times and their differences. Along with the increasing lightning current front times, the overvoltage of the model with corona

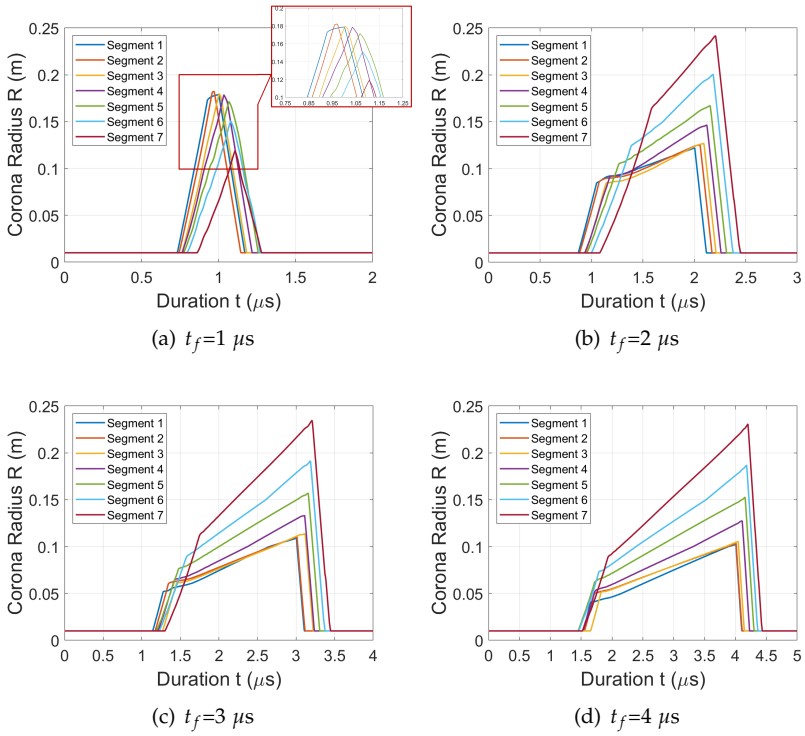

(a) t_f=1 μs (b) t_f=2 μs

(c) t_f=3 μs (d) t_f=4 μs

Fig. 4.6: Corona radius developing processes of every down-lead segment under different lightning current front times. Source: **J3**

is always lower than the overvoltage of the model without corona. However, the difference of the overvoltage crests increases from 1.41 % to 18.43 % first and then decreases to 16.15 %. The trend of the overvoltage difference is consistent with the trend of changing surge impedance, which is consistent with the trend of corona radius.

4.5.3 Influence on Backflashover Rate by Considering Corona on the Down-leads

BFR is linearly related to BF probability P_{BF} and ground lightning density N_g. P_{BF} is a joint result non-linearly contributed by soil resistivity and tower surge impedance. Thus, N_g is valued as 1.39 cases/km2·year, which is the worst case collected in Denmark in 2004. The soil condition is still classified into three levels as stated in *Chapter 3 Section 4*. P_{BF} and BFR provided by constant surge impedance model without considering corona effect (CSI model) and dynamic surge impedance model considering corona effect (DSI

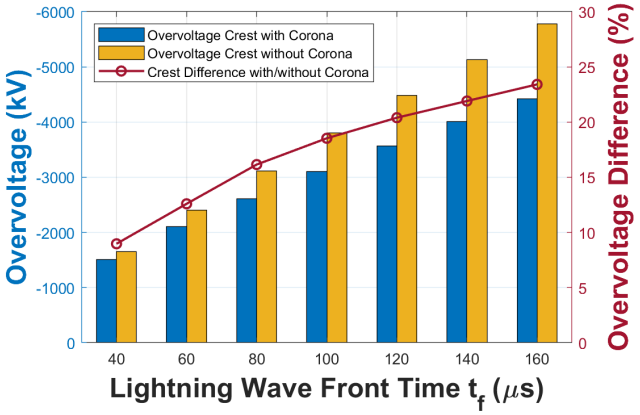

Fig. 4.7: Overvoltage crests of surge impedance models with and without corona under lightning current of different peaks and the difference of overvoltage crests between the two models. Source: **J3**

model) are listed in following Table 4.2.

Table 4.2: The statistics parameters of different soil classifications. Source: **J3**

Soil classification	P_{BF}		BFR [cases/100 km·yr]		
	DSI	CSI	DSI	CSI	Δ%
Low resistivity	0.007	0.008	0.12	0.13	7.7 %
Median resistivity	0.019	0.024	0.32	0.40	20.0 %
High resistivity	0.020	0.027	0.34	0.45	21.4 %

It can be found that the difference in BFR provided by the two models is the smallest under low soil resistivity. When soil resistivity is low, the overvoltage level caused by the same lightning current is also low. Thus, the corona developing process is limited to reducing surge impedance. As a result, the difference between BFR provided by the two models is the smallest under low soil resistivity and the largest under high soil resistivity.

The improvement in BFR caused by considering surge corona is very effective, which can be reflected in the following Chapter that considering corona effect makes the BFR of composite pylons comparatively equivalent to the BFR of traditional metallic towers. It means, from the aspect of BF performance, composite pylon can be an alternative for traditional metallic towers. Thus, the importance of considering corona effect for lightning transient studies on thin-wire grounding devices is stressed out.

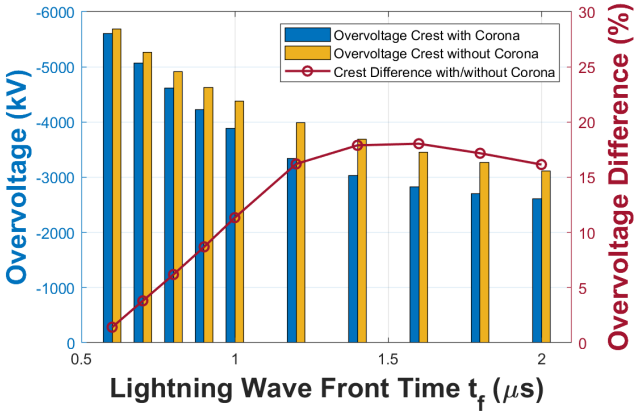

Fig. 4.8: Overvoltage crests of surge impedance models with and without corona under lightning current of different front times and the differences of overvoltage crests between the two models. Source: **J3**

4.6 Summary

In this chapter, a simplified dynamic surge impedance model for thin-wire vertical conductors considering voltage-dependent surge corona is proposed. The model describes the relationship between corona development and the surge overvoltage, it focuses on the macro effect of corona on the surge response of conductors, and it ignores the micro plasma dynamics inside corona. Firstly, current surge impedance models to simulate the transient response of traditional metallic towers are reviewed, and it is pointed out that corona effect is neglected because the change in surge impedance caused by corona is really small. However, for thin-wire conductors, the corona effect cannot be ignored because the extent corona can reach in a lightning surge is comparative to the size of thin-wire conductors. Secondly, the corona dynamics is introduced, which is the simulation foundation of the following description about establishing the novel model. Then, the corona developing process under different lightning current waveforms is presented through an ideal model shaped as a vertical cylindrical conductor. Finally, the simulation of down-leads is achieved by dividing a down-lead into several segments. The corona developing process of every segment is presented. The overvoltage level and BFR provided by the constant surge impedance model and dynamic surge impedance model are compared to stress out the importance of considering corona effect in lightning transient studies for thin-wire grounding devices.

Related Publications

J3. **H. Zhang**, M. Ghomi, Q. Wang, F. Faria da Silva, C. L. Bak, and K. Yin, "Backflashover performance of a novel composite pylon with external grounding down-lead modeled in dynamic surge impedance considering corona effect," *IEEE Trans. Power Delivery.*, 2022, Status: Under review.

Main contribution:

A simplified dynamic surge impedance model considering corona effect has been proposed. The model is employed on a vertical cylindrical grounded conductor, and the corona developing process related with lightning current amplitude and front time is presented.

C3. **H. Zhang**, K. Yin, Q. Wang, K. Y. See, F. Faria da Silva, and C. L. Bak, "A Simplified Dynamic Surge Impedance Model with Corona Effect for Grounding Down-Leads of Composite Pylons under Lightning Surges," *Proc. of ICLP*, Cape Town, South Africa, 2022, Status: Accepted

Main contribution:

The simplified dynamic surge impedance model considering corona effect has been revised that dynamic corona expansion velocity related with overvoltage is obtained . The model is employed on a down-lead by dividing the down-lead into several segments. The BF performance of the composite pylon with or without novel model is compared to stress out the importance of considering corona effect.

Chapter 5

Backflashover Performance Analysis on Engineering Application of Transmission Lines Supported by Composite Pylons

5.1 Comparison of Backflashover Performance with Traditional Steel Lattice Transmission Towers

5.1.1 Background

At the moment when the novel composite pylon is planned to be cast into industry, the potential of its safety and reliability should be investigated and confirmed in the first place. Various steel lattice towers still take the majority in the transmission power grid. A compelling way is to compare its BF performance with the traditional steel lattice towers in service at present.

Because the phase conductors are fixed on the crossarms directly without insulators, the new pylon looks more compact and shorter in appearance. There is a scarcity of knowledge on analyzing the lightning protection performance of such an uncommon transmission pylon. Previous research pays concentration to shielding failure performance. [114] assesses its BF performance based on simulations. Some models with too many approximations, such as constant footing resistance, critical flashover (CFO) determination,

and single-parameter lightning waveshape are utilized, so the simulated technique should be improved. When analyzing BF performance, numerous features between the unique completely composite pylon and typical steel lattice towers must be highlighted. To begin with, OHLs supported by composite pylons are low in height, and thus, have shorter spans than OHLs supported by typical steel lattice towers, which minimizes the overvoltage tail duration [115]. Secondly, the down-leads of composite pylons are quite thin, thus their surge impedance is higher than that of the conducting body of steel lattice towers to conduct lightning impulse current. Thirdly, ceramic or glass insulators are the mainstream of the insulators on conventional OHLs, whose flashover characteristics are investigated comprehensively. Novel pylons' cross-arms, which are more akin to post insulators made of polymers, have different flashover features from ceramic suspending insulators [116].

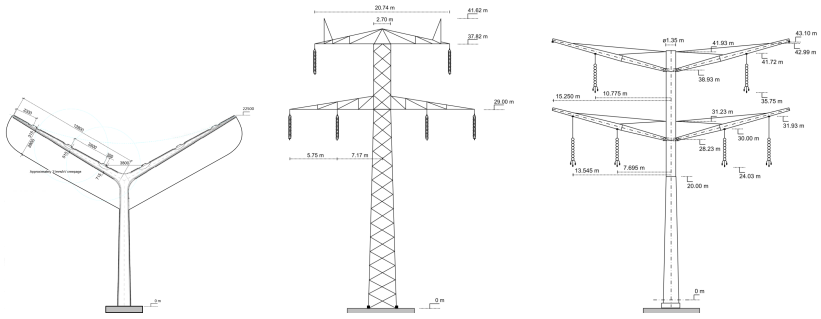

(a) Composite pylon (b) Donau tower (c) Eagle tower

Fig. 5.1: The configuration and dimensions of compsoite pylon and two steel lattice towers (not in real relative scale). Source: **J2** [117]

Looking into the fundamental engineering application for the revolutionary composite pylon, the BF performance is compared to two traditional steel lattice towers that have been erected in Denmark at present, namely Donau tower and Eagle tower. Fig. 5.1 (a), (b), and (c) depict the configuration and dimensions of the composite pylon and two steel lattice towers.

In this research from **J2**, FDI model is adopted as the tower footing model for all three towers. The footing condition is set as a vertical electrode buried in a two-layer soil. The length and the cross section radius of the electrode are $L = 3$ m and $r = 15$ mm respectively. The soil is characterized by resistivity of 100 Ω·m and 1000 Ω·m for upper and lower layer respectively. The relative electric permittivity is set as 10 [117]. Down-leads on composite pylons are simulated by the constant surge impedance model without considering corona effect. The revised dynamic surge impedance model of down-leads is proposed after the publication of **J2**.

5.1.2 Comparison of Backflashover Probability and Backflashover Rate between Composite Pylon and Steel Lattice Towers

The BF performance evaluation procedure accords to as stated in *Chapter 2*. MCM collects the BF probability of every lightning stroke of varied current amplitude and front times to calculate total BF probability as spectrums.

Fig. 5.2 shows an example of the spectrum of the composite pylon. The probability of one lightning stroke causing BF is represented by a single point in the spectrum. The front time and lightning current are the x-ordinates and y-ordinates of the point, respectively. The BF probability is represented by the color of the point. Because all lightning flash characteristics are collected according to their statistical probability distribution, lightning BF probability P_{BF} can be computed by dividing the sum of BF probability of all lightning strokes $\Sigma\ P\ (I_c)$ by the number of lightning strokes N_{total}.

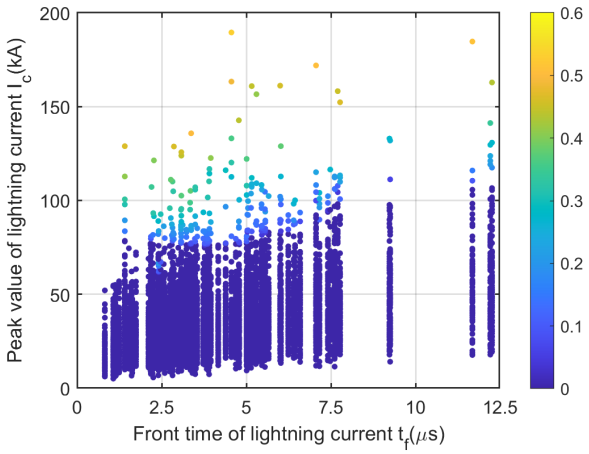

Fig. 5.2: An example of the spectrum to present BF probability among quantities of lightning strokes for composite pylon. Source: **J2** [117]

The prerequisites impacting the BFR of transmission towers studied are presented in Table 5.1 after the computation of lightning BF probability P_{BF}. It can be found that the BFR of the composite pylon with down-leads modeled of constant surge impedance is much higher than that of steel lattice towers, which mainly results from the high surge impedance of down-leads and shorter insulation length on composite pylons. It has been analyzed in *Chapter 4* that corona effect on down-leads should not be ignored and can reduce the surge impedance. Thus, the BF probability and BFR of composite pylon provided by the dynamic surge impedance model are computed again and listed together with the above results, as shown in Table 5.2.

When compared to the metallic tower bodies of Donau and Eagle tow-

Table 5.1: Prerequisites impacting BFR of the three transmission towers. Source: **J2** [117]

Tower type	Composite pylon	Donau tower	Eagle tower
Ground flash density N_g [cases/km^2 · yr]		1.39	
Tower height H [m]	22.50	41.62	43.10
Shielding distance D [m]	21.28	20.74	27.09
Line flash density N_d [cases/100 km · yr]]	20.26	28.30	29.60
Insulation length L [m]	2.8	3.2	3.72
CFO [kV]	1960	2240	2604
BF probability P_{BF}	0.027	0.013	0.012
BFR [cases/100 km · yr]	0.45	0.32	0.30

Table 5.2: BFR of composite pylon with constant and dynamic surge impedance model, and two steel lattice towers.

Tower type	BF probability P_{BF}	BFR [cases/100 km · yr]
Composite pylon (Constant surge impedance)	0.027	0.45
Composite pylon (Dynamic surge impedance)	0.021	0.35
Donau tower	0.013	0.32
Eagle tower	0.012	0.30

ers, the down-leads on composite pylon have a larger surge impedance, even though the surge impedance is reduced by the existence of surge corona. Thus, under the same lightning current, the overvoltage rising at the composite pylon head is higher. The insulation length of the composite pylon is shorter than both steel lattice towers. Thus, the overvoltage is more likely to lead to BF. As a consequence of these two prerequisites, the BF probability of composite pylon is much higher than that of steel lattice towers. However, the composite pylon has a lower height and a shorter shielding distance than steel lattice towers, which means fewer lightning strokes may be attracted to the composite pylon. After all, composite pylon has a BFR of 0.35 cases per 100 kilometers per year, which is comparatively equivalent to the BFR of steel lattice towers. In summary, from the aspect of BF performance, the composite pylon can be an alternative to traditional steel lattice towers.

5.1.3 Comparison of Overvoltage on Double Circuits between Composite Pylon and Steel Lattice Towers

The three transmission towers in this research are capable of supporting double-circuit OHLs at 400 kV. On steel lattice towers, lightning surge current passes through the tower body to the earth, regardless of which shield wires are terminated. Overvoltage increases at the suspending end of insulators, perhaps causing both circuits to BF at the same time. According to a Queensland study, double circuit failures account for 4.7 percent of outage issues on a 275 kV transmission line [118]. In Korea, multi-circuit outages account for 33.7 percent of all lightning-related accidents [119]. Despite the fact that the risk of a double circuit outage is small, double circuit outages sometimes result in catastrophic power disruption accidents. Two down-leads connecting shield wires and the ground are split independently for composite pylons. When lightning terminates one of the shield wires, excessive overvoltage only increases on one of the down-leads, posing a risk of BF.

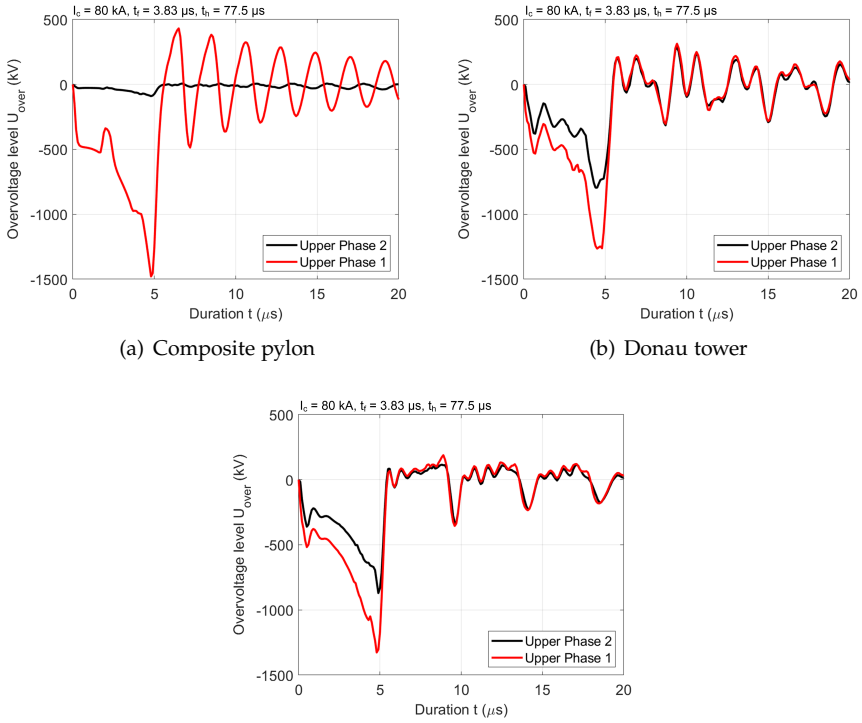

(a) Composite pylon

(b) Donau tower

(c) Eagle tower

Fig. 5.3: Overvoltage to the upper phase conductors of double circuits when lightning strikes at shield wire of one circuit. Source: **J2** [117]

When lightning terminates at shield wires of one circuit, the overvoltage across cross-arm of composite pylon and insulators on steel lattice towers to the top phase conductors of double circuits can be observed in Fig. 5.3. Overvoltage on composite pylons is recorded between the tip of down-lead and upper phase conductor across cross-arm. Overvoltage on steel lattice towers is recorded between the ends of the insulator suspending upper phase conductor. In the three cases, the parameters of injected lightning current are the same (80 kA, 3.83/77.5 μs). Lightning strokes hit the shield wires of circuit 1. Overvoltage waveforms in circuit 1 are shown as red curves, which is in the same side with shield wires hit by lightning strokes. Overvoltage waveforms in the other circuit are shown as black curves. It can be found that the overvoltages of both circuits on steel lattice towers are of closely high amplitudes [117]. However, the overvoltage in circuit 1 on composite pylon is quite high while the overvoltage in circuit 2 is of lower amplitude [117].

The BF probability of all six cases are computed and summarized in following Table 5.3. For steel lattice towers, although lightning strokes hit only one of shield wires, both circuits are probable to occur BF at the same moment [117]. To be noted, the simultaneous flashover may be overstated in simulation than in reality because flashover simulation mainly focuses on voltage rather than energy. Simultaneous flashover highly probably happens and lead to catastrophic consequences, only if the lightning current is really huge. For composite pylon, only the phase conductor in the same circuit with the hit shield wire is faced with higher BF probability, whereas the other circuit has a negligible risk to occur BF [117]. In summary, compared with traditional steel lattice towers, OHLs supported by composite pylons do not suffer from simultaneous BF of double circuits.

Table 5.3: Maximum and BF probability of the overvoltage threatening both circuits on the three transmission towers. Source: **J2** [117]

Tower type	Circuit No.	Overvoltage [kV]	BF probability P_{BF}
Composite pylon	1	-1479.20	0.4027
	2	-90.21	0
Donau tower	1	-1264.62	0.3251
	2	-795.18	0.0735
Eagle tower	1	-1326.80	0.3541
	2	-871.25	0.0950

5.1.4 Comparison of Overvoltage of Three Phases between Composite Pylon and Steel Lattice Towers

The overvoltages of three phases in the same circuit of the three towers are shown in Fig. 5.4. All three cases have the identical lightning current parameters (80 kA, 2/77.5 μs). As for the composite pylon, the overvoltages are measured at the locations on the down-lead where are nearest to the phase conductors. As for the two steel lattice towers, the overvoltages are measured at the locations suspending the insulators and phase conductors. From the results, it can be found that the overvoltages on the down-lead are closely high and all three phase conductors are faced with BF of close risk [117]. However, for steel lattice towers, the overvoltages at the suspending ends of upper phase are far greater than the other two phases. It can be discovered that tower layout has a significant impact on the overvoltage of different phases according to their locations on the tower [117].

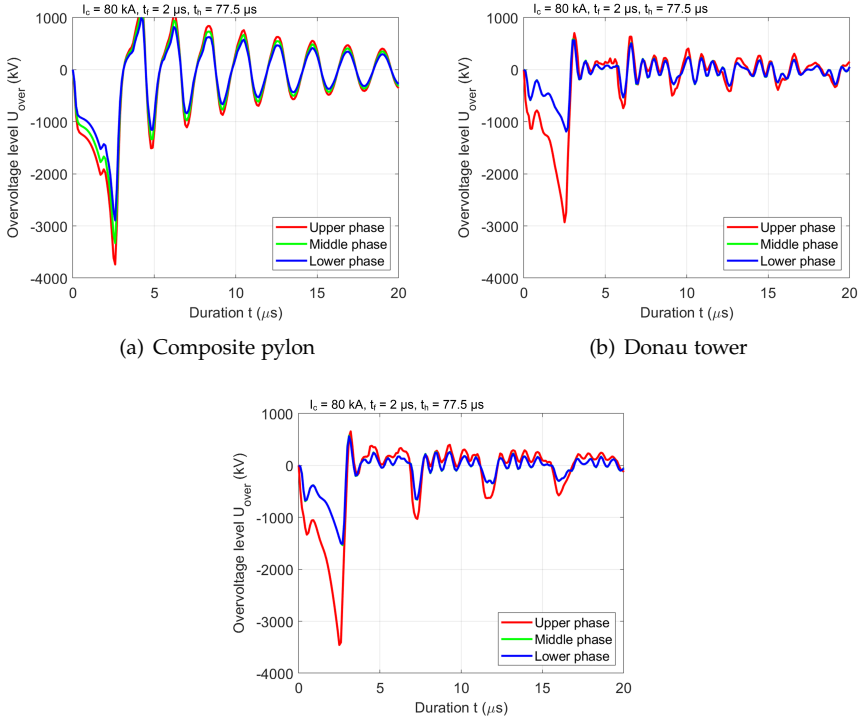

(a) Composite pylon

(b) Donau tower

(c) Eagle tower

Fig. 5.4: Overvoltage across cross-arm (composite pylon) and insulators (metallic towers) to the conductors of three phases when lightning strikes at shield wire. Source: **J2** [117]

Surge arresters are widely-used devices to suppress overvoltage and protect OHLs. If the surge arresters are installed at all three phases, this countermeasure certainly has the optimum BF protection performance. Considering the cost of surge arresters, it is more economic to install arresters on only one or two phases. The default surge arrester model in PSCAD is selected to Table 5.4 summarizes the BFR of three towers using different strategies of surge arrester installation. One is to install surge arresters solely on the upper phases (MOV-Upper). The other one is to install surge arresters on all three phases (MOV-3-phase).The compared group is without surge arresters (No MOV) [117].

Table 5.4: Maximum and BF probability of the overvoltage threatening both circuits on the three transmission towers. Source: **J2** [117]

Tower type	MOV strategy	BFR [cases/100 km·yr]
Composite pylon	No MOV	0.4526
	MOV-Upper	0.3037 (-32.90%)
	MOV-3-phase	0.0633 (-86.01%)
Donau tower	No MOV	0.3176
	MOV-Upper	0.0825 (-74.02%)
	MOV-3-phase	0.0622 (-80.41%)
Eagle tower	No MOV	0.2992
	MOV-Upper	0.0794 (-73.46%)
	MOV-3-phase	0.0591 (-80.24%)

Telling from the BFR results of the three towers, installing surge arresters on three phases is the technical best strategy and installing upper-phase surge arresters is still better than no surge arresters. However, for the two steel lattice towers, the BFR of installing 3-phase surge arresters is only a little lower than that of installing surge arresters solely on upper phase [117]. For composite pylons, installing 3-phase surge arresters has obviously lower BFR than solely installing upper-phase surge arresters. Compared with the BFR without surge arresters, the BFR after installing surge arrester on upper phase decreases 32.90 %, while the BFR after installing surge arresters on three phases decreases 86.01% [117]. Thus, for steel lattice towers, it is suggested to install surge arresters only on the upper phase out of the economy. However, installing surge arresters on all three phases of composite pylon can improve BF performance effectively but cost a lot.

It should be emphasized that the aforementioned findings are based only on BF performance. Surge arresters must also be addressed from the standpoint of shielding failure in the event that lightning hits the phase conductors directly across shield wires.

5.2 Partially-grounding Scheme of Overhead Lines Supported with Fully Composite Pylons

5.2.1 Background

The fully composite pylon is featured by its insulated pylon shaft. The term "partially grounded transmission lines" (PGTLs) refers to a plan where not all pylons are grounded out of economic and aesthetic considerations [120]. A PGTL is created as an OHL segment that is supported by a number of non-grounded pylons. It is still required to build grounding equipment at both ends of a PGTL to provide a conducting channel in the event that lightning strikes the shield wires [21]. Steel transmission towers, composite pylons with grounding down-leads, or steel tension towers at the corners of PGTLs can all be erected as grounding equipment. The traveling wave theory states that an overvoltage at a lightning striking location will remain high until the ground's negative wave reflection reaches the striking spot [121]. Thus, PGTLs create a longer distance between the lightning hitting location and the grounding end, resulting in more severe lightning overvoltage. Higher overvoltage amplitude will result from a greater striking distance if the reflection time is less than the lightning front. Longer striking distance will result in overvoltage with a longer duration if the reflection time exceeds the lightning front. Both situations severely test the insulation's strength, which causes BF. [120].

For conventional OHLs, several studies have revealed that the overvoltage caused by lightning hitting mid-span is approximately 1.2 to 2.0 times higher than that with tower top terminated by lightning [42, 122, 123]. BF is less likely to happen at mid-span than at the tower, despite the fact that the overvoltage at mid-span is larger because to the stronger insulation strength of the air gap at mid-span than the insulator surface on the tower. Therefore, critical lightning current of flashover when lightning strikes at pylon head, I_{c1}, is smaller than critical lightning current of flashover when lightning strikes at mid-span, I_{c2}. In light of this circumstance, the BFR of all transmission lines is calculated by multiplying the BF probability by a coefficient that is equal to the ratio of the probabilities that I_{c1} and I_{c2} will occur. The ratio relating to the probability distribution of lightning current for different spans in conventional OHLs lies in a small range between 0.58 and 0.67. 0.6 is therefore chosen as the compromised value [120].

For a PGTL, the distance between the lightning strike and the closest grounding device may typically be greater than most transmission line spans today, resulting in an overvoltage that has a higher amplitude and a longer duration. From another aspect, to sustain such a high overvoltage, the insulation strength at the cross-arm on a non-grounded pylon within a PTGL is

often weaker than the air gap at mid-span [120]. Therefore, the ratio of the occurring probability of I_{c1} and I_{c2} increases along with the increasing length of a PGTL. As a consequence, BF performance of a PGTL faces with severe situation.

5.2.2 Overvoltage of Different Footing Resistance and Soil Resistivity in PGTLs

In the OHLs where every pylon is grounded, decreasing footing resistance and soil resistivity of grounded pylons can enhance BF performance effectively. However, for PGTLs neither of the two strategies are effective.

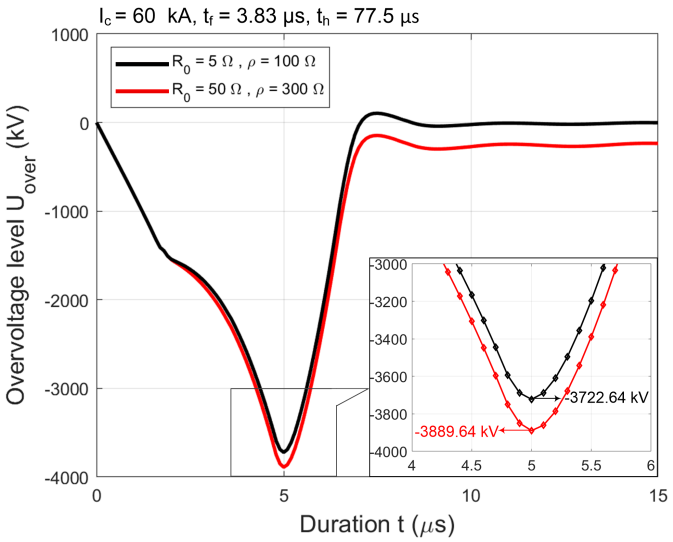

Fig. 5.5: Overvoltage wave fronts of two combinations of grounding parameters. Source: **J1** [120]

Overvoltage wave fronts shaped by various grounding parameters are investigated. In Fig. 5.5, overvoltage wave fronts of an example of a 500-m-long PGTL within only one non-grounded pylon in the center is shown of two combinations of grounding parameters. A lightning flash with the amplitude of 60 kA (3.83/77.5 μs) terminates in the middle. The maximum overvoltage when the grounded pylons are of lower footing resistance and soil resistivity is -3722.64 kV, which is only 4.5 % lower than when the grounded pylons are of higher footing resistance and soil resistivity, which is -3889.47 kV [120]. The span designed for composite pylons is 250 m, so the 500 m PGTL within one non-grounded pylon is the shortest scheme. The effect of decreasing footing resistance and soil resistivity will become even more insignificant in the PGTL schemes of longer length. The differences of the maximum

overvoltage on the PGTLs of 1000 m, 1500 m and 2000 m and a strike at the middle of the span are 89.69 kV, 1.85 kV and 0 kV [120]. Moreover, at an precision level of 0.0001, the tiny differences of overvoltage have little influence on BFR results.

In summary, when the lightning hits a non-grounded pylon, decreasing footing resistance and soil resistivity of grounded pylons at the both ends of PGTLs has only a minor influence on the amplitude of overvoltage and hence the BFR.

5.2.3 Overvoltage of Lightning Location in PGTLs

Once lightning flashes hit the shield wires in the middle of a PGTL, the overvoltage wave will flow towards opposite directions along the shield wires to both ends, reach the ground potential via the grounded pylons, be reflected and backtrack to rise up. Except the rare case that lightning hits right middle, the traveling distances to the two ends are generally not the same. Hereby, D_{near} denotes the nearer traveling distance between lightning location and one of the grounded pylons, while D_{far} denotes the longer one.

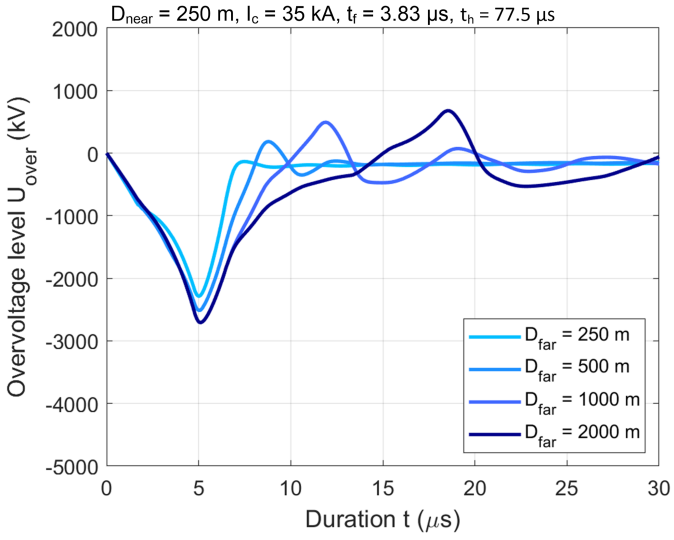

Fig. 5.6: Overvoltage wave fronts of same D_{near} and different D_{far}. Source: **J1** [120]

Fig. 5.6 and Fig. 5.7 show the overvoltage at lightning locations in PGTLs with different distance to grounded pylons. The waveshape of the lightning impulse is 35 kA (3.83/77.5 μs). When the D_{near} is the same, the overvoltage waveshapes provided by different D_{far} are similar, particularly in the wave front period. The maximum values of overvoltage range from -2289.55 kV to

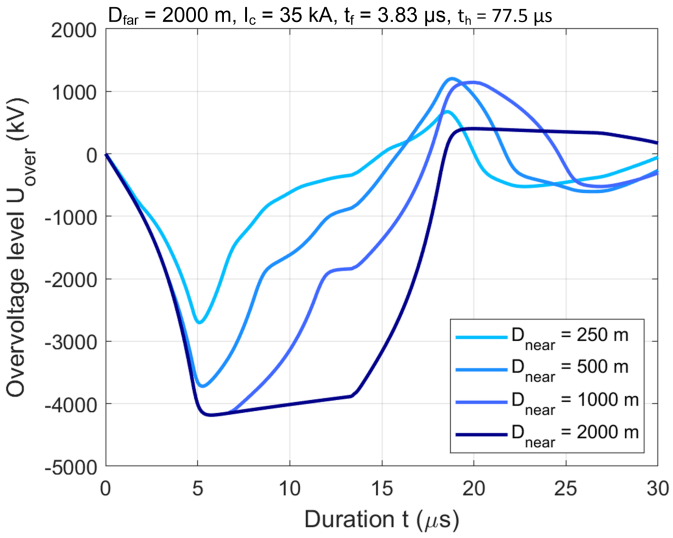

Fig. 5.7: Overvoltage wave fronts of same D_{far} and different D_{near}. Source: **J1** [120]

-2708.74 kV, increasing by 18.31 %. If lightning current amplitude is lower, the dispersion is even less [120]. On the contrary, when D_{far} is the same, the overvoltage waveshapes provided by different D_{near} are not alike. The overvoltage crests range from -2708.74 kV to -4182.65 kV, increasing by 54.41%. The disparity among the overvoltage waveshapes also widens further [120]. When D_{near} increases, the overvoltage waveshape shifts from a 'V' shape to a 'U' shape, with a flat bottom appearing. This is due to the fact that the time it takes for the overvoltage at the striking point to reach its peak is less than the time it takes for the ground reflection wave to reach the striking point. The waveshape of the overvoltage is compatible with the form of the lightning current before the arrival of the reflection wave. By superimposing the reflection wave on top of the overvoltage wave, the overvoltage wave is chopped before the arrival of the reflection wave. When overvoltage wave propagates on shield wires after lightning hitting, corona will dampen the energy, which will reduce overvoltage amplitude. If the traveling distance is longer, damping effect of corona will become more obvious [124].

In summary, in PGTLs, the distance to the nearest grounded equipment determines the overvoltage waveshape majorly. If the distance to the nearest grounded pylon is longer, the resulted overvoltage will be of higher crest and longer wave front.

5.2.4 Backflashover Rate of Different Distances of PGTLs

BFR is defined as the product of the number of lightning flashes hitting on 100 km lines each year, and the BF probability of lightning flashes. BF probability is resulted from lightning overvoltage, which is mainly determined by the distance to the nearest grounded pylon as discussed in the previous section.

The BF probability when lightning hits the PGTLs related to the distances to nearest grounded pylon is shown in the Fig. 5.8 as red dashed line. If the distance between the lightning location and the nearest grounded pylon increases, the overvoltage crest and wave front duration also increases resulting in the increase of the BF probability. The BF probability stabilizes at 0.6149 when the nearest distance exceeds 750 m [120].

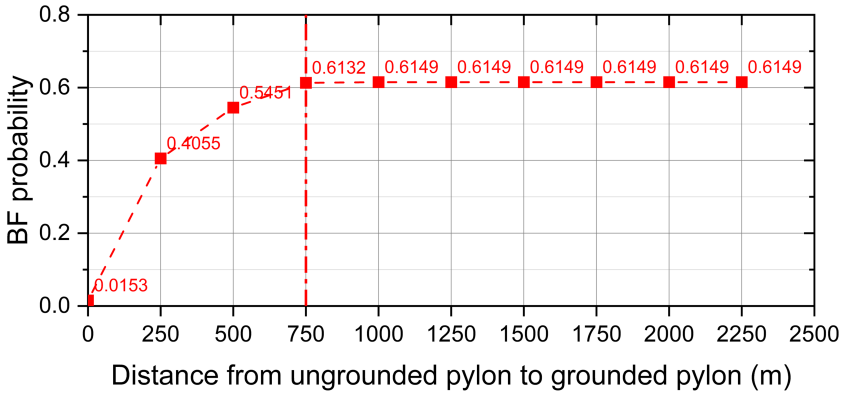

Fig. 5.8: BF probability of different distances to nearest grounded pylon. Source: **J1** [120]

Not only may lightning flashes hit pylon heads, but they can also hit in the mid-span. The overvoltage caused by lightning hitting in the mid-span is smaller than the overvoltage caused by the same lightning hitting the pylon head. Thus, a coefficient K less than 1 is adopted. Hereby, along with the increasing distance between non-grounded pylon and grounded pylon, K grows to approach 1 gradually. As a result, BFR can be computed by equation (2.7). The BFR of different distances to nearest grounded pylon is shown in Fig. 5.9 as blue dashed line, which grows to approach 17.3161 cases per 100 km each year when the distance between non-grounded pylon and grounded pylon keeps increasing [120].

In *Chapter 5 Section 2.2*, the ineffectiveness of reducing footing resistance and soil resistivity to improve BF performance of PGTLs is pointed out. Increasing the insulation length between the shield wire tip and the top phase

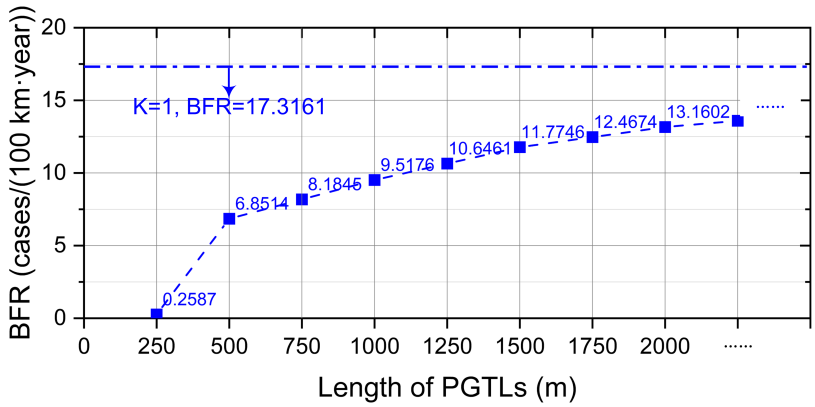

Fig. 5.9: BFR of different distances to nearest grounded pylon. Source: **J1** [120]

conductor is another option. As seen in equation (2.7), extending insulation length will increase the pylon height and shield wires corridor width at the same time, which means more lightning flashes will be attracted to the shield wires. The relationship between BFR and the distance to grounded pylon provided by different insulation lengths are depicted in following Fig. 5.10. As can be shown, extending insulation length has limited effect in practice.

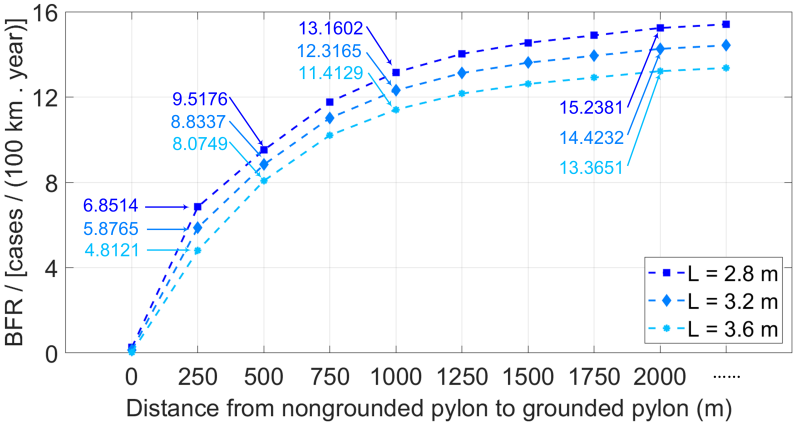

Fig. 5.10: Effect of increasing insulation distance L on BFR of different PGTLs distances. Source: **J1** [120]

In summary, the BFR of PGTLs increases in parallel with the distance to the nearest grounded pylon, until it reaches a limit value. In addition to

decreasing footing resistance and soil resistivity, extending insulation length has limited effect in practice either.

5.3 Lightning Protection Performance of the Overhead Lines Supported by Fully Composite Pylons with External Grounding Down-leads

As a call-back to *Chapter*1, the basic question of this entire project is "how many backflashover cases probably occur on the overhead lines supported by fully composite pylons with external grounding down-leads." From the all above analysis and discussion, it can be found that it is difficult to give a uniform answer for BFR, because BFR is highly-related to many uncertain factors, such as flash density, lightning current statistics, footing electrode type and dimension, and soil resistivity. Whereas, the answer can be given according to specific circumstances.

Flash ground density N_g is valued as 1.39 cases/km^2·year according to the worst case in Denmark in 2005. Additionally, BFR is linear to N_g. The footing electrode is shaped as a cylindrical conductor buried vertically inside the soil, whose cross-section radius and length are 15 mm and 3 m respectively. The down-lead is modeled considering corona effect. For the pylon footing model, MCM-CDI model and FDI model focus on two different physical phenomenons of grounding, so the results provided by the two models are both shown. In MCM-CDI model, soil resistivity is classified into three levels. In FDI model, the soil is characterized by resistivity of 100 Ωm and 1000 Ωm for upper and lower layers respectively.

Under the circumstance of the above presuppositions, the BFR of the OHLs supported by fully composite pylons with external grounding down-leads is shown in the following Table 5.5.

Table 5.5: Summary of BFR of OHLs supported by fully composite pylons with external grounding down-leads using different footing models

Footing model	Soil condition	P_{BF}	BFR [cases/100 km · year]
FDI model	ρ_{upper}=100 Ωm ρ_{lower}=1000 Ωm	0.021	0.35
MCM-CDI model	Low-ρ soil	0.007	0.12
	Median-ρ soil	0.019	0.32
	High-ρ soil	0.020	0.34

In the previous research, the shield failure flashover rate of this type of

composite pylon has been calculated as 0.0008 cases/100 km·year [8]. BFR provided by MCM-CDI model of median-resistivity soil is adopted as 0.3187 cases/100 km·year to give an integrating result of lightning protection performance. The number of flashes attracted to the 100-km OHLs each year N_d can be calculated as 28.1614 cases/100 km·year by equation 2.8. The theoretical lightning protection performance of the 400 kV composite pylon is shown in Table 5.6. In summary, the risk of lightning outages of OHLs supported by composite pylons is 1.1346 % among all lightning flashes each year.

Table 5.6: Theoretical lightning protection performance of OHLs supported by fully composite pylons with external grounding down-leads

400 kV composite pylon	Non-outage [cases/100 km · year]	Lightning outage [cases/100 km · year]
Shielding success	27.8419 (98.8654 %)	0.3187 (1.1317 %)
Shielding failure	0.0008 (0.0029 %)	
Total of lightning strokes	28.1614 (100 %)	

5.4 Summary

This chapter presents the analysis of two engineering applications. Firstly, the BF performance of the fully composite pylon of 400 kV with external grounding down-leads by contrast with two conventional steel lattice towers widely constructed in Denmark has been investigated. Compared with steel lattice towers under the same lightning conditions, the compact configuration of composite pylon may attract fewer lightning flashes, but the larger surge impedance makes it presents higher overvoltage, resulting in slightly higher BFR. The BFR of the composite pylon is 0.35 cases per 100 km per year, which is comparatively equivalent to that of Donau tower and Eagle tower. All three towers are capable of supporting double circuits. Compared with steel lattice towers, OHLs supported by composite pylons do not experience simultaneous BF of double circuits attributed to separated grounding down-leads. In the same circuit, where one shield wire is hit by lightning, the overvoltages on the down-lead of the composite pylon are closely high. Thus, from the aspect of BF, the effect of equipping upper phase of composite pylon with surge arresters is not as good as on steel lattice towers, while equipping three phases of the composite pylon with surge arresters has an excellent effect on improving BFR but costs a lot. Secondly, the fully composite pylon is featured in its insulated shaft body, so the BF performance of a partial grounding scheme of OHLs has been investigated. For partially grounded transmission lines supported by composite pylons, when the lightning hits the non-grounded

pylon, decreasing footing resistance and soil resistivity of grounded pylons at both ends is not effective. Extending insulation length has a limited effect to some extent. Lightning overvoltage is determined by the distance to the nearest grounded pylon and a longer distance to the nearest grounded pylon will result in overvoltage with a larger crest and longer wave front. BF probability and BFR grow as the distance of partially grounded transmission lines became longer, but are limited to a particular value, which depends on the natural lightning current probability distribution and the threshold electric field when flashover develops. Finally, the BFR of OHLs supported by fully composite pylons with external grounding down-leads is summarized under specific circumstances, and the theoretical lightning protection performance is presented combined with previous research. The risk of lightning outages of OHLs supported by composite pylons is 1.1346 % among all lightning flashes each year. Through the engineering applications, a prospect of the composite pylon can be foreseen because of its advantages of safety, reliability, and economy.

Related Publications

J1. **H. Zhang**, Q. Wang, F. Faria da Silva, C. L. Bak, K. Yin, and H. Skouboe, "Backflashover Performance Evaluation of the Partially Grounded Scheme of Overhead Lines with fully Composite Pylons," *IEEE Trans. Power Delivery.*, vol. 37, no. 2, pp. 823-832, Apr. 2021.

Main contribution: The BF performance of a partial grounding scheme of OHLs supported by the novel fully composite pylon has been investigated.

J2. **H. Zhang**, M. Ghomi, Q. Wang, F. Faria da Silva, C. L. Bak, K. Yin, and H. Skouboe, "Comparison of Backflashover performance between a novel composite pylon and metallic towers," *Electric Power Systems Research.*, vol. 196, pp. 107263, July. 2021.

Main contribution:

The BF performance of the fully composite pylon of 400 kV with external grounding down-leads with two conventional metallic towers widely installed in Denmark has been investigated. Surge arrester installation planning has been analyzed.

Chapter 6

Conclusions

This chapter summarizes the results and outcomes of the research during the Ph.D. project *"Transient Lightning Impulse Performance Analysis of a Fully Composite Pylon with an External-grounding Down-lead"*. The scientific and engineering contributions are highlighted following. The future research perspectives are discussed in the end.

6.1 Project Summary

In this Ph.D. project, the main research focuses on evaluating the lightning BF performance of OHLs supported by a novel composite pylon via simulating tools. The research path provides a complete structure, including BF performance evaluation procedure, optimization on simulating models of transmission system components, and investigation of tentative engineering applications. In this section, a brief summary of this project is presented.

In *Chapter 1*, the research background of the composite pylon is introduced and discussed. Because the pylon body and cross-arms are designed to be manufactured with insulated materials, a bare conductor as grounding down-lead is adopted to be installed outside the pylon to bring ground potential to shield wires. The previous research foundation of this type of composite pylon is reviewed, which focused on air clearance and insulated distance, lightning shielding performance, and electrical performance testing methods. Thus, the demand to evaluate lightning BF performance is put forward. Then the development of transmission towers fully or partially made of composite materials is reviewed, as well as the grounding schemes applied. After that, lightning transient analysis based on traveling wave theory is introduced, which is the basic research tool used in this project. Meanwhile, the importance of accurate transient models used in lightning simulations is stressed out.

In *Chapter 2*, the methods to calculate BFR are presented. Analytical methods recommended by CIGRE and IEEE have advantages in application simplicity but lead to doubts about accuracy because of simplifications and assumptions in the representation of transmission system components. Then, a BFR evaluation procedure based on MCM is proposed, which is the key approach in this project. Because the principle of MCM is to approximate the target results by quantities of sampling, which is applied to lightning current waveform parameters and soil resistivity in this project, the adequacy of sample size is necessary to be verified.

The following two chapters, *Chapter 3* and *Chapter 4* present the modeling validation and improvement of two crucial components in the lightning studies of composite pylons respectively, the pylon footing model and the grounding down-lead model. For the pylon footing model, two models are adopted in different conditions. Current-dependent impedance model concentrates on soil ionization and the simplicity of its analytical formulations makes it convenient when considering various soil conditions. Frequency-dependent impedance model concentrates on the high-frequency response of the electrical parameters of pylon footing and soil layer. For the grounding down-lead model, a novel dynamic surge impedance model considering the corona effect is proposed. The novel model neglects the micro plasma dynamics of the corona phenomenon and concentrates on the change of surge impedance of thin-wire conductors, which makes it possible to be implemented into EMTPSS.

In *Chapter 5*, the BF performance evaluation procedure within simulating models discussed above is applied in engineering. Firstly, the BF performance of the composite pylon should be assessed in comparison with traditional metallic transmission towers. Although the BFR of composite pylon is slightly higher than conventional transmission towers, it eliminates the danger of simultaneous outage of the double circuit. After that, a unique feature of the composite pylon is that its insulated pylon body makes it desirable not to grounded every pylon in transmission lines. It is found that if partially grounding transmission lines, a longer traveling distance for lightning current to ground will cause an overvoltage with higher amplitude and a rather longer wave front. Besides, the amplitude of the overvoltage is mainly dependent on the distance to the nearest grounded pylon. As for countermeasures, improving pylon footing conditions is not effective anymore, and increasing insulation distance has a limited effect to some extent. Future emphasis may lie in the application and coordination of surge arresters. Finally, the BFR of OHLs supported by fully composite pylons with external grounding down-leads is summarized, and the theoretical lightning protection performance is presented combined with previous research on shield failure.

6.2 Research Contributions

In this section, the major contributions achieved in this Ph.D. project are summarized as the response to the project objectives in *Chapter 1*.

The scientific contributions are listed as follows:

- **Improvement of Monte Carlo method used to evaluate the statistical result of back-flashover performance considering environmental factors**

  The transmission lines supported by composite pylon are designed to be installed on large-scale land and operate for years. From the aspect of lightning flashes, the waveform and amplitude of every lightning flash terminating at OHLs are of randomness and uncertainties. From the aspect of the soil layer, the electrical parameters of the soil where pylons stand are also different from pylon to pylon. Considering the uncertainties of those environmental factors and their non-linear effect on BF performance, MCM is improved to give a statistical result for BFR evaluation.

- **Development of a dynamic surge impedance model considering corona effect for thin-wire grounding devices**

  Traditional transmission tower surge impedance models all neglect the corona effect because the dimension of the surge corona sheath is relatively small by contrast to tower size. However, the corona effect cannot be ignored when thin-wire conductors are adopted as grounding devices. Therefore, a dynamic surge impedance model considering the corona effect is proposed. The importance of the corona effect for modeling thin-wire conductors is stressed out. Corona sheath can effectively reduce the surge impedance of thin-wire conductors, thus providing evidence for the application of thin-wire conductors as grounding devices in transmission systems.

The engineering contributions are listed as follows:

- **Calculation of backflashover rate of the overhead lines supported by composite pylons**

  Generally speaking, the BFR should be given according to specific environmental factors. Taking Danish factors as a case study, where the soil is ranked into median soil resistivity and ground lightning density is 1.39 cases/km^2·year, the BFR of OHLs supported by composite pylons is 0.3 cases/100 km·year.

- **Comparison of lightning transient performance of composite pylons to conventional metallic tower**

After the down-leads of composite are modeled considering the corona effect, the surge impedance of down-leads and the overvoltage level are reduced, which makes the BFR of the composite pylon comparative with two conventional metallic transmission towers. Meanwhile, it eliminates the danger of simultaneous outage of double circuits that possibly occurs in traditional OHLs. Therefore, composite pylons are capable to being cast into operation because it has the same safety and reliability, and advantages of aesthetics and economy.

- **Validation of the partially-grounded scheme that not all pylons in the transmission lines supported by composite pylons are grounded**

  The validation of a 400 kV partially grounded transmission line is studied. It is found that lightning overvoltage at a non-grounded pylon is mainly dependent on the distance to the nearest grounded pylon. There is a constant coefficient to consider that the overvoltage caused by lightning terminating in the span is smaller than lightning terminating at the pylon head. This coefficient is revised and given recommended value when applied in partially grounded transmission lines.

6.3 Research Perspectives

This project provides a complete process to evaluate the BF performance of the novel 400 kV composite pylon with external grounding down-leads from improvement on simulating models to validation on engineering applications. However, the fully composite pylon is still in design and experimental test processes and its configuration, junctions, dimensions, and materials frequently change. Therefore, the following researches should be addressed for next-step research for casting into operation.

6.3.1 Future Work in the Aspect of Simulation

- The flashover characteristics of cross-arm need to be studied furthermore. Flashover on metallic towers mainly occurs across the insulators. However, flashover location is more complicatedin composite pylons. Flashover possibly occurs from shield wire to upper phase conductor across the surface of cross-arm, and from the down-leads through the air gap across cross-arm to phase conductor. The flashover model used in PSCAD for backflashover studies needs to be

- The pylon footing model can be extracted as a specialized project, which is not studied comprehensively in this research. A more advanced model to take both frequency-dependence and soil ionization effect into

account can be studied deeply and developed to simulate the lightning performance of pylon footing better.

- The dynamic coupling effect between the down-leads with corona and phase conductors has not been considered into the current model, which needs further study to improve the modeling accuracy.
- The application of surge arresters is only studied preliminarily and tentatively. The surge arrester model is simply described by non-linear volt-ampere curve. A more accurate surge arrester model needs to be developed for lightning protection studies of composite pylons and the scheme of installation of surge arresters needs to be proposed after balancing economics and insulation coordination performance.

6.3.2 Future Work in the Aspect of Experiment

- The flashover model used in this project is based on a typical model used for insulator flashover on metallic towers. In view of the particularity of flashover characteristics on the composite pylon, the flashover model can be improved after obtaining parameters from a specific flashover tests on a real cross-arm.
- The novel dynamic surge impedance model considering the corona effect for thin-wire conductors is proposed based theoretical assumption, which contains approximations and simplifications. The model needs to be revised and verified by comparing with experimental results.
- A long-term onsite test of the composite pylon should be carried out before casting into operation. Among this, comprehensive lightning protection performance tests include shielding failure test, lightning withstand test, and dry/wet/polluted flashover tests.

6.3.3 Future Work in the Aspect of Application

- Some engineering application details should be studied for preventive research, for instance, the application and selection of surge arresters, the application of grading rings, and the selection of grounding mesh.
- The fully composite pylon aims to replace conventional lattice tower. Some specific conditions should also be considered, for instance, constructing composite pylons at the incoming of substations, and connecting OHLs supported by composite pylons with power cable lines or gas insulated lines.

- Some other conditions to applying composite pylons should be considered to utilize its advantages better. Because of the anti-corrosion of composite materials, the composite pylon is prior to being installed in coastal regions. The lightning protection performance, especially pollution flashover characteristics of composite pylon installed in such regions should be studied.
- There is another plan to bring ground potential to shield wires, which is to install grounding cables inside the crossarms and pylon body. The lightning transient performance of these two plans is expected to be compared. Their effectiveness and the visual impact to the whole tower configuration should be discussed.

References

[1] Petroleum British, "BP Statistical Review of World Energy 2022." https://www.bp.com/en/global/corporate/energy-economics/statistical-review-of-world-energy.html/Accessed June, 2022.

[2] L. Bird, M. Milligan, and D. Lew, "Integrating variable renewable energy: Challenges and solutions," tech. rep., National Renewable Energy Lab.(NREL), Golden, CO (United States), 2013.

[3] M. Sarmento and B. Lacoursiere, "A state of the art overview: composite utility poles for distribution and transmission applications," in *2006 IEEE/PES Transmission & Distribution Conference and Exposition: Latin America*, pp. 1–4, IEEE, 2006.

[4] T. K. Sørensen, J. Holbøll, and S. Mikkelsen, *Composite based EHV AC overhead transmission lines*. PhD thesis, Technical University of Denmark, Department of Electrical Engineering, 2010.

[5] BYSTRUP, "Power Pylons of the Future - EUROPEAN COMPOSITE PYLON." https://www.compositepylon.com/Accessed April, 2022.

[6] T. Jahangiri, C. L. Bak, F. F. da Silva, and B. Endahl, "Determination of minimum air clearances for a 420kv novel unibody composite crossarm," in *2015 50th International Universities Power Engineering Conference (UPEC)*, pp. 1–6, IEEE, 2015.

[7] T. Jahangiri, Q. Wang, C. L. Bak, F. F. da Silva, and H. Skouboe, "Electric stress computations for designing a novel unibody composite crossarm using finite element method," *IEEE Transactions on Dielectrics and Electrical Insulation*, vol. 24, no. 6, pp. 3567–3577, 2017.

[8] Q. Wang, T. Jahangiri, C. L. Bak, F. F. da Silva, and H. Skouboe, "Investigation on shielding failure of a novel 400-kv double-circuit composite tower," *IEEE Transactions on Power Delivery*, vol. 33, no. 2, pp. 752–760, 2017.

[9] T. Jahangiri, C. L. Bak, F. da Silva, and B. Endahl, "Electric field and potential distribution in a 420 kv novel unibody composite cross-arm," in *Proceedings of the Nordic Insulation Symposium*, 2015.

[10] Q. Wang, C. L. Bak, F. da Silva, and E. Bystrup, "A state of the art review-methods to evaluate electrical performance of composite cross-arms and composite-based pylons," in *2016 IEEE Electrical Insulation Conference (EIC)*, pp. 501–506, IEEE, 2016.

[11] T. Jahangirl, C. L. Bak, F. M. F. da Silva, B. Endahl, and J. Holbøll, "Assessment of lightning shielding performance of a 400 kv double-circuit fully composite pylon," in *Cigré Session 2016*, pp. C4–205, 2016.

[12] Q. Wang, C. L. Bak, F. Silva, and H. Skouboe, "Scale model test on a novel 400 kv double-circuit composite pylon," in *International Conference on Power System Transients*, 2017.

[13] Q. Wang, T. Jahangiri, C. L. Bak, F. M. F. da Silva, and H. Skouboe, "Experimental evaluation of shielding angles' effects on lightning performance in a 400 kv ac double-circuit composite pylon," in *CIGRÉ Symposium 2017*, CIGRE (International Council on Large Electric Systems), 2017.

[14] J. He, X. Wang, Z. Yu, and R. Zeng, "Statistical analysis on lightning performance of transmission lines in several regions of china," *IEEE Transactions on Power Delivery*, vol. 30, no. 3, pp. 1543–1551, 2014.

[15] C. Zachariades, I. Cotton, S. Rowland, V. Peesapati, P. Green, D. Chambers, and M. Queen, "A coastal trial facility for high voltage composite cross-arms," in *2012 IEEE International Symposium on Electrical Insulation*, pp. 78–82, IEEE, 2012.

[16] Q. Wang, X. Yang, H. Li, Z. Guo, and Z. Peng, "Computation and analysis of the electric field distribution and voltage-sharing characteristics for 1000 kv composite tower," in *2016 IEEE International Conference on Dielectrics (ICD)*, vol. 2, pp. 1048–1051, IEEE, 2016.

[17] X. Yang, N. Li, Z. Peng, J. Liao, and Q. Wang, "Potential distribution computation and structure optimization for composite cross-arms in 750 kv ac transmission line," *IEEE Transactions on Dielectrics and Electrical Insulation*, vol. 21, no. 4, pp. 1660–1669, 2014.

[18] Y. Huangfu, S. Wang, X. Tao, S. Wang, B. Yang, G. Wang, and Y. Zhang, "Surge voltage and environmental electromagnetic field analysis for hv composite transmission tower under lightning strokes," in *2014 IEEE International Symposium on Electromagnetic Compatibility (EMC)*, pp. 445–450, IEEE, 2014.

[19] Z. Li, M. Dai, D. Gu, S. Deng, H. Li, and Q. Wei, "Study on grounding design for lightning of tubular composite material towers in 110kv overhead transmission line," in *2010 International Conference on High Voltage Engineering and Application*, pp. 473–476, IEEE, 2010.

[20] H. Li, S. Deng, Q. Wei, Y. Wu, and Q. Xiang, "Research on composite material towers used in 110kv overhead transmission lines," in *2010 International Conference on High Voltage Engineering and Application*, pp. 572–575, IEEE, 2010.

[21] C. Hu, T. Liu, K. Liu, T. Wu, B. Xiao, Y. Peng, Z. Su, P. Tang, and X. Le, "Investigation on 110kv composite material pole: Effects of grounding methods on insulation of conductor-pole gaps," in *2016 IEEE International Conference on High Voltage Engineering and Application (ICHVE)*, pp. 1–5, IEEE, 2016.

[22] T. Lu and X. Cui, "Transient analysis of wave processes for multi-conductor transmission lines with branches using fdtd," in *IEEE International Symposium on Electromagnetic Compatibility. Symposium Record (Cat. No. 00CH37016)*, vol. 2, pp. 699–703, IEEE, 2000.

[23] F. Gatta, A. Geri, and S. Lauria, "Backflashover simulation of hv transmission lines with concentrated tower grounding," *Electric Power Systems Research*, vol. 73, no. 3, pp. 373–381, 2005.

[24] J. Wu, J. He, B. Zhang, and R. Zeng, "Influence of grounding impedance model on lightning protection analysis of transmission system," *Electric Power Systems Research*, vol. 139, pp. 133–138, 2016.

[25] Cigré Working Group C4. 23, "Procedures for estimating the lightning performance of transmission lines—new aspects," *Technical Brochure*, vol. 839, 2021.

[26] J. A. Martinez and F. Castro-Aranda, "Tower modeling for lightning analysis of overhead transmission lines," in *IEEE Power Engineering Society General Meeting, 2005*, pp. 1212–1217, IEEE, 2005.

[27] B. Salarieh, H. J. De Silva, A. M. Gole, A. Ametani, and B. Kordi, "An electromagnetic model for the calculation of tower surge impedance based on thin wire approximation," *IEEE Transactions on Power Delivery*, vol. 36, no. 2, pp. 1173–1182, 2020.

[28] J. He, X. Zhang, P. Yang, S. Chen, and R. Zeng, "Attenuation and deformation characteristics of lightning impulse corona traveling along bundled transmission lines," *Electric power systems research*, vol. 118, pp. 29–36, 2015.

[29] J. He, B. Zhang, R. Zeng, and B. Zhang, "Experimental studies of impulse breakdown delay characteristics of soil," *IEEE transactions on power delivery*, vol. 26, no. 3, pp. 1600–1607, 2011.

[30] L. Grcev, "Time-and frequency-dependent lightning surge characteristics of grounding electrodes," *IEEE Transactions on Power Delivery*, vol. 24, no. 4, pp. 2186–2196, 2009.

[31] F. Gatta, A. Geri, S. Lauria, and M. Maccioni, "Simplified hv tower grounding system model for backflashover simulation," *Electric power systems research*, vol. 85, pp. 16–23, 2012.

[32] S. Visacro and R. Alipio, "Frequency dependence of soil parameters: Experimental results, predicting formula and influence on the lightning response of grounding electrodes," *IEEE Transactions on Power Delivery*, vol. 27, no. 2, pp. 927–935, 2012.

[33] S. Wang, Z. Li, J. Zhang, J. Wang, L. Cheng, T. Yuan, and B. Zhu, "Experimental study on frequency-dependent properties of soil electrical parameters," *Electric Power Systems Research*, vol. 139, pp. 116–120, 2016.

[34] L. D. Grcev, "Computer analysis of transient voltages in large grounding systems," *IEEE Transactions on power delivery*, vol. 11, no. 2, pp. 815–823, 1996.

[35] G. Ala, P. Buccheri, P. Romano, and F. Viola, "Finite difference time domain simulation of earth electrodes soil ionisation under lightning surge condition," *IET Science, Measurement & Technology*, vol. 2, no. 3, pp. 134–145, 2008.

[36] T. Harada, Y. Aihara, and Y. Aoshima, "Influence of switching impulse wave shape on flashover voltages of air gaps," *IEEE Transactions on Power Apparatus and Systems*, no. 3, pp. 1085–1093, 1973.

[37] C. P. Braz, A. Piantini, M. Shigihara, and M. C. d. E. S. Ramos, "Analysis of the disruptive effect model for the prediction of the breakdown characteristics of distribution insulators under non-standard lightning impulses," in *2012 International Conference on Lightning Protection (ICLP)*, pp. 1–7, IEEE, 2012.

[38] G. Krithika and S. Usa, "vt characteristics using extended disruptive effect model for impulses of varying front times," *IEEE Transactions on Dielectrics and Electrical Insulation*, vol. 22, no. 4, pp. 2191–2195, 2015.

[39] X. Chen, X. Wen, and L. Lan, "Application of the leader progression model in the insulation flashover criterion for lightning performance calculation," in *Proceedings of the Second International Conference on Mechatronics and Automatic Control*, pp. 459–466, Springer, 2015.

[40] M. Z. A. Ab Kadir and I. Cotton, "Implementation of the modified leader progression model in backflashover analysis," in *2006 IEEE International Power and Energy Conference*, pp. 516–521, IEEE, 2006.

[41] F. Gatta, A. Geri, S. Lauria, M. Maccioni, and A. Santarpia, "An atp-emtp monte carlo procedure for backflashover rate evaluation," in *2012 International Conference on Lightning Protection (ICLP)*, pp. 1–6, IEEE, 2012.

[42] A. R. Hileman, *Insulation coordination for power systems*. CRC Press, 2018.

[43] IEEE Working Group on Lightning Performance of Transmission Lines, "A simplified method for estimating lightning performance of transmission lines," *IEEE Transactions on Power Apparatus and Systems*, no. 4, pp. 918–932, 1985.

[44] F. Gatta, A. Geri, S. Lauria, M. Maccioni, and A. Santarpia, "An atp-emtp monte carlo procedure for backflashover rate evaluation: A comparison with the cigre method," *Electric Power Systems Research*, vol. 113, pp. 134–140, 2014.

[45] S. Shelemy and D. Swatek, "Monte carlo simulation of lightning strikes to the nelson river hvdc transmission lines," in *International Conference on Power System Transients*, pp. 1–6, 2001.

[46] A. Borghetti, C. A. Nucci, and M. Paolone, "An improved procedure for the assessment of overhead line indirect lightning performance and its comparison with the IEEE Std. 1410 method," *IEEE Transactions on Power Delivery*, vol. 22, no. 1, pp. 684–692, 2006.

[47] A. Borghetti, F. Napolitano, C. A. Nucci, and F. Tossani, "Application of the monte carlo method to lightning protection and insulation coordination practices," *Lightning Interaction with Power Systems*, vol. 2, pp. 1–25, 2020.

[48] F. H. Silveira, S. Visacro, and R. E. de Souza Filho, "Calculation of backflashover outage rate of transmission lines: A discussion on traditional methodologies and recent advances," in *2015 International Symposium on Lightning Protection (XIII SIPDA)*, pp. 226–230, IEEE, 2015.

[49] K. Yin, M. Ghomi, F. F. Da Silva, C. L. Bak, H. Zhang, Q. Wang, and H. Skouboe, "Lightning performance and formula description of a y-shaped composite pylon considering the effect of tower-footing impedance," in *2021 35th International Conference on Lightning Protection (ICLP) and XVI International Symposium on Lightning Protection (SIPDA)*, vol. 1, pp. 1–6, IEEE, 2021.

[50] J. Anderson, "Monte carlo computer calculation of transmission-line lightning performance," *Transactions of the American Institute of Electrical Engineers. Part III: Power Apparatus and Systems*, vol. 80, no. 3, pp. 414–419, 1961.

[51] P. Sarajcev, "Monte carlo method for estimating backflashover rates on high voltage transmission lines," *Electric Power Systems Research*, vol. 119, pp. 247–257, 2015.

[52] H. Zhang, Q. Wang, K. Yin, C. L. Bak, and F. F. da Silva, "Transient modelling and backflashover rate analysis of a fully composite pylon," in *The 16th IET International Conference on AC and DC Power Transmission (ACDC 2020)*, pp. 460–466, IET, 2020.

[53] C. R. Vogel, *Computational methods for inverse problems*. SIAM, 2002.

[54] T. Shindo and T. Suzuki, "A new calculation method of breakdown voltage-time characteristics of long air gaps," *IEEE transactions on power apparatus and systems*, no. 6, pp. 1556–1563, 1985.

[55] A. Pigini, G. Rizzi, E. Garbagnati, A. Porrino, G. Baldo, and G. Presavento, "Performance of large air gaps under lightning overvoltages: Experimental study and analysis of accuracy of predetermination methods," *IEEE Power Engineering Review*, vol. 9, no. 4, pp. 100–101, 1989.

[56] H. Motoyama, "Experimental study and analysis of breakdown characteristics of long air gaps with short tail lightning impulse," *IEEE Transactions on power delivery*, vol. 11, no. 2, pp. 972–979, 1996.

[57] R. V. Krejcie and D. W. Morgan, "Determining sample size for research activities," *Educational and psychological measurement*, vol. 30, no. 3, pp. 607–610, 1970.

[58] E. B. Robertson, "Grounding systems," in *Wescon/96*, pp. 182–188, IEEE, 1996.

[59] J. He, R. Zeng, and B. Zhang, *Methodology and technology for power system grounding*. Wiley, 2012.

[60] A. F. Imece, D. W. Durbak, and H. Elahi, "Modeling guidelines for fast front transients," *IEEE Transactions on Power Delivery*, vol. 11, no. CONF-950103-, 1996.

[61] A. Geri, "Behaviour of grounding systems excited by high impulse currents: the model and its validation," *IEEE Transactions on Power Delivery*, vol. 14, no. 3, pp. 1008–1017, 1999.

[62] A. Habjanic and M. Trlep, "The simulation of the soil ionization phenomenon around the grounding system by the finite element method," *IEEE Transactions on Magnetics*, vol. 42, no. 4, pp. 867–870, 2006.

[63] S. Visacro, R. Alipio, M. H. M. Vale, and C. Pereira, "The response of grounding electrodes to lightning currents: The effect of frequency-dependent soil resistivity and permittivity," *IEEE Transactions on Electromagnetic Compatibility*, vol. 53, no. 2, pp. 401–406, 2011.

[64] A. Mousa, "The soil ionization gradient associated with discharge of high currents into concentrated electrodes," *IEEE Transactions on Power Delivery*, vol. 9, no. 3, pp. 1669–1677, 1994.

[65] R. Alipio and S. Visacro, "Impulse efficiency of grounding electrodes: Effect of frequency-dependent soil parameters," *IEEE Transactions on Power Delivery*, vol. 29, no. 2, pp. 716–723, 2014.

[66] R. Smith-Rose, "Electrical measurements on soil with alternating currents," *Journal of the Institution of Electrical Engineers*, vol. 75, no. 452, pp. 221–237, 1934.

[67] J. H. Scott, R. D. Carroll, and D. R. Cunningham, "Dielectric constant and electrical conductivity measurements of moist rock: A new laboratory method," *Journal of Geophysical Research*, vol. 72, no. 20, pp. 5101–5115, 1967.

[68] C. L. Longmire and K. S. Smith, "A universal impedance for soils," tech. rep., Mission Research Corp Santa Barbara CA, 1975.

[69] M. Messier, "Another soil conductivity model," *internal rep., JAYCOR, Santa Barbara, CA*, 1985.

[70] D. Cavka, N. Mora, and F. Rachidi, "A comparison of frequency-dependent soil models: Application to the analysis of grounding systems," *IEEE Transactions on Electromagnetic Compatibility*, vol. 56, no. 1, pp. 177–187, 2013.

[71] M. Ghomi, C. L. Bak, and F. F. da Silva, "Frequency dependence of multilayer soil electrical parameters: Effects on ground potential rise," in *2021 35th International Conference on Lightning Protection (ICLP) and XVI International Symposium on Lightning Protection (SIPDA)*, vol. 1, pp. 01–08, IEEE, 2021.

[72] M. Ghomi, H. R. Mohammadi, C. L. Bak, F. M. F. da Silva, H. Khazraj, *et al.*, "Full-wave modeling of grounding system: Evaluation the effects of multi-layer soil and length of electrode on ground potential rise," in *International Conference on Power Systems Transients, IPST*, pp. 1–6, 2019.

[73] Y. Liu, N. Theethayi, R. Thottappillil, R. M. Gonzalez, and M. Zitnik, "An improved model for soil ionization around grounding system and its application to stratified soil," *Journal of Electrostatics*, vol. 60, no. 2-4, pp. 203–209, 2004.

[74] R. Shariatinasab and J. G. Safar, "Probabilistic evaluation of lightning performance of overhead distribution lines using monte carlo method," in *2012 Proceedings of 17th Conference on Electrical Power Distribution*, pp. 1–7, IEEE, 2012.

[75] D. A. Weston, *Electromagnetic compatibility: principles and applications*. CRC Press, 2017.

[76] C. Wagner and A. Hileman, "A new approach to the calculation or the lightning perrormance or transmission lines iii-a simplified method: Stroke to tower," *Transactions of the American Institute of Electrical Engineers. Part III: Power Apparatus and Systems*, vol. 79, no. 3, pp. 589–603, 1960.

[77] F. Dawalibi, W. Ruan, S. Fortin, J. Ma, and W. Daily, "Computation of power line structure surge impedances using the electromagnetic field method," in *2001 IEEE/PES Transmission and Distribution Conference and Exposition. Developing New Perspectives (Cat. No. 01CH37294)*, vol. 2, pp. 663–668, IEEE, 2001.

[78] M. A. Sargent and M. Darveniza, "Tower surge impedance," *IEEE Transactions on Power Apparatus and Systems*, no. 5, pp. 680–687, 1969.

[79] W. Chisholm, Y. Chow, and K. Srivastava, "Travel time of transmission towers," *IEEE Transactions on Power Apparatus and Systems*, no. 10, pp. 2922–2928, 1985.

[80] W. Chisholm, Y. Chow, and K. Srivastava, "Lightning surge response of transmission towers," *IEEE transactions on power apparatus and systems*, no. 9, pp. 3232–3242, 1983.

[81] T. Yamada, A. Mochizuki, J. Sawada, E. Zaima, T. Kawamura, A. Ametani, M. Ishii, and S. Kato, "Experimental evaluation of a uhv tower model for lightning surge analysis," *IEEE transactions on power delivery*, vol. 10, no. 1, pp. 393–402, 1995.

[82] A. Ametani, K. Adachi, and T. Narita, "An investigation of surge propagation characteristics on an 1100-kv transmission line," *Electrical Engineering in Japan*, vol. 147, no. 2, pp. 22–29, 2004.

[83] H. Motoyama, Y. Kinoshita, K. Nonaka, and Y. Baba, "Experimental and analytical studies on lightning surge response of 500-kv transmission tower," *IEEE transactions on power delivery*, vol. 24, no. 4, pp. 2232–2239, 2009.

[84] Y. Baba and M. Ishii, "Tower models for fast-front lightning currents," *IEEJ Transactions on Power and Energy*, vol. 120, no. 1, pp. 18–23, 2000.

[85] P. Mota, M. Chaves, and J. Camacho, "Power line tower lightning surge impedance computation, a comparison of analytical and finite element methods," in *International Conference on Renewable Energies and Power Quality (ICREPQ'12)*, 2012.

[86] R. A. De Araujo, S. Kurokawa, C. M. de Seixas, and B. Kordi, "Lightning-induced surge in transmission towers calculated using full-wave electromagnetic analysis and the method of moments," in *2018 13th IEEE International Conference on Industry Applications (INDUSCON)*, pp. 943–948, Ieee, 2018.

[87] A. Soares, M. A. O. Schroeder, and S. Visacro, "Transient voltages in transmission lines caused by direct lightning strikes," *IEEE Transactions on power delivery*, vol. 20, no. 2, pp. 1447–1452, 2005.

[88] T. H. Thang, Y. Baba, N. Nagaoka, A. Ametani, N. Itamoto, and V. A. Rakov, "Fdtd simulation of insulator voltages at a lightning-struck tower considering ground-wire corona," *IEEE transactions on power delivery*, vol. 28, no. 3, pp. 1635–1642, 2013.

[89] J. Takami, T. Tsuboi, K. Yamamoto, S. Okabe, Y. Baba, and A. Ametani, "Lightning surge response of a double-circuit transmission tower with incoming lines to a substation through fdtd simulation," *IEEE Transactions on Dielectrics and Electrical Insulation*, vol. 21, no. 1, pp. 96–104, 2014.

[90] C. Jordan, "Lightning computation for transmission line with overhead ground wires," *GE Review*, vol. 37, no. 4, pp. 180–186, 1934.

[91] C. Menemenlis and Z. T. Chun, "Wave propagation on nonuniform lines," *IEEE Transactions on Power Apparatus and Systems*, no. 4, pp. 833–839, 1982.

[92] H. Takahashi, "Confirmation of the error of jordan's formula on tower surge impedance," *IEEJ Transactions on Power and Energy*, vol. 114, no. 1, pp. 112–113, 1994.

[93] T. Hara and O. Yamamoto, "Modelling of a transmission tower for lightning-surge analysis," *IEE Proceedings-Generation, Transmission and Distribution*, vol. 143, no. 3, pp. 283–289, 1996.

[94] IEEE Working Group on Estimating Lightning Performance of Overhead Transmission Lines, "IEEE guide for improving the lightning performance of transmission lines," *IEEE Std*, pp. 1243–1997, 1997.

[95] A. De Conti, S. Visacro, A. Soares, and M. A. O. Schroeder, "Revision, extension, and validation of jordan's formula to calculate the surge impedance of vertical conductors," *IEEE transactions on electromagnetic compatibility*, vol. 48, no. 3, pp. 530–536, 2006.

[96] C. De Jesus and M. C. De Barros, "Modelling of corona dynamics for surge propagation studies," *IEEE transactions on power delivery*, vol. 9, no. 3, pp. 1564–1569, 1994.

[97] T. H. Thang, Y. Baba, N. Nagaoka, A. Ametani, J. Takami, S. Okabe, and V. A. Rakov, "A simplified model of corona discharge on overhead wire for fdtd

computations," *IEEE transactions on electromagnetic compatibility*, vol. 54, no. 3, pp. 585–593, 2011.

[98] T. H. Thang, Y. Baba, N. Itamoto, and V. A. Rakov, "Fdtd simulation of back-flashover at the transmission-line tower struck by lightning considering ground-wire corona and operating voltages," *Electric Power Systems Research*, vol. 159, pp. 17–23, 2018.

[99] T. Okada, Y. Baba, T. H. Tran, and V. A. Rakov, "On possible influence of corona discharge on the propagation speed of lightning surges along a tall grounded object," *IEEE Transactions on Electromagnetic Compatibility*, vol. 63, no. 1, pp. 172–180, 2020.

[100] J. J. Clade, C. H. Gary, and C. A. Lefevre, "Calculation of corona losses beyond the critical gradient in alternating voltage," *IEEE Transactions on Power Apparatus and Systems*, no. 5, pp. 695–703, 1969.

[101] M. Al Tai, H. Elayyan, D. German, A. Haddad, N. Harid, and R. Waters, "The simulation of surge corona on transmission lines," *IEEE Power Engineering Review*, vol. 9, no. 4, pp. 98–99, 1989.

[102] J. Guillier, M. Poloujadoff, and M. Rioual, "Damping model of travelling waves by corona effect along extra high voltage three phase lines," *IEEE transactions on power delivery*, vol. 10, no. 4, pp. 1851–1861, 1995.

[103] Y. Baba and V. A. Rakov, "Simulation of corona at lightning-triggering wire: Current, charge transfer, and the field-reduction effect," *Journal of Geophysical Research: Atmospheres*, vol. 116, no. D21, 2011.

[104] A. Smorgonskiy, E. Egüz, F. Rachidi, M. Rubinstein, and V. Cooray, "A model for the evaluation of the electric field associated with the lightning-triggering rocket wire and its corona," *Journal of Geophysical Research: Atmospheres*, vol. 120, no. 20, pp. 10–964, 2015.

[105] F. W. Peek, *Dielectric phenomena in high voltage engineering*. McGraw-Hill Book Company, Incorporated, 1920.

[106] A. Zalesski, "Trudy leningradskogo polytechniceskogo instituta," 1948.

[107] M. Robinson, "The corona threshold for coaxial cylinders in air at high pressures," *IEEE Transactions on Power Apparatus and Systems*, no. 2, pp. 185–189, 1967.

[108] R. Waters and W. Stark, "Characteristics of the stabilized glow discharge in air," *Journal of Physics D: Applied Physics*, vol. 8, no. 4, p. 416, 1975.

[109] G. Hartmann, "Theoretical evaluation of peek's law," *IEEE Transactions on industry applications*, no. 6, pp. 1647–1651, 1984.

[110] V. M. Cabrera and V. Cooray, "On the mechanism of space charge generation and neutralization in a coaxial cylindrical configuration in air," *Journal of electrostatics*, vol. 28, no. 2, pp. 187–196, 1992.

[111] S. Heckman and E. Williams, "Corona envelopes and lightning currents," *Journal of Geophysical Research: Atmospheres*, vol. 94, no. D11, pp. 13287–13294, 1989.

[112] COMSOL, "Atmospheric Pressure Corona Discharge in Air." `https://www.comsol.com/model/atmospheric-pressure-corona-discharge-in-air-44311` Accessed May, 2021.

[113] Phelps database, "Scattering cross sections data of Nitrogen." `https://fr.lxcat.net` Accessed July, 2021.

[114] K. Velitsikakis, F. M. F. da Silva, Q. Wang, C. L. Bak, and H. Skouboe, "Performance analysis for the innovative 400 kv double-circuit'y'composite tower under backflashover conditions," in *CIGRE International Colloquium on Lightning and Power Systems 2019*, CIGRE (International Council on Large Electric Systems), 2019.

[115] W. A. Chisholm, "New challenges in lightning impulse flashover modeling of air gaps and insulators," *IEEE Electrical Insulation Magazine*, vol. 26, no. 2, pp. 14–25, 2010.

[116] S. Venkataraman and R. Gorur, "Prediction of flashover voltage of non-ceramic insulators under contaminated conditions," *IEEE transactions on dielectrics and electrical insulation*, vol. 13, no. 4, pp. 862–869, 2006.

[117] H. Zhang, M. Ghomi, Q. Wang, F. F. da Silva, C. L. Bak, K. Yin, and H. Skouboe, "Comparison of backflashover performance between a novel composite pylon and metallic towers," *Electric Power Systems Research*, vol. 196, p. 107263, 2021.

[118] J. Gillespie and G. Stapleton, "Improving double circuit transmission line reliability through lightning design," *Cigré*, pp. B2–301, 2004.

[119] J. Kwak, J. Woo, E. Shim, H. Kim, and J. Moon, "Application of arrester to double circuit transmission line to enhance lightning performance and introduction about the obtained lightning waveforms by monitering systems," in *19th International Lightning Detection Conference, Tucson, Arizona, USA*, pp. 24–25, 2006.

[120] H. Zhang, Q. Wang, F. F. da Silva, C. L. Bak, K. Yin, and H. Skouboe, "Backflashover performance evaluation of the partially grounded scheme of overhead lines with fully composite pylons," *IEEE Transactions on Power Delivery*, vol. 37, no. 2, pp. 823–832, 2021.

[121] J. Li, *Measurement and analysis of overvoltages in power systems*. John Wiley & Sons, 2018.

[122] T. Udo, "Estimation of lightning shielding failures and mid-span backflashovers based on the performance of ehv double circuit transmission lines," *IEEE transactions on power delivery*, vol. 12, no. 2, pp. 832–836, 1997.

[123] N. Rugthaicharoencheep, W. Thansiphraserth, and A. Phayomhom, "Comparison voltage across insulator strings of 69 kv and 24 kv lines due to lightning strokes to top pole and mid span," in *2012 47th International Universities Power Engineering Conference (UPEC)*, pp. 1–5, IEEE, 2012.

[124] X. Liu, J. Yang, G. Liang, and L. Wang, "Modified field-to-line coupling model for simulating the corona effect on the lightning induced voltages of multiconductor transmission lines over a lossy ground," *IET Generation, Transmission & Distribution*, vol. 11, no. 7, pp. 1865–1876, 2017.

Part II

Papers

Paper I

Backflashover Performance Evaluation of the Partially Grounded Scheme of Overhead Lines With Fully Composite Pylons

Hanchi Zhang, *Student Member, IEEE*, Qian Wang, *Member, IEEE*, Filipe Faria da Silva, *Senior Member, IEEE*, Claus Leth Bak, *Senior Member, IEEE*, Kai Yin, *Student Member, IEEE*, and Henrik Skouboe

***Abstract*—A design of a fully composite pylon has been proposed for new-generation 400 kV transmission towers to save line corridors and to reduce visual impact. Correspondingly, a method of external down-leads is proposed to bring grounding potential to the shield wires, together with a plan that not all pylons are grounded called 'partially grounded transmission lines' (PGTLs). This paper investigates backflashover performance of a partial grounding scheme of overhead lines (OHLs) supported by composite pylons. The transient analysis was carried out in PSCAD based on Monte Carlo method. For OHLs with every pylon grounded, reducing footing resistance and soil resistivity can improve backflashover performance effectively, but for PGTLs, these two methods do not have obvious effect and increasing insulation distance has limited effect. When lightning strikes at PGTLs, overvoltage is mainly dependent on the distance to the nearest grounded pylon and a longer distance will cause overvoltage with larger amplitude and longer wave front duration. Therefore, backflashover rate also increases along with the distance to the nearest grounded pylon until reaching a value limited by the inceptive condition of flashover. A coefficient recommended by CIGRE TB 63 to estimate backflashover rate is discussed and modified when using in PGTLs.**

***Index Terms*—Backflashover rate, partially grounded, fully composite pylon, lightning overvoltage, grounding, OHLs.**

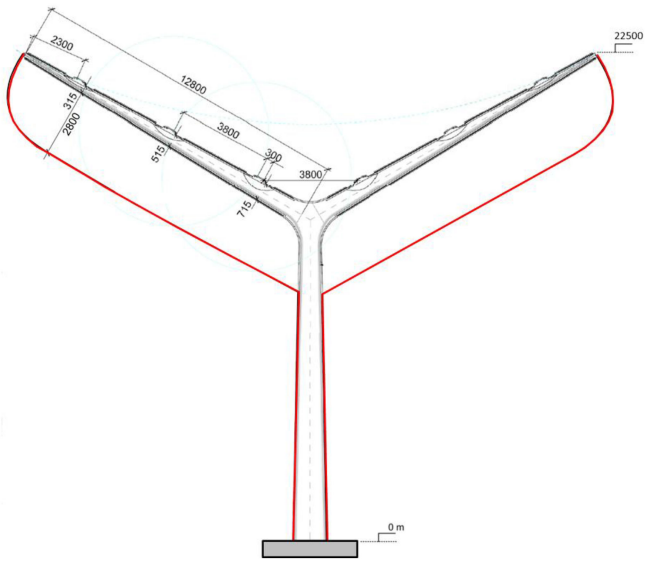

Fig. 1. The design concept of the novel 400 kV fully composite pylon with external grounding down-leads.

I. Introduction

In RECENT years, usage of overhead lines (OHLs) in transmission system has faced with great challenges, because of the increasing requirement for transmission capacity, along with the public opposing to the erection of more conventional metal lattice towers, which have negative visual impact. A fully composite pylon has been proposed to meet the requirements of compact structure and elegant appearance for new-generation transmission towers [1]. The configuration and dimension of the fully composite pylon is shown in Fig. 1. The pylon is in the shape of a 'Y' geometric configuration. Conductors are fixed by clamps on the surface of the cross-arm, which has an inclined angle of 30° from the horizontal ground plane. Two shield wires are installed at the tips of the two cross-arms. Because the pylon body are made of fiber reinforced plastic (FRP) and the cross-arms are design with sheds of silicon rubber on the surface, the pylon itself cannot conduct lightning current if struck by lightning flashes or when lightning flashes terminate at shield wires. Correspondingly, as one choice of grounding design, two bare-metal conductors downwards outside the pylon are used to conduct the lightning current to ground when shield wires are terminated by lightning flashes, which are shown as red lines in Fig. 1, and they are potential locations to install line surge arresters. An alternative of two conductors downwards inside the cross-arms and pylon body to ground is being considered and studied in [2], but it is not be addressed in present paper.

Out of economic and aesthetic considerations, a scheme where not all pylons are grounded is desirable and investigated in this paper, which is called 'partially grounded transmission lines' (PGTLs). PGTL is designed as a segment of OHLs, which is

Manuscript received November 11, 2020; revised February 28, 2021; accepted April 1, 2021. Date of publication April 8, 2021; date of current version March 24, 2022. Paper no. TPWRD-01661-2020. *(Corresponding author: Hanchi Zhang.)*

Hanchi Zhang, Qian Wang, Filipe Faria da Silva, Claus Leth Bak, and Kai Yin are with the Department of Energy Technology, Aalborg University, 9100 Aalborg, Denmark (e-mail: hazh@et.aau.dk; qiw@et.aau.dk; ffs@et.aau.dk; clb@et.aau.dk; kyi@et.aau.dk).

Henrik Skouboe is with BYSTRUP Architecture Design Engineering, 2100 København Ø, Denmark (e-mail: hs@bystrup.dk).

Color versions of one or more figures in this article are available at https://doi.org/10.1109/TPWRD.2021.3071926.

Digital Object Identifier 10.1109/TPWRD.2021.3071926

supported by several ungrounded pylons. At both ends of PGTL, it is still necessary to install grounding equipment providing a conducting path when lightning strikes on the shield wires [3]. The grounding equipment can be composite pylons with grounding down-leads, conventional steel transmission towers, or steel tension towers at the corner of PGTLs. According to the travelling wave theory, an overvoltage at a lightning strike location will go on increasing before the negative wave reflected from the ground reaches the striking point[4]. Thus, with a longer distance between the lightning striking point and the grounding point, the lightning overvoltage will become more severe. If the reflection time is shorter than the lightning front time, longer striking distance will cause higher overvoltage amplitude. If the reflection time is longer than the lightning front time, longer striking distance will cause overvoltage with longer duration. Both conditions stress the insulation strength heavily leading to backflashover (BF). Backflashover rate (BFR) is commonly used to evaluate backflashover performance of transmission lines, which is described as the number backflashovers of a transmission lines per 100 km per year.

For conventional OHLs, several papers have studied that the overvoltage with mid-span terminated by lightning is approximately 1.2 to 2.0 times higher than that with tower top terminated by lightning[5]–[7]. Although the overvoltage at mid-span is higher, the insulation strength of the air gap at mid-span is stronger than the insulator surface on the tower, thus backflashover is less likely to occur at mid-span than at the tower. Therefore, critical lightning current of flashover when lightning strikes at pylon head, I_{c1}, is smaller than critical lightning current of flashover when lightning strikes at mid-span, I_{c2}. Considering this situation, BFR of the entire transmission lines is obtained by the BF probability multiplying a coefficient, which equals to the ratio of the occurring probability of I_{c1} and I_{c2}. For variant spans in conventional OHLs, the ratio according to lightning current probability distribution is in a narrow range from 0.58 to 0.67[7]. Thus, 0.6 is selected as a compromised value.

For PGTL, the distance from lightning location to nearest grounded pylon may be generally longer than most spans in current transmission lines, which will causes overvoltage with higher amplitude and longer duration. On the other hand, insulation strength at cross-arm in ungrounded pylon within PTGL may be generally weaker than mid-span to withstand such severe overvoltage. Therefore, critical lightning current of flashover when lightning strikes at mid-span I_{c2} will be lower, and the ratio of the occurring probability of I_{c1} and I_{c2} increases along with the length of PGTL. The value of the coefficient used in BFR evaluation for PGTL of different length needs to be investigated and revised.

This paper deals with backflashover performance evaluation of the PGTLs supported by the novel composite pylons, using the simulation software PSCAD and the Monte Carlo Method (MCM) and it is organized as follows. Chapter II and III describe the modelling details for the backflashover analysis for composite pylons and propose a procedure to evaluate BFR using MCM. Chapter IV analyzes that the distance of PGTLs is the main factor affecting overvoltage, BF probability and BFR, while conventional methods like reducing footing resistance and soil resistivity, or increasing insulation distance do not have substantial effects. Chapter V analyzes the reason and influencing factor of the stabilization of BF probability and BFR with the increasing of distance to the nearest grounded pylon. Then, the equation used in conventional OHLs to estimate BFR is discussed, and modified when it is used for PGTLs.

TABLE I
THE MEDIAN AND LOG STANDARD DEVIATION OF THE LIGHTNING CURRENT PARAMETERS [7]

Variable	M, median	β, log std. deviation
I_c [>20 kA, kA]	33.3	0.605
S_m [kA/μs]	24.3	0.599
t_f [μs]	3.83	0.553
t_h [μs]	77.5	0.577

II. MODELLING OF TRANSMISSION LINES FOR BACKFLASHOVER ANALYSIS

A. Lightning Current Model

There exist several widely used lightning current simulation waveforms. The effect of lightning current waveforms on the backflashover withstand level is studied and summarized in [8]. Among all models, CIGRE lightning current model is used because of its consistency with the waveshape of lightning flashes in nature[9]. Four variables are used to shape the lightning current waveshape of the first stroke of the downward flash as recommended by CIGRE, namely, the lightning current amplitude I_c, the maximum steepness S_m, the front time (from 30% to 90%) t_f, and the tail time t_h. All the parameters yield to log-normal distribution[10]. The median *M* and log standard deviation β of the variables are shown in Table I.

In this paper, I_c and t_f are treated as the inter-related variables to shape the lightning current waveform. t_h is set as constant equal to its median after concluding that it has little effect on overvoltage level. S_m is set as per unit value determined by I_c and t_f and its base value is equal to the quotient by the medians of I_c and t_f.

B. OHL Model

The simulated double-circuit OHL is at rated voltage of 400 kV. At one end of the OHL, phase conductors are connected with a three-phase voltage source and shield wires are solidly grounded. At the other end, the OHL is connected to a load. The PGTL under research is set in the middle. At the ends of PGTL segment, two grounded pylons are modelled, then two 50 km OHLs are set from grounded pylons to voltage source and load respectively. The PGTL segment itself is divided into two parts, in order to simulate the lightning striking location with different distance to grounded pylon. The span is 250 m. The distance of PGTL depends on the amount of ungrounded pylons in PGTL. For instance, the shortest PGTL is 500 m within 1 ungrounded pylon. Fig. 2 shows the demonstration of OHL model with PGTL.

C. Down-Leads Model

The surge impedance of the down-leads varies according to the geometry, as the lightning wave travels from top to ground. To cope with this behavior, the down-leads model is established

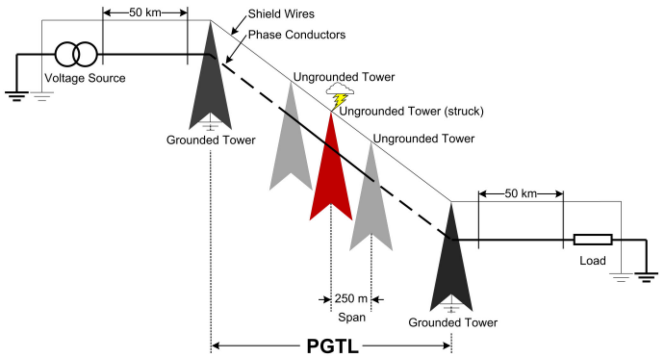

Fig. 2. The demonstration of OHL model within PGTL.

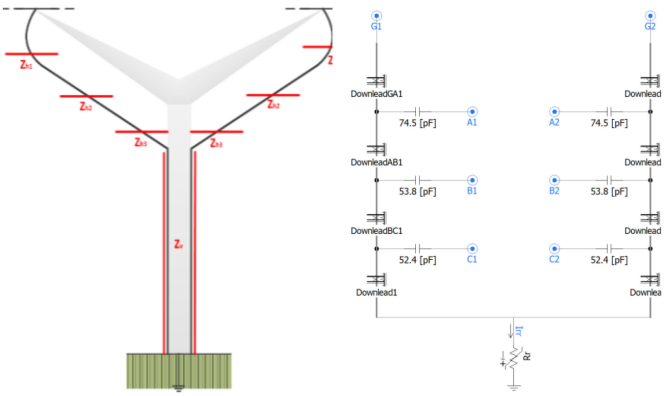

Fig. 3. The demonstration and model of grounding down-leads.

as a combination of several parts. The 'Bergeron Model' in PSCAD is used to simulate the transient characteristics of each part[11]. The down-lead is regarded as two types of conductors, the part along with pylon body is regarded as a vertical cylindrical conductor whose surge impedance Z_v can be calculated by (1) and the part along with the crossarm is regarded as combination of three horizontal cylindrical conductors whose surge impedance Z_h can be calculated by (2)[12],

$$Z_v = 60(\ln(h_v/r) - 1) \tag{1}$$

$$Z_h = 60\ln(2h_h/r) \tag{2}$$

where r is the radius of the down-leads and h is the height of different segment. To be noted, the height of the vertical part h_v is from earth bottom to top and the height of each horizontal segments h_h is from earth bottom to the center of each segment. Fig. 3 shows the demonstration of grounding down-leads and the model in PSCAD. The insulation capacitances are calculated by FEM software.

D. Tower Footing Impedance Model

After a lightning strike at shield wires of the pylon, the overvoltage waves will travel along the shield wires through the grounding down-leads to ground. A wave in opposite polarity will be reflected after it travels to the pylon base. A concentrated grounding system is selected for modelling pylon base, exhibiting current magnitude dependence from soil ionization[9]. The following current-dependence footing impedance model is used as equation (3) to simulate the footing impedance [13],

$$R_f = \frac{R_0}{\sqrt{1 + (I_R/I_g)}} \tag{3}$$

where R_0 is the pylon footing resistance at low frequency and low current, I_R is the lightning current through the footing resistance to ground and I_g is the threshold lightning current initialing the soil ionization described by (4) [14],

$$I_g = \frac{\rho E_0}{2\pi R_0^2} \tag{4}$$

where E_0 is the soil ionization electric field gradient and ρ is the apparent soil resistivity. E_0 can be also related to ρ, in the equation (5) [15],

$$E_0 = 241 \cdot \rho^{0.215} \tag{5}$$

TABLE II
RECOMMENDED VALUES FOR LEADER PROGRESSION MODEL OF LIGHTNING IMPULSE FLASHOVER

Configuration	Polarity	k [m²/(kV²·μs)]	E_l [kV/m]
Air gaps, post insulators, long-rod polymer insulators	Positive	0.8	600
	Negative	1.0	670
Cap-and-pin porcelain insulators, glass insualtors	Positive	1.2	520
	Negative	1.3	600

E. Leader Progression Model for Flashover

The leader progression method (LPM) considers the physical process of air gap discharge to describe the insulation surface flashover, which mainly consists of two stages: the streamer progression stage T_s and the leader progression stage T_l[16].

The streamer progression time can be calculated by (6)[17],

$$T_s = \frac{1}{k_1(E/E_{50\%}) - k_2} \tag{6}$$

where, E is the maximum electric field before insulation flashover and $E_{50\%}$ is the electric field under the 50% flashover voltage. k_1 and k_2 are the factors of streamer progression time, which are recommended to be 1.25 and 0.95 respectively[18].

The leader progression time can be calculated based on its velocity recommended by CIGRE as (7) [10],

$$\frac{dx}{dt} = ku(t)\left(\frac{u(t)}{D-x} - E_l\right) \tag{7}$$

where, x is the length of the leader, $u(t)$ is the voltage at the air gap, D is the length of insulation, E_l is the threshold electric field of leader progression and k is the factor of leader progression speed. E_l and k are related to the type of the insulators and the polarity of lightning impulse voltage, which are obtained from experiments and are shown in Table II.

For ungrounded pylon, the flashover characteristics between the shield wire and upper phase conductor along the crossarm are more similar to that of a long-rod polymer insulator instead of a cap-and-pin insulator with metallic connecting hardware, thus the parameters of long-rod polymer insulator are selected[19]. For grounded pylon, a flashover is also likely to occur between the down-lead and the phase conductor in the air gap, which

uses the same parameters as long-rod polymer insulators. Thus, these two situations can use the same leader progression model.

III. BFR Estimation Procedure

The BFR evaluation procedure based on the Monte Carlo method uses the statistical result of quantities of random lightning surges to evaluate the probability that the backflashover occurs [20]. The procedure consists of three steps: pre-processing step, numerical simulation step and post-processing step.

A. Pre-Processing Step

In pre-processing step, a large number, N_{total}, of lightning currents were generated. Because the front time of lightning current follows log normal probability distribution, a group of front times were generated using inverse transform sampling. Front time t_f and current amplitude I_c are inter-related. The median of log-normal distribution of I_c can be obtained according to the value of t_f in equation (8)[7],

$$M_I = 19.5 \cdot {t_f}^{0.39} \tag{8}$$

Then, based on every front time, a group of lightning current amplitudes can be generated based on their medians because of log-normal probability distribution. In this paper, the number of different front times is 100 and the number of different lightning current amplitudes corresponding to every front time is also 100, thus, the number of lightning currents N_{total} is 10000.

B. Numerical Simulation Step

In numerical simulation step, all lightning currents derived from the previous step were input into the OHLs model established in PSCAD as lightning impulse current source. The overvoltages between down-leads and nearest phase conductors were recorded.

The backflashover probability for every lightning current was estimated considering the operating voltage of the phase conductors. When using LPM to determine the occurrence of backflashover, *u(t)* in (7) is the voltage at the air gap, which is the difference between the voltages on the down-leads and the operating voltage *V* on the phase conductors. The operating voltage can be regarded as a constant during the lightning transients because of the relatively extremely short duration of overvoltage. The result after determination of LPM to a certain *u(t)* is only 1 (flashover) or 0 (not flashover). Hereby, the backflashover probability is related to the probability of the operating voltage in the whole AC cycle when flashover is determined to occur. The different operating voltage values from minimum to maximum are used to determine flashover occurrence with overvoltage together. A critical value of operating voltage V_i can be approached, which means the operating voltage higher than V_i can cause flashover with overvoltage, while the operating voltage lower than V_i cannot. The backflashover probability can be estimated as the ratio of the duration in one cycle when the operating voltage is above V_i for the whole AC period.

TABLE III
The Soil Resistivity and Soil Ionization Electric Field Gradient of Different Soil Types in Denmark

Soil type	Soil resistivity ρ [Ωm]	Soil ionization E-field E_0 [kV/m]
Sand	200-300	752.90-821.48
Sandy clay / clayey sand	50-500	558.85-916.84
Clay	100-200	648.66-752.90

C. Post-Processing Step

In post-processing step, the BFR is calculated after processing the results of backflashover probability of all lightning currents.

The BFR can be expressed in equation (9)[10],

$$BFR = K \cdot N_d \cdot \frac{\sum P(I_C)}{N_{total}} \tag{9}$$

where $\Sigma\ P(I_C)$ is the sum of the backflashover probability of every lightning current and N_{total} is the total number of lightning currents. N_d is the estimated number of lightning strikes that terminate on the 100-km line, which can be calculated by (10)[21],

$$N_d = N_g \cdot (D + 28H^{0.6})/10 \tag{10}$$

where N_g is the ground flash density describing the number of flashes that terminate on the ground per year per square kilometers. *H* is the pylon height and *D* is the horizontal distance between shield wires. *K* is a coefficient less than 1, considering that overvoltage at the shield wire caused by lightning flashes striking within the span is lower than that caused by lightning striking at the pylon head. Consequently, the BFR is reduced if lightning flashes striking within the span is considered. In conventional OHLs supported by steel towers, $K = 0.6$ is usually applied in the BFR estimation recommended by CIGRE TB 63 [10], [20], [22]–[24]. The value of *K* used in PGTLs is discussed in Chapter V.

IV. Results

A. BFR of Different Footing Resistance and Soil Resistivity in OHLs With Every Pylon Grounded

For OHLs with every pylon grounded, after lightning strikes at shield wires, the reflections of travelling waves from the tower base through the down-leads arrive at the pylon top much faster than those reflections from adjacent pylons [25]. According to (4) and (5), it can be found that two parameters, the soil resistivity and the footing resistance at low current determine the performance of tower footing impedance. Thus, the BFR of OHLs with every pylon grounded is influenced by these two parameters. The soil resistivity depends on local soil type. Hereby, the Danish soil conditions are selected as case study. The soil of Denmark can be classified into three major types, namely sand in the western and northern region, sandy clay or clayey sand in the center and clay in the southeastern region. The soil resistance and the soil ionization electric field gradient of different soil types are shown in the Table III [26].

Pylon footing resistance is set as 5 Ω, 10 Ω, 20 Ω, and 50 Ω. The BFR of OHLs supported by grounded composite pylons

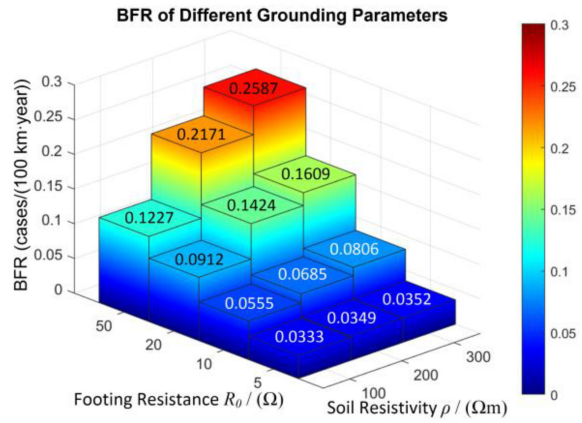

Fig. 4. BFR of OHLs with every pylon grounded of different grounding parameters.

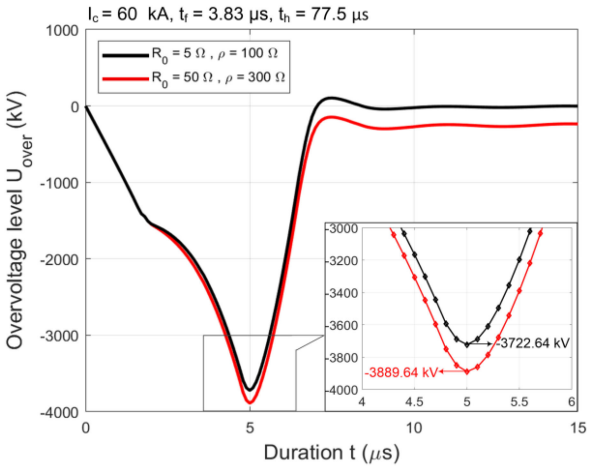

Fig. 5. Overvoltage wave fronts of two combinations of grounding parameters.

with different combination of pylon footing resistance and soil resistivity is summarized in Fig. 4.

It can be summarized that for OHLs supported by grounded composite pylons, reducing footing resistance and soil resistivity of grounded pylons can improve backflashover performance effectively, which is identical to the case of OHLs supported by steel lattice towers. When pylon footing resistance is low enough, the effect of reducing soil resistivity is limited.

B. Overvoltage of Different Footing Resistance and Soil Resistivity in PGTLs

Reducing footing resistance and soil resistivity of grounded pylons can improve backflashover performance effectively in the OHLs where every pylon is grounded. However, for PGTLs neither of the methods are effective.

The wave fronts of overvoltages of different grounding parameters are studied. Hereby, an example under the same lightning strike is shown in Fig. 5, where the PGTLs is 500 m long including only one ungrounded pylon in the middle. The lightning flash with the amplitude of 60 kA (3.83/77.5 μs) strikes in the middle. The maximum overvoltage when the grounded pylons are of lower footing resistance and soil resistivity is -3722.64 kV, which is only 4.5% lower than when the grounded

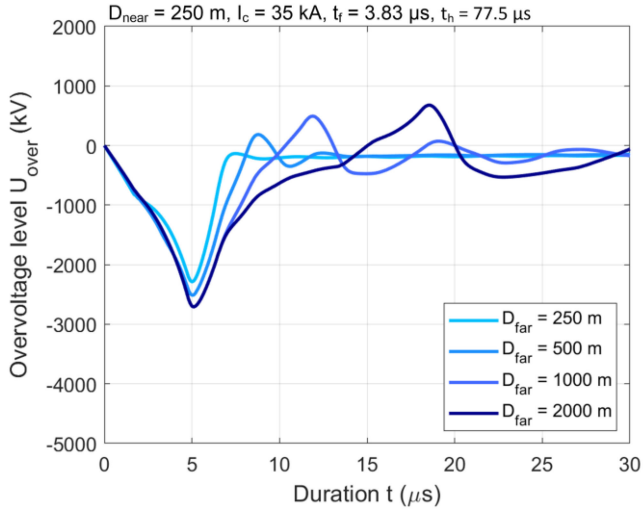

Fig. 6. Overvoltage wave fronts of same Dnear and different Dfar.

pylons are of higher footing resistance and soil resistivity, which is -3889.64 kV. For the span of 250 m, the 500 m PGTL with one ungrounded pylon is the shortest scheme. Along with the increasing of PGTL length, the effect of reducing footing resistance and soil resistivity will become even more limited. The differences of the maximum overvoltage on the PGTLs of 1000 m, 1500 m and 2000 m and a strike at the middle of the span are 89.69 kV, 1.85 kV and 0 kV. Moreover, the small differences in overvoltage cannot influence the BFR results obviously.

In summary, when the lightning strikes at the ungrounded pylon, reducing footing resistance and soil resistivity of grounded pylons at the both ends of PGTLs has limited effect on the amplitude of overvoltage and so as to the BFR.

C. Overvoltage of Lightning Location in PGTLs

Because the pylons within PGTLs are not grounded, when lightning flashes terminate at the shield wires, the overvoltage wave will travel to both ends in opposite directions on the shield wires and go into ground through the grounded pylons. The travelling distances to the two ends are different except when lightning strikes at right middle. Hereby, D_{near} is termed as the nearer travelling distance from lightning location to one of the grounded pylon while D_{far} is termed as the longer one.

The overvoltage at lightning location in PGTLs with different distance to grounded pylons can be seen in Fig. 6 and Fig. 7. The lightning surge is 35 kA (3.83/77.5 μs). If the D_{near} is the same, the overvoltage waveforms with different D_{far} are similar, especially in the wave front duration. The maximum values of overvoltage range from -2289.55 kV to -2708.74 kV, increasing by 18.31%. If lightning current amplitude is lower, the dispersion is even smaller. However, if D_{far} is the same, the overvoltage waveforms with different D_{near} are obviously different. The maximum values of overvoltage range from -2708.74 kV to -4182.65 kV, increasing by 54.41%. The discrepancy among the overvoltage waveshapes becomes also larger. Along with the increasing of D_{near}, the waveshape of the overvoltage changes from a 'V' shape to a 'U' shape, forming a flat bottom. This is because the time for the overvoltage at the striking point to reach

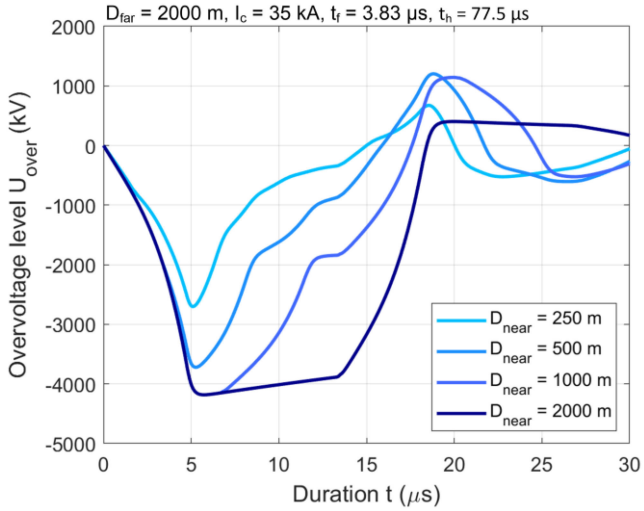

Fig. 7. Overvoltage wave fronts of same Dfar and different Dnear.

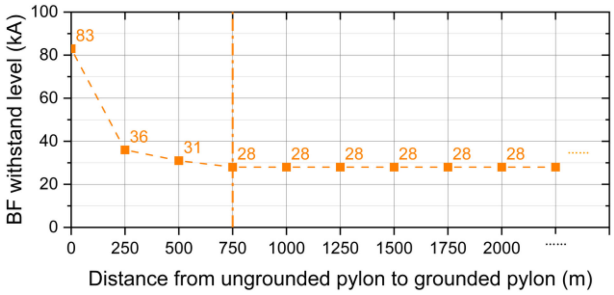

Fig. 8. BF withstand level of different distances to nearest grounded pylon.

its peak is shorter than that for the reflection wave from ground to reach the striking point. Before the arrival of the reflection wave, the waveshape of the overvoltage is consistent with the shape of the lightning current. After the arrival of reflection wave, the overvoltage wave is chopped by superimposing the reflection wave. During the propagation of overvoltage wave on shield wires after lightning striking, corona will damp the energy, which will reduce overvoltage amplitude. Along with the increase of travelling distance, damping effect of corona will become larger[27].

In summary, in PGTLs, lightning overvoltage is mainly dependent on the distance to the nearest grounded pylon. Longer distance to the nearest grounded pylon will cause overvoltage with larger amplitude and longer wave front.

D. BFR of Different Distances of PGTLs

According to (10), BFR is the product of the amount of lightning flashes terminating on 100 km lines per year and the backflashover probability caused by lightning flashes, based on MCM procedure. Backflashover probability is resulted from lightning overvoltage which is mainly dependent on the distance to the nearest grounded pylon as elaborated in the last section.

The backflashover withstand levels of the ungrounded pylons after lightning striking with different distances to nearest grounded pylons is shown in Fig. 8. For a grounded pylon, its BF withstand level is 83 kA. After After the nearest distance

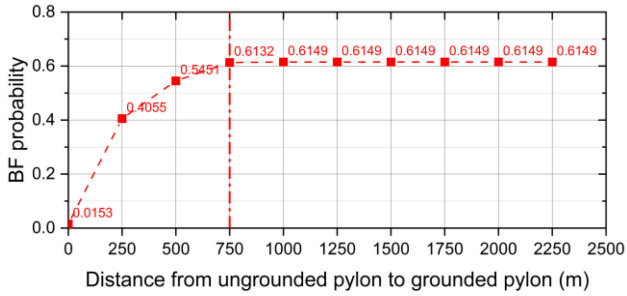

Fig. 9. BF probability of different distances to nearest grounded pylon.

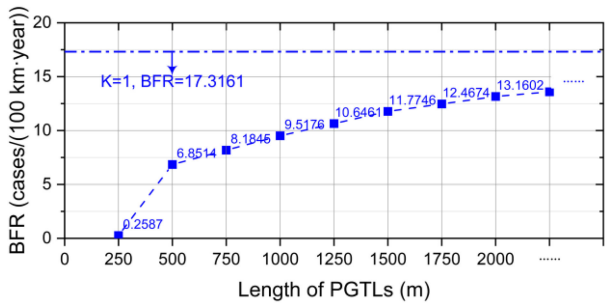

Fig. 10. BFR of different length of PGTLs.

increases to exceed 750 m, the BF withstand level stabilizes at 28 kA. The backflashover probability when lightning strikes at the PGTLs for different distances to nearest grounded pylon is shown in the Fig. 9. When the distance from the lightning location to the nearest grounded pylon increases, the BF probability also increases, because of the increase of the overvoltage amplitude and wave front duration. After the nearest distance increases to exceed 750 m, the BF probability stabilizes at 0.6149.

Lightning flashes may not only strike at pylons, but also strike in span. The overvoltage at the pylon caused by lightning flashes striking within the span is lower than that caused by the same lightning strike at the pylon head. Therefore, a coefficient K is considered which is less than 1. For PGTLs, the analysis of the value of K is discussed in next chapter. Hereby, K increases and approaches to 1, along with the increasing of the distance between ungrounded pylon and grounded pylon. Therefore, BFR can be calculated by equation (10). The BFR of different length of PGTL is shown in the Fig. 10, which increases and approaches to 17.3161 cases per 100 km per year along with the increase in the length of PGTL. To be noted, because the span is 250 m, the length of 250 m means the pylons in OHL are all grounded. A PGTL of 500 m has 1 ungrounded pylon, a PGTL of 750 m has 2 ungrounded pylon inside, and so on.

In Section IV.B, the ineffectiveness of reducing footing resistance and soil resistivity to improve backflashover performance of PGTLs was summarized. Another alternative method is increasing the insulation distance between the shield wire and the upper phase conductor. To be noted from equation (11), increasing insulation distance will increase the pylon height and shield wires corridor width, which means the OHLs will attract more lightning flashes. The BFRs along with different distance between ungrounded pylon and grounded pylon provided by

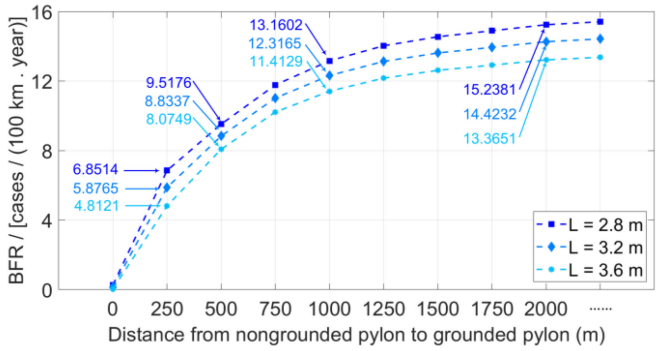

Fig. 11. Effect of increasing insulation distance L on BFR of different PGTLs distances.

different insulation distances are shown in following Fig. 11. It can be seen that increasing insulation distance has limited effect for practical application.

In summary, the BFR of PGTLs increases along with the distance to the nearest grounded pylon, until it reaches a limit value. Besides reducing footing resistance and soil resistivity, increasing insulation distance has limited effect for practical application either.

V. Discussion

A. Discussion on the Stabilization of BF Probability of Long-Distance PGTLs

The reason for the stabilization of the BF probability is explained and the determining factor is discussed in this chapter. The stabilization of the BF probability results from the stabilization of the maximum value of overvoltages along with the increase of the distance to the nearest grounded pylon. A distance over 750 m corresponds to a reflection wave travelling time that exceeds 5.36 μs, which is longer than the front time of 72.83% of the lightning currents, according to the cumulative distribution function of lightning current parameters. Therefore, the maximum value of overvoltages is not influenced by the majority of lightning impulses when travelling time exceeds 5.36 us. As a result, the BF probability stabilizes when distance to the nearest grounded pylon exceeds around 750 m.

The value of the maximum BF probability 0.6149 is limited by the threshold electric field of leader progression development E_l in (7). Based on the mechanism of leader progression, it is necessary for flashover occurrence that the electric field exceeds E_l and keeps over E_l continuously during the development of leader progression. When distance to the nearest grounded pylon increase over 750 m, the wave front of the overvoltage is long enough for the leader progression to develop as flashover. Once the inceptive condition of leader progression is satisfied, the longer duration of the 'U' shape bottom may ensure the occurrence of flashover. Thus, as the inceptive condition for leader progression, the threshold electric field E_l is significant to evaluate the flashover.

At present, the value of threshold electric field E_l is recommended by CIGRE when using leader progression model to determine the occurrence of flashover, which was derived from the results of experiments in [17]. Catering to the industrial demand, line post insulators and suspension insulators were tested and their E_l were analyzed under different impulse polarities. Given the lacking of experimental data, threshold electric field E_l of composite crossarm, one can refer to that of polymer insulators, because of similarity in electrical design. They both have sheds made of silicon rubber and composite material.

TABLE IV
The Test Conditions and Fitted Threshold Electric Field

Scholar	Gap type	Waveform	Polarity	E_l [kV/m]
Pigini 1989[17] & CIGRE 1991[10]	line post insulator	1.6/50	+	600
		0.5/50	−	670
Motoyama 1996[28]	rod-rod air gap	1.2/3.2	±	750
Xi 2014[29]	composite insulator	1.45/11	+	620
		1.56/49.2	−	570

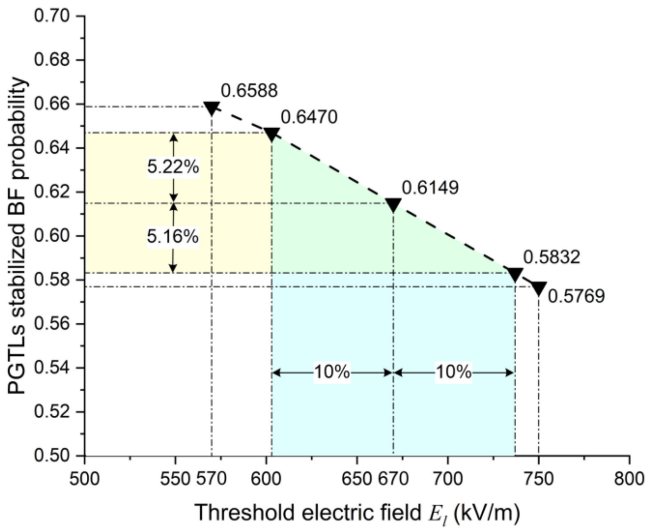

Fig. 12. Sensitivity analysis result of PGTLs stabilized BF probability to the threshold electric field E_l.

Despite this, a sensitivity analysis based on the different values of threshold electric field E_l, which were derived in experiments under different conditions. Among all, the values obtained by Motoyama[28] and Xi[29] present the highest and lowest under the negative lightning impulse. The tested models and conditions are summarized in Table IV. The sensitivity analysis results are shown in Fig. 12. When the value of E_l changes $\pm 10\%$, the deviation of BF probability is around $\pm 5\%$. The sensitivity coefficient is -0.52, whose absolute value less than 1. In summary, firstly, the stabilized BF probability is closely related to E_l. Secondly, although there is no such experimental data to provide exact value of E_l for crossarm, the simulating BF probability is also convincing considering the uncertainty of E_l in a probable range.

However, there still exist some differences between crossarm and polymer insulators. For instance, the air gap of crossarm is much longer than that of line post insulator and the E_l of insulators was tested under standard lightning impulse voltage[16], [17], [29]. From [28], for short tail lightning impulse, the value of E_l might be higher. In a word, the threshold electric

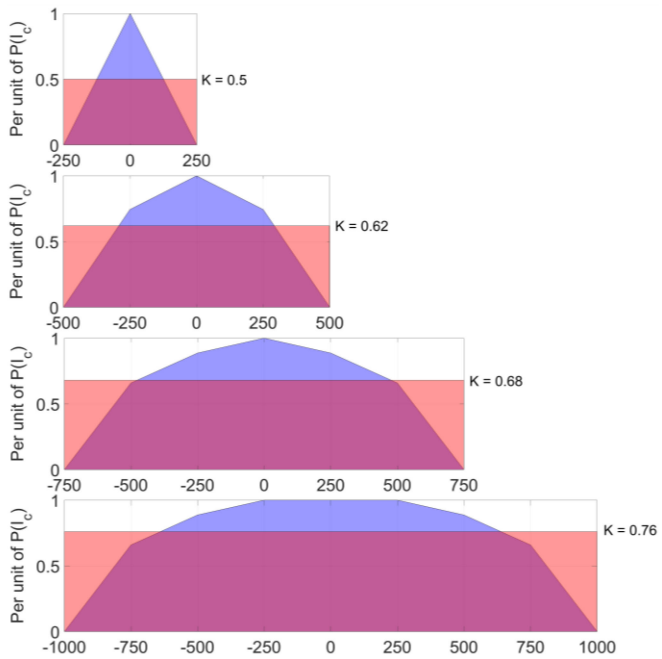

Fig. 13. Demonstration of the BF probability unitization and estimation of *K*.

field of leader progression used for crossarm is higher than the practical value recommended by CIGRE, which is necessary to be revised in experiments in further research. Thus, the actual BF performance might not be worse than simulating results.

B. Discussion on Span Flashover Coefficient K of Long-Distance PGTLs

In this section, the value of *K* is analyzed and discussed. In the past, most researchers used (10) to estimate BFR and $K = 0.6$ is recommended[7].

For PGTLs, the overvoltage caused by lightning flashes striking at the ungrounded pylon head in the middle of PGTLs is higher than at mid-span and at other pylon heads. Therefore, the backflashover probability at the ungrounded pylon in the middle of PGTLs is the highest. From middle to the grounded pylons, BF probability decreases. The value of *K* can be estimated by the unitization of BF probability.

The following Fig. 13 shows the estimation of *K* for the PGTLs of different distance for example. At the ends of the PGTLs, there are two grounded pylons. Within the PGTLs, there locate ungrounded pylons with the span of 250 m. The PGTLs length of 500 m, 1000 m, 1500 m, and 2000 m means the number of ungrounded pylons within PGTLs is 1, 3, 5, and 7 correspondingly. The origin of horizontal axis is where the middle ungrounded pylon locates. The first step is the unitization of BF probability, which means the highest BF probability is regarded as 1, and the unitized BF probability of other ungrounded pylons equals to the ratio of their BF probability to the highest BF probability. Thus, the unitized BF probability of the middle ungrounded pylon is 1 and the BF probability at grounded pylons are extremely low compared with that of middle pylon which can be regard as 0. From the middle ungrounded pylon to the grounded pylon, the unitized BF probability decreases from 1 to 0 and the height of every pylon is its unitized probability. The second step is the probability average. As a result of the first step, the blue region in Fig. 12 is the unitized BF probability distribution of every pylon in PGTLs. The red region is in the same area of the blue region, which averages the unitized BF probability of pylon to the entire line. Because of unitization, the height of red region is the value of *K*. Finally, the product of *K* multiplying the highest BF probability of pylon in PGTL is the BF probability of the entire line.

It can be derived that the value of K increases and approaches to 1 but always less than 1, along with the increasing of the distance of PGTLs. In this case, the *K* for PGTLs with different lengths, represented by the amount of ungrounded pylons *N* within PGTLs, can be induced in following equation (11). When *N* ranges from 1 to 4, *K* is from 0.5 to 0.65. To be concise in equation, before the amount of ungrounded pylons *N* increases to the critical amount for stabilization, *K* is compromised and unified as 0.6 here referring to the value recommended by CIGRE. When *N* exceeds 5, the BF probability starts to stabilize and the value of *K* is formulated by *N*.

$$K = \begin{cases} 0.6 & (1 \le N \le 4) \\ 1 - \frac{1.9}{N+1} & (N \ge 5) \end{cases} \tag{11}$$

VI. Conclusion

This paper investigated the backflashover performance of a partial grounding scheme of OHLs supported by a novel fully composite pylon. The OHLs was established and the transient analysis was carried out in PSCAD based on Monte Carlo method. A coefficient used in the equation estimating backflashover rate is discussed and modified when it is used in partial grounding OHLs. The following conclusions can be drawn:

1) For common OHLs supported by composite pylons without using PGTLs, reducing footing resistance and soil resistivity of grounded pylons can improve backflashover performance effectively according to the local soil characteristics in Denmark.
2) For PGTLs supported by composite pylons, when the lightning strikes at the ungrounded pylon, reducing footing resistance and soil resistivity of grounded pylons at the both ends of PGTLs does not have obvious effect. Increasing insulation distance has limited effect to some extent. Future emphasis may lie in the application and coordination of surge arresters.
3) For PGTLs supported by composite pylons, lightning overvoltage is mainly dependent on the distance to the nearer grounded pylon and longer distance to the nearest grounded pylon will cause overvoltage with larger amplitude and longer wave front duration. Future research will consider corona effect during the propagation of overvoltage on shield wires.
4) For PGTLs supported by composite pylons, BF probability and BFR increase along with the longer distance of PGTLs, but are limited to a certain value, which is determined by the lightning current probability distribution in the nature and the threshold electric field of leader progression development.

5) The value of the coefficient K to estimate BFR considering the lightning striking in mid-span of shield wire has been examined for PGTLs. K increases and approaches to 1, along with the increasing of the distance of PGTLs supported by composite pylons.

REFERENCES

[1] BYSTRUP, "Composite pylon," Accessed: Jun. 2019. [Online]. Available: https://www.powerpylons.com/composite-pylon

[2] T. Jahangiri, Q. Wang, C. L. Bak, F. F. da Silva, and H. Skouboe, "Electric stress computations for designing a novel unibody composite cross-arm using finite element method," *IEEE Trans. Dielectrics Elect. Insul.,* vol. 24, no. 6, pp. 3567–3577, Dec. 2017.

[3] C. Hu *et al.*, "Investigation on 110kV composite material pole: Effects of grounding methods on insulation of conductor-pole gaps," in *Proc. IEEE Int. Conf. High Voltage Eng. Application*, 2016, pp. 1–5.

[4] J. Li, *Measurement and Analysis of Overvoltages in Power Systems*. Hoboken, NJ, USA: Wiley, 2018.

[5] T. Udo, "Estimation of lightning shielding failures and mid-span backflashovers based on the performance of EHV double circuit transmission lines," *IEEE Trans. Power Del.*, vol. 12, no. 2, pp. 832–836, Apr. 1997.

[6] N. Rugthaicharoencheep, W. Thansiphraserth, and A. Phayomhom, "Comparison voltage across insulator strings of 69 kV and 24 kV lines due to lightning strokes to top pole and mid span," in *Proc. 47th Int. Univ. Power Eng. Conf.*, 2012, pp. 1–5.

[7] A. R. Hileman, *Insulation Coordination for Power Systems (POWER ENGINEERING)*. New York, NY, USA: Taylor & Francis Group, 1999.

[8] Y. Han, L. Li, H. Chen, and Y. Lu, "Influence of modeling methods on the calculated lightning surge overvoltages at a UHVDC converter station due to backflashover," *IEEE Trans. Power Del.,* vol. 27, no. 3, pp. 1090–1095, Jul. 2012.

[9] M. S. Banjanin and M. S. Savić, "Some aspects of overhead transmission lines lightning performance estimation in engineering practice," *Int. Trans. Elect. Energy Syst.,* vol. 26, no. 1, pp. 79–93, Jan. 2016.

[10] W. S. 33, "Guide to procedures for estimating the lightning performance of transmission lines," *CIGRE*, 1991, vol. 63.

[11] J. A. Martinez and F. Castro-Aranda, "Tower modeling for lightning analysis of overhead transmission lines," in *Proc. IEEE Power Eng. Soc. Gen. Meeting*, 2005, vol. 2, pp. 1212–1217.

[12] T. Hara and O. Yamamoto, "Modelling of a transmission tower for lightning-surge analysis," *IEE Proc. - Gener., Transmiss. Distrib.,* vol. 143, no. 3, pp. 283–289, 1996.

[13] T. Hara, Y. Yasuda, Y. Hirakawa, N. Hayanose, K. Nomura, and K. Kawabata, "Flashover analyses of 500 kV transmission towers with nonlinear and capacitive grounding impedance model," in *Proc. 11th Int. Symp. High Voltage Eng.*, Aug. 1999, vol. 2, pp. 292–295.

[14] A. M. Mousa, "The soil ionization gradient associated with discharge of high currents into concentrated electrodes," *IEEE Trans. Power Del.,* vol. 9, no. 3, pp. 1669–1677, Jul. 1994.

[15] F. E. Asimakopoulou, I. F. Gonos, and I. A. Stathopulos, "Methodologies for determination of soil ionization gradient," *J. Electrostatics,* vol. 70, no. 5, pp. 457–461, Oct. 2012.

[16] T. Shindo and T. Suzuki, "A new calculation method of breakdown voltage-time characteristics of long air gaps," *IEEE Trans. Power App. Syst.,* vol. PAS-104, no. 6, pp. 1556–1563, Jun. 1985.

[17] A. Pigini, G. Rizzi, E. Garbagnati, A. Porrino, G. Baldo, and G. Pesavento, "Performance of large air gaps under lightning overvoltages: Experimental study and analysis of accuracy predetermination methods," *IEEE Trans. Power Del.,* vol. 4, no. 2, pp. 1379–1392, Apr. 1989.

[18] X. Chen, X. Wen, and L. Lan, "Application of the leader progression model in the insulation flashover criterion for lightning performance calculation," in *Proc. 2nd Int. Conf. Mechatronics Autom. Control*, W. Wang, Ed. Cham: Springer International Publishing, 2015, pp. 459–466.

[19] D. Filipović-Grčić, B. Filipović-Grčić, D. Brezak, I. Uglešić, and A. Tokić, "Leader progression model application for calculation of lightning critical flashover voltage of overhead transmission line insulators," in *Proc. Int. Conf. Lightning Protection*, Sept. 2012, pp. 1–8.

[20] P. Sarajcev, "Monte Carlo method for estimating backflashover rates on high voltage transmission lines," *Electric Power Syst. Res.,* vol. 119, pp. 247–257, Feb. 2015.

[21] A. J. Eriksson, "An improved electrogeometric model for transmission line shielding analysis," *IEEE Trans. Power Del.,* vol. 2, no. 3, pp. 871–886, Jul. 1987.

[22] F. H. Silveira, S. Visacro, and R. E. Souza, "Lightning performance of transmission lines: Assessing the quality of traditional methodologies to determine backflashover rate of transmission lines taking as reference results provided by an advanced approach," *Electric Power Syst. Res.,* vol. 153, pp. 60–65, Dec. 2017.

[23] F. M. Gatta, A. Geri, S. Lauria, M. Maccioni, and A. Santarpia, "An ATP-EMTP Monte Carlo procedure for backflashover rate evaluation: A comparison with the CIGRE method," *Electric Power Syst. Res.,* vol. 113, pp. 134–140, Aug. 2014.

[24] F. M. Gatta, A. Geri, S. Lauria, M. Maccioni, and A. Santarpia, "An ATP-EMTP Monte Carlo procedure for backflashover rate evaluation," in *Proc. Int. Conf. Lightning Protection*, Sept. 2012, pp. 1–6.

[25] J. A. Gutierrez R, *et al.*, "Nonuniform transmission tower model for lightning transient studies," *IEEE Trans. Power Del.,* vol. 19, no. 2, pp. 490–496, Apr. 2004.

[26] K. Adhikari, "Soil mapping in denmark using digital soil mapping techniques," Ph.D. dissertation, AArhus Univ., 2013.

[27] X. Liu, J. Yang, G. Liang, and L. Wang, "Modified field-to-line coupling model for simulating the corona effect on the lightning induced voltages of multi-conductor transmission lines over a lossy ground," *IET Gener., Transmiss. Distrib.*, vol. 11, no. 7, pp. 1865–1876. [Online]. Available: https://digital-library.theiet.org/content/journals/10.1049/iet-gtd.2016.1340

[28] H. Motoyama, "Experimental study and analysis of breakdown characteristics of long air gaps with short tail lightning impulse," *IEEE Trans. Power Del.,* vol. 11, no. 2, pp. 972–979, Apr. 1996.

[29] X. Wang, Z. Yu, and J. He, "Breakdown process experiments of 110- to 500-kV insulator strings under short tail lightning impulse," *IEEE Trans. Power Del.,* vol. 29, no. 5, pp. 2394–2401, Oct. 2014.

Hanchi Zhang (Student Member, IEEE) was born in Liaoning, China, in 1993. He received the bachelor's and master's degrees in electrical engineering from North China Electric Power University, Beijing, China, in 2016 and 2019, respectively. He is currently working toward the Ph.D. degree in electrical engineering with the Department of Energy Technology, Aalborg University, Aalborg, Denmark. His research interests include lightning protection, electromagnetic transients, and insulation coordination.

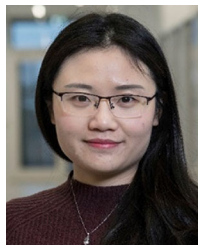

Qian Wang (Member, IEEE) was born in Hubei Province, China, in 1990. She received the bachelor's degree in electrical engineering from the Wuhan University of Technology, Wuhan, China, in 2012, the master's degree in high voltage engineering from the Huazhong University of Science and Technology, Wuhan, China, in 2015, and the Ph.D. degree in high voltage engineering from the Department of Energy Technology, Aalborg University, Aalborg, Denmark in 2018. She is currently an Assistant Professor with Aalborg University. Her research interests include electrical design or testing of innovative, composite-based transmission towers, and insulation in modern power electronic components.

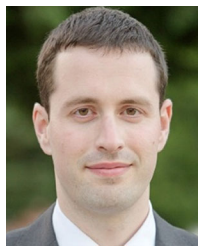

Filipe Faria da Silva (Senior Member, IEEE) received the M.Sc. degree in electrical and computers engineering from the Instituto Superior Técnico, Lisbon, Portugal, in 2008 and the Ph.D. degree in electric power systems from Aalborg University, Aalborg, Denmark, in 2011. In 2008, he was with EDP-Labelec and from 2008 to 2011, with Danish TSO Energinet. He is currently an Associate Professor with the Department of Energy Technology, Aalborg University, where he is also Semester Coordinator for the Electrical Power System and High Voltage Engineering Master Program and the Leader of the Modern Power Transmission Systems Research Program. His research interests include power cables, electromagnetic transients and insulation coordination, power quality, network stability, HVDC transmission, and HV phenomena.

Claus Leth Bak (Senior Member, IEEE) was born in Arhus, Denmark, on April 13th, 1965. He received the B.Sc. degree (Hons.) in electrical power engineering, the M.Sc. degree in electrical power engineering from the Department of Energy Technology, Aalborg University, Aalborg, Denmark, in 1992 and 1994, respectively, the Ph.D. degree in 2015 with the thesis EHV/HV underground cables in the transmission system. After his studies, he was a Professional Engineer with Electric Power Transmission and Substations with specializations within the area of Power System Protection with NV Net Transmission System Operator. In 1999, he was an Assistant Professor with the Department of Energy Technology, Aalborg University, where he is currently a Full Professor. He has supervised or co-supervised more than 45 PhD's and more than 50 MSc theses. His main research interests include corona phenomena on overhead lines, composite transmission towers, power system modeling and transient simulations, underground cable transmission, power system harmonics, power system protection, composite materials for EHV power pylons, and HVDC-VSC Offshore transmission networks. He is the author or coauthor of app. 370 publications. He is the Chair of the Danish Cigré National Committee, a Member of CIGRE Technical Council and Cigré SC C4 AG1. He is the Head of the Energy Technology Ph.D. program (+ 130 PhD's) and the Section of Electric Power Systems and Microgrids and is a Member of the Ph.D. Board with the Faculty of Engineering and Science. He was the recipient of the DPSP 2014 Best Paper Award, the PEDG 2016 Best Paper Award, the CIGRE Distinguished Member Award (2020), and the CIGRE TC Award (2020).

Kai Yin (Student Member, IEEE) received the B.Sc. degree in electrical engineering and the M.Sc. degree in high voltage and insulation technology from North China Electric Power University, Beijing, China, in 2015 and 2018, respectively. He is currently working toward the Ph.D. degree with the Department of Energy Technology, Aalborg University, Aalborg, Denmark. His research interests include lightning protection, insulating materials, and flashover mechanism.

Henrik Skouboe received the B.Sc. degree from the Royal Danish Academy of Fine Arts, Copenhagen, Denmark, in 1998. After that, he was worked on all types of transmission line projects from planning, alignment, and routing, to designing, optimization, and detailing. In 2010, he joined the architecture company Partner and the Director, Bystrup, Denmark. He is currently the Head of the company's department for infrastructure with projects, such as power line planning, design, procurement, and control.

Paper II

Electric Power Systems Research 196 (2021) 107263

Contents lists available at ScienceDirect

Electric Power Systems Research

journal homepage: www.elsevier.com/locate/epsr

Comparison of Backflashover performance between a novel composite pylon and metallic towers☆☆

H. Zhang [a,*], M. Ghomi [a], Q. Wang [a], F.Faria da Silva [a], C.L. Bak [a], K. Yin [a], H. Skouboe [b]

[a] Department of Energy Technology, Aalborg University, Aalborg 9100, Denmark
[b] BYSTRUP Architecture Design Engineering, København Ø 2100, Denmark

ARTICLE INFO

Keywords:
Backflashover rate
Fully composite pylon
Lightning overvoltages
Monte Carlo method
PSCAD
Frequency-dependent footing model

ABSTRACT

A design of a fully composite pylon with external grounding down-leads has been proposed for new-generation 400 kV transmission towers, able to save lines corridors and to reduce visual impact. This paper investigates and compares the backflashover performance of a composite pylon and two conventional metallic towers, which have been widely installed in Denmark. The transient models of overhead lines and all three towers were established respectively and the transient analysis was carried out in PSCAD. Monte Carlo method was used to estimate backflashover rate. The backflashover rate of composite pylon is 0.4526 cases per 100 km per year, which is in the same range, but slightly higher than that of metallic towers. The separated grounding down-leads of double circuits on composite pylon eliminates the danger of simultaneous backflashover of double circuits, which exists in transmission lines supported by metallic towers. After comparing the overvoltages to three phases of the three towers from backflashover, it is worthy considering that the installation of surge arresters at all three phases of composite pylon has a strong impact on the backflashover rather, but for the two metallic towers only the surge arresters at the upper phase has an impact.

1. Introduction

In recent years, usage of overhead lines (OHLs) in transmission system has been faced with great challenges, because of the increasing requirement for transmission capacity along with the public opposing to erect more conventional metallic towers, which have negative visual impact. A proposal for a fully composite pylon has been designed to meet the requirements of compact structure and elegant appearance for new-generation transmission towers [1]. The fully composite pylon is in shape of a 'Y' geometric configuration, shown in Fig. 1. (a). Conductors are fixed by clamps on the surface of the cross-arm, which has an inclined angle of 30° from the horizontal ground plane. Two shield wires are installed at the tips of the two cross-arms respectively. The cross-arms and the pylon body are made of fiber reinforced plastic (FRP). Therefore, the pylon itself cannot conduct lightning current if struck by lightning flashes. Correspondingly, as one choice of grounding schemes, two bare-metal conductors are installed outside the pylon to conduct the lightning current to ground when shield wires are terminated by lightning flashes, which are shown in Fig. 1. (a).

By contrast, variant metallic towers are still the mainstream in transmission power grid at present. Two types of conventional metallic towers, which have been widely installed in Denmark, namely Donau tower and Eagle tower, are selected as comparison to assess the backflashover performance of the novel composite pylon [2]. The configuration and dimension of two metallic towers are shown in Fig. 1. (b) and (c).

The novel pylon has a more compact configuration and reduced height due to elimination of insulator strings. However, there is little experience and research on the lightning performance evaluation of a pylon with such an unusual electric design. In [3], the backflashover evaluation based on constant footing resistance, critical flashover determination and single-variable lightning waveform is performed, but the simulation procedure can be improved. Considering differences between the novel fully composite pylon and conventional metallic towers, several features need to be emphasized when evaluating backflashover performance. Firstly, compared to the OHLs supported by conventional metallic towers, the OHLs supported by composite pylons have more compact configuration with shorter spans, which reduces the

☆ Paper submitted to the International Conference on Power Systems Transients (IPST2021) in Belo Horizonte, Brazil June 6–10, 2021.

* Corresponding author.
E-mail addresses: hazh@et.aau.dk (H. Zhang), qiw@et.aau.dk (Q. Wang), ffs@et.aau.dk (F.Faria da Silva), clb@et.aau.dk (C.L. Bak), kyi@et.aau.dk (K. Yin), hs@bystrup.dk (H. Skouboe).

https://doi.org/10.1016/j.epsr.2021.107263
Received 3 November 2020; Received in revised form 28 February 2021; Accepted 7 April 2021
Available online 30 April 2021

tail time of transient overvoltage at insulation [4]. Secondly, compared to the metallic tower body as lightning current grounding path, the grounding down-leads of composite pylons have larger inductance. Thirdly, mainstream, both theoretical and experimental research on insulation flashover for OHLs is based on ceramic insulators. The polymeric cross-arms of novel pylons, which are more similar to polymeric insulators, tend to have shorter dry-arc distance than ceramic ones [5].

This paper deals with the PSCAD implementation of Monte Carlo Method (MCM) for the backflashover rate (BFR) evaluation of the novel fully composite pylon and its backflashover performance is compared with two widely-installed metallic towers in Demark. Chapter II describes the modeling details for the backflashover analysis of composite pylons and proposes a procedure to evaluate BFR using MCM. Results in Chapter III shows that although BFR of composite pylon is higher than metallic towers, composite pylon will not suffer simultaneous backflashover of double circuits, but the backflashover on three phases are the same severe.

2. Simulation model and procedure for Backflashover analysis

2.1. Lightning current model

CIGRE lightning current model is used because of its consistency with the waveshape of lightning flashes in the nature. Four variables are used in analytical expressions to shape the lightning current waveshape of the first stroke of the downward flash recommended by CIGRE [6], namely lightning current amplitude I_c, maximum steepness S_m, front time (from 30% to 90%) t_f, and tail time t_h. All the parameters yield to log-normal distribution.

In this paper, I_c and t_f are treated as variables to shape the lightning current waveform. t_h is set as constant equal to its median after concluding that it has little effect on overvoltage level. S_m is set as per unit value determined by I_c and t_f and its base value is equal to the quotient by the medians of I_c and t_f.

2.2. OHL model

The simulated double-circuit OHL is 100 km long, at the rated voltage of 400 kV and highest system voltage of 420 kV. At one end of the OHL, phase conductors are connected with a three-phase voltage source and shield wires are solidly grounded. At the other end, the OHL is connected to a load. The tested transmission tower under research is set in the middle, 50 km to both ends of the whole line. Six adjacent transmission towers are modelled in details because the tower in longer distance have little impact on the overvoltage at the head of tower struck by lightning. The span is 250 m. Fig. 2 shows a schematic of the model. In the study of the three transmission towers, only the model of different towers is replaced.

2.3. Down-leads and tower model

The surge impedance of the down-leads varies according to the geometry, as the lightning wave travels from top to ground. To cope with this behavior, the models based on non-uniform transmission lines is considered [7].

The tower model is established by horizontal cylindrical conductors representing cross-arms and vertical cylindrical conductors representing tower bodies. The down-leads model is established as a combination of horizontal and vertical segments. The part along with pylon body is treated as a vertical cylindrical conductors and the part along with the cross-arm is treated as three horizontal cylindrical conductors. The 'Bergeron Model' in PSCAD is used to simulate the transient characteristics of each segment [8]. The surge impedance of vertical segments Z_v can be calculated as Eq. (1) and surge impedance of horizontal segments Z_h can be calculated as Eq. (2) [9],

$$Z_v = 60(\ln(h_v / r) - 1) \tag{1}$$

$$Z_h = 60\ln(2h_h / r) \tag{2}$$

where r is the radius of each segment and h is the height of different segment. To be noted, the height of the vertical part h_v is from earth bottom to top and the height of each horizontal segments h_h is from earth bottom to the center of each segment.

2.4. Frequency-dependent tower footing impedance model

In lightning studies estimating backflashover rate for transmission lines, modeling of grounding systems plays an important role, because the lightning current contains a very high frequency. With this regard, if the high frequency grounding system impedance is not sufficiently low, the resultant overvoltages may reach a level leading to insulation failure. In recent years, the full-wave electromagnetic field methods have

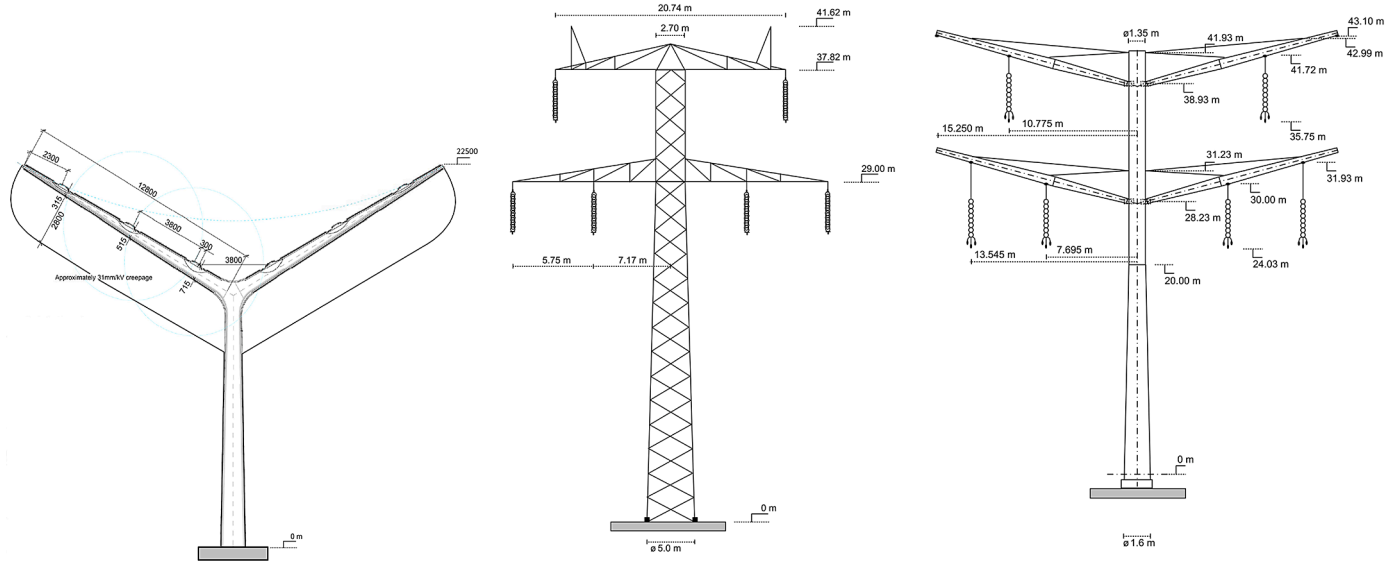

(a) Composite pylon (b) Donau tower (c) Eagle tower

Fig. 1. The sketch and configuration of all three transmission towers (not in real relative scale).

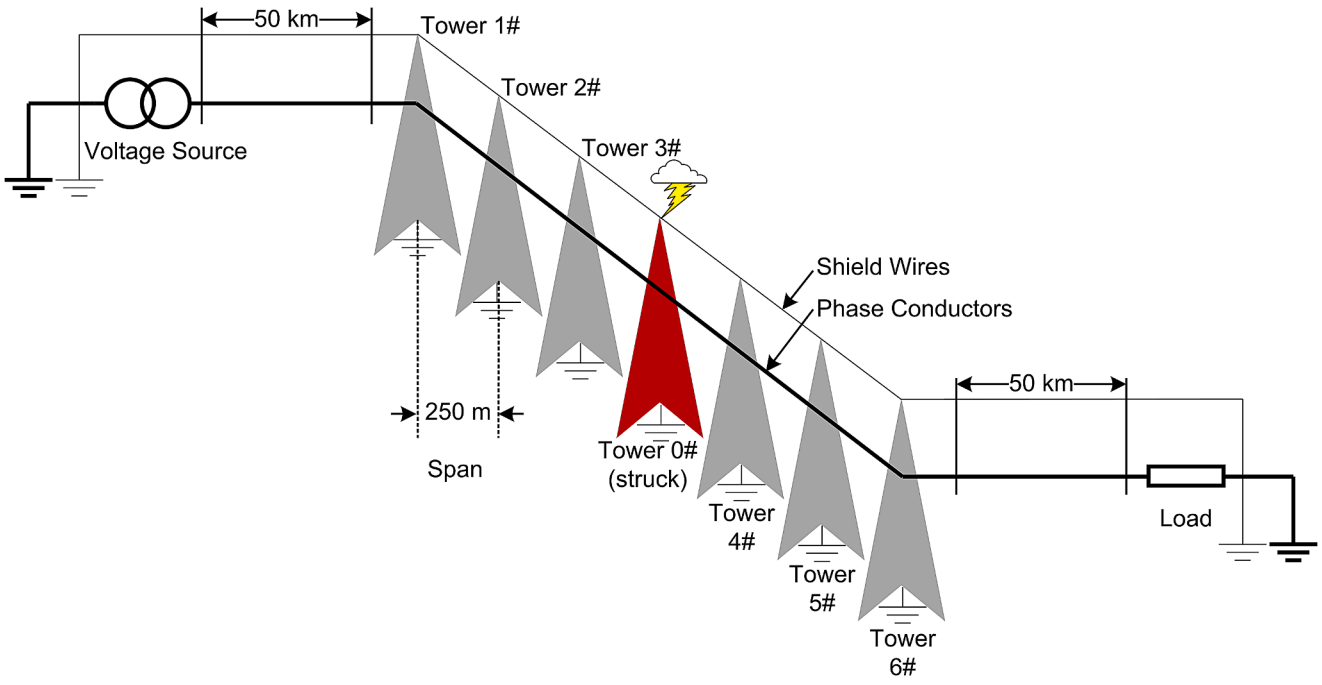

Fig. 2. The demonstration of OHL lines model.

been applied for modeling tower grounding system based on both the time and frequency domain numerical solution of Maxwell's equations, for instance, the finite difference time domain (FDTD) method [10], the finite element method (FEM) [11] and the method of moment (MoM) [12].

This paper adopts the same approach presented in [13-16] for frequency dependent modeling of grounding system. Firstly, the grounding system impedance matrix over the frequency range of interest is obtained by applying the full-wave approach MoM solution to Maxwell's equations. In this method, the governing electric field integral equation is formulated for the induced currents along the grounding conductor segments by making use of the MoM, which provides the current distribution along the grounding segments. Then, a rational approximation of the grounding system admittance matrix is obtained by making use of vector fitting techniques in the frequency domain [17]. Finally, the obtained rational approximation is employed to generate a model of the grounding system expressed in the form of state-space equations, which can be simulated and expressed for in the time-domain blocks in electromagnetic transient software.

In this paper, the footing condition is set as a vertical electrode buried in a two-layer soil. The length and the cross section radius of the electrode are $L = 3$ m and $r = 15$ mm respectively. The soil is characterized by resistivity of 100 Ω•m and 1000 Ω•m for upper and lower layer respectively. The relative electric permittivity is set as 10.

2.5. Leader progression model for flashover

Leader progression method (LPM) considers the physical process of air gap discharge to describe insulation surface flashover, which mainly consists of two stages: the streamer progression stage T_s and the leader progression stage T_l. T_s can be calculated as follow [18],

$$T_s = \frac{1}{k_1(E/E_{50\%}) - k_2} \tag{6}$$

where E is the maximum electric field before insulation flashover while $E_{50\%}$ is the electric field under CFO. k_1 and k_2 are the factors of streamer progression time, which are recommended to be 1.25 and 0.95 respectively.

T_l can be calculated based on its velocity recommended by CIGRE as follow,

$$\frac{dx}{dt} = ku(t)\left(\frac{u(t)}{D-x} - E_l\right) \tag{7}$$

where x is the length of the leader, $u(t)$ is the voltage between the air gap, D is the length of insulation, E_l is the threshold electric field of leader progression and k is the factor of leader progression speed. E_l and k are related to the type of the insulators and the polarity of the lightning impulse voltage, which are obtained from experiments [19].

2.6. BFR estimation procedure

The BFR evaluation procedure based on MCM uses the statistical result of quantities of single random lightning protection case to evaluate backflashover (BF) probability. The procedure consists of three steps: pre-processing step, numerical simulation step and post-processing step.

In pre-processing step, a large number, N_{total}, of lightning currents are generated to simulate the randomness and statistics of lightning flashes in the nature. Because the front time of lightning current follows log normal distribution, a group of front times are generated using inverse transform sampling. The median of log-normal distribution of I_c can be obtained according to the value of t_f in Eq. (8) [20],

$$M_I = 19.5 \cdot {t_f}^{0.39} \tag{8}$$

With every front time, a group of lightning current amplitudes can be generated. The number of different front times is 100 and the number of different lightning current amplitudes corresponding to every front time is also 100, thus, the number of lightning currents N_{total} is 10,000.

In numerical simulation step, all lightning currents derived from last step were input in OHLs model in PSCAD as lightning impulse current source.

The BF probability for every lightning current was estimated considering the operating voltage on phase conductors. When using LPM to determine the occurrence of backflashover, $u(t)$ in Eq. (7) is the voltage at the air gap, which is the difference between the overvoltages and the operating voltage V on phase conductors. The operating voltage

can be regarded as a constant during lightning transients, because of the relatively extremely short duration of overvoltage. The result after determination of LPM to a certain $u(t)$ is only 1 (flashover) or 0 (not flashover). Thus, there is a critical operating voltage V_i. The voltage difference between overvoltage and the operating voltage larger than V_i can definitely cause flashover, and the voltage difference between overvoltage and the operating voltage smaller than V_i cannot cause flashover. The BF probability can be estimated as the ratio of the duration in one cycle when the operating voltage is above V_i for the whole AC period.

In post-processing step, BFR is calculated after processing the results of BF probability of all lightning currents.

The BFR can be expressed in Eq. (9) [20],

$$BFR = 0.6 \cdot N_d \cdot \frac{\sum P(I_c)}{N_{total}} \tag{9}$$

where $\Sigma\ P(I_c)$ is the sum of the backflashover probability of every lightning current and N_{total} is the total number of lightning currents. N_d is the estimated number of lightning strikes that terminate on the 100-km line, which can be calculated by Eq. (10),

$$N_d = N_g \cdot \left(D + 28H^{0.6}\right) \cdot 10^{-1} \tag{10}$$

where N_g is the ground flash density describing the number of flashes that terminate on the ground per year per square kilometers. H is the tower height and D is the horizontal distance between shield wires. The numerical multiplicative coefficient 0.6 considers that overvoltage at the shield wire caused by lightning flashes striking within the span is lower than those striking at the pylon head. Consequently, BFR is reduced by 40% if mid-span striking is considered.

3. Results

3.1. Comparison of BF probability and BFR between composite pylon and metallic towers

The evaluation of total BF probability is based on MCM collecting every BF probability of quantities of lightning flashes with different front times and currents. The BF probabilities of the three transmission towers of all the lightning flashes with different front times and currents are shown as spectrums in Fig. 3.

A single spot in spectrum represents BF probability of a single lightning flash. The x-ordinate and y-ordinate of the spot are the front time and lightning current respectively. The color of spot represents the BF probability. Because the parameters of all lightning flashes are sampled following to their statistical probability distribution, lightning BF probability P_{BF} can be obtained by the sum of BF probabilities of all lighting flashes $\Sigma P(I_c)$ divided by the amount of lightning flashes N_{total}. It can be found that both metallic towers provide similar results and under lightning currents with front time shorter than around 3 μs composite pylon also has similar backflashover performance. However, under lightning currents with longer front time, compared with the results from metallic towers, the minimum lightning current to cause back-flashover on composite pylon is lower, and BF probability caused by same lightning current is higher. As a result, lightning BF probability P_{BF} provided by composite pylon is higher than metallic towers.

After calculating the total lightning BF probability P_{BF}, the factors influencing BFR of the three towers are summarized in the Table 1. Compared with Donau tower and Eagle tower at the same lightning conditions, the composite pylon has lower height, which will attract fewer flashes, higher surge impedance, which will cause higher over-voltage, and shorter insulation distance, which means flashover is easier to occur at the same overvoltage. As a result, the BFR of composite pylon is 0.4526 cases per 100 km per year, which is a little higher than that of Donau tower and Eagle tower.

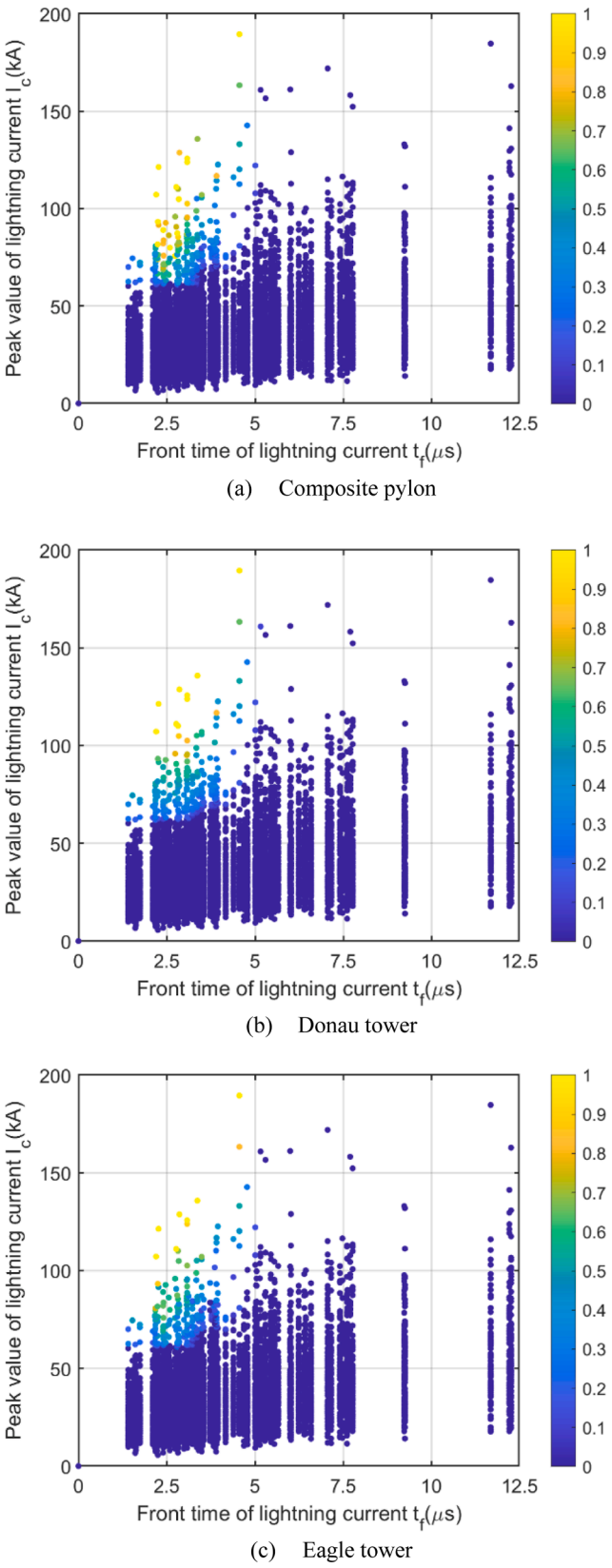

Fig. 3. BF probability spectrum after MCM.

3.2. Comparison of overvoltage of double circuit between composite pylon and metallic towers

All three transmission towers are designed to support double-circuit

Table 1
Factors influencing BFR of three transmission towers.

Tower type	Composite pylon	Donau tower	Eagle tower
Ground flash density N_g [cases/km^2•year]	1.39		
Tower height H [m]	22.50	41.62	43.10
Shielding distance D [m]	21.28	20.74	27.09
Line flash density N_d [cases/100 km•year]	20.26	28.3	29.60
DC footing resistance R_0 [Ω]	50		
Insulation length L [m]	2.8	3.2	3.72
CFO [kV]	1960	2240	2604
Total BF probability P_{BF}	0.0267	0.0134	0.0121
BFR [cases/100km•year]	0.4526	0.3176	0.2992

OHLs at 400 kV. For metallic towers, no matter which shield wires is struck, lightning current travels through the tower body to ground. High overvoltage rises across insulators, which may cause backflashover of both circuits. A review from Queensland Transmission Company shows that 4.7% of the outage faults of a 275 kV transmission line were double circuit outages [21]. Multi-circuit outages account for 33.7% of total lightning caused faults in Korea [22]. Although the probability of double circuit outage is lower than single circuit outage, double circuit outages often lead to especially severe power interruption problems. For composite pylons, two down-leads are separated from shield wires to ground individually. When one of shield wires is struck by lightning, high overvoltage only rises on one of the down-leads, which solely faces with the danger of backflashover.

Fig. 4 shows the overvoltage across cross-arm of composite pylon and insulators on metallic towers to the upper phase conductors of double circuits when lightning strikes at shield wires of one circuit. For composite pylons, the overvoltage is measured from tip of down-lead across cross-arm to upper phase conductors. For metallic towers, the overvoltage is from suspending points across insulators to upper phase conductors. The lightning parameters are the same for all three cases (80 kA, 3.83/77.5 μs) and the shield wires of circuit 1 is struck. Red lines show the overvoltage waveforms across insulation to the upper phase conductors in circuit 1, which is in the same side with shield wires struck by lightning. Black lines show the overvoltage waveforms across insulation to the upper phase conductors in the other circuit. It can be observed that, for Donau tower and Eagle tower, the overvoltages of both circuits are closely high. However, for composite pylon, the overvoltage in circuit 1 is of a quite high amplitude while the overvoltage in circuit 2 is of lower amplitude. The opposite phase between the overvoltage oscillations of double circuits shows the overvoltage in circuit 2 of composite pylon is caused by induction of the overvoltage in circuit 1 instead of direct lightning current, which results in lower amplitude.

The BF probability of all six cases are calculated according to MCM procedure introduced above and summarized in following Table 2. For Donau tower and Eagle tower, although lightning flash strikes only one of shield wires, both circuits are probable to occur backflashover at the same time. For composite pylon, the phase conductor in the same circuit with the struck shield wire is faced with higher BF probability, but the other circuit has little probability to occur backflashover.

In order to prevent the backflashover of both circuits under the strike of a single lightning flash, differential insulation may be adopted in conventional OHLs supported by metallic towers, to sacrifice one circuit with weaker insulation to protect the other circuit with stronger insulation [23]. By contrast, backflashover cases may occur at both circuits randomly in composite pylons and solely occur at the circuit with weaker insulation in metallic towers, which overloads insulation strength and shortens lifetime of insulators in metallic towers.

In summary, compared with conventional metallic towers, OHLs supported by composite pylons are not faced with simultaneous backflashover of double circuits. Compared with conventional metallic towers with differential insulation, OHLs supported by composite pylons

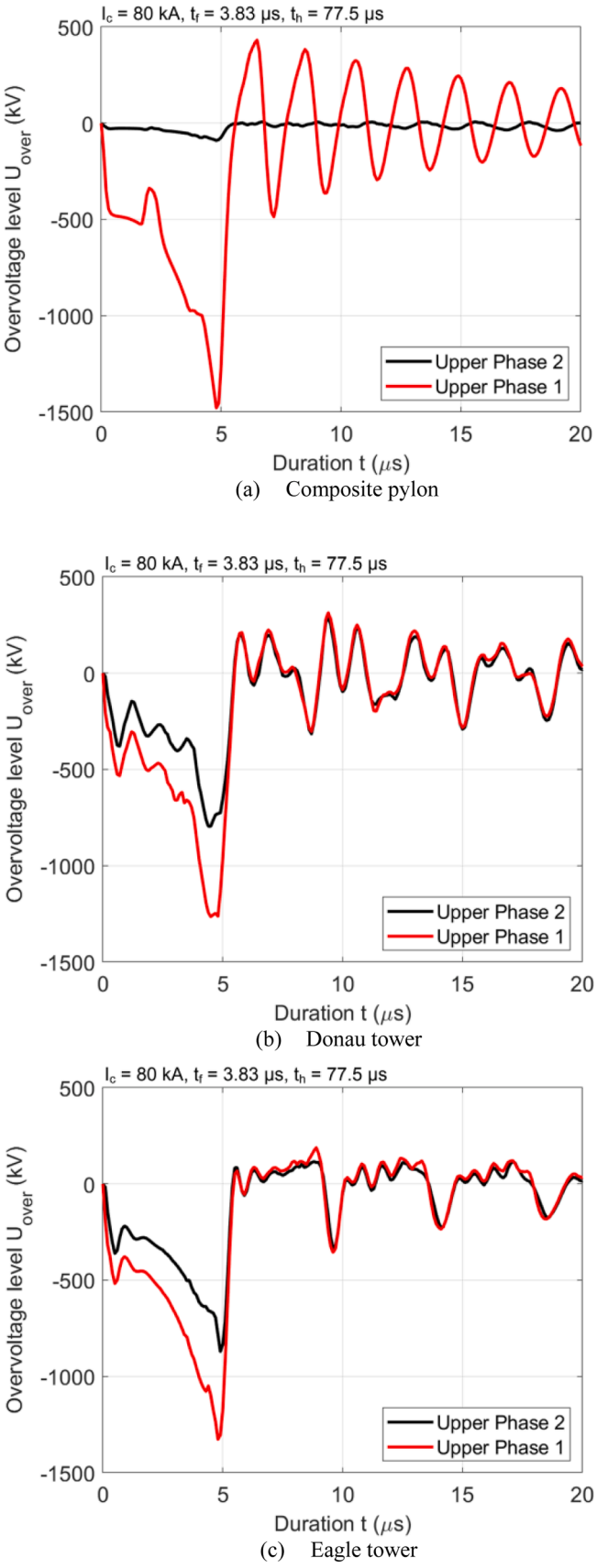

Fig. 4. Overvoltage across cross-arm (composite pylon) and insulators (metallic towers) to the upper phase conductors of double circuits when lightning strikes at shield wire of one circuit.

Table 2
Maximum and BF probability of the overvoltages threatening both double circuits of three transmission towers under the lightning (80 kA, 3.83/77.5 μs).

Tower type	Circuit No.	Max. overvoltage [kV]	BF probability
Composite pylon	1	−1479.20	0.4027
	2	−90.21	0
Donau tower	1	−1264.62	0.3251
	2	−795.18	0.0735
Eagle tower	1	−1326.80	0.3541
	2	−871.25	0.0950

have longer lifetime.

3.3. Comparison of overvoltage of three phases between composite pylon and metallic towers

The overvoltages of three phases in the same circuit of the three towers are shown in Fig. 5. The lightning parameters are the same for all three cases (80 kA, 2/77.5 μs). As for the composite pylon, the overvoltages are measured at the locations on the down-lead nearest to the phase conductors. As for the two metallic towers, the overvoltages are measured at the locations suspending the insulators and phase conductors. From the results, it can be found that the overvoltages on the down-lead of the composite pylon are of closely amplitudes and all three phase conductors are faced with backflashover of close probability. However, for metallic towers, the overvoltages at the suspending points of upper phase are far higher than the other two phases. In other words, the tower configuration has an important impact on the overvoltage of different phases according to their locations on the tower.

The application of surge arresters is a widely used method to protect transmission lines. If the surge arresters are installed at all three phases, this countermeasure will certainly have a best backflashover protection performance than if no surge arresters are installed. Considering the cost of surge arresters, it is economic to minimize the number of surge arresters if possible. The default surge arrester model in PSCAD is selected and Table 3 summarizes the BFR of the three towers using three different strategies of surge arrester installation. The first strategy is without surge arresters (No MOV). The second is to install surge arresters only on the upper phases (MOV-Upper). The third is to install surge arresters on all three phases (MOV-3-phase).

From the BFR results of the three towers, installing surge arresters on three phases leads to the best performance and installing upper-phase surge arresters is still better than no surge arresters, both results in accordance with the expectations. However, for the two metallic towers, the BFR of installing 3-phase surge arresters is only slightly lower than that of installing a surge arrester only on the upper phase. For composite pylons, installing 3-phase surge arresters has obviously lower BFR than installing only upper-phase surge arresters. Compared with the BFR without surge arresters, the BFR after installing surge arrester on upper phase decreases 32.90%, while the BFR after installing surge arresters on three phases decreases 86.01%. Thus, for metallic towers, it is not recommended to install surge arresters on all three phases out of economy, but it is worthy to consider installing surge arresters on all three phases of composite pylon for good backflashover performance.

To be noted, the above conclusions are only investigated from the aspect of backflashover performance. The installation of surge arresters is also need to be examined from the aspect of shielding failure in case that lightning directly strikes at the phase conductors.

4. Conclusions

This paper investigated and compared the backflashover performance of a novel fully composite pylon of 400 kV with external grounding down-leads with two conventional metallic towers widely installed in Denmark. The transient models of OHLs and all three towers were established and the transient analysis was carried out in PSCAD.

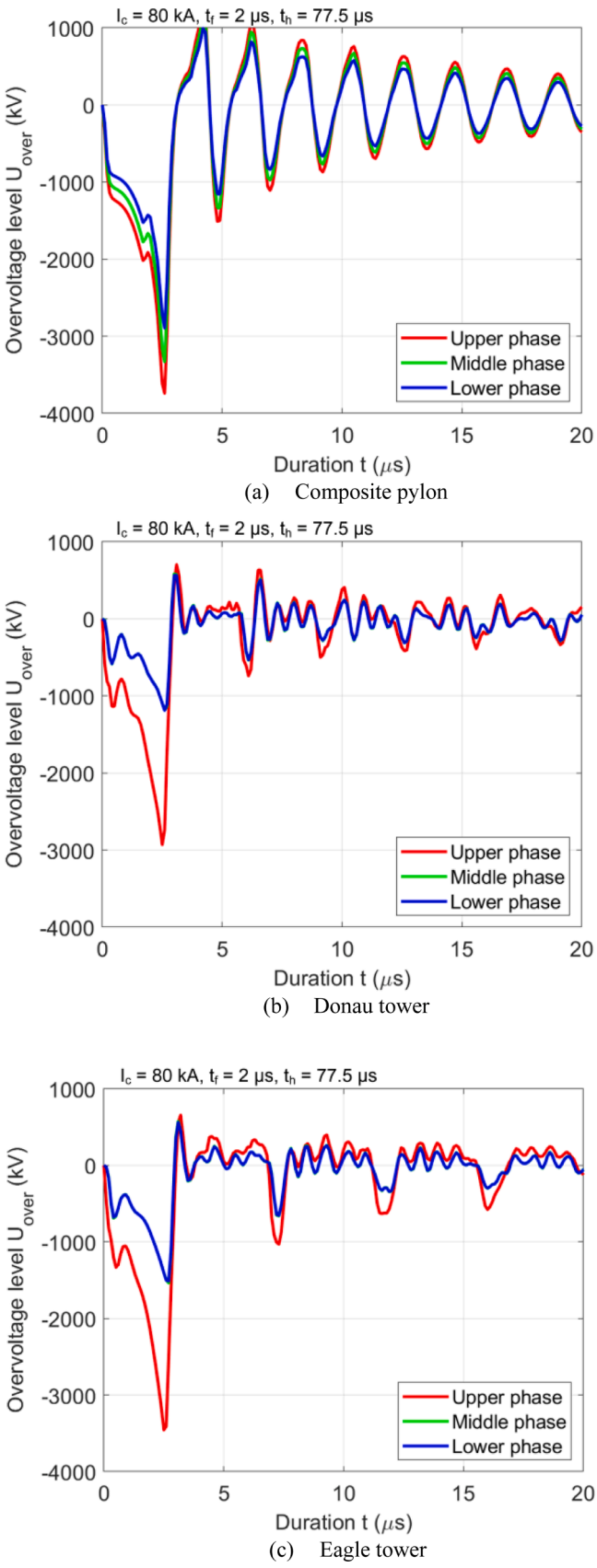

Fig. 5. Overvoltage across cross-arm (composite pylon) and insulators (metallic towers) to the conductors of three phases when lightning strikes at shield wire.

Table 3
Maximum and BF probability of the overvoltages threatening both double circuits of three transmission towers.

Tower type	Method	BFR [cases/100km•year]
Composite pylon	No MOV	0.4526
	MOV-Upper	0.3037(−32.90%)
	MOV-3-phase	0.0633(−86.01%)
Donau tower	No MOV	0.3176
	MOV-Upper	0.0825(−74.02%)
	MOV-3-phase	0.0622(−80.41%)
Eagle tower	No MOV	0.2992
	MOV-Upper	0.0794(−73.46%)
	MOV-3-phase	0.0591(−80.24%)

Monte Carlo method was used to simulate the randomness of lightning current waveforms in the nature in order to estimate the backflashover rate. Methods to improve the backflashover performance of composite pylons were proposed and analyzed. The following conclusions can be drawn:

(1) Compared with conventional metallic towers at the same lightning conditions, the compact configuration of composite pylons and larger surge impedance may attract fewer lightning flashes, but it presents higher overvoltage, resulting in higher BFR. The BFR of composite pylon is 0.4526 cases per 100 km per year, which is higher than Donau tower and Eagle tower.
(2) All three towers are designed to support double circuits. Compared with conventional metallic towers, OHLs supported by composite pylons are not faced with simultaneous backflashover of double circuits attributed to separated grounding down-leads.
(3) In the same circuit, where the shield wire is struck by lightning, the overvoltages on the down-lead of composite pylon are of closely amplitude, whereas the overvoltages across the upper phase insulators on the metallic towers are far higher than those of the other two phases. Thus, from backflashover, it might be worthy considering that all three phases of composite pylon are installed with surge arresters.

Credit author statement

Hanchi Zhang: Conceptualization, Methodology, Software, Writing - Original Draft Preparation
Mohammad Ghomi: Methodology, Software
Qian Wang: Supervision
Filipe Faria da Silva: Supervision, Software
Claus Leth Bak: Supervision
Kai Yin: Software
Henrik Skouboe: Supervision

Declaration of Competing Interest

The authors declare that they have no known competing financial interests or personal relationships that could have appeared to influence the work reported in this paper.

References

[1] BYSTRUP. "THE COMPOSITE PYLON." https://www.powerpylons.com/composite-pylon (accessed).
[2] T. Ebdrup, D. Olason, K. Pederson, C.L. Bak, F.F. Silva, Comparison of overhead line lightning performance based on two different tower geometries, in: Presented at the Cigré International colloquium on lightning and power systems, Lyon, 2014.
[3] K. Velitsikakis, F.M.F. da Silva, Q. Wang, C.L. Bak, H. Skouboe, Performance analysis for the innovative 400kV Double-Circuit'Y'Composite tower under backflashover conditions. CIGRE International Colloquium on Lightning and Power Systems 2019, CIGRE (International Council on Large Electric Systems, 2019.
[4] W.A. Chisholm, New challenges in lightning impulse flashover modeling of air gaps and insulators, IEEE Electric. Insulat. Mag. 26 (2) (2010) 14–25, https://doi.org/10.1109/MEI.2010.5482551.
[5] S. Venkataraman, R.S. Gorur, Prediction of flashover voltage of non-ceramic insulators under contaminated conditions, IEEE Trans. Dielectric. Electric. Insulat. 13 (4) (2006) 862–869, https://doi.org/10.1109/TDEI.2006.1667747.
[6] W. S., Guide to procedures for estimating the lightning performance of transmission lines, CIGRE 63 (1991).
[7] J.R. Martí, A. Tavighi, Frequency-dependent multiconductor transmission line model with collocated voltage and current propagation, IEEE Transactions on Power Delivery 33 (1) (2018) 71–81, https://doi.org/10.1109/TPWRD.2017.2691343.
[8] J.A. Martinez, F. Castro-Aranda, Tower modeling for lightning analysis of overhead transmission lines, in: IEEE Power Engineering Society General Meeting, 2005 2, 2005, pp. 1212–1217, https://doi.org/10.1109/PES.2005.1489355, 16-16 June 2005.
[9] T. Hara, O. Yamamoto, Modelling of a transmission tower for lightning-surge analysis, IEE Proceedings - Generation, Transmission and Distribution 143 (3) (1996) 283–289, https://doi.org/10.1049/ip-gtd:19960289.
[10] M. Tsumura, Y. Baba, N. Nagaoka, A. Ametani, FDTD simulation of a horizontal grounding electrode and modeling of its equivalent circuit, IEEE Trans. Electromagnetic Compatib. 48 (4) (2006) 817–825, https://doi.org/10.1109/TEMC.2006.884448.
[11] L. Qi, X. Cui, Z. Zhao, H. Li, Grounding performance analysis of the substation grounding grids by finite element method in frequency domain, IEEE Trans. Magn. 43 (4) (2007) 1181–1184, https://doi.org/10.1109/TMAG.2007.892283.
[12] V.A. Toseva, L. Grcev, K.E.K. Drissi, High frequency performance of ground rod in two-layer soil, in: IEEE EUROCON 2017 -17th International Conference on Smart Technologies, 2017, pp. 914–918, https://doi.org/10.1109/EUROCON.2017.8011244, 6-8 July 2017[Online]. Available: https://ieeexplore.ieee.org/document/8011244/.
[13] L. Grcev, Modeling of grounding electrodes under lightning currents, IEEE Trans. Electromagnetic Compatib. 51 (3) (2009) 559–571, https://doi.org/10.1109/TEMC.2009.2025771.
[14] L. Grcev, Impulse efficiency of ground electrodes, IEEE Trans. Power Del. 24 (1) (2009) 441–451, https://doi.org/10.1109/TPWRD.2008.923396.
[15] M. Ghomi, C.L. Bak, F.M.F. da Silva, Frequency dependence of multilayer soil electrical parameters: effects on ground potential rise, in: International conference on Lightning protection: ICLP2020, 2020.
[16] M. Ghomi, C.L. Bak, F.M.F. da Silva, Frequency dependence of multilayer soil electrical parameters: effects on the input impedance of grounding systems, in: 16th International conference on AC and DC power transmission.: IET event, 2020.
[17] B. Gustavsen, Computer code for rational approximation of frequency dependent admittance matrices, IEEE Trans. Power Del. 17 (4) (2002) 1093–1098.
[18] A. Pigini, G. Rizzi, E. Garbagnati, A. Porrino, G. Baldo, G. Pesavento, Performance of large air gaps under lightning overvoltages: experimental study and analysis of accuracy predetermination methods, IEEE Trans. Power Del. 4 (2) (1989) 1379–1392, https://doi.org/10.1109/61.25625.
[19] X. Chen, X. Wen, L. Lan, Application of the leader progression model in the insulation flashover criterion for lightning performance calculation, in: W. Wang (Ed.), Proceedings of the Second International Conference on Mechatronics and Automatic Control, Cham, Springer International Publishing, 2015, pp. 459–466, 2015//.
[20] A.R. Hileman, *Insulation Coordination for Power Systems* (POWER ENGINEERING), Taylor & Francis Group, 1999.
[21] J. Gillespie, G. Stapleton, Improving double circuit transmission line reliability through lightning design, Cigré (2004) B2–301.
[22] J. Kwak, J. Woo, E. Shim, H. Kim, J. Moon, Application of arrester to double circuit transmission line to enhance lightning performance and introduction about the obtained lightning waveforms by monitering systems, in: 19th International Lightning Detection Conference, Tucson, Arizona, USA, 2006, pp. 24–25.
[23] W. C4.301, Use of surge arresters for lightning protection of transmission lines, CIGRE Tech. Brochur. (2010).

Paper III

Backflashover Performance of a Composite Pylon with External Grounding Down-leads Modeled in Dynamic Surge Impedance Model considering Corona Effect

Hanchi Zhang, Mohammad Ghomi, Kai Yin, Qian Wang, Filipe Faria da Silva, Claus Leth Bak

AAU Energy
Aalborg University
Aalborg, Denmark
Email: hazh@energy.aau.dk

***Abstract*— Design of a novel 400 kV fully composite pylon utilizes external down-leads to bring grounding potential to earth wires. In lightning transient studies, the effect of the corona on the surge impedance of the thin-wire down-leads should not be neglected. A simplified dynamic surge impedance model for thin-wire conductors considering voltage-dependent surge corona is proposed and implemented on the grounding down-leads of the composite pylon. The model describes the relationship between corona development and surge overvoltage, it focuses on the macro effect of corona on the surge response of conductors, and it ignores the micro plasma dynamics inside the corona. Higher applied lightning current peaks will cause longer corona radius and cause more reduction on overvoltage. If the front time of applied lightning impulse current increases, the maximum corona radius increases first and then decreases, because the corona development is dominated by expansion velocity and critical streamer-tip electric field in succession. The dynamic surge impedance model shows a reduction of the overvoltage at the top of the conductor by 10% to 20% approximately compared with a constant surge impedance model without considering corona. The backflashover rate of composite pylon is reduced by 22.2 %, which is comparable to metallic towers. The necessity to consider corona effect in the lightning transients research of thin-wire grounding devices is stressed out and the composite pylons with thin-wire grounding down-leads can be an alternative of metallic towers.**

***Index Terms*—corona effect, fully composite pylon, lightning overvoltage, EMT, COMSOL**

I. INTRODUCTION

The increasing power demand requires the construction of additional power plants and transmission lines. In the past decades, many concepts of composite pylons have emerged to meet the requirements of more efficient, durable, and compact transmission towers[1]. If the pylon is fully made of composite materials, it raises a challenge that a method is needed to bring the ground potential to shield wires when lightning strikes. A direct method is installing grounding down-leads outside the pylon body to conduct lightning current to the ground, as shown in Fig.1. The external grounding down-leads are marked as red lines.

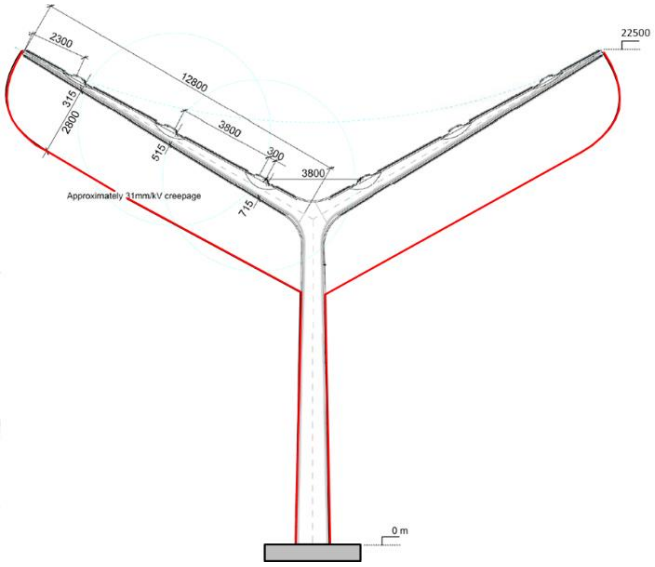

Fig. 1 A sketch of the configuration of the fully composite pylon with external grounding down-leads.

When a lightning flash strikes at the shield wires of the overhead lines, the lightning current passing through both the metallic tower and the down-leads of composite tower will cause corona discharge at the edges of conductive paths. In lightning electromagnetic transient studies, the tower is represented by means of one or several surge impedance sections that are assembled taking into account the tower structure[2]. The tower models neglect surge corona because of the relatively small corona radius compared with tower size. However, the grounding down-leads anticipated to install on

composite pylons are very thin, with a cross-section radius of a few centimeters, which is comparable to the corona developing radius during a lightning surge. Corona discharge around the down-leads decreases the surge impedance of the down-leads, distorts the wavefronts of overvoltage, and enhances the coupling effect between down-leads and phase conductors. Thus, the impact of surge corona on the transient performance of the grounding down-leads cannot be neglected.

The surge corona modeling for overhead lines has been studied for several decades. There are two main ways to model corona. One is to obtain a q-v curve by experiments first and then, reproduce the specific q-v curve by constructing linear, piecewise linear, or nonlinear circuits[3, 4]. However, it is practical for simulation to reproduce the q-v curve without field tests. Therefore, the other way is to attempt to reproduce the q-v curve from the geometrical configuration of the conductor and physical process. Some finite element method (FEM) simulating tools are used, but the modeling of plasma dynamics inside the corona makes the calculation quite time-consuming[5]. Recent research has simplified the corona dynamics then corona can be modeled by the finite-difference time-domain (FDTD) method in the simulation of large-scale transmission lines[6-8]. Another model considering the corona physical process is the corona shell model, which points out that space charges generated by the corona form a shell around the conductor[9]. This concept simplifies the modeling of corona around the thin-wire conductors considerably. The corona shell model was initially proposed for the calculation of steady-state corona, and it was applied to surge corona [10, 11]. There is little modeling research to be referred for the surge corona on grounding down-leads in the lightning study of composite pylons. The main difference lies in the vertical position in space of down-leads whereas overhead lines are horizontal. The corona modeling of trigger-wire of lightning triggering rockets can be referred because the trigger-wires and down-leads can be regarded as vertical cylinders and the presence of corona is regarded as the increasing radius of the cylinders[12, 13].

This paper proposed a simplified dynamic surge impedance model of thin-wire grounding down-leads considering voltage-dependent surge corona for the backflashover performance evaluation of a composite pylon. The model describes the relationship between dynamic corona development and surge overvoltage and focuses on the macro effect of corona on the surge response of conductors. The micro plasma dynamics inside corona are neglected, such as particle conservation with recombination, streamer development, and ionization. The corona effect is transferred into the circuit model, which is convenient to be implemented into EMT software. Section II introduces the basic modeling details of the entire transmission system and the procedure to evaluate backflashover rate. Section III reviews the surge corona dynamics and introduces the modeling details of surge corona development. The results are presented and discussed in Section IV. The corona developing processes under different lightning current waveforms are simulated, and the dominant factors determining different stages of corona development are analyzed. The reduction of considering surge corona on the lightning overvoltage and the backflashover rate is addressed, thus the importance of considering the corona effect for lightning transient studies on thin-wire grounding devices is stressed out.

II. MODELLING

A. Lightning Current Source Model

CIGRE lightning current model is used because of its consistency with the waveshape of lightning flashes in the nature. Four variables are used in analytical expressions to shape the lightning current waveshape of the first stroke of the downward flash, as recommended by CIGRE[14], namely lightning current peak amplitude I_c, maximum steepness S_m, front time (from 30% to 90%) t_f, and tail time t_h.

In this paper, I_c and t_f are treated as the variables to shape the lightning current waveform. t_h is set as constant as 75 μs because corona development is irrelevant to the wave tail of overvoltage. S_m is set as per unit value determined by I_c and t_f and its base value is equal to the quotient of I_c and t_f. Lightning channel impedance is set as 400 Ω [14].

B. Down-lead Model with Voltage-dependent Corona

The configuration of the down-lead is special, and the electric field distribution is different at the surface of the down-lead at different heights. Thus, the down-lead is divided into seven segments to get a more accurate simulation of corona sheath development. The dimension of every segment is shown in Fig. 2 on the left side. The bending and inclining segments are approximated into vertical and horizontal segments as shown in Fig. 2 on the right side.

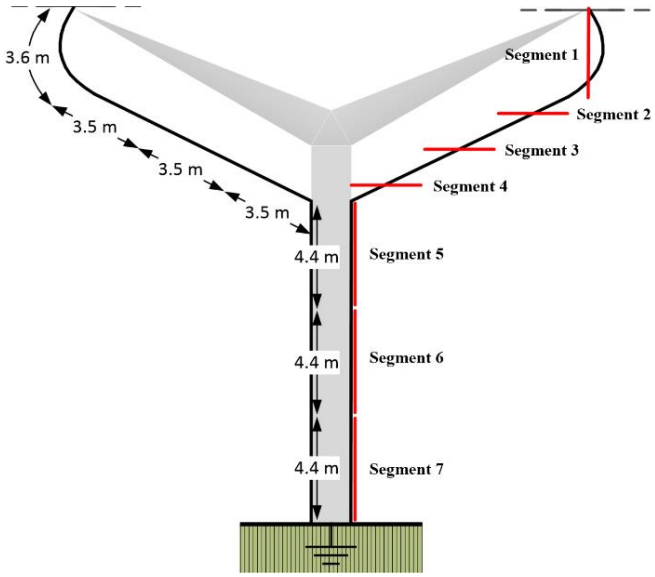

Fig. 2 The demonstration of down-lead segments and dimension

The surge impedance of the vertical cylindrical conductor has been evaluated for decades and Sargent's model is adopted. The corona sheath is regarded as the increasing radius of the conductor. Thus, the surge impedance of the vertical segments and the horizontal segment is described by the sum of conductor radius and corona radius, as described in equation (1) and (2) respectively [15],

$$Z_v = 60(\ln(\frac{h}{r+r_{cr}})-1) \quad (1)$$

$$Z_h = 60\ln(\frac{2h}{r+r_{cr}}) \quad (2)$$

where h is the height of the conductor, r is the cross-section radius of the conductor, and r_{cr} is the radius of corona sheath, which is voltage-dependent as described in the next chapter.

C. Other Simulating Models and Backflashover Rate Evaluation Procedure

The pylon footing is simulated by frequency-dependent model as described in [16]. The footing electrode is shaped as a cylindrical conductor buried vertically inside the soil, whose cross-section radius and length are 15 mm and 3 m respectively. The soil is modeled into two layers. The soil resistivity of upper and lower layers is 100 Ωm and 1000 Ωm.

The flashover is simulated by the leader progression model. The modeling details are identical as described in [17]. The transmission line model is established in PSCAD.

The evaluation procedure of backflashover rate (BFR) is the same as described in [17], which is based on the Monte Carlo method.

III. Description of Corona Development

Corona is the partial breakdown of the air in the vicinity of a conductor applied high electric stress. The physical properties of surge corona in the air are introduced at first.

One of the necessary conditions for corona to onset is that the electric field around the stressed conductor exceeds a critical threshold, namely corona inception electric field E_{cr} [18]. Correspondingly, the overvoltage causing E_{cr} is termed as corona inception overvoltage V_{cr}.

The other condition is the free electrons in high electric field area to induce a self-sustained electron avalanche. The occurrence of a specific electron and ionization to create space charge takes a certain time, namely statistical time lag, t_s [5].

The expansion of the corona sheath is governed by the guiding electric field E_g, which is the sum of the electric field created by conductor potential and the electric field created by space charges in the corona. The expansion velocity equals to the streamer velocity v_{cr}.

Corona effect only occurs when the applied voltage is increasing. Thus, the corona only expands and develops during wave front of impulse overvoltage instead of wave tail. A critical electric field at the streamer-tip of the corona sheath E_b is necessary for streamer propagation, which determines the maximum expansion radius of the corona sheath.

In summary, once the impulse overvoltage on the conductor rises and exceeds V_{cr}, the corona will onset after a delay of t_s. Then, corona expands at the velocity of v_{cr} and the electric field at the streamer's tip is limited by E_b until the overvoltage starts decreasing.

A. Corona Inception Electric Field

The corona inception electric field E_{cr} (kV/mm) of cylindrical conductors was investigated experimentally by Peek[18]. Afterwards, some more practical equations to evaluate E_{cr} were produced based on Peek's law[19, 20]. The equation by Hartmann is adopted[21],

$$E_{cr} = m \cdot 2.594 \cdot \left(1+\frac{0.1269}{r^{0.4346}}\right) \quad \text{[kV/mm]} \quad (2)$$

where m is the roughness coefficient of the conductor surface and equals to 0.5, r is the conductor radius in mm.

As a result, the corona inception electric field E_{cr} is calculated as 3 kV/mm. This value is imported into electric field evaluation of the vertical conductor in COMSOL to calculate critical voltage V_{cr}. According to the software results, V_{cr} from Segment 1 to Segment 7 is equal to 690 kV, 640 kV, 610 kV, 480 kV, 380 kV, 330 kV, and 300 kV.

B. Statistical Time Lag

Statistical time lag t_s is generally not related to the electric field and other electrostatic parameters but is related to air pressure, temperature, and other air conditions. Thus, it is directly referred to the experimental results of other scholars. In [5], t_s varies from 0.4 μs to 0.7 μs. In [22], t_s varies from 0.45 μs to 0.88 μs. In this paper, t_s is considered as 0.6 μs.

C. Corona Expansion and Shrinking Velocity

After electric field on the surface of conductor exceeds E_{cr}, corona effect onsets. The expansion velocity of corona concluded in [5] ranges from 0.3 m/μs to 2 m/μs under the voltage ranging from 300 kV to 500 kV. Besides, [23] reported the radial speed of negative corona streamer from conductor surface in coaxial cylindrical electric field equals to around 0.1 m/μs, while [24] also reported 0.1 m/μs as the speed for positive corona streamers. The highest speed in the literature is 4.4 m/μs [25]. In the recent simulating research on surge corona using FDTD, v_{cr} is estimated as a constant of 1 m/μs[8, 26, 27].

Corona expansion velocity v_{cr} is generally related to electric field. In COMSOL Plasma Module, a 1-D air corona discharge model is established. A simplified set of reactions that correctly describes the creation and destruction of electrons, ions and molecules of nitrogen in a background of dry air is used. The corona developing process under different voltage is shown in Fig. 3. It can be found that the corona radius approximately increases at a uniform velocity at the beginning and keeps constant gradually. Thus, v_{cr} is regarded as a constant related to voltage, and their relationship is fitted and imported into PSCAD.

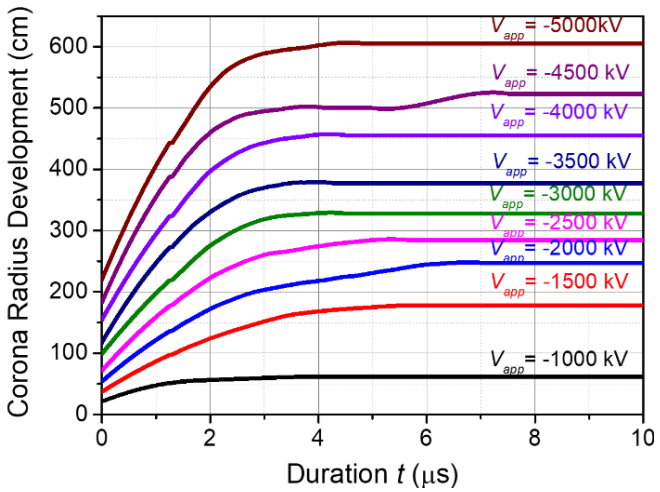

Fig. 3 Corona radius development process under different applied voltage

When the overvoltage reaches its crest, it decreases, and the corona will shrink until extinct. It is assumed that the corona shrinking velocity is equal to 1 m/s.

D. Streamer-tip Electric Field

A critical electric field at the streamer's tip limits the expansion of the corona, which determines the maximum extent of the radially expanding corona region. The critical streamer-tip electric fields at positive and negative polarity are as follows[28]. Only negative polarity is studied in this paper.

$$E_{bp} = 0.5 \quad \text{[kV/mm]} \tag{3}$$

$$E_{bn} = 1.5 \quad \text{[kV/mm]} \tag{4}$$

The corona sheath is assumed as an ideal conductor with a conductivity of 40 μS/m[8]. Electric field is produced both by conductor potential and the space charge in the corona. The space charge density distribution related to electric field is described by equation (5),

$$E(r) = \frac{Q}{2\pi\varepsilon_0 r} + \frac{Q}{2\pi\varepsilon_0 (2h - r)} \quad \text{[V/m]} \tag{5}$$

where $E(r)$ is the radial electric field, Q is the space charge per meter, h is the height from ground flat to top of vertical conductor, and r is the radial distance from center. For h>>r, equation (5) can be simplified into equation (6), then the space charge density distribution can be expressed by equation (7),

$$E(r) = \frac{Q}{2\pi\varepsilon_0 r} \quad \text{[V/m]} \tag{6}$$

$$\rho(r) = \frac{Q}{\pi r^2} = \frac{E(r)\cdot\varepsilon_0}{r} \quad \text{[C/m}^3\text{]} \tag{7}$$

Then equation (7) is given to the domain of corona, together with electric potential on the conductor to calculate the total electric field at the surface of corona. For every maximum corona radius, the applied voltage on conductor that causes the electric field at the surface of corona equal to E_b is calculated. Because the height of every segment to ground is different, the voltage to produce the same for every segment is also different. The relationship of corona radius and applied voltage is fitted in curves as shown in Fig. 4. As can be seen, maximum corona radius is related to overvoltage, thus is indirectly related to time, marked as $r_{max}(t)$.

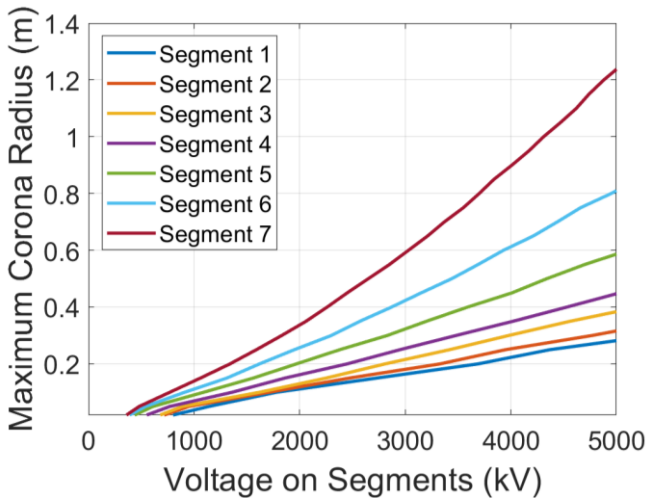

Fig. 4 Maximum corona radius limited by critical streamer-tip electric field under different polarities and amplitude of overvoltage on the conductor

E. Corona Radius

Based on above analysis and assumptions, a time-variant voltage-dependent surge impedance model is proposed to describe the expansion of corona during a lightning transient. When overvoltage on the down-lead exceeds V_{cr}, corona onsets. During expansion, $r_{cr}(t)$ is restricted by both the expansion velocity v_{cr} and the maximum expansion radius $r_{max}(t)$. When overvoltage reaches its crest and starts decreasing, corona starts shrinking at the shrinking velocity, which is numerically equal to expansion velocity v_{cr}, until corona extinguishes. Thus, it can be described as equation (8), where t_0 is the time when $r_{cr}(t_0)$ equals to 0.

$$r_{cr}(t) = \begin{cases} \min\{v_{cr}\cdot(t - t_s - t_{cr}), r_{max}(t)\}, & 0 < t \le t_f \\ r_{cr}(t_f) - v_{cr}\cdot(t - t_f), & t_f < t < t_0 \end{cases} \quad \text{[m]} \tag{8}$$

IV. Results and Discussion

A. Influence of Corona Developing on Surge Impedance and Overvoltage

The overvoltage, surge impedance, and corona radius influence each other in every time step. The surge impedance is in negative correlation with corona radius, and overvoltage is impacted by surge impedance. Then overvoltage induces the development of corona radius. When overvoltage meets the maximum, surge impedance is the lowest and corona radius is the largest, then corona starts shrinking.

Fig. 5 shows the mutual influence among overvoltage, surge impedance, and corona radius of Segment 1 as an example. The lightning current is of 80 kA/2 μs. When overvoltage exceeds V_{cr}, after a delay of t_s, corona starts developing at the velocity of v_{cr}. The stage of statistical time lag is marked in the blue shadow and the stage that corona develops at v_{cr} is marked in the red shadow. When the electric field of streamer's tip reaches E_{bn}, the electric field keeps constant as E_{bn} and limits the corona radius to change with the curve in Fig. 4. The stage that corona develops limited by E_{bn}

is marked in the orange shadow. When overvoltage meets crest and starts decreasing, surge impedance is the lowest and corona radius is the largest, then corona starts shrinking. The stage when corona shrinks is marked in the yellow shadow.

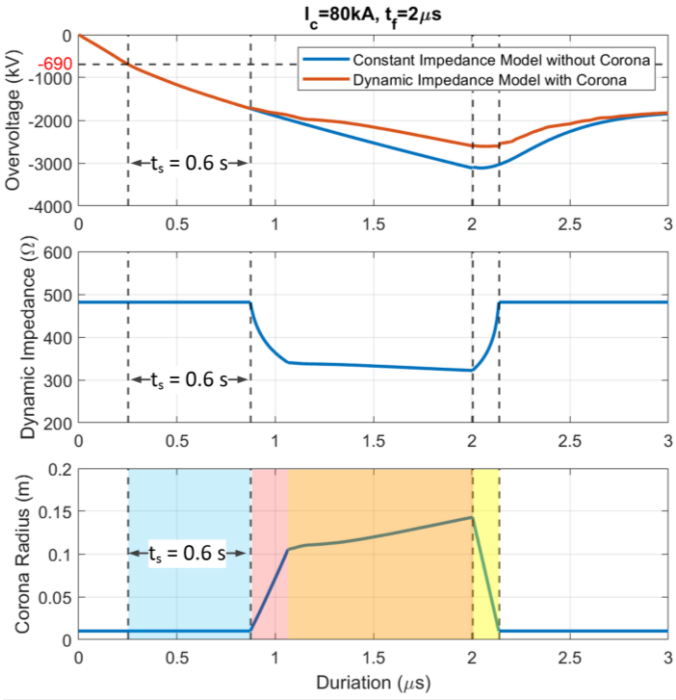

Fig. 5 Relationship among overvoltage at the top of conductor, surge impedance, and corona radius during one lightning impulse case

B. Corona Development of a single segment under different lighnting peaks and front timnes

The corona developing processes of Segment 1 under lightning current with different peaks and front times are presented as an example.

Fig. 6 shows the corona radius developing processes under the lightning currents of the same front time (2 μs) and different peaks, from 40 kA to 160 kA at the increment of 20 kA. As a result, the maximum radius that the corona can reach ranges from 0.076 m to 0.253 m. Because the front times of the lightning current keep the same, the corona radius also reach the maximum at around the same time. Looking through into the corona initial stage, higher lightning current peak will exceed V_{cr} earlier, so the corona onsets at an earlier time.

Fig. 7 (a) shows the corona radius developing processes under the lightning currents of the same peak amplitude (80 kA) and different front times, from 0.6 μs to 4 μs.

Firstly, if the front time is even shorter than 0.6 μs, there is not adequate time for corona to onset and develop because t_s is 0.6 μs. Then the corona developing processes can be classified into two cases. The first case is shown in Fig. 7 (b). The front time increases from 0.6 μs to 0.9 μs, and the maximum corona radius increases from 0.097 m to 0.239 m. In this case, the front time is short, thus, the overvoltage as well as the electric field can reach quite high magnitudes, but the electric field at the streamer-tip is always lower than E_{bn}. Therefore, the corona radius only depends on v_{cr}, and a longer front time leads to developing a longer corona radius. This stage is termed the v_{cr}-dominant stage in this paper. The other case is shown in Fig. 7 (c). The front time increases from 1.2 μs to 4 μs, and the maximum corona radius decreases from 0.206 m to 0.132 m. Along with the increasing front time, the corona developing process is limited by E_{bn} gradually. Therefore, longer front time causes lower overvoltage as well as shorter maximum corona radius. This stage is termed the E_{bn}-dominant stage in this paper.

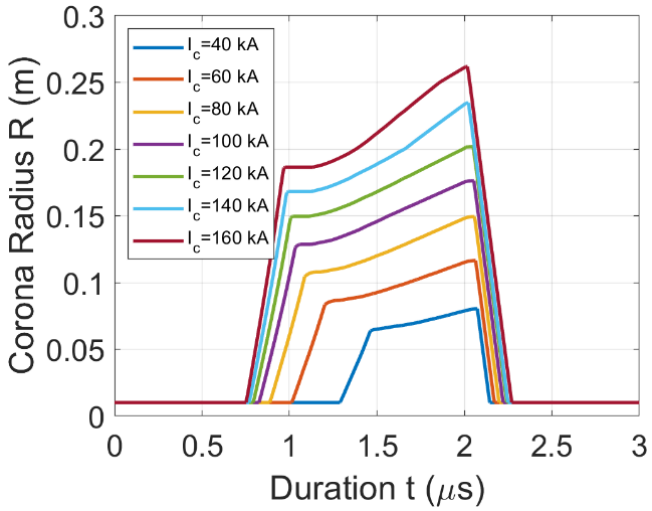

Fig. 6 Corona radius developing processes under different lightning current peaks from 40 kA to 160 kA at an increment of 20 kA

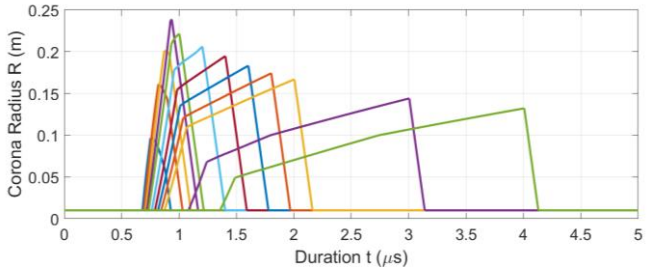

Fig. 7 (a) Corona radius developing processes under different lightning current front times from 0.6 μs to 4 μs

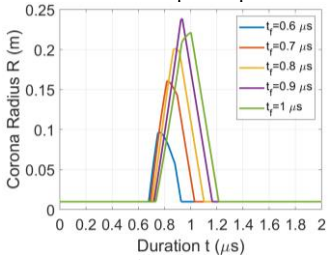

(b) Front time from 0.6 μs to 1 μs at an increment of 0.1 μs

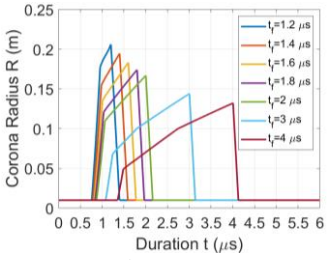

(c) Front time from 1.2 μs to 2 μs at an increment of 0.2 μs and to 4 μs

C. Corona Development of every Segment at different height

The height where every segment locates from ground influences the electric distribution, and the corona developing process.

Corona developing processes of every down-lead segment are shown in Fig. 6. If the lightning front time is short around 1 μs, as shown in Fig. 8 (a), corona development is mainly dominated by expansion velocity. Segment 7 is the nearest to ground, thus the voltage applied on it is the smallest, it is the last one to reach E_{cr}. In the v_{cr}-dominant stage, the maximum extent that corona on Segment 7 can reach is the shortest one, and the maximum corona radius of the other segments from low to high also ranges from short to long. To be noted, Segment 1 in this case has come into the E_{bn}-dominant stage, thus its maximum corona radius is shorter than that of Segment 2. In Fig. 8 (b), (c), and (d), the lightning front time is long enough for the corona on all segments to come into the E_{bn}-dominant stage. Although the segments at low height initial corona later, the relatively low voltage makes their v_{cr}-dominant stage longer. As a result, the maximum corona radius of the segments from low to high ranges from long to short.

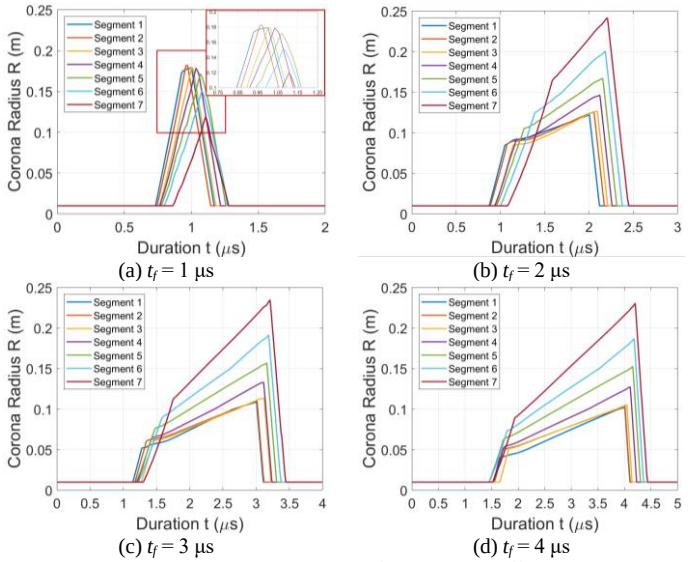

(a) t_f = 1 μs (b) t_f = 2 μs

(c) t_f = 3 μs (d) t_f = 4 μs

Fig. 8 Corona radius developing processes of segments at different height.

D. *Influence on Overvoltage Crest by Considering Corona on the Down-leads.*

The surge impedance of the model considering corona is dynamic to the overvoltage. A constant surge impedance model based on equation (1) without considering corona is established for comparison.

Fig. 9 shows the overvoltage crests of the two models under the lightning current of the same front time (2 μs) and different peaks and their differences. Along with the increasing of lightning current peak, the overvoltage of the model with corona is always smaller than the overvoltage of the model without corona and the difference of the overvoltage crests increases from 8.97 % to 23.41 %. It results from the decreasing surge impedance, which is due to the increasing corona radius. Fig. 10 shows the overvoltage crests of the two models under the lightning current of the same peak amplitude (80 kA) and different front times and their differences. Along with the increasing of lightning current front times, the overvoltage of the model with corona is always lower than the overvoltage of the model without corona. However, the difference of the overvoltage crests increases from 1.41 % to 18.43 % first and then decreases to 16.15 %. The trend of the overvoltage difference is consistent with the trend of changing surge impedance, which is consistent to the trend of corona radius.

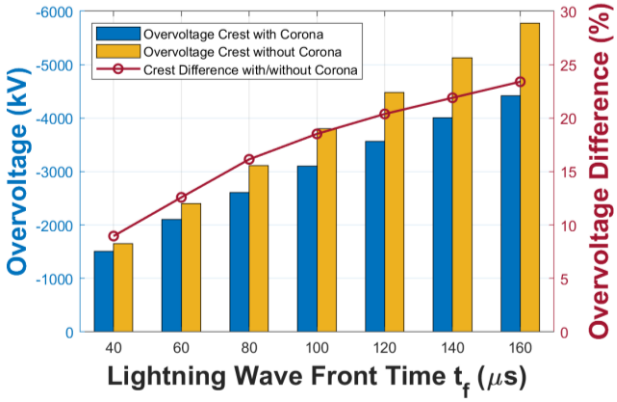

Fig. 9 Overvoltage crests of surge impedance models with and without corona under lightning current of different peaks and the difference of overvoltage crests between the two models

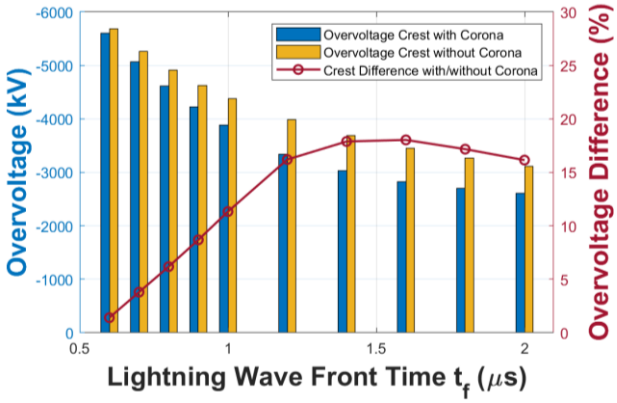

Fig. 10 Overvoltage crests of surge impedance models with and without corona under lightning current of different front times and the differences of overvoltage crests between the two models

E. *Influence on Backflashove Rate by Considering Corona on the Down-leads*

BFR is linearly related to backflashover probability P_{BF} and flash ground density N_g. P_{BF} is a joint result non-linearly contributed by the pylon footing condition and surge impedance. Thus, N_g is valued as 1.39 cases/km^2·year, which is the worst case collected in Denmark in 2004. Pylon footing model is described in above Section II. C. P_{BF} and BFR provided by constant surge impedance model without considering corona effect (CSI model) and dynamic surge impedance model considering corona effect (DSI model) are listed in following Table I.

TABLE I

THE MEDIAN AND LOG STANDARD DEVIATION OF THE LIGHTNING CURRENT PARAMETERS

Surge Impedance Model	PBF	BFR [cases/100 km·year]
CSI model	0.027	0.45
DSI model	0.021	0.35
Δ%	22.2 %	

It can be found that the difference in BFR provided by the two models is 22.2 %. The improvement in BFR caused by considering surge corona is very effective.

In [29], BFR of this composite pylon is quite higher than the BFR of two conventional metallic lattice towers serving widely in Denmark, Donau tower and Eagle tower, which are 0.32 cases/100 km·year and 0.30 cases/100 km·year. The compact structure makes composite pylons attract fewer lightning flashes, but the higher surge impedance of the thin-wire grounding down-leads results in much higher BFR than conventional metallic towers. When the surge corona on down-leads is not neglected anymore, the BFR of composite pylon is comparable to conventional lattice towers. It means, from the aspect of BF performance, composite pylon with external grounding down-leads can be an alternative for traditional metallic towers. Thus, the importance of considering corona effect for lightning transient studies on thin-wire grounding devices is stressed out.

F. Discussion on the Limitation of the Novel Dynamic Surge Impedance Model Considering the Corona Effect

The modeling parameters, especially statistical time lag, are discussed firstly. In the dynamic surge impedance model, some modeling parameters are calculated by finite element method, such as corona inception voltage and corona expansion velocity, while some modeling parameters are referred from the research of other scholars, such as streamer-tip electric field. Only statistical time lag is estimated as a constant value based the research of other scholars. The statistical time lag truly impacts overvoltage and backflashover performance. On the one hand, if the front time of lightning current is shorter than the statistical time lag, corona does not develop. On the other hand, the longer statistical time lag is, the shorter duration of corona development will be. Thus, longer statistical time lag may result in higher BFR. Statistical time lag is random with uncertainties, and its variation does not influence the final BFR linearly. In the future research, the statistical time lag is expected to be processed by the Monte Carlo method together with lightning current parameters.

The enhancement on coupling effect of surge corona has not been considered in this research. In the design of composite pylon, there are two down-leads paralleling downward along the surface of the pylon shaft. The increasing corona sheath can enhance the coupling effect between the two down-leads. When the surge current passes through one of the down-leads, the overvoltage will be further distorted and reduced if the enhancement of the coupling effect is considered. Besides, the coupling effect between the down-leads paralleling with the cross-arm and the phase conductors will induce an overvoltage on the phase conductors also. The dynamic surge impedance model will be revised considering the enhancement on coupling effect with other conductors.

V. CONCLUSIONS

This paper proposed a simplified dynamic surge impedance model for thin-wire conductors considering voltage-dependent surge corona and implemented the model on the external grounding down-leads of a 400 kV fully composite pylon. The corona development is simulated as the increasing radius of the cylindrical conductor. Thus, the surge impedance of the conductor with corona can change with the corona radius depending on lightning overvoltage. The surge corona developments on down-leads of different height under different waveforms of lightning current are simulated. The effect of considering surge corona on the overvoltage and backflashover performance of composite pylons is summarized. The importance of modelling surge corona effect in the research on lightning transient performance of thin-wire conductors is emphasized. The following conclusions are drawn.

Surge corona developing processes and overvoltage under different lightning current waveforms are simulated and summarized. Higher applied lightning current peaks will cause longer corona radius and cause more reduction on overvoltage. If the front time of applied lightning impulse current increases, the maximum corona radius will increase first and decrease because the corona development is dominant by the expansion velocity and the critical streamer-tip electric field in succession.

The overvoltage caused by the dynamic surge impedance model and constant surge impedance model without corona is compared. The dynamic surge impedance model reduces the overvoltage at the top of conductor by 10 % to 20 % approximately. As a result, the backflashover rate provided by dynamic surge impedance model is reduced by 22.2 %, which is comparable to conventional lattice towers. Therefore, it is necessary to consider corona effect in the research on lightning transient performance of thin-wire grounding devices. From the aspect of BF performance, composite pylon with external grounding down-leads can be a qualified option for next-generation transmission towers as an alternative of traditional metallic towers.

Finally, the limitations of the proposed dynamic surge impedance model are discussed. The randomness of statistical time lag and coupling effect with other conductors will be studied in the future work to simulate the lightning performance of the thin-wire grounding devices better.

REFERENCES

[1] BYSTRUP. "THE COMPOSITE PYLON." https://www.powerpylons.com/composite-pylon (accessed.

[2] B. Salarieh, H. M. J. D. Silva, A. M. Gole, A. Ametani, and B. Kordi, "An Electromagnetic Model for the Calculation of Tower Surge Impedance Based on Thin Wire Approximation," *IEEE Transactions on Power Delivery*, vol. 36, no. 2, pp. 1173-1182, 2021.

[3] K. C. Lee, "Non-Linear Corona Models in an Electromagnetic Transients Program (EMTP)," *IEEE Transactions on Power Apparatus and Systems*, vol. PAS-102, no. 9, pp. 2936-2942, 1983.

[4] P. S. Maruvada, D. H. Nguyen, and H. Hamadani-Zadeh, "Studies on modeling corona attenuation of dynamic overvoltages," *IEEE Transactions on Power Delivery*, vol. 4, no. 2, pp. 1441-1449, 1989.

[5] C. d. Jesus and M. T. C. d. Barros, "Modelling of corona dynamics for surge propagation studies," *IEEE Transactions on Power Delivery*, vol. 9, no. 3, pp. 1564-1569, 1994.

[6] T. H. Thang *et al.*, "A Simplified Model of Corona Discharge on Overhead Wire for FDTD Computations," *IEEE Transactions on Electromagnetic Compatibility*, vol. 54, no. 3, pp. 585-593, 2012.

[7] T. H. Thang, Y. Baba, N. Itamoto, and V. A. Rakov, "FDTD simulation of back-flashover at the transmission-line tower struck by lightning considering ground-wire corona and operating voltages," *Electric Power Systems Research*, vol. 159, pp. 17-23, 2018/06/01/ 2018.

[8] T. Okada, Y. Baba, T. H. Tran, and V. A. Rakov, "On Possible Influence of Corona Discharge on the Propagation Speed of Lightning Surges Along a Tall Grounded Object," *IEEE Transactions on Electromagnetic Compatibility*, vol. 63, no. 1, pp. 172-180, 2021.

[9] J. J. Clade, C. H. Gary, and C. A. Lefevre, "Calculation of Corona Losses Beyond the Critical Gradient in Alternating Voltage," *IEEE Transactions on Power Apparatus and Systems*, vol. PAS-88, no. 5, pp. 695-703, 1969.

[10] M. A. Al-Tai, H. S. B. Elayyan, D. M. German, A. Haddad, N. Harid, and R. T. Waters, "The simulation of surge corona on transmission lines," *IEEE Transactions on Power Delivery*, vol. 4, no. 2, pp. 1360-1368, 1989.

[11] J. F. Guillier, M. Poloujadoff, and M. Rioual, "Damping model of travelling waves by corona effect along extra high voltage three phase lines," *IEEE Transactions on Power Delivery*, vol. 10, no. 4, pp. 1851-1861, 1995.

[12] Y. Baba and V. A. Rakov, "Simulation of corona at lightning-triggering wire: Current, charge transfer, and the field-reduction effect," *Journal of Geophysical Research: Atmospheres*, vol. 116, no. D21, 2011.

[13] A. Smorgonskiy, E. Egüz, F. Rachidi, M. Rubinstein, and V. Cooray, "A model for the evaluation of the electric field associated with the lightning-triggering rocket wire and its corona," *Journal of Geophysical Research: Atmospheres*, vol. 120, no. 20, pp. 10,964-10,973, 2015.

[14] CIGRE Working Group 01 SC. 33, "Guide to procedures for estimating the lightning performance of transmission lines," *CIGRE Technical Brochure 63*, 1991.

[15] T. Hara and O. Yamamoto, "Modelling of a transmission tower for lightning-surge analysis," *IEE Proceedings - Generation, Transmission and Distribution*, vol. 143, no. 3, pp. 283-289, 1996.

[16] M. Ghomi, H. Zhang, C. Leth Bak, F. Faria da Silva, and K. Yin, "Integrated model of transmission tower surge impedance and multilayer grounding system based on full-wave approach," *Electric Power Systems Research*, vol. 198, p. 107355, 2021/09/01/ 2021.

[17] H. Zhang, Q. Wang, F. M. F. d. Silva, C. L. Bak, K. Yin, and H. Skouboe, "Backflashover Performance Evaluation of the Partially Grounded Scheme of Overhead Lines with fully Composite Pylons," *IEEE Transactions on Power Delivery*, pp. 1-1, 2021.

[18] F. W. Peek, *Dielectric phenomena in high voltage engineering*. McGraw-Hill Book Company, Incorporated, 1920.

[19] M. Robinson, "The Corona Threshold for Coaxial Cylinders in Air at High Pressures," *IEEE Transactions on Power Apparatus and Systems*, vol. PAS-86, no. 2, pp. 185-189, 1967.

[20] R. T. Waters and W. B. Stark, "Characteristics of the stabilized glow discharge in air," *Journal of Physics D: Applied Physics*, vol. 8, no. 4, pp. 416-426, 1975/03/11 1975.

[21] G. Hartmann, "Theoretical Evaluation of Peek's Law," *IEEE Transactions on Industry Applications*, vol. IA-20, no. 6, pp. 1647-1651, 1984.

[22] J. He, X. Zhang, P. Yang, S. Chen, and R. Zeng, "Attenuation and deformation characteristics of lightning impulse corona traveling along bundled transmission lines," *Electric Power Systems Research*, vol. 118, pp. 29-36, 2015/01/01/ 2015.

[23] V. M. Cabrera and V. Cooray, "On the mechanism of space charge generation and neutralization in a coaxial cylindrical configuration in air," *Journal of Electrostatics*, vol. 28, no. 2, pp. 187-196, 1992/07/01/ 1992.

[24] S. J. Heckman and E. R. Williams, "Corona envelopes and lightning currents," *Journal of Geophysical Research: Atmospheres*, vol. 94, no. D11, pp. 13287-13294, 1989.

[25] K. H. Schneider, "Positive discharges in long air gaps at Les Renardières—1975 results and conclusions," *Electra*, vol. 53, pp. 311-352, 1977.

[26] T. H. Thang *et al.*, "FDTD computation of lightning surges on overhead wires in the presence of corona discharge," in *2011 7th Asia-Pacific International Conference on Lightning*, 1-4 Nov. 2011 2011, pp. 85-88."

[27] T. H. Thang, Y. Baba, N. Nagaoka, A. Ametani, N. Itamoto, and V. A. Rakov, "FDTD Simulations of Corona Effect on Lightning-Induced Voltages," *IEEE Transactions on Electromagnetic Compatibility*, vol. 56, no. 1, pp. 168-176, 2014.

[28] T. Tran Huu *et al.*, "Modeling of corona discharge on a transmission line conductor struck by lightning for FDTD calculations," in *2010 Asia-Pacific International Symposium on Electromagnetic Compatibility*, 12-16 April 2010 2010, pp. 1309-1312."

[29] H. Zhang *et al.*, "Comparison of Backflashover performance between a novel composite pylon and metallic towers," *Electric Power Systems Research*, vol. 196, p. 107263, 2021/07/01/ 2021.

Paper IV

Electric Power Systems Research 198 (2021) 107355

Contents lists available at ScienceDirect

Electric Power Systems Research

journal homepage: www.elsevier.com/locate/epsr

Integrated model of transmission tower surge impedance and multilayer grounding system based on full-wave approach

M. Ghomi *, H. Zhang, C. Leth Bak, F. Faria da Silva, K. Yin

Department of Energy Technology, Aalborg University, Aalborg, Denmark

ARTICLE INFO

Keywords:
Harmonic impedance
Method of moment
Multilayer grounding system
Tower surge impedance

ABSTRACT

In this paper, a full-wave approach based on the method of moment (MoM) is proposed to investigate the harmonic impedance of a tower and its connected ground electrode in the frequency domain. The accuracy of the results is validated in comparison with NEC-4. The proposed numerical method is also employed for the evaluation of a full-sized HVDC tower harmonic impedance. The main contribution is the assessment of the harmonic impedance of a real tower with detailed geometrical information connected to the multi-layer grounding system. The validity of the transmission line method is evaluated through comparison with the results computed using the developed full-wave approach at the high frequency. In addition, the simulation results assure that a real tower's harmonic impedance could be smaller than the value estimated for very simplified models at the high frequencies. When the full-wave method is applied and the precise model of the ground electrode is considered, the harmonic impedance of the tower in the frequency domain and consequently, the transient impedance in the time domain are different, while the grounding system is assumed to be a perfectly conducting plane. These differences can become very significant, especially close to the resonant frequencies. The harmonic impedance of power transmission towers is strongly influenced by the connected grounding system.

1. Introduction

ONe of the leading causes of a power transmission line (PTL) unscheduled outages are a lightning surges. Seven out of twelve significant blackouts that occurred in 2019 were reported to be due to a lightning strike to the PTLs [1]. The transient behavior of the transmission tower, which is struck by lightning, is vital in determining the basic impulse level (BIL). Accordingly, the detailed tower and grounding system modeling (GSM) are indispensable in the transient analysis. The lightning impulse is often specified by its wide-band frequency contents from dc to several MHz. The transient overvoltage quantities depend on some different parameters like lightning current waveform, GSM, mechanical specifications, construction, shield wire, and surge impedance characteristics of a tower or its transient impedance [2]. Significantly, the grounding system (GS) and the tower surge impedance (TSI) have considerable effects on the lightning performance of the PTLs. The available models of the tower in the Electromagnetic Transient Programs, such as ATP-EMTP [3] PSCAD/EMTDC [4], indicate some of the assumptions that limit its applicability at the high frequencies. Additionally, for the GSM, the resistive model has been utilized, which is not perfect for lightning studies. The tower impedance changes from the tower top to the tower bottom as the wave travels. A proper GS can provide a low-impedance path for the lightning currents into the soil to dampen the occurred transient overvoltages. However, the modeling of GSs is exceedingly difficult, because of its dynamic behaviors such as a multilayer structure [5], [6], and the frequency dependency of soil resistivity and permittivity [7]. The theoretical methods of the harmonic impedance calculation are based on quasi-static or full-wave approaches. The quasi-static techniques, such as circuit theory or transmission-line model (TLM) [8] fail to provide precise results when used for the estimation of the harmonic impedance. Also, the main limiting factor of the quasi-static approaches is low computational efficiency, which makes them prohibitively slow, in particular for the harmonic impedance calculations. The electrical dimensions of the problem should be much smaller than the smallest wavelength of the flowing current in the TLM. The full-wave methods can be presented as the most accurate results over a wide frequency range [9]. The numerical solution of Maxwell's equations can be performed using the finite element method (FEM) [10], the method of moments (MoM) [11], the finite-difference time-domain (FDTD) method [12]. The practical

* Corresponding author.
E-mail addresses: mhg@et.aau.dk (M. Ghomi), hazh@et.aau.dk (H. Zhang), clb@et.aau.dk (C. Leth Bak), ffs@et.aau.dk (F. Faria da Silva), kyi@et.aau.dk (K. Yin).

https://doi.org/10.1016/j.epsr.2021.107355
Received 30 November 2020; Received in revised form 13 April 2021; Accepted 3 May 2021
Available online 24 May 2021

method is defined as a direct method in which an excitation current is injected at the top of the tower.

To estimate the surge impedance, several approaches have been using based on analytical and practical methods. It is worth noting that diverse expressions have been employed to determine the surge impedance, which was entirely dependent on the waveform of excitation current, the magnitude of the excitation current, and induced voltages. Hence, there is no agreement on the determination of surge impedance in the time domain [13].

In the time domain, tower transient behavior and the measured value of surge impedance are related to the angle and direction of excitation waveform [13], [16], and [18]. In the frequency domain, the harmonic impedance of the tower is a function of electromagnetic specifications and geometry of the system [13]. Therefore, using procedures based on the frequency domain is well suited to illustrate TSI [17]. The same approach for the tower surge impedance calculation has been used to appraise GS modeling. Therefore, among these techniques, MoM can be considered as an efficient approach in the frequency-domain because 1) it uses the thin-wire approximation with deducting two-dimensional surface integration to the one-dimensional line, 2) the harmonic impedance is not excitation waveform-dependent [18], [13]. To carry on with the attempts performed in [19], a numerical simulation is presented for harmonic impedance calculation of the integrated model. This model consists of detailed modeling of the tower and a GS in the frequency-domain unitedly.

This paper is organized as follows. In Section II, the developed full-wave approach is demonstrated concisely. The proposed method validation is investigated in Section III. The used delta-gap excitation model and the harmonic impedance analysis of the simple tower considering different GS configurations are shown in Section IV. Finally, the simulation results of the tower geometry impact on harmonic impedance considering multi-layer GS are analyzed as a proposed integrated model in Section V. Conclusion notes are described in Section VI.

2. Approach description

This section is a general description of the theory of dielectric layers modeling and the procedure of MoM implementation [20]. The problem is defined by representing each layer with a thickness d, resistivity ρ_0, permittivity ε, and permeability μ. This procedure is based on the developed concept for appraisal of arbitrary microstrip structures in a multilayer medium [21].

Fig. 1 shows a three-layered medium which is separated by two planar interfaces. A vertical wire of length h along the z-axis of the multi-layer medium is considered [22]. The source and observation point could be assumed in any layer of interest. For mathematical modeling, the mixed-potential integral equation (MPIE) is utilized [23]. These potentials consist of vector and scalar. J_s is the current density on the surface S of the perfect electric conductors (PECs) placed in a layered media is obtained by applying boundary conditions on the surface of the

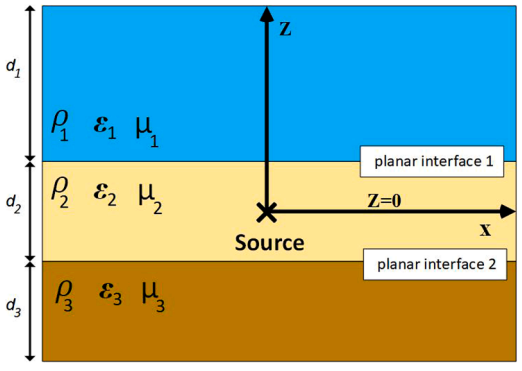

Fig. 1. Illustration of multi-layer medium.

elements of the model given in (1)

$$-\hat{a} \times E_s(r) = \hat{a} \times E_i(r) \tag{1}$$

where $E_i(r)$, $E_s(r)$, and r are the incident electric field, scattered field, and the position vector defined according to the rectangular coordinate system, respectively. The expression of electric current density $J_s(r)$ and surface charge density $\rho_s(r)$ are related to in (2)

$$\nabla . J_s(r) + j\omega\rho_s(r) = 0 \tag{2}$$

where ω and ρ_s are the angular frequency and density of electric charge, respectively. The MPIE formulation is obtained by fulfilling the boundary condition at the surface of elements and are given in (3)

$$E_s(r) = [-j\omega A(r) - \nabla V(r)] \tag{3}$$

where $A(r)$ and $V(r)$ being potential of magnetic vector and electric scalar potential, respectively. The gradient operator is ∇. By substituting (3) into (1) gives (4)

$$\hat{a} \times [j\omega A(r) + \nabla V(r)] = \hat{a} \times E_i(r), \ r \text{ on } S \tag{4}$$

In this paper, the presented formula in (5) is selected as a Greens functions form for the magnetic vector potential [24]. The potentials could be explained in terms of Green's functions, which are obtained on the base of spectral-domain Greens functions for microstrip structures given in (6) and (7)

$$\overline{\boldsymbol{G}}_A = \begin{pmatrix} G_{xx} & G_{xy} & G_{xz} \\ G_{yx} & G_{yy} & 0 \\ G_{zx} & 0 & G_{zz} \end{pmatrix} \tag{5}$$

$$V(r) = \int_S \boldsymbol{G}_v(r|r')\rho_s(r')dS' \tag{6}$$

$$A(r) = \int_S \boldsymbol{G}_A(r|r')\cdot J_s(r')dS' \tag{7}$$

where $\boldsymbol{G_A}$ and $\boldsymbol{G_v}$ are magnetic vector and electric scalar potential Green's function, respectively. The spatial domain Green's functions are determined easily using inverse Fourier transform of its spectral pairs [24].

$$G_{A,v} = \frac{1}{2\pi}\int_0^\infty \widetilde{G}_{A,v}(k_\lambda)J_0(k_\lambda\lambda)k_\lambda \mathrm{d}k_\lambda \tag{8}$$

where $k_\lambda = (k_x^2 + k_y^2)^{0.5}$, and k_x, k_y are wave vector components in the each layer on xy plane. ρ is J_0 is first kind Bessels function, and $\widetilde{G}_{A,v}$ is the Green's function for spectral domain [23]. The radial distance between the source segment and the point for calculating the electric field is λ. It should be pointed out that Sommerfeld integrals presented in (8) is solved numerically.

3. Model verification

The validation of the models against experimental results is the most crucial part of the modeling. However, there has not been a comprehensive comparison between modeling and experimenting with the input impedance of towers connected to a ground electrode buried in multi-layer soil. The fundamental reasons for the lack of comparison are: 1) the measured voltage is path-dependent at the high frequencies between any two points, 2) there are complexities of measuring each layer's electrical parameters in a multi-layer soil structure. Due to the noted practical limitations for validation, NEC-4, as a widely accepted numerical electromagnetic code, is applied to investigating the presented method [25].

In this section, to verify the proposed method, a very simple case, consisting of a tower and vertical ground electrode (VGE), is applied. An

antenna theory approach [13] is well suited to the frequency domain analysis of layered microstrip structures to calculate the Green's functions for multi-layer media, which are basically shown by Sommerfeld's integrals and formulas in the spatial and spectral domain, respectively.

Fig. 2 shows the tower geometrical configuration, and the junction point between the tower and ground electrode is used to excite the ground surface by a 1-V voltage source. A 0.4-m cylindrical tower with a 5-mm diameter is considered. The soil is characterized by a resistivity of 10 Ω.m and a relative permittivity of 10. This integrated model, tower, and GS are simulated numerically using a full-wave method.

Figs. 3 (a) and (b) present the absolute value and phase angle of the current distribution vector along with the integrated model at higher frequencies, namely 10 MHz. The obtained results through NEC-4 are also illustrated in Fig. 3 along the *z*-axis. It can be seen that two methods predict similar behavior in the estimation of current distribution. This approach's usefulness is validated from the excellent consensus between the proposed method's results and computed results by NEC-4. It is seen that the proposed method can compute the distribution of current along with the integrated model precisely. The differences between absolute values in Fig. 3(a) refers to the selected basis function for the excitation source at the excitation terminal. The terminal is excited by an ideal voltage source of magnitude V_s in the integrated model. The triangular basis functions are employed. If $\delta \longrightarrow 0$, the induced terminal current passes into the ideal voltage source, and subsequently, it will expand to the half-subsectional basis function. An incident field is provided by the delta-gap voltage source at the excitation terminal.

4. Analysis of harmonic impedance of the integrated model in the frequency domain

The most relevant contribution of lightning impulse for the outage rate of PTLs comes out from the tower surge impedance and the tower-footing GSs. The typical tower surge impedance characteristic and dynamic behavior of GSs are analyzed in detail elsewhere (e.g., [7]). According to the measurement expenses, complications of working on high-frequency phenomena, and the towers' diversity, few measurement results are presented. Also, the detailed information about the tested towers and their GS condition is not accessible. Numerical solvers are widely used to analyze the harmonic impedance of towers and GSs.

4.1. Harmonic impedance calculation based on MoM

The harmonic impedance is extremely helpful in the transient analysis. It is given by (9)

$$Z_{input}(f) = \frac{V(f)}{I(f)} \tag{9}$$

where $I(f)$ and $V(f)$ are phasors of the injected current and the steady-state harmonic electric potential at the injection point in reference to the remote terminal, respectively(see [29], [31]). It depends on the electromagnetic characteristics and the geometry of the medium, and not on excitation. The input harmonic impedance of the integrated model can be calculated from the MoM matrix directly. Based on MoM, a full-wave frequency-domain approach, the integrated model is divided into *N* small segments. Accordingly, a lower number of segments needs to be taken into account (see [24]).

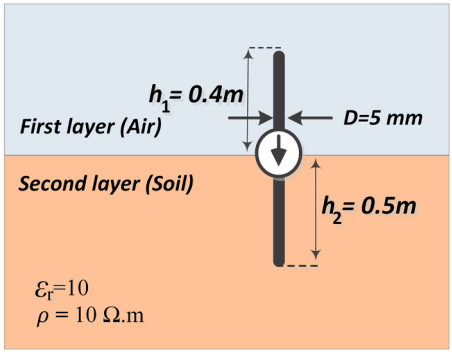

Fig. 2. Vertical electrode buried in soil which is connected to very simple tower.

4.1.1. Excitation model

Two theoretical models can be applied to an excitation source modeling, namely, delta-gap and impressed current models [26]. In this part, the modeling of the delta-gap excitation approach is reviewed concisely. According to the presented model in [26], the tower is excited by the voltage source V_s, applied within a tiny gap region of length $\delta \longrightarrow 0$ and across the reference plate (perfect electric conductor (PEC)) and the excitation terminal (see Fig. 4(a)). To obtain finite input impedance, a nontrivial voltage must always be induced across the gap, which has a width of almost zero. Thin wire approximation is employed to compute the distributed currents along all conductors in the mentioned case. To avoid the first segment current discontinuity, the first segment is utilized to create the induced terminal current at each frequency. Within the MoM methodology, Fig. 4(b) shows the expanded finite series of current distribution on the surface of conductors, which is located on the multi-layer medium. To solve (4), the electric current density on the conductors surface (tower and vertical ground electrode) can be defined as follow:

$$J_s(r') = I^t f_t(r') + \sum_{n=1}^{N} I^c f_n(r') \tag{10}$$

where the half-subsectional basis function, $f_t(r')$, generates terminal current and $f_n(r')$ represents full-subsection basis functions. I^t and I^c denote the induced current coefficient that is associated with half-subsectional basis function and the unknown coefficients that are associated with the triangular basis functions, respectively [27]. The voltage source of the delta gap at the tower top creates the incident excitation field given by (11)

$$E_i = V_s \delta(r - r')\hat{a} \tag{11}$$

where r' is the terminal and r is the distance along with the integrated model. As presented in Fig. 4(b), the induced terminal current, I^t, goes along the voltage source, which expands into a half-subsectional basis function, also located at r_n. The identical MPIE governing the surface current, J_s, on the surfaces of the integrated model conductors is given by (12)

$$\int G_A(r|r')\cdot J_S(r')dS' + V_s\delta(r - r')\hat{a} = 0 \tag{12}$$

4.1.2. Integration path influence on the harmonic impedance

It is well known that the voltage between two points along a determined path in the general case is given by (13)

$$V_s = \int_s \vec{E}_{total}\cdot\vec{dl} = \Delta V(r) - \frac{\partial}{\partial t}\int \vec{A}\cdot\vec{dl} \tag{13}$$

$$\vec{E}_{total} = \vec{E}_i + \vec{E}_s \tag{14}$$

where *S* shows the integration path on the excitation terminal. In the case of an electrostatic field, the voltage value is not dependent on the integration path and it is unique. Once the current distribution has been computed along with the components, the electric field can be computed at any point by summing the contributions due to the currents in each segment. In this situation, the last term of (13) is zero and the voltage is exactly different from electric scalar potentials.

Generally speaking, for a dynamic electromagnetic field, the electric

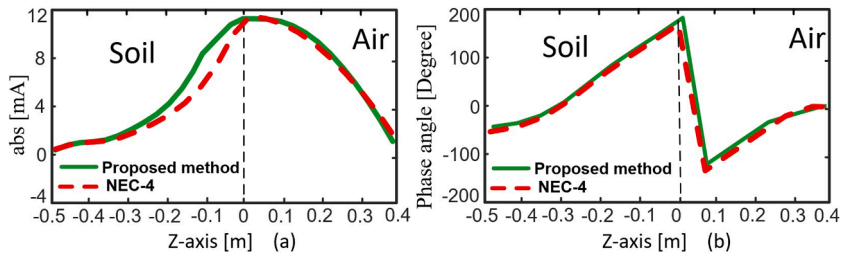

Fig. 3. Current distribution along the ground electrode and tower at 10 MHz. (a) absolute value (b) phase angle.

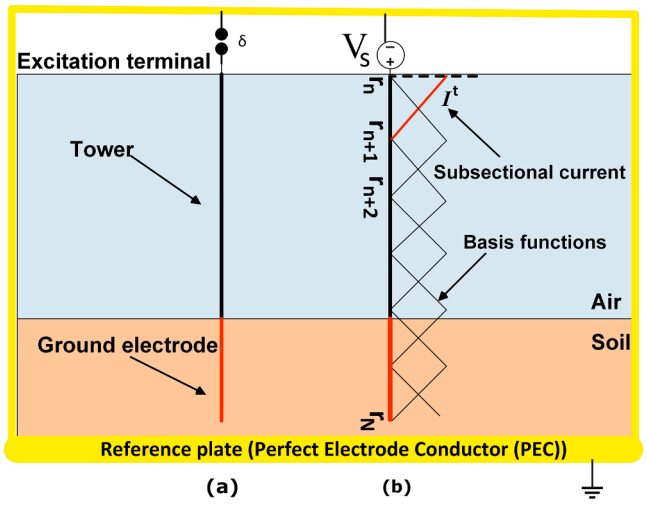

Fig. 4. Setup for the calculation of harmonic impedance of the integrated model. (a) delta-gap excitation generator, (b) triangular basis functions, and the segmented integrated model.

field is not conservative and the integral of the electric field between any two points is path-dependent. Due to this issue and to determine a unique voltage, the gradient of the scalar potential calculated along a unique straight path extends to the remote ground reference point. The path-dependent voltage is estimated by (15) expression based on Faraday's law.

$$V'(r) - V(r) = \frac{\partial}{\partial t}\int \vec{B}\cdot\overrightarrow{dS} \tag{15}$$

where $V'(r)$, $V(r)$, and B are voltages obtained along a path on S and magnetic flux density, respectively. The input impedance at the excitation terminal is calculated as follows:

$$Z_{input}(f) = \frac{V_s}{I^t} = -\frac{\int_S \vec{E}_{total}\cdot\vec{dl}}{I^t} \tag{16}$$

One way to circumvent the problem of path dependence is to use the scalar potential instead of the voltage as the integral of the electric field over a given path. Such an approach has the benefit that the scalar potential is uniquely derived. Hence, with this assumption, the voltage or the integrated value is independent of the integration path [13]. Adaptive Simpson's integration is employed to evaluate the integrals over the finite interval, while Mosig's method of averages is applied to assess the integrals over the infinite interval, which features a very fast convergence [32].

4.1.3. Terminal length effect on the harmonic impedance

The presence of the excitation terminal can create a parasitic inductance [30]. It can be estimated by (17)

$$L = 0.2 \times h \times \left(\ln\frac{2h}{b} + \frac{0.223b}{h} + 0.5\right)[nH] \tag{17}$$

where h and b are the length and width of the excitation terminal in mm, respectively. For instance, for a conductor radius of 12.5 mm, the port width is set to 25 mm. The terminal's impedance magnitude (ωL) for several port lengths in the maximum frequency of 10 MHz is given in Table 1. This table shows that to achieve a negligible impedance, the excitation terminal length must be no longer than 100 mm. This length is considered for the excitation segment.

4.1.4. Moment impedance matrix

In this part, the impedance matrix of the system is obtained by making use of the MoM solution to Maxwell's equations. Maxwell's equations are reduced to a matrix form by applying to (12). The electric field at the observation point will be computed once finding the current of each segment. The moment impedance matrix is defined by (18). Also, the impedance matrix can be expressed by (19). Eventually, by formulating the problem as a close form matrix, given by (20), unknown coefficients vector is computed [27].

$$\begin{pmatrix} Z_{1,1} & \cdots & Z_{1,N+1} \\ \vdots & \ddots & \vdots \\ Z_{1+N,1} & \cdots & Z_{1+N,N+1} \end{pmatrix}\begin{pmatrix} I^t \\ \vdots \\ 0 \end{pmatrix} = \begin{pmatrix} V_s \\ \vdots \\ 0 \end{pmatrix} \tag{18}$$

$$\begin{pmatrix} Z^{tt} & Z^{tc} \\ Z^{ct} & Z^{cc} \end{pmatrix}\begin{pmatrix} I^t \\ I^c \end{pmatrix} = \begin{pmatrix} V_s \\ 0 \end{pmatrix} \tag{19}$$

where $Z^{ii}(f)$ and $Z^{ij}(f)$ represent self and mutual impedance, respectively which $i,j \in \{t,c\}$. I^c can be obtained from the following resultant matrix equations:

$$[z][I] = [V_s] \tag{20}$$

where $[z]$, $[I]$, and $[V_s]$ are the moment impedance matrix, the unknown coefficients vector, and the excitation vector, respectively. Finally, for the wide frequency range, the relation between the terminal voltage and induced current in an impedance matrix form is obtained from the moment impedance matrix by manipulation of (19). Z_{input} is given as follow:

$$Z_{\text{input}}(f) = Z^{tt}(f) - Z^{tc}(f)(Z^{cc}(f))^{-1}Z^{ct}(f) \tag{21}$$

where $Z_{\text{input}}(f)$ is the calculated harmonic impedance. From Fig. 6, the proposed method for calculating long integration path harmonic impedance converges to the impedance estimated by the conventional

Table 1
Excitation Terminal Impedance Magnitude.

Terminal Length (mm)	Impedance (Ω)
10	0.10484
50	1.25520
100	3.31200
1000	61.4200

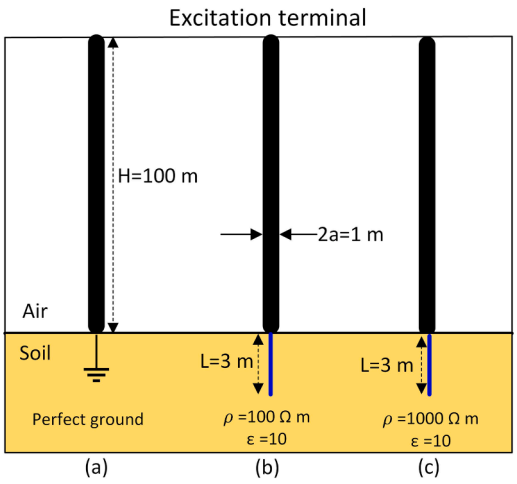

Fig. 5. Geometry of the two-layer medium. (a) tower end is connected to PEC adapted from [13], (b) integrated model which tower end is connected to vertical electrode buried in soil resistivity of 100 Ωm, and (c) resistivity of 1000 Ωm.

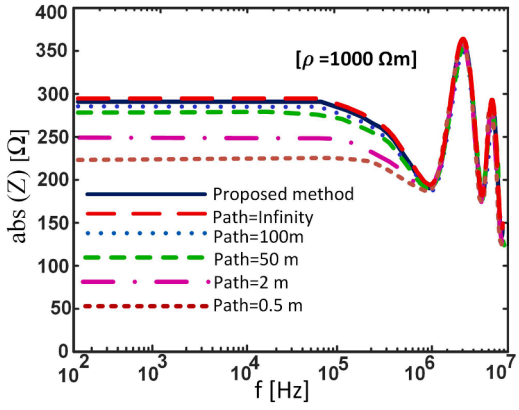

Fig. 6. Integration path effect on the harmonic impedance absolute value of integrated model shown in Fig. 5(c) [ρ= 1000 Ωm].

method for long integration path.

4.2. Grounding system effect on integrated model harmonic impedance

To assess the GS effect on the harmonic impedance of a tower, a cylindrical tower is considered. The specification of this case is adapted from [13]. The configurations are shown in Fig. 5. The tower is placed in the upper layer, and the depth of the first layer is equal to the tower length. The upper layer medium is an air, which is supposed to be lossless and characterized by magnetic permeability μ_0 and permittivity ε_0. The input impedance of the problem is calculated with and without a real model of the GS. The end of the tower is connected to the zero-potential ground, PEC (see Fig. 5(a)), and in the Figs. 5(b) and (c), the tower is connected to the VGE length of 3-m buried in soil with a resistivity of 100 and 1000 Ωm, respectively. The related permittivity of soil is set to 10.

To further appraise the impact of the integration path on the harmonic impedance, various lengths (0.5, 2, 50, 100-m) of the integration path are taken into account. The harmonic impedance of the integrated model is illustrated in Fig. 6. It is clear from the figure that the harmonic impedance strongly depends on the length of the integration path (Paths in Fig. 6). In this paper, the concept of remote terminal voltage which is presented by *Grcev* as a scalar potential [13] is used for validating the calculated harmonic impedance of the integrated model, which was presented as a direct characterization in Section IV-A-4. The corresponding voltage for the *infinity* case is almost equivalent to the scalar potential. The path-dependence effect on harmonic impedance is visible at frequencies under 700 kHz. It is clear that the applied method must be rigorously checked for the impact of path dependency on the harmonic impedance.

Fig. 7 shows the obtained harmonic impedance using TLM and MoM, which have the same results up to the first frequency (FRF) of 0.75 MHz when assuming a PEC. The full-wave approach can calculate the minimum and maximum values of input harmonic impedance at the higher frequencies more accurately than the TLM method, which does not calculate zero or infinite accurately. The high deviations at the specific frequencies may be attributed to radiation loss, which the full-wave model considers. The TLM method does not consider the mutual coupling between the adjacent segments, so it is expected that they might lead to differences in the high-frequency response. In the TLM, the VGE is supposed to have zero resistivity and the tower is simulated by a surge impedance whose value is calculated by (22)

$$Z_c = 60\ln\frac{H_{tower}}{a_{tower}} \tag{22}$$

where H_{tower} and a_{tower} are the height and radius of the tower in meters, respectively. Z_c has a value of 317.9 Ω for the tower radius of 0.5 m and the tower height of 100 m [13], [15]. The detailed formulation of the grounding system modeling using the TLM can be found in [14]. It is assumed that the 3-m vertical electrode is buried in the soil with two different resistivities of [ρ= 100 Ω.m, Fig. 5(b)] and [ρ= 1000 Ω.m, Fig. 5(c)]. The influence of an accurate model of the GS on the input impedance is illustrated. It may be noted in Figs. 7 and 8 that the TLM model greatly overestimates the values of harmonic impedance at high frequencies. Also, the harmonic impedance of the integrated model has a different behavior from the estimated harmonic impedance of the tower, which is connected to the perfect GS. This dissimilarity at the frequency of resonance and different behavior at high frequency may be ascribed to change system transfer function in the frequency domain and radiation losses. The subsequent stroke impulse with a larger front rise rate has higher frequency contents in comparison with the first stroke impulse [29]. It is worth noting that the use of the TLM could be revised principally at the lightning studies [13].

5. Impact of tower geometry on harmonic impedance considering multilayer soil

In this section, to further assess the applicability of the proposed

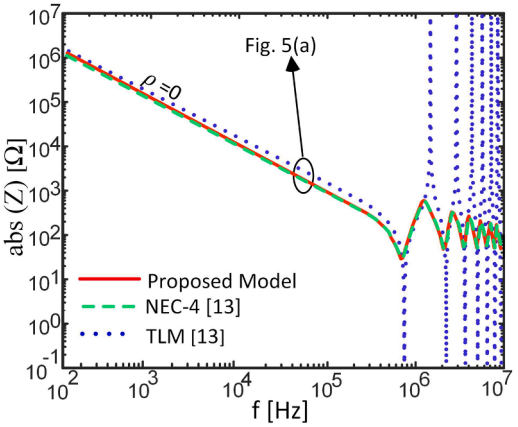

Fig. 7. Geometry of the two-layer medium. (a) tower end is connected to PEC adapted from [13], (b) integrated model which tower end is connected to vertical electrode buried in soil resistivity of 100 Ωm, and (c) resistivity of 1000 Ωm.

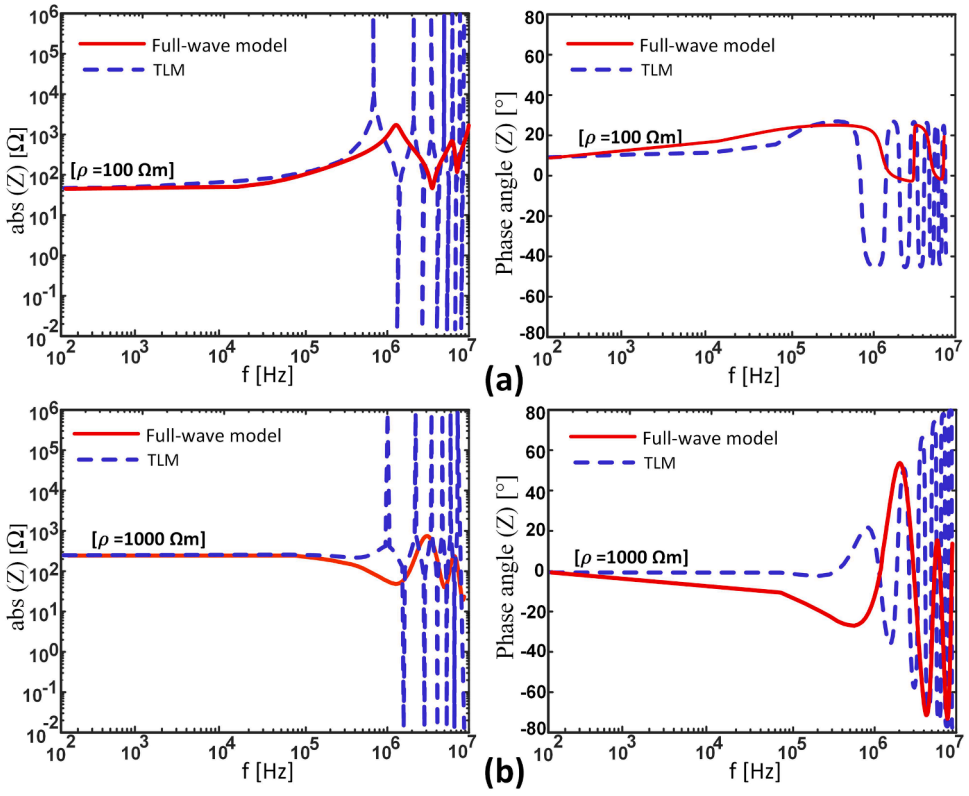

Fig. 8. Harmonic impedance of tower and its connected VGE [absolute value (left column) and phase angel (right column)] shown in Fig. 5(b) [ρ= 100 Ωm] and Fig. 5(c) [ρ= 1000 Ωm]. Full-wave model: red line, TLM model: blue dashed line. (For interpretation of the references to colour in this figure legend, the reader is referred to the web version of this article.)

integrated model, the input impedance of the typical full-sized HVDC tower is investigated compared to an approximated model of the towers in the frequency domain [17]. The tower is simulated with three levels of detail. Firstly, in a very simplified model, only the main cylinder with a height of 89.5 m and simple cross arm is considered [*tower*(*a*), Fig. 9 (a)]. Next, the simplified model, four legs and cross arm with the width of 20 m are added to the geometry [*tower*(*b*), Fig. 9(b)]. Finally, all members and components of the steel lattices tower are taken into account in [(*tower*(*c*), Fig. 9(c)] as a complex model. The equivalent model of the presented integrated model in the frequency domain, the medium of the integrated model, and the top view of the real tower are shown, respectively in Figs. 9(d), (e), and (f). For each case, the harmonic impedance is calculated up to 10 MHz. The full-wave method based on MoM solutions to Maxwell's equations is used for evaluating the harmonic impedance observed from the tower top. This model has been extensively used to determine the transient surge impedance in lightning studies. It is worth noting that the real tower structure is much more complicated compared with the very simple equivalents (see Fig. 9) [28]. The influence of the tower elements on the harmonic impedance with an accurate model of GS is analyzed unitedly in this study.

All towers are connected to the VGE buried in uniform and multi-layer soil structures. To this aim, two configurations of the soil layers are defined in Table 2 with resistance values of 100 and 1000 Ωm. A soil permittivity is set to 10 for all cases. The electrode is 3-m long and has a diameter of 30 mm. The input impedance seen from the tower top is determined as the harmonic impedance in the frequency domain, as explained in section IV-B.

Fig. 10 shows simulation results of the computed harmonic

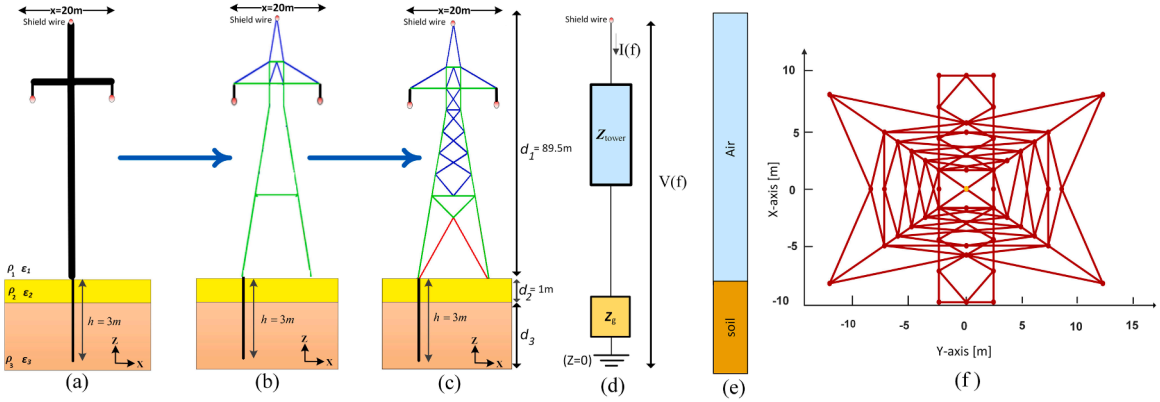

Fig. 9. HVDC tower side view. (a) very simplified structure, (b) simplified structure, (c) real tower, (d) frequency-dependent representation of tower which is connected to the ground electrode, (e) medium of integrated model, (f) 2-D top view of the simulated real tower in the X-Y plane.

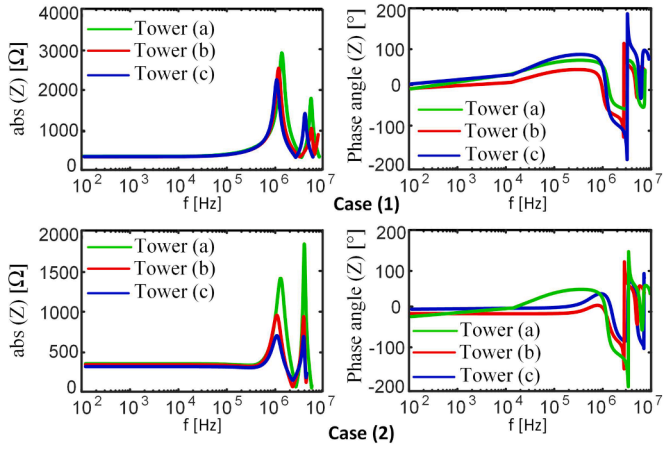

Fig. 10. Influence of tower model on the harmonic impedance [absolute value and phase angle] of the integrated model. The ground electrode of towers is buried in the uniform soil (see cases 1 and 2 in Table 2).

Table 2
Adopted Values of The Soil Resistivity.

Ground structures	ρ_1(Ω.m)	ρ_2(Ω.m)
Case 1 (uniform soil)	100	100
Case 2 (uniform soil)	1000	1000
Case 3 (multilayer soil)	100	1000
Case 4 (multilayer soil)	1000	100

impedance of the tower, which is connected to the VGE with the adopted parameters in Table 2 for case 1. In this case, the maximum value of harmonic impedance magnitude for the presented tower has a noticeable difference between the simplified towers (tower (a) and (b)) and the complex model of the tower.

For case 2, the soil is characterized by the resistivity of 1000 Ωm. Towers are connected to this GS. According to Fig. 10, the obtained harmonic impedance of a very simplified tower is markedly higher than the obtained results for Figs. 9(b) and (c). The peak values of the harmonic impedance magnitude are 23 and 140 for cases 1 and 2, respectively. The LF harmonic impedance is the same for all towers in each case. The values of R_{LF} are 33.9 and 313 Ω for the case of 1 and 2, respectively. It can be seen that all towers have the same response at low frequencies up to FRF. For instance, in case 1, the FRF value is different and changes from 1.4 MHz for the tower (a) to 0.92 MHz for the tower (c). It varies from 1.2 MHz for the tower (a) to 1 MHz for the tower (c) in case 2.

To further analyze the influence of the tower-footing GS on the harmonic impedance of the integrated model, the same VGE with a length of 3-m buried in a multi-layer soil is taken into account in cases of 3 and 4. The upper soil layer depth is set to d_2 =1m. The electrical parameters of soil are given in Table 2. The obtained results associated with the harmonic impedance (amplitude and phase angle) observed from the tower top are shown in Fig. 11.

For case 3, the maximum value of harmonic impedance magnitude is significantly distinct between the illustrated towers in Fig. 9. The maximum value of input impedance for the tower in Fig. 9(a) has appeared in the second resonant frequency at 4MHz, but the peak value of the harmonic impedance of the complex tower model occurs at 6 MHz. The results show different behavior for the simplified and complex models depending on the differences related to the maximum values of harmonic impedance at resonance frequencies [see Fig. 11(a)]. A predicted impedance using a full-wave approach might be smaller than the predicted values for a very simplified tower. Differences could become very significant, especially close resonant frequencies.

To supplementary evaluate the effect of the buried VGE in multi-

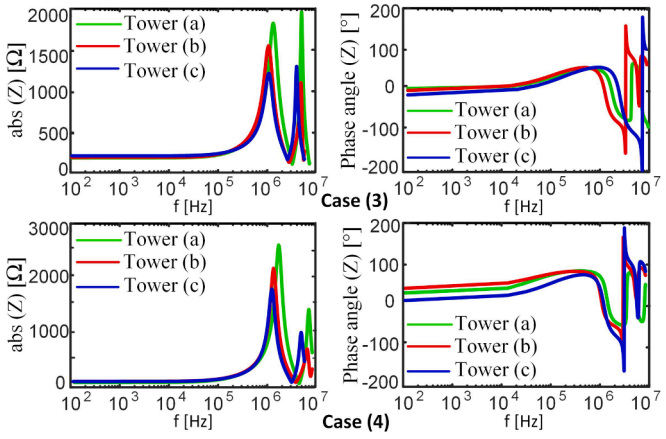

Fig. 11. Influence of a tower model on harmonic impedance [absolute value and phase angle] of the integrated model. The ground electrode of towers is buried in the multilayer soil (see cases 3 and 4 in Table 2).

layer soil on the integrated model harmonic impedance, the upper and lower soil layers are, respectively, characterized by resistivity of $\rho_1 = 1000\Omega m$ and $\rho_2 = 100\Omega m$, both having the same relative electric permittivity of 10. (see case 4 in Table 2). The magnitude and phase angle of the harmonic impedance of this case is demonstrated in Fig. 11 (b). From the results shown here, it is observed that the harmonic impedance is a function of different parameters such as the tower's geometry and electromagnetic characteristics of medium and tower footing GS specifications. The influence of the tower elements and the exact model of the GS on the peak value of harmonic impedance magnitude is briefly presented in Table 3.

6. Conclusions

This paper can be regarded as a continuation of the work developed by *Grcev* and *Ametani* in [13] and [17]. A precise full-wave MoM-based solution of Maxwell's equations for calculating the harmonic impedance's integrated model was proposed. The contributions of this paper are listed as follows:

a) A comprehensive methodology based on the full-wave approach was introduced, which can directly provide the integrated model's harmonic impedance consisting of a tower and grounding system.
b) The impedance vectors, including the self and mutual impedances, are calculated in the multi-layer medium using MoM matrix directly, which differs from the approach adopted in [13] and [17].
c) Simulations are implemented to solve the full-wave Maxwell's equations regarding the tower's detailed model and the grounding system's real geometry.
d) The correctness of the theoretical procedure, TLM, is examined through comparison with the obtained results of the integrated model based on the developed full-wave approach.
e) In all cases, (tower (a) and (b)), overestimate the peak value of the harmonic impedance in comparison to the detailed model at the specific frequencies. However, the input harmonic impedance of the tower in the frequency domain, and consequently, the transient impedance in the time domain, was different as long as the GS is assumed a perfectly conducting plane. The related differences for cases 1, 2, 3, and 4 are 23, 140, 57, and 47% in the frequency domain. It can bring about notable errors in transient impedance values in the time domain.
f) The frequencies of resonance, the minimum and maximum values of the harmonic impedance, varied when the system transfer function is changed based on the GS model.

Table 3
Comparison of Max.Values of the Integrated Model Input Impedance.

Cases	$R_{LF}[\Omega]$	$\lvert Z\rvert_m[\Omega]$			%diff($\lvert Z\rvert_m$)	FRF(MHz)		
		(a)	(b)	(c)		(a)	(b)	(c)
1	33.9	2924	2650	2371	23	1.4	1.13	0.92
2	313	1828	963	759	140	1.2	0.95	1
3	93.5	2070	1530	1315	57	1.7	0.91	1.02
4	42.6	2576	2275	1751	47	1.8	1	1.1

g) The exact model of the tower and grounding system could be necessary for the back-flashover rate approximation and other surge performances associated with the PTLs. These are significant factors in optimizing the cost of insulation coordination and the protection systems.

Funding

No funding was received for this work.

Intellectual Property

We confirm that we have given due consideration to the protection of intellectual property associated with this work and that there are no impediments to publication, including the timing of publication, with respect to intellectual property. In so doing we confirm that we have followed the regulations of our institutions concerning intellectual property.

Research Ethics

We further confirm that any aspect of the work covered in this manuscript that has involved human patients has been conducted with the ethical approval of all relevant bodies and that such approvals are acknowledged within the manuscript.

IRB approval was obtained (required for studies and series of 3 or more cases)

Written consent to publish potentially identifying information, such as details or the case and photographs, was obtained from the patient(s) or their legal guardian(s).

Authorship

All listed authors meet the ICMJE criteria. We attest that all authors contributed significantly to the creation of this manuscript, each having fulfilled criteria as established by the ICMJE.

One or more listed authors do(es) not meet the ICMJE criteria.

We confirm that the manuscript has been read and approved by all named authors.

We confirm that the order of authors listed in the manuscript has been approved by all named authors.

Contact with the Editorial Office

This author submitted this manuscript using his/her account in IPST 2021/EVISE.

We understand that this Corresponding Author is the sole contact for the Editorial process (including EVISE and direct communications with the office). He/she is responsible for communicating with the other authors about progress, submissions of revisions and final approval of proofs.

We confirm that the email address shown below is accessible by the Corresponding Author, is the address to which Corresponding Author EVISE account is linked, and has been configured to accept email from the editorial office of American Journal of Ophthalmology Case Reports: mhg@et.aau.dk

Someone other than the Corresponding Author declared above submitted this manuscript from his/her account in EVISE: CLB@et.aau.dk

We understand that this author is the sole contact for the Editorial process (including EVISE and direct communications with the office). He/she is responsible for communicating with the other authors, including the Corresponding Author, about progress, submissions of revisions and final approval of proofs.

CRediT authorship contribution statement

M. Ghomi: Conceptualization, Methodology, Software, Writing - original draft. **H. Zhang:** Methodology, Software. **C. Leth Bak:** Supervision, Writing - original draft. **F. Faria da Silva:** Supervision, Software, Writing - original draft. **K. Yin:** Software.

Declaration of Competing Interest

No conflict of interest exists.

References

[1] List of major power outages, List of major power outages, https://en.wikipedia.org/wiki/.
[2] L. Grcev, M. Popov, On high-frequency circuit equivalents of a vertical ground rod, IEEE Trans. Power Del. 20 (2) (2005) 1598–1603.
[3] J. Mahseredjian, S. Dennetiere, L. Dube, B. Khodabakhchian, L. Gerin-Lajoie, On a new approach for the simulation of transients in power systems, Elect. Power Syst. Res. 77 (11) (2007) 1514.
[4] PSCAD/EMTDC, User'S manual: ver.4.2, Manitoba HVDC Research Centre, 2005.
[5] M. Ghomi, H. Mohammadi, H. Karami, Full-wave modeling of grounding system: evaluation the effects of multi-layer soil and length of electrode on ground potential rise, International Conference on Power Systems Transients, IPST (2019) 1–6.
[6] M. Ghomi, C.L. Bak, F.F.d. Silva, Frequency Dependence of Multilayer Soil Electrical Parameters: Effects on the Input Impedance of Grounding Systems. 16th International conference on AC and DC power transmission.ACDC, 2020.
[7] A. Ametani, Y. Kasai, J. Sawada, A. Mochizuki, T. Yamada, Frequency-dependent impedance of vertical conductors and a multiconductor tower model, Proc. Inst. Elect. Eng., Gen., Transm. Dist. 141 (1994) 339–345.
[8] Z. Feng, X. Wen, X. Tong, Impulse characteristics of tower grounding devices considering soil ionization by the time-domain difference method, IEEE Trans. Power Delivery 30 (4) (2015) 1906–1913.
[9] M.A. Sargent, M. Darveniza, Tower surge impedance, IEEE Trans. Power App. Syst. PAS-88 (1969) 680–687.
[10] A. Sunjerga, F. Rachidi, M. Rubinstein, Calculation of the grounding resistance of structures located on elevated terrain, IEEE Trans. Electromagn. Compat. (2018) 1–5.
[11] L. Grcev, A. Kuhar, V. Arnautovski-Tasova, Evaluation of high-frequency circuit models for horizontal and vertical grounding electrodes, IEEE Trans. Power Delivery 33 (6) (2018) 3065–3074.
[12] Y. Baba, N. Nagaoka, A. Ametani, Modeling of thin wires in a lossy medium for FDTD simulations, IEEE Trans. Electromagn. Compat. 47 (1) (2005) 54–60.
[13] L. Grcev, F. Rachidi, On tower impedances for transient analysis, IEEE Trans. Power Delivery 19 (3) (2004) 1238–1244.
[14] C.R. Paul, Analysis of multiconductor transmission lines, IEEE Press, 2007.
[15] CIGRE, WG01 SC33, To procedures for estimating the lightning performance of transmission lines, a. eriksson (CH), l. dellera (IT), g. baldo (IT), c. h. bouquegneau (BE), h. darvenisa (AU), j. elovaara (FI), e. garbagnati (IT), c. gary (FR), Cigre Tb 63 (01) (1991) 64.
[16] H. Motoyama, Y. Kinoshita, K. Nonaka, Y. Baba, Experimental and analytical studies on lightning surge response of 500-kv transmission tower, in IEEE Transactions on Power Delivery 24 (4) (2009) 2232–2239.
[17] A. Ametani, N. Triruttanapiruk, K. Yamamoto, Y. Baba, F. Rachidi, Impedance and admittance formulas for a multistair model of transmission towers, in IEEE Transactions on Electromagnetic Compatibility. 10.1109/TEMC.2020.2976644.

[18] B. Salarieh, H.M.J. De Silva, A.M. Gole, A. Ametani, B. Kordi, An electromagnetic model for the calculation of tower surge impedance based on thin wire approximation, in IEEE Transactions on Power Delivery 36 (2) (2021) 1173–1182.
[19] T. Noda, S. Yokoyama, Thin wire representation in finite difference time domain surge simulation, IEEE Trans. Power Del. 17 (3) (2002) 840–847.
[20] K.A. Michalski, D. Zheng, Electromagnetic scattering and radiation by surfaces of arbitrary shape in layered media, I. Theory, in IEEE Transactions on Antennas and Propagation 38 (3) (1990) 335–344.
[21] K.A. Michalski, D. Zheng, Electromagnetic scattering and radiation by surfaces of arbitrary shape in layered media, II. Implementation and results for contiguous half-spaces, in IEEE Transactions on Antennas and Propagation 38 (3) (1990) 345–352.
[22] B. Markovski, L. Grcev, V. Arnautovski-Toseva, Fast and accurate transient analysis of large grounding systems in multilayer soil, in IEEE Transactions on Power Delivery10.1109/TPWRD.2020.2985926.
[23] J.R. Mosig, F.E. Gardiol, Analytical and numerical techniques in the green's function treatment of microstrip antennas and scatterers, IEE Proc. HMicrow., Opt. Antennas 130 (2) (1983) 175–182.
[24] G. Dural, M.I. Aksun, Closed-form green's functions for general sources and stratified media, IEEE Trans. Microw. Theory Tech. 43 (7) (1995) 1545–1552.
[25] G.J. Burke, Numerical electromagnetic code (NEC-4), method of mo- ments, Lawrence Livermore Nat. Lab., Livermore, CA, USA, UCRL- MA-109338 (1992).
[26] G.V. Eleftheriades, J.R. Mosig, On the network characterization of planar passive circuits using the method of moments, IEEETrans. Microw. Theory Techn. 44 (3) (1996) 438–445.
[27] L. Grcev, Modeling of grounding electrodes under lightning currents, IEEE Trans. Electromagn. Compat. 51 (3) (2009) 559–571.
[28] M. Ishii, Y. Baba, Numerical electromagnetic field analysis of tower surge response, in IEEE Transactions on Power Delivery 12 (1) (1997) 483–488, https://doi.org/10.1109/61.568275.
[29] L. Grcev, Impulse efficiency of ground electrodes, IEEE Trans. Power Del. 42 (24) (2009) 441–451.
[30] C.R. Paul, Inductance: Loop and partial, Wiley-IEEE Press, 2010.
[31] F.P. Dawalibi, W. Ruan, S. Fortin, J. Ma, W.K. Daily, Computation of power line structure surge impedances using the electromagnetic field method, 2001 IEEE/PES transmission and distribution conference and exposition, Developing New Perspectives (Cat. No.01CH37294), Atlanta, GA, USA (2001) 663668.
[32] J.R. Mosig, T.K. Sarkar, Comparison of quasi-static and exact electromagnetic fields from a horizontal electric dipole above a lossy dielectric backed by an imperfect ground plane, IEEE Trans. Microw. Theory Tech. MTT-34 (4) (1986) 379–387.

Paper V

TRANSIENT MODELLING AND BACKFLASHOVER RATE ANALYSIS OF A FULLY COMPOSITE PYLON

Hanchi Zhang[1], Qian Wang[1], Kai Yin[1], Claus L Bak[1], F. Faria da Silva[1]*

[1]Aalborg University, Aalborg, Denmark
**qiw@et.aau.dk*

Keywords: FULLY COMPOSITE PYLON, BACKFLASHOVER RATE, PSCAD, MONTE CARLO METHOD

Abstract

A proposal for a fully composite pylon has been designed to meet the requirements of compact structure and elegant appearance for new-generation 400 kV transmission towers, able to save lines corridors and reduce visual impact. Correspondingly, a method of external down-lead has been proposed to bring grounding potential to the shield wires. Based on this design, in this paper, lightning overvoltage level of the fully composite pylon is investigated by using transient simulation tools and backflashover performance is evaluated through Monte Carlo method. An equivalent distributed parameter model of the pylon is established, with the stray capacitances of phase conductors calculated in advance. Monte Carlo method is used to simulate the randomness of lightning current waveform in the nature. The overvoltage levels are simulated in PSCAD to determine the occurrence of backflashover. The backflashover rate (BFOR) is estimated by accumulate the probability of backflashover after repeated random sampling of lightning current. Simulating results show that the BFOR is 0.074 flashes/100 km·year and the overvoltage level calculated becomes lower in the modified model considering stray capacitances. Effects of both the lightning peak current and the tail time on the probability of backflashover occurrence is also summarized.

1. Introduction

In recent years, usage of overhead lines in transmission system has been faced with great challenges, because of the increasing requirement for transmission capacity along with the public opposing to erect more conventional metal lattice towers, which have negative visual impact. A proposal for a fully composite pylon has been designed to meet the requirements of compact structure and elegant appearance for new-generation transmission towers, which has the advantages of saving lines corridors and reducing visual impact[1]. The fully composite pylon is in the shape of a 'Y' geometric configuration, shown in Fig. 1. Conductors are fixed by clamps on the surface of the cross-arm which has an inclined angle of 30° from the horizontal ground plane, thus the conductors are in a diagonal form. Two shield wires are installed at the tips of the two cross-arms respectively. The cross-arms and the body are made of fibre reinforced plastic (FRP) so the pylon itself can not conduct lightning current anymore. Correspondingly, two bare-metal down conductors downwards outside the pylon are used to conduct the lightning current to ground when shield wires are terminated by lightning flashes, which are shown as red lines in Fig. 1.

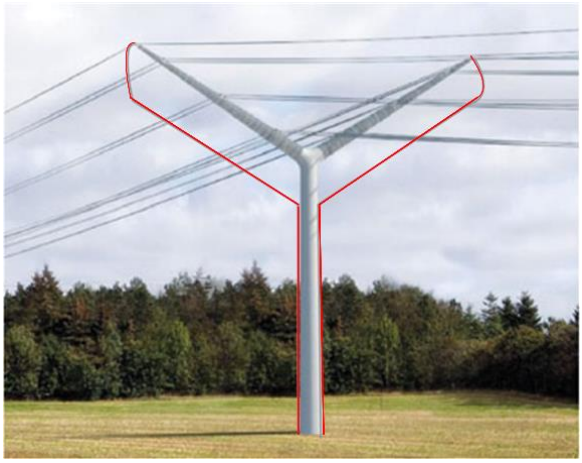

Fig. 1 The picture of the novel 400 kV fully composite pylon

The novel pylon has a more compact size and reduced height due to the elimination of insulator strings. However, there is little experience and research on the lightning performance evaluation about a pylon with such an unusual configuration and electric design. High voltage overhead lines are exposed to lightning strikes, which may cause flashover threatening the safe and steady operation of power grid[2]. If the flashover occurs when the lightning flash strikes directly on the phase conductors bypassing the shield wires, the rate of this condition per 100 km-years of the transmission line is termed the shield failure flashover rate (SFFOR). Direct lightning strikes to shield wires can increase the electric potential of the shield wires in a short time, which may also provoke a flashover between shield wires and conductors. The rate of this condition per 100 km-years of the transmission line is termed the backflashover rate (BFOR)[3].

The SFFOR of this pylon has been studied comprehensively in previous studies. The lightning shield performance of the pylon was investigated based on the electro-geometric model (EGM) and found that there existed an unprotected zone in the middle span of the pylon[4]. The lightning shield performance of the pylon was investigated furthermore based on the method of scale model test, it was proved that shield failure happened in the middle of pylon[5]. To optimize the lightning shield performance, two different shield angles, -60 ° and -70 °, were investigated via both the electro-geometric model (EGM) and scale model tests. And -60 ° can provided better shield performance[6]. According to the above experience, the possibility of lightning shield failure was deeply investigated via both the revised electro-geometric model (EGM) and scale

model tests[7], and it was proved to be practically negligible. Operating experience showed that for the overhead lines over 500 kV, lightning strike accidents were majorly caused by the shield failure of lightning striking towers and shield wires. However, for the overhead lines below 500 kV, lightning strike accidents were majorly caused by the backflashover when lightning striking towers and shield wires [8]. Therefore, the research on BFOR of this 400 kV fully composite pylon is as significant as SFFOR.

The present paper uses the mathematical calculation function of Matlab and the electromagnetic transient analysis function of PSCAD to deal with the BFOR evaluation procedure based on Monte Carlo method. The Monte Carlo method is used to simulate the randomness of lightning current waveform in the nature in order to approach the probability of backflashover[9]. The procedure consists of three steps: pre-processing, numerical simulation and post-processing. In the first step, inverse transform sampling is used in Matlab to create a set of different lightning current waveshapes, with peak current and wave tail time as variables following log-normal distribution, to simulate the statistics of lightning flashes in the nature. In the second step, the OHL transmission system with the novel pylons is established in PSCAD and after inserting the lightning current set from Matlab, the overvoltage level of the certain points on the down-lead is calculated. In the third step, the backflashover is determined in Matlab according to the comparison of the overvoltage level and critical flashover voltage and the BFOR is estimated by the numerical results from the repeated random sampling[10].

2. Methodology

2.1. Transmission line modelling

2.1.1 Configuration of the pylon and wires coordination

The configuration of the fully composite pylon and coordinates of the phase conductors and shield wires are shown in Fig. 2, by setting the horizon as the x-axis and the symmetry axis of the pylon as the y-axis.

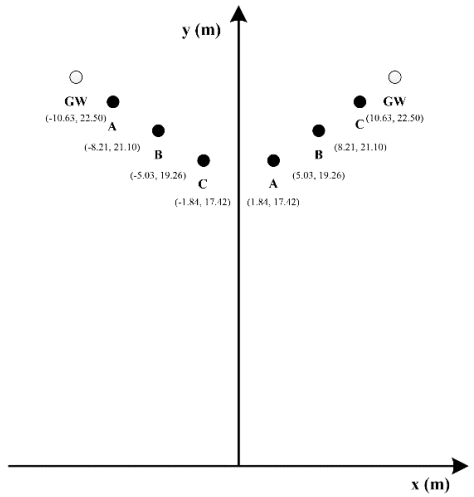

Fig. 2 The configuration of the fully composite pylon and coordinates of the phase conductors and shield wires

2.1.2 OHL Model

The simulated 400 kV/50 Hz double-circuit OHL is 100 km long. The pylon stroke by lightning flash is in the middle of the whole line and the neighbouring two pylons are modelled, the span between which is 250 m. The OHL is simulated in PSCAD by the means of 'Bergeron Model'. At one end of the OHL, phase conductors are connected with a three-phase voltage source and shield wires are solidly grounded. At the other end, the OHL is connected to a load. Corona effect that influence the effective radius of OHL is not simulated for simplification reason.

2.1.3 Down-lead Model

Because the novel pylon body is made of composite materials, the external down-lead is the only path to conduct lightning current to ground. The down-leads can be and regarded as cylindrical bare conductors.

The down-leads can be modelled by a 'Bergeron Model' in PSCAD. The Bergeron Model is represented by a distributed inductance, capacitance and lumped resistance property to approximate system losses[11]. In this paper, one down-lead is divided into two parts, one is the vertical part along with the pylon body and the other is the approximately horizontal part along with the cross-arm, where the overvoltages need to be simulated. The former is modelled in PSCAD by the means of 'Bergeron Model'. Because the length of the latter is relatively short, it is modelled by several RLC-Pi-equivalent circuits so as to the distributed capacitance can be modelled more precisely by considering stray capacitances together[12]. The stray capacitances are calculated by the finite element analysis software COMSOL, the simplified model and results calculated are shown in Fig. 3. The physical model is simply one cross-arm with three phase conductors, one shield wire and an external down-lead surrounded by air. The colorbar shows the electric potential on the cross-arm

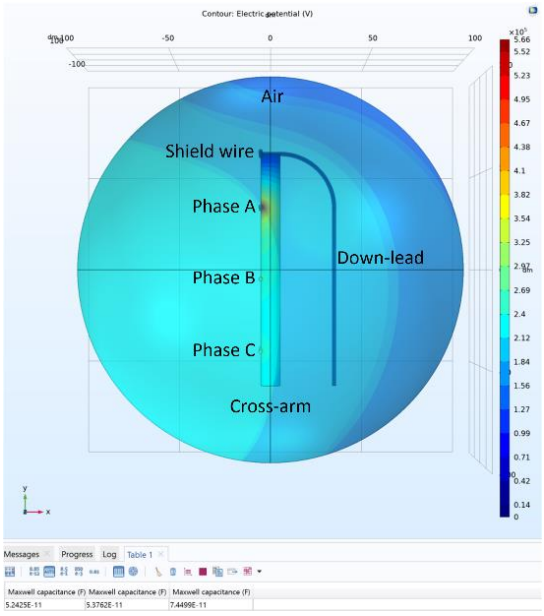

Fig. 3 The model and simulating results of stray capacitances in COMSOL

Given that the radius of the down-lead r is 8 mm, the resistivity ρ is 3.78 × 10^{-8} Ω m and the permeability is equal to μ_0 the permeability of vacuum, the resistance R and inductance L per unit can be calculated at power frequency. R is equal to 0.19 Ω/km and L is equal to 0.047 mH/km. A generic value of 50 Ω is used to represent grounding resistance. The sketch of the down-lead model established in PSCAD is shown in Fig. 4.

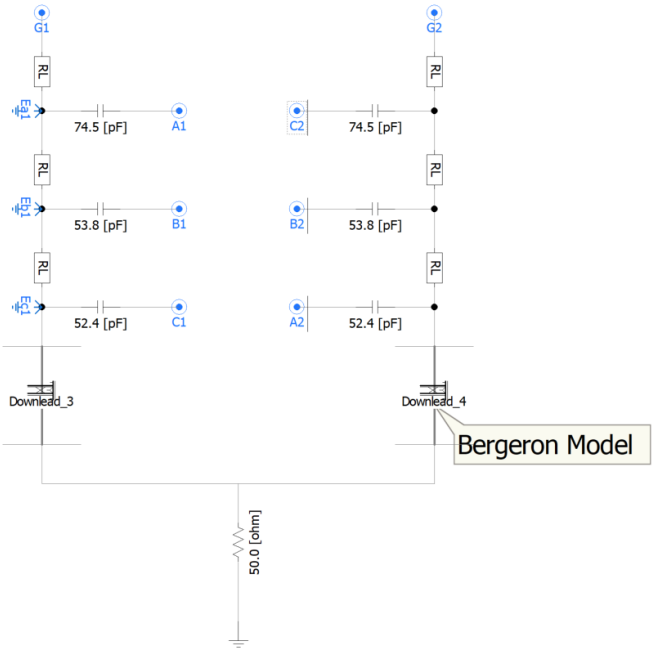

Fig. 4 The sketch of the down-lead model established in PSCAD

2.1.4 Lightning Model

A direct lightning that strikes to one of the shield wires connected to the grounding down-lead is modelled as an ideal current source in parallel with a resistance, which represents the lightning-channel surge impedance[13]. This value ranges from 400 Ω to 1000 Ω and here is set as 400 Ω[14]. The waveform is selected as CIGRE type, which is a piecewise function shaped by four variables, namely the peak of the lightning current I_F, the maximum steepness S_m, the front time (from 30% to 90%) t_f, and the time to half t_h.

2.2. Procedure to estimate BFOR

A simple but approximate deterministic formulation is used to estimate the BFOR (the amount of backflashovers per 100 km lines per year), as shown in equation (1)[3],

$$BFOR = 0.6 \times N_d \times P(I_c) \quad \text{[flashes/100 km·year]} \ (1)$$

where N_d is the estimated number of lightning strikes which terminate on the 100 km line, and $P(I_c)$ is the cumulative probability that a overvoltage caused by lightning current I equals or exceeds the critical flashover voltage level, which is defined as the voltage level where the probability of flashover occurrence is 50%. The numerical multiplicative coefficient 0.6 takes it into consideration that backflashovers within the span can be neglected whereas the voltages caused by the strokes to shield wires along the span practically are lower than those to pylons[15].

2.2.1 Lightning incidences

Ground flash density N_g is used to describe the number of flashes which terminate on the ground per year per square kilometers. The estimated number of lightning strikes which terminate on the lines N_d can be calculated by N_g and shadow area using equation (2),

$$N_d = N_g \times A \quad \text{[flashes/ km·year]} (2)$$

The red area shielded by the grounding wires shown in Fig. 5 is called shadow area, where if the lightning terminates within, it will be attracted to the lines. D is the horizontal distance between the grounding wires, H is the height of the pylon, and R is the protective radii which is related to H, as shown in equation (3)[16],

$$R = 14 \times H^{0.6} \quad \text{[m]} (3)$$

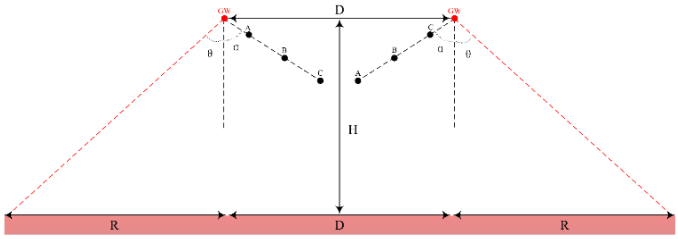

Fig. 5 The demonstration of shielding shadow area

Therefore, the estimated number of lightning strikes which terminate on a 100 km line can be changed into equation (4)[2],

$$N_d = N_g \times (D + 28 \times H^{0.6}) \times 10^{-1} \ \text{[flashes/100 km·year]} (4)$$

2.2.2 Lightning current variables

Analytical expressions to simulate the lightning current waveshape of the first stroke of the downward flash are proposed and recommended CIGRE. Four variables are used to shape the lightning current wave, namely the peak of the lightning current I_F, the maximum steepness S_m, the front time (from 30% to 90%) t_f, and the time to half t_h. All the parameters yield to log-normal distribution. The statistical parameters median M and log standard deviation β of the variables are shown in Table 1[3].

Table 1 The median M and log standard deviation β of the lightning current parameters

Variable	M, median	β, log std. deviation
I_F (>20 kA, kA)	33.3	0.605
S_m (kA/μs)	24.3	0.599
t_f (μs)	3.83	0.553
t_h (μs)	77.5	0.577

In this paper, the peak of the lightning current I_F and the time to half , or in another term, wave tail time t_h are treated as the

variables to shape the lightning current waveform. The front time t_f is equal to the median and the steepness can be determined by I_F and t_f.

2.2.3 Generating the lightning set

Because the probability distributions of the variables follow a log-normal distribution, several mathematical methods can be used to create a set of lightning flashes.

The function in Matlab 'lognrnd' can generate a group of random numbers when the median and log standard deviation of the log-normal distribution are known.

Inverse transform sampling (ITS) can be used when the cumulative distribution function F(x) is known or can be derived by integrating the probability distribution function f(x). Then the inverse function of F(x), $F^{-1}(x)$ can be obtained. According, the random sampling of uniform distribution can be done easily by computer, if u is an element generated by uniform distribution, $x=F^{-1}(u)$ is a sampling element of f(x). As a result, the sampling set of f(x) can be generated from the sampling set of uniform distribution.

In this paper, ITS is adopted to generate the set of random numbers because the cumulative distribution function of log-normal distribution is known. Besides, acceptance-rejection sampling (ARS) and Markov chain-Monte Carlo sampling (MCMCS) can also be used, however they are of lower computational efficiency compared to ITS.

2.2.4 Lightning polarity and CFO

Given that 90% of the lightning flashes to ground are negative while other 10% are positive, the lightning current set is divided into two parts proportionally. For instance, the set size created in this study is 100000, thus 90000 of them are negative lightning flashes and 10000 are positive lightning flashes.

The critical flashover (CFO) is defined as the voltage level where there is 50% probability for flashover to occur, which is determined by the distance of a specific air gap and the environmental factors. Given the environmental condition is wet due to rain, the equations of the CFO under different lightning polarity are selected as follows[15],

$$\mathrm{CFO}_{\mathrm{neg,wet}} = 605 \times \mathrm{D}_{\mathrm{flash}} \quad [\mathrm{kV}] \quad (5)$$

$$\mathrm{CFO}_{\mathrm{pos,wet}} = 560 \times \mathrm{D}_{\mathrm{flash}} \quad [\mathrm{kV}] \quad (6)$$

where D_{flash} is the gap distance when flashover happens. The overvoltages simulated from positive and negative lightning currents need to be compared with corresponding CFO respectively.

2.2.5 Phase angle of the operating voltage

The phase angle of the three-phase system is assumed as a uniformly distributed variable between 0° and 360°. Compared with the period of operating voltage, the duration of overvoltage is very short. When calculating the difference between overvoltage and operating voltage, the phase angle must be taken into consideration.

For a certain lightning current input, the occurrence of the backflashover depends on whether the difference of the overvoltage on the down-lead and the operating voltage exceed CFO. It can be transferred that the occurrence of the backflashover depends on whether the overvoltage exceed the sum of operating voltage and CFO. As shown in Fig. 6 to be specific, if the overvoltage is below the sum of CFO and minimum value of operating voltage, the backflashover won't occur, thus the probability of the backflshover equals to 0. If the overvoltage is below the sum of CFO and maximum value of operating voltage, the backflashover will definitely occur, thus the probability of the backflshover equals to 1. When the overvoltage is between the above two conditions, the occurrence of backflashover depends on the operating voltage at certain phase angle, thus the probability of backflashover can be estimated by the the relation between the operating voltage amplitude and the phase angle, as shown in equation (7),

$$\mathrm{P}\left(\mathrm{V_{over}} - \mathrm{V_{phase}} \geq \mathrm{CFO}\right) = 1 - \frac{\mathrm{t}}{\mathrm{T}} \quad (7)$$

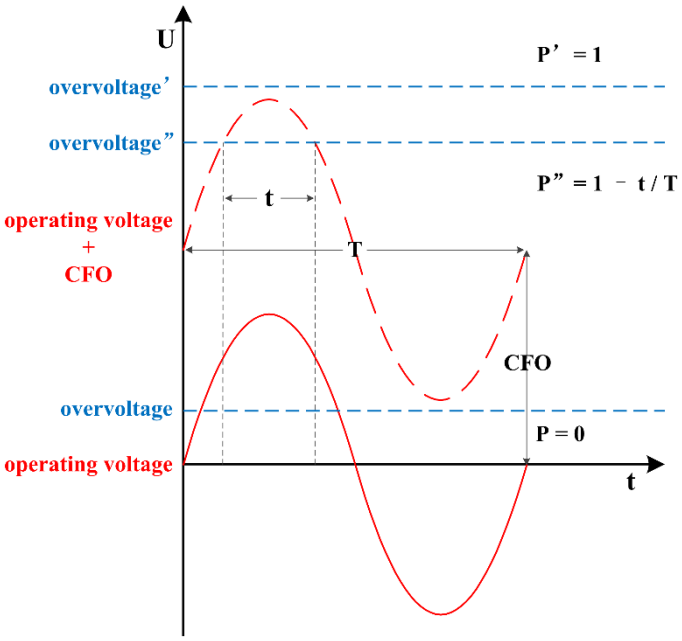

Fig. 6 The demonstration of calculating the backflashover probability under a certain overvoltage

For all the lightning currents input, given that the sample set size of lightning currents is large enough, the probability of backflashover can be estimated by the discrete statistical method. The probability of backflashover $P(I_c)$ is equal to the ratio of the cumulative probabilities of backflashover under every negative and positive lightning flash, which are calculated above among the total number of the lightning flashes input. Thus $P(I_c)$ can be equated as follows in equation (8),

$$\mathrm{P}(\mathrm{I_c}) = 0.5 \times \frac{0.9 \times \sum \mathrm{P}(|\mathrm{V_o} - \mathrm{V_{ph}}| \geq \mathrm{CFO_n}) + 0.1 \times \sum \mathrm{P}(|\mathrm{V_o} - \mathrm{V_{ph}}| \geq \mathrm{CFO_p})}{\mathrm{N_{total}}} \quad (8)$$

where V_o is overvoltage on the down-leads, V_{ph} is the operating voltage of the phase conductors, CFO_n and CFO_p are negative critical flashover voltage and positive critical flashover voltage respectively, and N_{total} is the total number of the lightning flashes input. The numerical multiplicative coefficient 0.5 represents the 50% probability for flashover to occur based on the definition of CFO.

3. Results

3.1. Outcome of the procedure

For the case under study, the parameters of the BFOR estimation can be specified or calculated.

The worst case of ground flash density N_g in Denmark was during 2001-2005, which was equal to 1.39 flashes/km^2[2]. According to the configuration of the pylon, the height of the pylon H is 22.5 m and the horizontal distance between the grounding wires D is 21.28 m. Therefore, the estimated number of lightning strikes which terminate on the 100 km line N_d is equal to 27.5 flashes/100 km·year.

The set size of lightning peak current is 1000 and the set size of lightning wave tail time is 100, thus the total number N_{total} of the input lightning flashes is 100000. According to the simulating results, the number of negative lightning flashes that cause backflashover is 876.43 while the number of positive lightning flashes that cause backflashover is 1127.14 among 100000 flashes. Therefore, the cumulative probability that the overvoltage caused by lightning current equals or exceeds CFO, $P(I_c)$, is equal to 0.0045.

In summary, the BFOR of this case is 0.074 flashes/100 km·year. Referred to the '110 (66) kV-500 kV Overhead Transmission Line Operation Specifications' published by China State Grid in 2005[17], which regulated that the criterion of the BFOR of 220 kV OHL is 0.221 flashes/100 km·year, the BFOR of this case is rather lower than the criterion value.

3.2. Effect of stray capacitances on overvoltage

Capacitors can provide the high-pass path for high frequency wave. Therefore, when the stray capacitances are taken into consideration and modelled in the transient analysis for the down-lead after lightning striking, the transient steep lightning current would be dispersed partially. Fig. 7 (a) shows the overvoltages on the down-lead without considering stray capacitances, whereas Fig. 7 (b) shows the overvoltages considering stray capacitances. It can be found that the maximum magnitude of the overvoltage is by 24.28% lower when modelling stray capacitances.

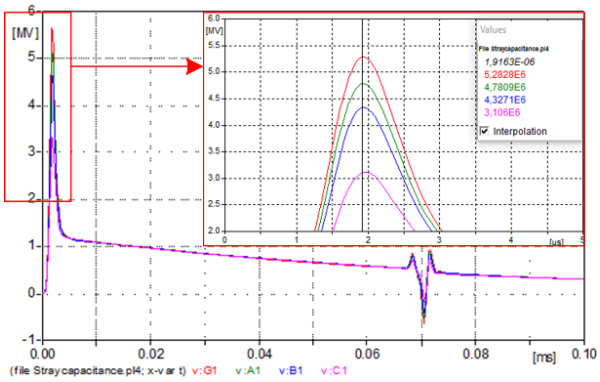

(a)

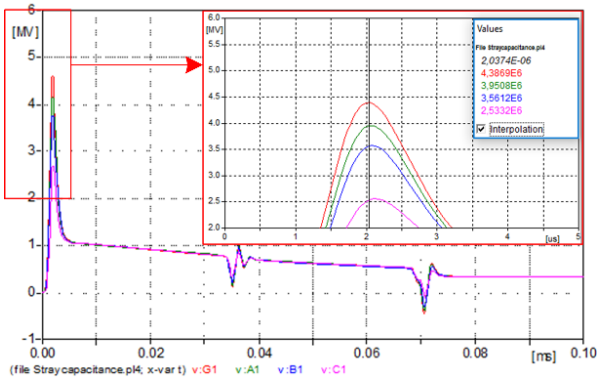

(b)

Fig. 7 (a)The overvoltages on the down-lead modelled without stray capacitances (b) The overvoltages on the down-lead modelled with stray capacitances

3.3. Effect of lightning current parameters on backflashover

The random values of peak value and tail time of lightning current are sampled independently. In Fig. 8, the graph (a) shows the probability distribution function (PDF) in histogram of tail time of lightning current t_h and the graph (b) shows the PDF in histogram of in histogram of peak value of lightning current I_f . The graph (c) in Fig. 8 shows the probability of backflashover under the lightning flashes with different peak values and tail times. Every point on the graph (c) in Fig. 8 represent one lightning waveform shaped by one combination of a peak current and a tail time and its colour represents the probability of backflashover occurrence when the shield wire is terminated by this lightning flash.

It can be seen that along with the increase of the peak value of the lightning current or the increase of the tail time, the probability of the backflashover increases because the overvoltage levels rises up. The curves of the critical probability of 0 and 1 can be plotted and shown as the long-dash red curve and short-dash red curve in graph (c) respectively. The relation between I_f and t_h to result in

backflashover can be fitted and described in rectangular hyperbolic functions as follows equation (9) and (10),

$$I_f = \frac{7229}{t_h} + 139.6 \quad \text{[kA]} \quad (9)$$

$$I_f = \frac{5141}{t_h} + 52.78 \quad \text{[kA]} \quad (10)$$

When the peak current and tail time of a lightning flash can be located beyond the short-dash curve, it can be determined that this lightning will result in backflashover. Conversely, if the peak current and tail time of a lightning flash can be located below the long-dash curve, it can be determined that this lightning will not result in backflashover. if the peak current and tail time of a lightning flash can be located between the two curves, the occurrence of backflashover depends on the phase angle of operating voltage at that time.

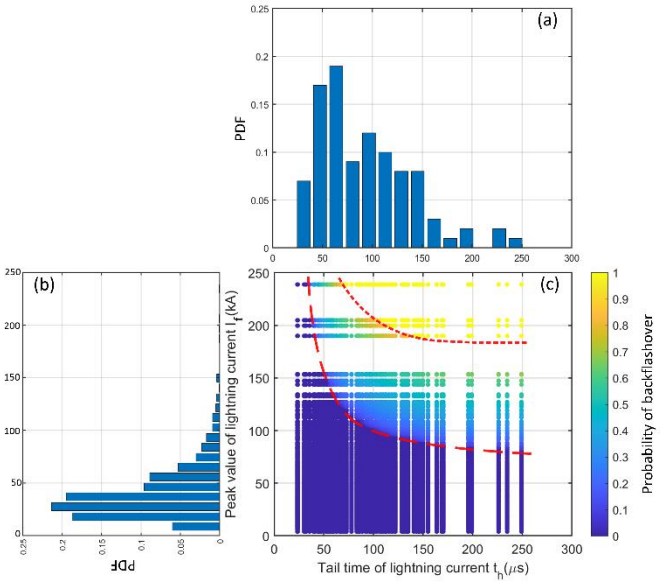

Fig. 8 (a) PDF of tail time of lightning current t_h (b) PDF of peak value of lightning current I_f (c) The probability of backflashover under the lightning flashes with different peak values and tail times

4. Conclusion

This paper investigates the backflashover performance of a novel fully composite pylon of 400 kV with external grounding down-leads. The transmission system model was established and the transient analysis was carried out in PSCAD. Monte Carlo method was used to simulate the randomness of lightning current waveform in the nature in order to estimate the backflashover rate. The following conclusions can be drawn:

- After Monte Carlo procedure, the BFOR of this case is estimated to 0.074 flashes/100 km·year, which is rather lower than the criterion in industrial standards.
- The stray capacitances were considered and calculated in the study, which will decrease the maximum magnitude of overvoltage when lightning striking compared with the case ignoring stray capacitances. Thus the modelling of stray capacitances is recommended and necessary to accord with practical conditions.
- The relationship of both peak current and tail time to the probability of backflashover occurrence is summarized and described in equations. The threshold of the lightning waveform to result in backflashover is fitted which can be referred in the following research on lightning protection performance.

5. References

[1] T. Jahangiri, C. L. Bak, F. F. d. Silva, and B. Endahl, "Determination of minimum air clearances for a 420kV novel unibody composite cross-arm," in *2015 50th International Universities Power Engineering Conference (UPEC)*, 2015, pp. 1-6.

[2] T. Ebdrup, D. Olason, K. Pederson, C. L. Bak, and F. F. Silva, "Comparison of overhead line lightning performance based on two different tower geometries," presented at the Cigré International colloquium on lightning and power systems, Lyon, 2014.

[3] *Guide to procedures for estimating the lightning performance of transmission lines*, 1991.

[4] T. Jahangirl, C. L. Bak, F. M. F. d. Silva, B. Endahl, and J. Holbøll, "Assessment of Lightning Shielding Performance of a 400 kV Double-Circuit Fully Composite Pylon," presented at the Cigré Session 2016, Paris France, 2016. Article in proceedings.

[5] Q. Wang, C. L. Bak, F. F. Silva, and H. Skouboe, "Scale model test on a novel 400 kV double-circuit composite pylon," presented at the International Conference on Power System Transients, 2017.

[6] Q. Wang, T. Jahangiri, C. L. Bak, F. F. d. Silva, and H. Skouboe, "Experimental evaluation of shielding angles' effects on lightning performance in a 400 kV AC double-circuit composite pylon," in *CIGRÉ Symposium 2017*, 2017.

[7] Q. Wang, T. Jahangiri, C. L. Bak, F. F. d. Silva, and H. Skouboe, "Investigation on Shielding Failure of a Novel 400-kV Double-Circuit Composite Tower," *IEEE Transactions on Power Delivery*, vol. 33, no. 2, pp. 752-760, 2018.

[8] J. He, X. Wang, Z. Yu, and R. Zeng, "Statistical Analysis on Lightning Performance of Transmission Lines in Several Regions of China," *IEEE Transactions on Power Delivery*, vol. 30, no. 3, pp. 1543-1551, 2015.

[9] F. M. Gatta, A. Geri, S. Lauria, M. Maccioni, and A. Santarpia, "An ATP-EMTP Monte Carlo procedure for backflashover rate evaluation," in *2012 International Conference on Lightning Protection (ICLP)*, 2012, pp. 1-6.

[10] P. Sarajcev, "Monte Carlo method for estimating backflashover rates on high voltage transmission lines," *Electric Power Systems Research*, vol. 119, pp. 247-257, 2015/02/01/ 2015.

[11] F. F. d. Silva, "Comparison of Bergeron and frequency-dependent cable models for the simulation of electromagnetic transients," in *2016*

51st International Universities Power Engineering Conference (UPEC), 2016, pp. 1-6.
[12] N. N. Akihiro Ametani, Yoshihiro Baba, Teruo Ohno, Koichi Yamabuki, *Power System Transients: Theory and Applications*. CRC Press, 2016.
[13] "IEEE Guide for Improving the Lightning Performance of Electric Power Overhead Distribution Lines," *IEEE Std 1410-2004 (Revision of IEEE Std 1410-1997)*, pp. 1-50, 2004.
[14] Z. G. Datsios, P. N. Mikropoulos, and T. E. Tsovilis, "Effects of Lightning Channel Equivalent Impedance on Lightning Performance of Overhead Transmission Lines," *IEEE Transactions on Electromagnetic Compatibility*, vol. 61, no. 3, pp. 623-630, 2019.
[15] A. R. Hileman, *Insulation Coordination for Power Systems* (POWER ENGINEERING). Taylor & Francis Group, 1999.
[16] A. J. Eriksson, "The Incidence of Lightning Strikes to Power Lines," *IEEE Transactions on Power Delivery*, vol. 2, no. 3, pp. 859-870, 1987.
[17] *110 (66) kV-500 kV Overhead Transmission Line Operation Specifications*, 2005.

Paper VI

Evaluation of Lightning Backflashover Rate of a Fully Composite Pylon using Monte Carlo Method on Environmental Factors

Hanchi Zhang, Mohammad Ghomi, Kai Yin, Qian Wang, Filipe Faria da Silva, Claus Leth Bak
Department of Energy Technology
Aalborg University
Aalborg East 9220, Denmark
Email: hazh@energy.aau.dk

***Abstract*— Design of a 400 kV fully composite pylon with external down-leads to bring grounding potential to earth wires has been proposed to meet the requirements of saving lines corridors and reducing visual impact. The backflashover performance of the pylon is investigated by EMT and the Monte Carlo method is employed on lightning current waveform parameters and soil resistivity. The backflashover rates of the pylon are estimated for different soil conditions and ground flash density in a broad variation. A case study in Denmark is exampled and compared with the backflashover rate of a conventional transmission tower. Because of the non-linearity of the relationship between backflashover probability and the value of soil resistivity, selecting constant soil resistivity for transmission tower footing model in high-resistivity region may overestimate the BFR.**

***Index Terms*-- backflashover rate, fully composite pylon, soil resistivity, Monte Carlo method, EMT**

I. INTRODUCTION

Modernization of overhead transmission lines has met huge challenges, because the capacity demand for transmission lines keeps growing increasingly and the public opposes the erection of traditional lattice towers, which impacts visual environment. A scheme of a fully insulating pylon has been developed for next-generation transmission towers, which has the prominent features of compact structure and aesthetic appearance[1]. The fully insulating pylon looks in a 'Y'-shape appearance, demonstrated in Fig. 1. Both of the cross-arms and the pylon shaft are manufactured with composite materials. Phase conductors are clamped on the top of the cross-arms and the angle between two cross-arms is of 120°. Each of earth wires is fixed at the tip of each cross-arm. When lightning flashes strike on the pylon or earth wires, the pylon itself can no longer serve as the access for lightning current to ground. As one option of grounding approaches to conducting the lightning current, two bare conducting wires are planned to install from the earth wires along the pylon shaft to ground externally, which are denoted in red in the following Fig. 1.

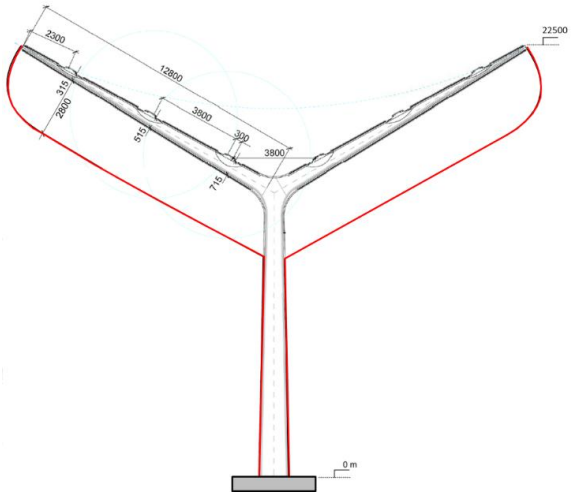

Fig. 1. Sketch of the 400 kV fully composite pylon with external grounding down-leads

As one of the significant indices to assess the lightning protection performance of overhead lines (OHLs), backflashover rate (BFR) is a statistical result correlating the electrical stress of lightning and the electrical strength of insulation, both having a probabilistic nature. Some simplified mathematical methods were recommended by CIGRE and IEEE, respectively, based on observational and experimental data[2, 3]. Both methods intend to calculate the lightning withstand level, then estimate BFR based on the probability that lightning current exceeds the level. In [4], the probability distributions of both lightning crest current and front time are taken into consideration, along with their correlation coefficient. In order to simulate the statistical uncertainties of lightning events, Monte Carlo method (MCM) is generally used to solve such problem and it has an excellent consistence to observation data[5]. A standard MCM for lightning

performance evaluation of transmission lines needs a large amount of lightning events, which are characterized by different lightning current waveshape parameters and different lightning stroke locations[6]. For evaluation of backflashover rate, lightning stroke location is generally omitted, while lightning current crest and lightning front time are selected as key parameters for MCM, which are implemented in EMT software[7, 8]. Besides the lightning parameters, tower footing resistance also affects backflashover performance of the towers significantly. However, at present, MCM is only applied on the pre-ionization footing resistance of the tower[9, 10]. It has been ignored that the pre-ionization footing resistance of the tower is closely related to soil resistivity, which also varies in a wide range from tower to tower randomly.

The concept of fully composite pylon makes a step forward for next-generation transmission towers to integrate economy, reliability and aesthetics together. A general evaluation on backflashover performance is necessary to be proposed considering broad variation of environmental factors, such as lightning waveform and soil resistivity. In particular, for the regions with high soil resistivity that has large dispersion, selecting a constant soil resistivity value for footing model might introduce error into backflashover evaluation from reality. This paper applies MCM on both lightning current parameters and soil resistivity, especially high soil resistivity with large dispersion on backflashover performance evaluation. The paper is organized as follows. Section II to III describe the simulating models of the transmission system within composite pylons for lightning transient analysis and put forward a procedure to estimate BFR based on MCM for both lightning current parameters and soil resistivity. The results of backflashover performance with varying lightning parameters and soil conditions are presented and compared with constant soil resistivity, and the integrated lightning protection performance is analyzed and compared with a traditional metallic tower in Section IV. Section V discusses the deviation of the BF probability by applying MCM on soil resistivity and constant soil resistivity.

II. MODELLING

A. General Simulating Models

The Fig. 2 demonstrates a schematic of the transmission lines model. The pylon struck by lightning is placed in the middle. Only other six adjacent pylon models are established considering the pylons in longer distance do not have obvious influence on the overvoltage at the struck pylon. The span is 250 m.

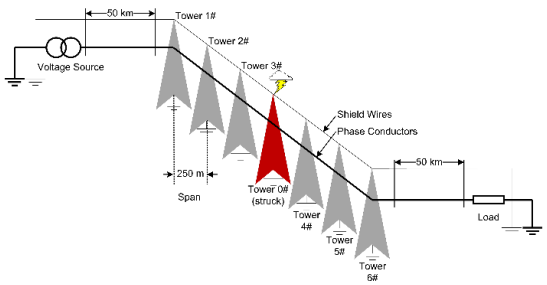

Fig. 2 The demonstration of OHL lines model

A direct lightning that strikes at one of the earth wires connected to the grounding down-lead is modelled. CIGRE model is adopted as lightning impulse source. The grounding down-leads are modelled by a combination of several segments characterized by surge impedance. The backflashover is modelled based on leader progression method, describing the insulation surface flashover based on the physical process of the discharge development in the air. The modelling details of the above components during the simulation can be referred in [11].

B. Current-dependent Pylon Footing Impedance Model

The influence of the pylon footing surge impedance on the transient overvoltage at the top of down-leads is related to the magnitude and frequency of injecting lightning current. For large-scale metallic lattice tower, a grounding grid is commonly used because of the large-size tower base, and it mostly exhibits frequency-dependence. A composite pylon with a relatively small-size pylon base and a concentrated grounding system is desirable, and it mostly exhibits current dependence. Therefore, current-dependent model is established and the footing resistance can be calculated as a function of injecting current in equation (1)[12],

$$R_f = \frac{R_0}{\sqrt{1+(I_R / I_g)}} \tag{1}$$

where R_0 is low-current footing resistance, I_R is the lightning current injecting into ground and I_g is the critical current to ionize the surrounding soil described by equation (2),

$$I_g = \frac{\rho E_0}{2\pi R_0^{\,2}} \tag{2}$$

where E_0 is the electric field gradient for soil ionization and ρ is the soil resistivity. The relationship of them can be described in the equation (3),

$$E_0 = 241 \cdot \rho^{0.215} \tag{3}$$

The footing device is set as an electrode buried vertically. R_0 of a single vertical electrode is also related to ρ and the dimension, in equation (4),

$$R_0 = \frac{\rho}{2\pi L}\left(\ln\frac{4L}{r} - 1\right) \tag{4}$$

where the length L and the radius r of the electrode are 3 m and 15 mm respectively. Equation (4) can be simplified into equation (5),

$$R_0 = 0.3\rho \tag{5}$$

The soil types are ranked into three levels: low-resistivity soil (fills-ashes, cinders, brine wastes), median-resistivity soil (clay, shale, gumbo, loam) and high-resistivity soil (gravel, sand, stones, with little clay and loam). Reference [13] provides the soil resistivities of different soil types with their average, minimum and maximum values. The distribution of soil resistivity follows log normal distribution, approximately. The average is regarded as μ, the median of log normal distribution and the minimum and maximum are regarded as $\mu \pm 3\sigma$, the confidential interval of 99.7%. As a result, σ, the deviation of distribution can be obtained. The probability

distributions of the three types of soil are shown in Fig. 3 and the statistics parameters are shown in Table I.

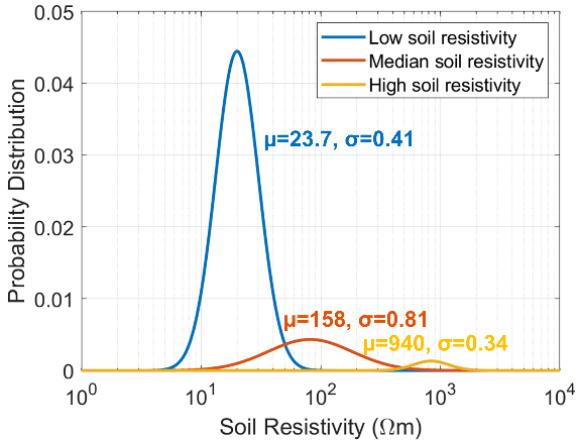

Fig. 3. The probability distribution of different soil classifications

TABLE I THE STATISTICS PARAMETERS OF DIFFERENT SOIL CLASSIFICATIONS

Soil classification	Soil resistivity [Ωm]			
	Min.	Ave., μ	Max.	Dev., σ
Low resistivity	5.9	23.7	70	0.41
Median resistivity	10.2	158	1350	0.81
High resistivity	590	940	4580	0.34

III. BFR ESTIMATION PROCEDURE

A. *Pre-processing step*

In the pre-processing step, a large amount of soil resistivity and lightning currents were generated to simulate the broad variation of natural soil condition and lightning flashes. A pool of lightning waveforms and a pool of soil resistivity were generated randomly based on inverse transform sampling respectively[14].

The random sampling of lightning currents is of two correlated parameters, front time t_f and current crest I_c. A pool of t_f were generated at first. The distribution of I_c is correlated to t_f. After generating the front time pool, the median of log-normal distribution of I_c can be calculated by each value of t_f in the pool by equation (6)[2],

$$M_I = 19.5 \cdot t_f^{\,0.39} \tag{6}$$

Then, corresponding to every t_f, there produces one median of I_c following log-normal distribution. Given that the deviation of I_c, a pool of lightning current crests can be generated also based on inverse transform sampling.

The sizes of front time pool and current crest pool are both 100, thus, the size of lightning current waveform pool N_{total} is 10000. The size of soil resistivity pool of every soil type M_{total} is 100. The adequacy of the sample size is proved as follows.

According to the Central Limit Theorem, the confidence interval can be calculated as follows,

$$CI = (\bar{x} - z^* \times \frac{s}{\sqrt{n}}, \bar{x} + z^* \times \frac{s}{\sqrt{n}}) \tag{7}$$

where $\bar{x}$ is the sample mean and z^* is the statistic associated with a certain confidence interval. In case of a 90% confidence interval, z^* equals to 1.64, approximately. s is the sample standard deviation and n is the sample size. Thus, estimation precision level can be described in following equation (8),

$$\phi = z^* \times \frac{s}{\sqrt{n}} \tag{8}$$

The estimation precision levels of front time and lightning current crest are 0.0907 and 0.1095, and take 2.37% and 0.33% of the medians. The estimation precision levels of three soil resistivity are 0.0413, 0.0814 and 0.0342, and take 0.17%, 0.05% and 0.03‰ of the medians. At a 90% confidence interval, the sample size with a precision level lower than 5% is enough to provide reliable results using MCM.

B. *Numerical simulation step*

The major task in this step is to obtain the lightning overvoltage between down-leads and nearest phase conductors on the pylon struck by lightning and calculate backflashover (BF) probability. The transmission system has already been established in PSCAD. The lightning current waveform pool and three-type soil resistivity pools obtained in last step were input in as lightning impulse current source and pylon grounding condition respectively.

The AC voltage on phase conductors is considered when estimating the BF probability for each lightning current and soil resistivity. When determining backflashover, the voltage function $u(t)$ in leader progression method equals to the voltage difference between the AC voltage V on phase conductors and the overvoltages on the down-leads. The duration of lightning transients is extremely instant compared with AC period, thus the change of AC voltage can be neglected and AC voltage can be treated as a constant. A critical AC voltage V_i is defined first. $u(t)$ higher than V_i can definitely cause flashover, while $u(t)$ lower than V_i cannot cause flashover. As a result, the BF probability can be calculated as the probability that the AC voltage is higher than V_i in one AC period.

C. *Post-processing step*

All the results of BF probability from last step are processed in this step. The BF probability of each lightning current $P(I)$ is calculated first by processing the results of BF probability under all conditions of soil resistivity $P(\rho)$. Then, BFR is evaluated by processing the results of BF probability of all lightning waveforms.

The BF probability of every lightning current can be expressed in equation (9),

$$P(I) = \frac{\sum P(\rho)}{M_{total}} \tag{9}$$

where $P(I)$ is the BF probability of one lightning current, $\Sigma P(\rho)$ is the sum of the BF probability under all soil resistivity of one certain soil type and M_{total} is the total number of input soil resistivity. Then, the final BFR can be expressed in equation (10)[2],

$$BFR = 0.6 \cdot N_d \cdot \frac{\sum P(I)}{N_{total}} \tag{10}$$

where $\Sigma P(I)$ is the sum of BF probability of each lightning waveform. N_d is the statistical amount of lightning flashes striking on a 100-km OHL per year. $\Sigma P(I)/N_{total}$ is termed as BF probability, P_{total}.

N_d depends on the lightning density and tower configuration in equation (11),

$$N_d = N_g \cdot (D + 28H^{0.6}) \cdot 10^{-1} \quad (11)$$

where N_g is the ground flash density, terming the amount of flashes that strike on per-square-kilometer ground every year. D is the horizontal width of earth wires and H is the height from pylon bottom to earth wire. The overvoltages caused by lightning flashes terminating within the span is smaller than the overvoltages caused by those terminating at the pylon head. Thus, the numerical multiplicative coefficient 0.6 takes it into consideration that the BFR should be reduced to 60% approximately if lightning flashes terminate at mid-span[2].

In order to assess N_g, different regions proposed different gradings based on local meteorological conditions[15, 16]. Referred to those standards, a classification to assess N_g is set so that the backflashover performance can be evaluated under different lightning conditions, as shown in Table II.

TABLE II THE CLASSIFICATION OF LIGHTNING DENSITY

Lightning density level	Ground flash density range [case/km^2·year]
Low lightning density	$N_g \leq 2$
Median lightning density	$2 < N_g \leq 4$
High lightning density	$4 < N_g \leq 6$
Extra high lightning density	$N_g > 6$

IV. RESULTS

A. Comparison of backflashover probability of the composite pylon with constant soil resistivity footing model and MCM on soil resistivity footing model

The sampling of soil resistivity for MCM follows the log normal distribution, which is defined by median and deviation. Therefore, the BF probability of composite pylon is evaluated with the pylon footing model of constant soil resistivity and the pylon footing model of soil resistivity dealt by MCM. The results are shown and compared in following Fig. 4.

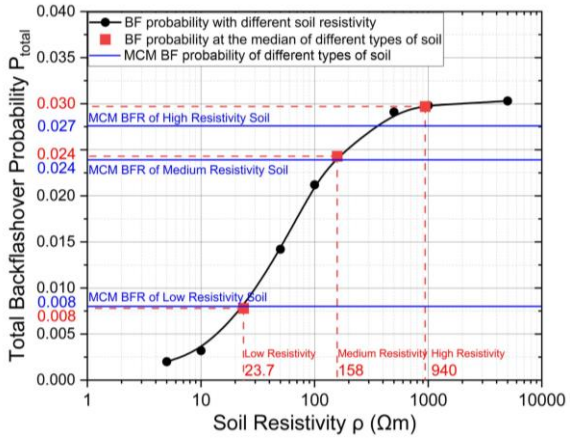

Fig. 4 MCM BF probability of different types of soil v.s. BF probability at the median of different types of soil

The relationship of BF probability and constant soil resistivity is shown as the black dot-line. The red dots represent three specific values of BF probability at the soil resistivities that equal to the medians of soil resistivity distribution of different types, as listed in Table II. The blue lines show the levels of BF probability when MCM is applied on soil resistivity distribution of different types. It can be found that when soil resistivity is lower than around 500 Ωm, BF probability is approximately linear to the log of soil resistivity. When soil resistivity is higher than 500 Ωm, BF probability is not closely sensitive to the change of soil resistivity. For low-resistivity soil and medium-resistivity soil, the MCM BF probability is close to the BF probability of the median soil resistivity. However, for high-resistivity soil, the MCM BF probability has a larger deviation, around 10% smaller than the BF probability of the median soil resistivity.

B. Results of lightning protection performance of the 400 kV composite pylon compared with metallic towers

After obtaining BF probability, BFR can be calculated considering ground flash density and pylon geometry as formulated in equation (10) and (11). The BFRs of the composite pylon under different ground flash density and soil conditions are calculated and presented in Table III. To be noted, BFR is linear to N_g.

TABLE III THE BFRS OF THE 400 KV COMPOSITE PYLON UNDER DIFFERENT GROUND FLASH DENSITY AND SOIL CONDITIONS

Soil type	BFR [case/100 km·year]			
	Low N_g	Median N_g	High N_g	Extra high N_g
Low-ρ soil	0 ~ 0.3	0.3 ~ 0.5	0.5 ~ 0.8	0.8 ~
Median-ρ soil	0 ~ 0.7	0.7 ~ 1.4	1.4 ~ 2.3	2.3 ~
High-ρ soil	0 ~ 1.0	1.0 ~ 2.3	2.3 ~ 3.3	3.3 ~

Considering the future on-site test will be carried out in Denmark, a case study is carried out based on Danish meteorological and geological conditions. The worst case of ground flash density N_g in Denmark was selected, which was equal to 1.39 cases/km^2 during 2001-2005. Most soil in Denmark is clay or sandy clay, which is classified as median-resistivity soil[17]. Thus, the BF probability resulted by the lightning flashes terminating on earth wires is equal to 0.024. The BFR is evaluated as 0.4 cases/100 km·year.

The 400 kV Donau tower which has been widely installed in Denmark is referred for comparison[18]. The Donau tower model was established based on the multi-conductor lossless line model. Lightning current pool, tower footing impedance pool and other external factors were the same as those in the simulating model of the composite pylon. The different factors influencing backflashover performance of composite pylon and Donau tower are summarized in Table IV. Looking into the composite pylon, its compact configuration makes it attract fewer lightning flashes. The larger surge impedance of down-leads will cause larger overvoltage. The air clearance between down-leads and phase conductors is shorter than the length of suspension insulators on Donau tower. When the same overvoltage level rises up on the composite pylon as on Donau tower, flashover has higher probability to occur. In total, the estimated BFR of composite pylon is only a bit higher than that of Donau tower, which equal to 0.3 cases/100

km·year, but composite pylon has other advantages of saving corridors, reducing cost and improving visual impact.

TABLE IV THE COMPARISON OF FACTORS INFLUENCING BACKFLASHOVER RESULTS BETWEEN COMPOSITE PYLON AND DONAU TOWER

Tower type	Composite pylon	Donau Tower
Tower height H [m]	22.5	41.62
Earth wire distance D [m]	21.28	20.74
Air clearance L [m]	2.8	3.2
BF probability $P(I_C)$	0.024	0.018
BFR [cases/100 km·yr]	0.4	0.3

V. DISCUSSION ON MCM APPLIED ON SOIL RESISTIVITY IN BFR EVALUATION FOR COMPOSITE PYLONS

The deviation between MCM result and constant median result is due to the non-linearity of the relationship between backflashover probability and the log of soil resistivity. MCM is prior to solve such non-linear problem.

For low-resistivity soil and medium-resistivity soil, the values of soil resistivity in sample are lower than 500 Ωm, BF probability is approximately linear to the log of soil resistivity. Because soil resistivity yields to log-normal distribution, the linearity between BF probability and the log of soil resistivity results in the small deviation between the MCM BF probability and the BF probability of the median soil resistivity. However, for high-resistivity soil, most values of which are larger than around 500 Ωm, the relationship of BF probability is not linear to the log of soil resistivity and it presents an increasing and concave trend. Thus, it can be inferred that the MCM BF probability is much lower than the BF probability of the median soil resistivity.

The turning point of the linearity between BF probability and the log of soil resistivity is related to the insulation level of the transmission pylon. If the insulation level is higher, the slope of the BF probability-to-log of soil resistivity relationship will be smaller, which means the turning point will locate at higher soil resistivity and vice versa.

In summary, if current-dependence footing model with constant soil resistivity is adopted in backflashover study for a transmission tower installed in high resistivity region, the BFR is probably overestimated because of the non-linearity between BF probability and the log of soil resistivity, and the dispersion of soil resistivity.

VI. CONCLUSIONS

This paper proposed a general evaluation on the backflashover performance of a novel fully composite pylon considering broad variation of environmental factors. To deal with the broad variation, Monte Carlo method is employed on both lightning current parameters and soil resistivity. The sample size for MCM is examined also.

Firstly, the non-linearity of the relationship between backflashover probability and the log of soil resistivity is concluded. A turning point of soil resistivity exists. Before the point, BF probability is approximately linear to the log of soil resistivity, while after the point BF probability is not closely sensitive to the change of soil resistivity.

Then, there is a large deviation between the MCM BF probability and the BF probability of the constant median soil resistivity for high resistivity soil, but similar results for low and medium resistivity soils. Thus, if current-dependent footing model with constant soil resistivity is adopted in backflashover study for a transmission tower installed in high resistivity region, the BFR is probably overestimated.

REFERENCES

[1] BYSTRUP. "THE COMPOSITE PYLON." https://www.powerpylons.com/composite-pylon (accessed.

[2] A. R. Hileman, *Insulation Coordination for Power Systems* (POWER ENGINEERING). Taylor & Francis Group, 1999.

[3] IEEE Working Group on Lightning Performance of Transmission Lines, "A Simplified Method for Estimating Lightning Performance of Transmission Lines," *IEEE Transactions on Power Apparatus and Systems*, vol. PAS-104, no. 4, pp. 918-932, 1985.

[4] P. Chowdhuri, "Parametric effects on the induced voltages on overhead lines by lightning strokes to nearby ground," *IEEE Transactions on Power Delivery*, vol. 4, no. 2, pp. 1185-1194, 1989.

[5] J. G. Anderson, "Monte Carlo Computer Calculation of Transmission-Line Lightning Performance," *Transactions of the American Institute of Electrical Engineers. Part III: Power Apparatus and Systems*, vol. 80, no. 3, pp. 414-419, 1961.

[6] A. Borghetti, F. Napolitano, C. A. Nucci, and F. Tossani, "Application of the Monte Carlo method to lightning protection and insulation coordination practices," *Lightning Interaction with Power Systems*, vol. 2, pp. 1-25, 2020.

[7] F. M. Gatta, A. Geri, S. Lauria, M. Maccioni, and A. Santarpia, "An ATP-EMTP Monte Carlo procedure for backflashover rate evaluation: A comparison with the CIGRE method," *Electric Power Systems Research*, vol. 113, pp. 134-140, 2014/08/01/ 2014.

[8] P. Sarajcev, "Monte Carlo method for estimating backflashover rates on high voltage transmission lines," *Electric Power Systems Research*, vol. 119, pp. 247-257, 2015/02/01/ 2015.

[9] S. Shelemy and D. Swatek, "Monte Carlo simulation of lightning strikes to the Nelson River HVDC transmission lines," in *International Conference on Power System Transients*, 2001, pp. 1-6."

[10] R. Shariatinasab and J. G. Safar, "Probabilistic evaluation of lightning performance of overhead distribution lines using Monte Carlo method," in *2012 Proceedings of 17th Conference on Electrical Power Distribution*, 2-3 May 2012 2012, pp. 1-7."

[11] H. Zhang *et al.*, "Comparison of Backflashover performance between a novel composite pylon and metallic towers," *Electric Power Systems Research*, vol. 196, p. 107263, 2021/07/01/ 2021.

[12] CIGRE Working Group 01 SC. 33, "Guide to procedures for estimating the lightning performance of transmission lines," *CIGRE Technical Brochure 63*, 1991.

[13] D. Weston, *Electromagnetic Compatibility: Principles and Applications, Revised and Expanded*. CRC Press, 2001.

[14] C. R. Vogel, *Computational methods for inverse problems*. Siam, 2002.

[15] A. Mäkelä, S.-E. Enno, and J. Haapalainen, "Nordic Lightning Information System: Thunderstorm climate of Northern Europe for the period 2002–2011," *Atmospheric Research*, vol. 139, pp. 46-61, 2014/03/15/ 2014.

[16] X. Jiao, H. Xing, Q. Zhang, and J. Zhou, "Meteorological risk identification and assessment of offshore wind farms," in *IOP Conference Series: Earth and Environmental Science*, 2020, vol. 514, no. 3: IOP Publishing, p. 032016."

[17] K. Adhikari, "Soil mapping in Denmark using digital soil mapping Techniques," 2013.

[18] T. Ebdrup, D. Olason, K. Pederson, C. L. Bak, and F. F. Silva, "Comparison of overhead line lightning performance based on two different tower geometries," presented at the Cigré International colloquium on lightning and power systems, Lyon, 2014."

Paper VII

A Simplified Dynamic Surge Impedance Model with Corona Effect for Grounding Down-Leads of Composite Pylons

Hanchi Zhang[1], Kai Yin[1], Kye Yak See[2], Qian Wang[1], Filipe Faria da Silva[1], Claus Leth Bak[1]

AAU Energy[1]
Aalborg University
Aalborg, Denmark

[2]School of Electrical and Electronic Engineering
Nanyang Technological University
Singapore, Singapore

Email: hazh@energy.aau.dk

***Abstract*— Design of a novel 400 kV fully composite pylon utilizes external down-leads to bring grounding potential to earth wires. In lightning transient studies, the corona effect on the thin-wire down-leads should not be neglected. A simplified dynamic surge impedance model for thin-wire vertical conductors considering voltage-dependent surge corona is proposed. The model describes the relationship between corona development and the surge overvoltage, it focuses on the macro effect of corona on the surge response of conductors, and it ignores the micro plasma dynamics inside the corona. Higher applied lightning current peaks will cause a longer corona radius and cause more reduction in overvoltage. If the front time of applied lightning impulse current increases, the maximum corona radius increases first and then decreases, because the corona development is dominated by expansion velocity and critical streamer-tip electric field in succession. The dynamic surge impedance model shows a reduction of the overvoltage at the top of the conductor by 40% approximately compared with a constant surge impedance model without considering corona, which shows it is necessary to consider the corona effect in the lightning transients research of thin-wire grounding devices.**

***Index Terms*—corona effect, fully composite pylon, lightning overvoltage, EMT, COMSOL**

I. INTRODUCTION

The increasing power demand requires the construction of additional power plants and transmission lines. In the past decades, many concepts of composite pylons have emerged to meet the requirements of more efficient, durable, and compact transmission towers[1]. If the pylon is fully made of composite materials, it raises a challenge that a method is needed to bring the ground potential to shield wires when lightning strikes. A direct method is installing grounding down-leads to conduct lightning current to the ground.

When a lightning flash strikes at the shield wires of the overhead lines, the lightning current passing through both metallic towers and the down-leads of the composite tower will cause corona discharge at the edges of conductive paths. In lightning electromagnetic transient studies, the tower is represented by means of one or several surge impedance sections that are assembled taking into account the tower structure[2]. The tower models neglect surge corona because of the relatively small corona radius compared with tower size. However, the grounding down-leads anticipated to install on composite pylons are very thin, with a cross-section radius of several centimeters, which is comparable to the corona developing radius during a lightning surge. Corona discharge around the down-leads decreases the surge impedance of the down-leads, distorts the wavefronts of overvoltage, and enhances the coupling effect between down-leads and phase conductors. Thus, the impact of surge corona on the transient performance of the grounding down-leads cannot be neglected.

The surge corona modeling for overhead lines has been studied for several decades. There are two main ways to model corona. One is to obtain a q-v curve by experiments first and then, reproduce the specific q-v curve by constructing linear, piecewise linear, or nonlinear circuits[3, 4]. However, it is practical for simulation to reproduce the q-v curve without field tests. Therefore, the other way is to attempt to reproduce the q-v curve from the geometrical configuration of the conductor and physical process. Some finite element method (FEM) simulating tools are used, but the modeling of plasma dynamics inside the corona makes the calculation quite time-consuming[5]. Recent research has simplified the corona dynamics then corona can be modeled by the finite-difference time-domain (FDTD) method in the simulation of large-scale transmission lines[6-8]. Another model considering the physical process of the corona is the corona shell model, which points out that space charges generated by the corona form a shell around the conductor[9]. This concept simplifies the modeling of corona around the thin-wire conductors considerably. The corona shell model was initially proposed for the calculation of steady-state corona and recently, it was applied to surge corona [10, 11]. There is little modeling

research to be referred for the surge corona on grounding down-leads in the lightning study of composite pylons. The main difference lies in the vertical position in space of down-leads whereas overhead lines are horizontal. The corona modeling of trigger-wire of lightning triggering rockets can be referred to because the trigger-wires and down-leads can be regarded as vertical cylinders and the presence of corona is regarded as the increasing radius of the cylinders[12, 13].

This paper proposed a simplified dynamic surge impedance model for thin-wire vertical conductors considering voltage-dependent surge corona. The model describes the relationship between dynamic corona development and surge overvoltage and focuses on the macro effect of corona on the surge response of conductors. The micro plasma dynamics inside corona are neglected, such as particle conservation with recombination, streamer development, and ionization. The corona effect is transferred into the circuit model, which is convenient to be implemented into EMT software. The corona developing processes under different lightning current waveforms are simulated and the overvoltage produced by the models with and without corona is compared. Only negative polarity lightning cases are studied in this paper.

II. MODELING

A. Lightning Current Source Model

CIGRE lightning current model is used because of its consistency with the waveshape of lightning flashes in nature. Four variables are used in analytical expressions to shape the lightning current waveshape of the first stroke of the downward flash, as recommended by CIGRE[14], namely lightning current peak amplitude I_c, maximum steepness S_m, front time (from 30% to 90%) *of*, and tail time t_h.

In this paper, I_c and t_f are treated as the variables to shape the lightning current waveform. t_h is set as constant as 75 μs because corona development is irrelevant to the wave tail of overvoltage. S_m is set as per the unit value determined by I_c and t_f and its base value is equal to the quotient of I_c and t_f. Lightning channel impedance is set as 400 Ω [14].

B. Down-lead Model with Voltage-dependent Corona

The surge impedance of the vertical cylindrical conductor has been evaluated for decades and Sargent's model is adopted. The corona sheath is regarded as the increasing radius of the conductor. Thus, the surge impedance of the thin-wire conductor is described by the sum of conductor radius and corona radius, as described in equation (1) [15],

$$Z = 60(\ln(\sqrt{2}\frac{2h}{r+r_{cr}})-1) \quad (1)$$

where h is the height of the conductor, r is the cross-section radius of the conductor, and r_{cr} is the radius of the corona sheath, which is voltage-dependent as described in the next chapter.

C. Other modeling assumptions

Because the height of the down-lead is 20 m, the traveling time for lightning current from the top of the down-lead to the ground is around 0.06 μs, which is very short in a lightning transient. The overvoltage is supposed to be the same along the conductor in the vertical direction at the same time. The expansion of the corona surrounding the conductor in the vertical direction is also supposed as uniform. Therefore, the down-lead with corona sheath is modeled as a cylindrical conductor with a time-variant voltage-dependent radius.

Some parameters are calculated by COMSOL, and the model in COMSOL is shown in Fig. 1 with the dimension of every part. The down-lead is in the configuration of a vertical cylindrical conductor with a height of 20 m from the ground flat and a cross-section radius of 0.01 m. A 5-meter part of the conductor is buried in soil and the ideal grounding layer is set as a hemisphere with a radius of 10 m. Corona is modeled in a cylindrical shell surrounding the conductor.

In order to illustrate the sole impact of variable surge impedance of down-lead on overvoltage, the footing impedance of the down-lead is set as constant as 10 Ω.

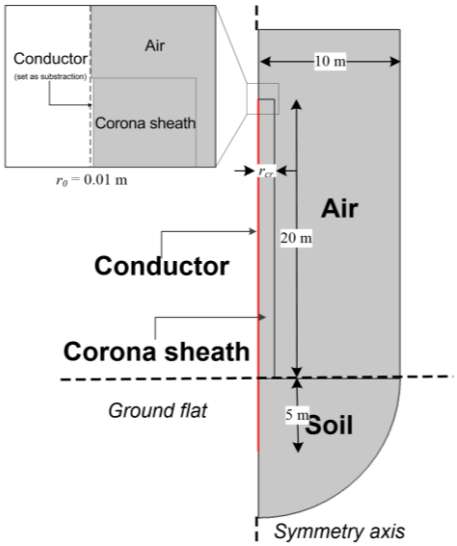

Fig. 1 A sketch of the geometry model established in COMSOL for parameter evaluation and its dimension

III. DESCRIPTION OF CORONA EXPANSION

Corona is the partial breakdown of the air in the vicinity of a conductor applied to high electric stress. The physical properties of surge corona in the air are introduced at first.

One of the necessary conditions for corona to onset is that the electric field around the stressed conductor exceeds a critical threshold, namely corona inception electric field E_{cr} [16]. Correspondingly, the overvoltage causing E_{cr} is termed as corona inception overvoltage V_{cr}.

The other condition is the free electrons in a high electric field area to induce a self-sustained electron avalanche. The occurrence of a specific electron and ionization to create space charge takes a certain time, namely statistical time lag, t_s [5].

The expansion of the corona sheath is governed by the guiding electric field E_g, which is the sum of the electric field created by conductor potential and the electric field created by

space charges in the corona. The expansion velocity equals the streamer velocity v_{cr}.

The corona effect only occurs when the applied voltage is increasing. Thus, the corona only expands and develops during wave front of impulse overvoltage instead of wave tail. A critical electric field at the streamer-tip of the corona sheath E_b is necessary for streamer propagation, which determines the maximum expansion radius of the corona sheath.

In summary, once the impulse overvoltage on the conductor rises and exceeds V_{cr}, the corona will onset after a delay of t_s. Then, corona expands at the velocity of v_{cr}, and the electric field at the streamer's tip is limited by E_b until the overvoltage starts decreasing.

A. Corona Inception Electric Field

The corona inception electric field E_{cr} (kV/mm) of cylindrical conductors was investigated experimentally by Peek[16]. Afterward, some more practical equations to evaluate E_{cr} were produced based on Peek's law. The equation by Hartmann is adopted[17],

$$E_{cr} = m \cdot 2.594 \cdot \left(1 + \frac{0.1269}{r^{0.4346}}\right) \quad \text{[kV/mm](2)}$$

where m is the roughness coefficient of the conductor surface and equals 0.5, and r is the conductor radius in mm.

As a result, the corona inception electric field E_{cr} is calculated as 3 kV/mm. This value is imported into the electric field evaluation of the vertical conductor in COMSOL to calculate critical voltage V_{cr}. According to the software results, V_{cr} at the bottom of the conductor equals 430 kV, while V_{cr} at the top of the conductor equals 240 kV. Out of simplification, V_{cr} is unified as 350 kV.

B. Statistical Time Lag

Statistic time lag t_s is generally not related to the electric field and other electrostatic parameters but is related to air pressure, temperature, and other air conditions. Thus, it is directly referred to the experimental results of other scholars. In [5], t_s varies from 0.4 μs to 0.7 μs. In [18], t_s varies from 0.45 μs to 0.88 μs. In this paper, t_s is considered as 0.6 μs.

C. Corona Expansion and Shrinking Velocity

After the electric field on the surface of the conductor exceeds E_{cr}, the corona effect onsets. The expansion velocity of corona concluded in [5] ranges from 0.3 m/μs to 2 m/μs under the voltage ranging from 300 kV to 500 kV. Besides, [19] reported the radial speed of negative corona streamer from conductor surface in coaxial cylindrical electric field equals to around 0.1 m/μs, while [20] also reported 0.1 m/μs as the speed for positive corona streamers. The highest speed in the literature is 4.4 m/μs [21]. Corona expansion velocity v_{cr} is generally related to the electric field, but out of simplification and referring to relevant simulating research using FDTD, v_{cr} is estimated as a constant of 1 m/μs[8, 22, 23].

When the overvoltage reaches its crest, it decreases, and the corona will shrink until extinct. It is assumed that the corona shrinking velocity is equal to the expansion velocity.

D. Streamer-tip Electric Field

A critical electric field at the streamer's tip limits the expansion of the corona, which determines the maximum extent of the radially expanding corona region. The critical streamer-tip electric fields at positive and negative polarity are as follows[24]. Only negative polarity is studied in this paper.

$$E_{bp} = 0.5 \quad \text{[kV/mm](3)}$$

$$E_{bn} = 1.5 \quad \text{[kV/mm](4)}$$

The corona sheath is assumed as an ideal conductor with a conductivity of 40 μS/m[8]. The electric field is produced both by conductor potential and the space charge in the corona. The space charge density distribution related to electric field is described by equation (5),

$$E(r) = \frac{Q}{2\pi\varepsilon_0 r} + \frac{Q}{2\pi\varepsilon_0 (2h - r)} \quad \text{[V/m](5)}$$

where $E(r)$ is the radial electric field, Q is the space charge per meter, h is the height from ground flat to the top of vertical conductor, and r is the radial distance from the center. For h>>r, equation (5) can be simplified into equation (6), then the space charge density distribution can be expressed by equation (7),

$$E(r) = \frac{Q}{2\pi\varepsilon_0 r} \quad \text{[V/m](6)}$$

$$\rho(r) = \frac{Q}{\pi r^2} = \frac{E(r) \cdot \varepsilon_0}{r} \quad \text{[C/m}^3\text{](7)}$$

Then equation (7) is given to the domain of the corona, together with the electric potential on the conductor to calculate the total electric field at the surface of the corona. For every maximum corona radius, the applied voltage on the conductor that causes the electric field at the surface of the corona equal to E_b is calculated. The relationship of corona radius and the applied voltage is fitted in curves as shown in Fig. 2. As can be seen, maximum corona radius is related to overvoltage, thus is indirectly related to time, marked as $r_{max}(t)$.

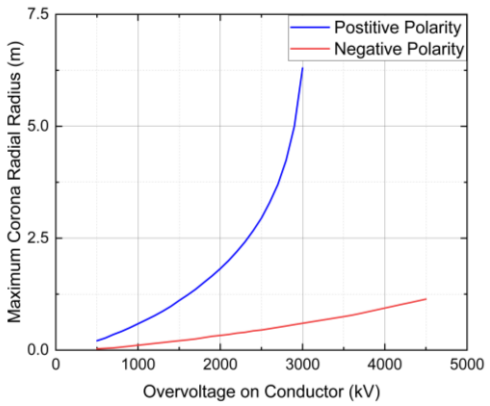

Fig. 2 Maximum corona radius limited by critical streamer-tip electric field under different polarities and amplitude of overvoltage on the conductor

E. Corona Radius

Based on the above analysis and assumptions, a time-variant voltage-dependent surge impedance model is proposed

to describe the expansion of corona during a lightning transient. When overvoltage on the down-lead exceeds V_{cr}, corona onsets. During expansion, $r_{cr}(t)$ is restricted by both the expansion velocity v_{cr} and the maximum expansion radius $r_{max}(t)$. When overvoltage reaches its crest and starts decreasing, corona starts shrinking at the shrinking velocity, which is numerically equal to expansion velocity v_{cr}, until corona extinguishes. Thus, it can be described as equation (8), where t_0 is the time when $r_{cr}(t_0)$ equals 0.

$$r_{cr}(t)=\begin{cases}\min\{v_{cr}\cdot(t-t_s-t_{cr}),r_{max}(t)\}, & 0<t\le t_f\\ r_{cr}(t_f)-v_{cr}\cdot(t-t_f), & t_f<t<t_0\end{cases}\ \text{[m]} \quad (8)$$

IV. Results

A. Influence of Corona Developing on Surge Impedance and Overvoltage

The overvoltage, surge impedance, and corona radius influence each other in every time step. The surge impedance is in negative correlation with corona radius, and overvoltage is impacted by surge impedance. Then overvoltage induces the development of corona radius. When overvoltage meets the maximum, surge impedance is the lowest, and corona radius is the largest, then corona starts shrinking.

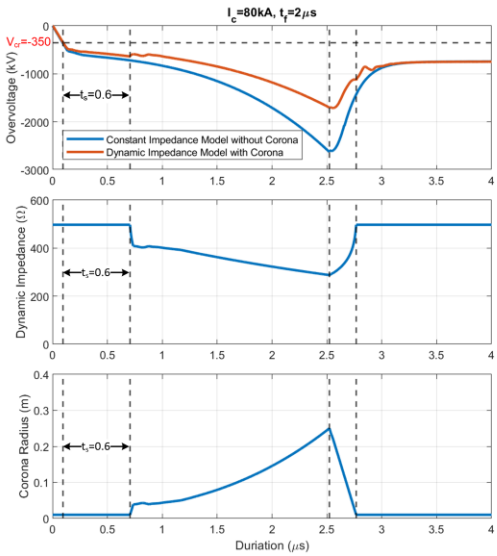

Fig. 3 Relationship among overvoltage at the top of conductor, surge impedance, and corona radius during one lightning impulse case

Fig. 3 shows an example of the mutual influence among overvoltage, surge impedance, and corona radius. The lightning current is of 80 kA/2 μs. When overvoltage exceeds V_{cr}, after a delay of t_s, corona starts developing at the velocity of v_{cr}. When the electric field of the streamer's tip reaches E_{bn}, the electric field keeps constant and limits the corona radius to change with the curve in Fig. 2. When overvoltage meets crest and starts decreasing, surge impedance is the lowest, and corona radius is the largest, then corona starts shrinking.

B. Corona Development with Different Lightning Current Peaks

Fig. 4 shows the corona radius developing processes under the lightning currents of the same front time (2 μs) and different peaks, from 50 kA to 200 kA at the increment of 10 kA. As a result, the maximum radius that the corona can reach ranges from 0.14 m to 0.79 m. Because the front times of the lightning current keep the same, the corona radius also reaches the maximum at the same time. Looking through into the corona initial stage, the higher lightning current peak will exceed V_{cr} earlier, so the corona onsets at an earlier time.

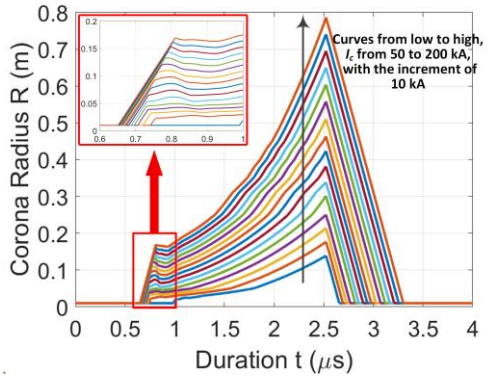

Fig. 4 Corona radius developing processes under different lightning current peaks from 50 kA to 200 kA at an increment of 10 kA

C. Corona Development with Different Lightning Current Front Times

Fig. 5 (a) shows the corona radius developing processes under the lightning currents of the same peak amplitude (80 kA) and different front times, from 0.5 μs to 4 μs.

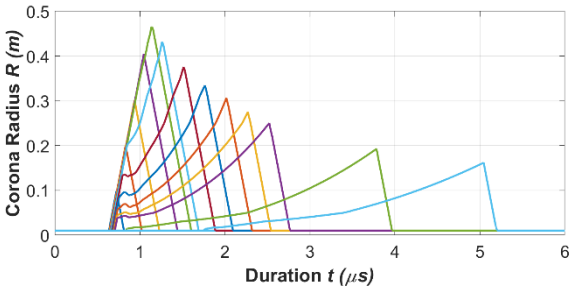

Fig. 5 (a) Corona radius developing processes under different lightning current front times from 0.5 μs to 4 μs

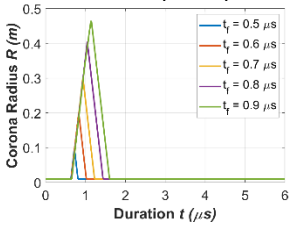

(b) Front time from 0.5 μs to 0.9 μs at an increment of 0.1 μs

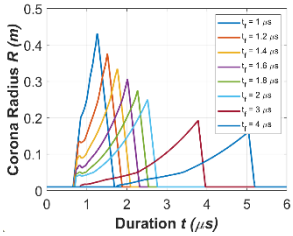

(c) Front time from 1 μs to 2 μs at an increment of 0.2 μs and to 4 μs

Firstly, if the front time is even shorter than 0.5 μs, there is not adequate time for corona to onset and develop because t_s is 0.6 μs. Then the corona developing processes can be classified into two cases. The first case is shown in Fig. 5 (b). The front time increases from 0.5 μs to 0.9 μs, and the maximum corona radius increases from 0.10 m to 0.47 m. In this case, the front time is short, thus, the overvoltage, as well as the electric field, can reach quite high magnitudes, but the electric field at the

streamer-tip is always lower than E_{bn}. Therefore, the corona radius only depends on v_{cr}, and a longer front time leads to developing a longer corona radius. The other case is shown in Fig. 5 (c). The front time increases from 1 μs to 4 μs, and the maximum corona radius decreases from 0.43 m to 0.16 m. Along with the increasing front time, the corona developing process is limited by E_{bn} gradually. Therefore, longer front time causes a shorter maximum corona radius.

D. Influence on Overvoltage Crest by Considering corona on the Down-leads.

The surge impedance of the model considering corona is dynamic to the overvoltage. A constant surge impedance model based on equation (1) without considering corona is established for comparison.

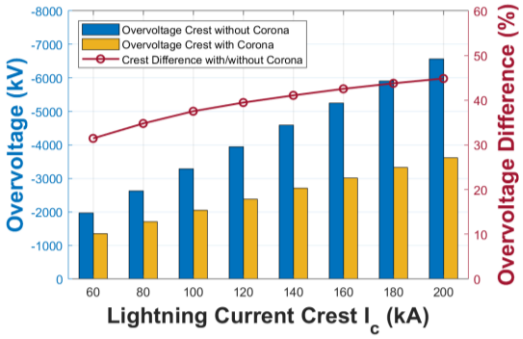

Fig. 6 Overvoltage crests of surge impedance models with and without corona under lightning current of different peaks and the difference in overvoltage crests between the two models

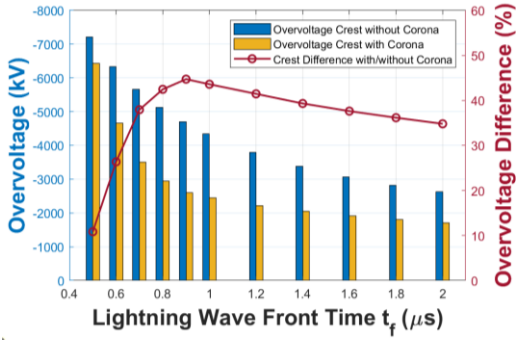

Fig. 7 Overvoltage crests of surge impedance models with and without corona under lightning current of different front times and the differences in overvoltage crests between the two models

Fig. 6 shows the overvoltage crests of the two models under the lightning current of the same front time (2 μs) and different peaks and their differences. Along with the increasing lightning current peak, the overvoltage of the model with corona is always smaller than the overvoltage of the model without corona and the difference between the overvoltage crests increases from 29.04 % to 44.86 %. It results from the decreasing surge impedance, which is due to the increasing corona radius. Fig. 7 shows the overvoltage crests of the two models under the lightning current of the same peak amplitude (80 kA) and different front times and their differences. Along with the increasing lightning current front times, the overvoltage of the model with corona is always lower than the overvoltage of the model without corona. However, the difference of the overvoltage crests increases from 10.83 % to 44.71 % first and then decreases to 23.69 %. The trend of the overvoltage difference is consistent with the trend of changing surge impedance, which is consistent with the trend of corona radius.

V. Discussion on Sensitivity and Error Caused by the Simplification of Modelling Parameters

In the modeling of corona dynamics, three parameters are valued as constant out of simplifications, namely corona inceptive voltage V_{cr}, statistic time lag t_s, and corona expansion and shrinking velocity v_{cr}, which possibly lead to errors in the simulating results and need examination. Subject to the page limit, only the impact of v_{cr} is discussed here. The value of v_{cr} reviewed in previous literature is from 0.1 m/μs to 4.4 m/ μs. Thus, the value of v_{cr} is within this range.

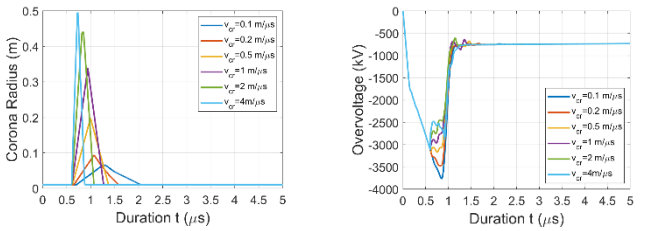

(a) (b)

Fig. 8 Corona radius developing processes (a) and overvoltage (b) caused by the new model at different v_{cr} under lightning with a front time of 0.8 μs

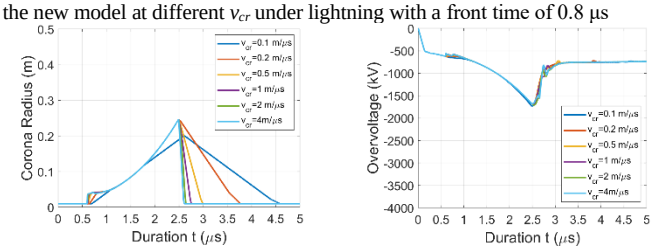

(a) (b)

Fig. 9 Corona radius developing processes (a) and overvoltage (b) caused by the new model at different v_{cr} under lightning with a front time of 2 μs

From the results in the last section, corona expansion velocity v_{cr} influences the development of surge corona dominantly when lightning front time is short. Thus two lightning currents with a front time of 0.8 μs and 2 μs are selected as examples and the lightning current peak amplitude is the same, 80 kA. The corona radius developing processes and overvoltage in the two cases are shown in Fig. 8 and Fig. 9 respectively. When lightning current is of short front time, larger v_{cr} makes corona reach a longer extent. As a result, the peak of overvoltage is reduced by the decreasing surge impedance. However, when lightning current is of longer front time, the major factor to impact corona development is critical streamer's tip electric field E_{bn}. Even though v_{cr} determines the time of corona sheath from the largest extent to extinct, the largest extent that corona can reach is limited by E_{bn}. As a result, v_{cr} hardly impacts the overvoltage level.

Even though under the slow front lightning flashes the value of v_{cr} has a limited impact on the overvoltage level, its impact on the results caused by fast front lightning flashes cannot be ignored. Corona expansion velocity is generally related to electric field, but there is no concise, precise, and well-acknowledged analytical equation to describe the relationship in large-scale corona phenomenon. In [19-21, 25],

the average velocity is experimentally calculated, and the results vary in a quite wide range. Thus, valuing corona expansion velocity deserves further studies and discussion. Although the velocity of corona expansion and shrinking should be different because of their different mechanisms in the physical process, the shrinking velocity does not influence the extent of corona development.

VI. CONCLUSIONS

This paper proposed a simplified dynamic surge impedance model for thin-wire vertical conductors considering voltage-dependent surge corona and emphasized the importance of modeling surge corona effect in the research on the lightning transient performance of thin-wire conductors. The corona development is simulated as the increasing radius of the vertical cylindrical conductor. Thus, the surge impedance of the conductor with corona can change with the corona radius depending on lightning overvoltage. The following conclusions are drawn.

Surge corona developing processes and overvoltage under different lightning current waveforms are simulated and summarized. Higher applied lightning current peaks will cause a longer corona radius and cause more reduction in overvoltage. If the front time of applied lightning impulse current increases, the maximum corona radius will increase first and decrease because the corona development is dominated by expansion velocity and critical streamer-tip electric field in succession.

The overvoltage caused by the dynamic surge impedance model and constant surge impedance model without corona is compared. The dynamic surge impedance model reduces the overvoltage at the top of a conductor by 40% approximately. Therefore, it is necessary to consider the corona effect in the research on the lightning transient performance of thin-wire grounding devices.

The simplified value of corona expansion and shrinking velocity is discussed and examined. Different value of corona velocity has little impact on the overvoltage caused by slow front lightning flashes but has a large impact on the overvoltage caused by fast front lightning flashes. Therefore, the value of corona expansion velocity needs further studies and discussion because of its wide range in previous research.

REFERENCES

[1] BYSTRUP. "THE COMPOSITE PYLON." https://www.powerpylons.com/composite-pylon (accessed.

[2] B. Salarieh, H. M. J. D. Silva, A. M. Gole, A. Ametani, and B. Kordi, "An Electromagnetic Model for the Calculation of Tower Surge Impedance Based on Thin Wire Approximation," *IEEE Transactions on Power Delivery*, vol. 36, no. 2, pp. 1173-1182, 2021.

[3] K. C. Lee, "Non-Linear Corona Models in an Electromagnetic Transients Program (EMTP)," *IEEE Transactions on Power Apparatus and Systems*, vol. PAS-102, no. 9, pp. 2936-2942, 1983.

[4] P. S. Maruvada, D. H. Nguyen, and H. Hamadani-Zadeh, "Studies on modeling corona attenuation of dynamic overvoltages," *IEEE Transactions on Power Delivery*, vol. 4, no. 2, pp. 1441-1449, 1989.

[5] C. d. Jesus and M. T. C. d. Barros, "Modelling of corona dynamics for surge propagation studies," *IEEE Transactions on Power Delivery*, vol. 9, no. 3, pp. 1564-1569, 1994.

[6] T. H. Thang *et al.*, "A Simplified Model of Corona Discharge on overhead Wire for FDTD Computations," *IEEE Transactions on Electromagnetic Compatibility*, vol. 54, no. 3, pp. 585-593, 2012.

[7] T. H. Thang, Y. Baba, N. Itamoto, and V. A. Rakov, "FDTD simulation of back-flashover at the transmission-line tower struck by lightning considering ground-wire corona and operating voltages," *Electric Power Systems Research*, vol. 159, pp. 17-23, 2018/06/01/ 2018.

[8] T. Okada, Y. Baba, T. H. Tran, and V. A. Rakov, "On Possible Influence of Corona Discharge on the Propagation Speed of Lightning Surges Along a Tall Grounded Object," *IEEE Transactions on Electromagnetic Compatibility*, vol. 63, no. 1, pp. 172-180, 2021.

[9] J. J. Clade, C. H. Gary, and C. A. Lefevre, "Calculation of Corona Losses Beyond the Critical Gradient in Alternating Voltage," *IEEE Transactions on Power Apparatus and Systems*, vol. PAS-88, no. 5, pp. 695-703, 1969.

[10] M. A. Al-Tai, H. S. B. Elayyan, D. M. German, A. Haddad, N. Harid, and R. T. Waters, "The simulation of surge corona on transmission lines," *IEEE Transactions on Power Delivery*, vol. 4, no. 2, pp. 1360-1368, 1989.

[11] J. F. Guillier, M. Poloujadoff, and M. Rioual, "Damping model of travelling waves by corona effect along extra high voltage three phase lines," *IEEE Transactions on Power Delivery*, vol. 10, no. 4, pp. 1851-1861, 1995.

[12] Y. Baba and V. A. Rakov, "Simulation of corona at lightning-triggering wire: Current, charge transfer, and the field-reduction effect," *Journal of Geophysical Research: Atmospheres*, vol. 116, no. D21, 2011.

[13] A. Smorgonskiy, E. Egüz, F. Rachidi, M. Rubinstein, and V. Cooray, "A model for the evaluation of the electric field associated with the lightning-triggering rocket wire and its corona," *Journal of Geophysical Research: Atmospheres*, vol. 120, no. 20, pp. 10,964-10,973, 2015.

[14] CIGRE Working Group 01 SC. 33, "Guide to procedures for estimating the lightning performance of transmission lines," *CIGRE Technical Brochure 63*, 1991.

[15] M. A. Sargent and M. Darveniza, "Tower Surge Impedance," *IEEE Transactions on Power Apparatus and Systems*, vol. PAS-88, no. 5, pp. 680-687, 1969.

[16] F. W. Peek, *Dielectric phenomena in high voltage engineering*. McGraw-Hill Book Company, Incorporated, 1920.

[17] G. Hartmann, "Theoretical Evaluation of Peek's Law," *IEEE Transactions on Industry Applications*, vol. IA-20, no. 6, pp. 1647-1651, 1984.

[18] J. He, X. Zhang, P. Yang, S. Chen, and R. Zeng, "Attenuation and deformation characteristics of lightning impulse corona traveling along bundled transmission lines," *Electric Power Systems Research*, vol. 118, pp. 29-36, 2015/01/01/ 2015.

[19] V. M. Cabrera and V. Cooray, "On the mechanism of space charge generation and neutralization in a coaxial cylindrical configuration in air," *Journal of Electrostatics*, vol. 28, no. 2, pp. 187-196, 1992/07/01/ 1992.

[20] S. J. Heckman and E. R. Williams, "Corona envelopes and lightning currents," *Journal of Geophysical Research: Atmospheres*, vol. 94, no. D11, pp. 13287-13294, 1989.

[21] K. H. Schneider, "Positive discharges in long air gaps at Les Renardières—1975 results and conclusions," *Electra*, vol. 53, pp. 311-352, 1977.

[22] T. H. Thang *et al.*, "FDTD computation of lightning surges on overhead wires in the presence of corona discharge," in *2011 7th Asia-Pacific International Conference on Lightning*, 1-4 Nov. 2011 2011, pp. 85-88."

[23] T. H. Thang, Y. Baba, N. Nagaoka, A. Ametani, N. Itamoto, and V. A. Rakov, "FDTD Simulations of Corona Effect on Lightning-Induced Voltages," *IEEE Transactions on Electromagnetic Compatibility*, vol. 56, no. 1, pp. 168-176, 2014.

[24] T. Tran Huu *et al.*, "Modeling of corona discharge on a transmission line conductor struck by lightning for FDTD calculations," in *2010 Asia-Pacific International Symposium on Electromagnetic Compatibility*, 12-16 April 2010 2010, pp. 1309-1312."

[25] T. M. P. Briels, J. Kos, G. J. J. Winands, E. M. van Veldhuizen, and U. Ebert, "Positive and negative streamers in ambient air: measuring diameter, velocity and dissipated energy," *Journal of Physics D: Applied Physics*, vol. 41, no. 23, p. 234004, 2008/11/20 2008.

Paper VIII

35th International Conference on Lightning Protection
XVI International Symposium on Lightning Protection
20th to 26th September 2021 - Sri Lanka
ICLP-SIPDA SRI LANKA 2021

Lightning performance and formula description of a Y-shaped composite pylon considering the effect of tower-footing impedance

Kai Yin
Department of Energy
Aalborg University
Aalborg, Denmark
kyi@et.aau.dk

Mohammad Ghomi
Department of Energy
Aalborg University
Aalborg, Denmark
mhg@et.aau.dk

Filipe Faria da Silva
Department of Energy
Aalborg University
Aalborg, Denmark
ffs@et.aau.dk

Claus Leth Bak
Department of Energy
Aalborg University
Aalborg, Denmark
clb@et.aau.dk

Hanchi Zhang
Department of Energy
Aalborg University
Aalborg, Denmark
hazh@et.aau.dk

Qian Wang
Department of Energy
Aalborg University
Aalborg, Denmark
qiw@et.aau.dk

Henrik Skouboe
Bystrup Architecture Design & Engineering
Vermundsgade 40A, 2100
København Ø, Denmark
hs@bystrup.dk

***Abstract*—This paper presents systematic research on the lightning performance of a novel Y-shaped composite pylon for 400 kV transmission lines and the feasibility of empirical formulas for this kind of tower when considering the effect of tower-footing impedance. The transient overvoltage response to a lightning surge at the tip of the pylon is modeled in PSCAD/EMTDC. Compared with the Donau tower, the composite pylon shows a similar backflash rate (BFR) level. Then, we use qualitative analysis based on lumped parameter model and distributed parameter model to predict the critical flashover current (I_c) of the composite pylon. We find that the calculated results exhibit higher error deflection when the existing empirical formulas are applied in the Y-shaped pylon. Furthermore, the simulated lightning performance has a lower sensitivity to varied tower-footing impedance compared with empirical formula calculation. The special structure of the Y-shaped pylon, the discontinuity in surge impedance and the soil ionization are analyzed to account for the role of tower-footing impedance on lightning performance. Finally, we improve the accuracy of the empirical formulas to the Y-shaped pylon lightning performance and discuss the effect of the footing impedance on the BFR.**

Keywords— BFR, tower-footing impedance, surge impedance, composite pylon, empirical formula

I. INTRODUCTION

Composite towers have been regarded as next-generation towers for transmission lines due to their lower environmental, visual and economic impacts [1]. Compared with traditional transmission towers, the application of a composite pylon can reduce both the line corridor areas and the use of steel [2], decreasing the cost of component transportation and assembly [2]. In recent years, the increase of new renewable energy leads to a growing demand for new overhead lines and towers [3]. A composite pylon, which has a 'Y' shape with an integrated cross-arm without insulator strings, is a promising substitute for the traditional transmission tower. A proposal that a bare grounding conductor through the cross-arm is designed as downlead system to provide zero potential for the shield wire. The mast of the pylon body is composed of a vertical steel cylindrical mast with a radius of 1 m. Low-density polyethylene (LDPE) is used as filling material inside the cross-arm to curb the partial discharge and to guarantee enough insulation between phase conductors and downlead [4].

Lightning performance is an essential factor to the safe and reliable operation of transmission overhead lines (OHLs). There are two kinds of lightning failures of OHLs. One is flashover caused by a direct lightning strike to phase conductors (shielding failure), and the other is the back flashover between the shield wire and phase conductor. To date, there are just a few scientific works on shielding failure of the composite pylon. Claus Leth Bak et al. [2] studied the lightning performance of the novel pylon and showed that transmission lines supported by the Y composite pylon have

978-1-6654-2346-5/21/$31.00 ©2021 IEEE

a lower probability of being struck by lightning and the shielding failure flashover rate is nearly zero. Subsequently, a scale model was built, and the relevant experiments were performed. The test results verified the lightning performance evaluation of the composite pylon [5].

Additionally, the backflash rate (BFR) of the composite pylon has never been studied to date. The tower grounding system and the soil resistivity play an important role in the backflash rate (BFR). The ground system for Y-shaped pylon including the downlead routing and electrode shape is largely different from traditional ones, as will be seen in section II. In engineering practice, empirical formulas are often used to evaluate the BFR [6]. Whether the lightning performance of the composition pylon can be predicted by the traditional empirical formulas with acceptable error is also unclear. Thus, it is of great importance to carry out the research work on BFR of the novel pylon considering the variation of tower-footing impedance.

In this paper, PSCAD/EMTDC is employed to investigate the transient overvoltage response of a novel composite pylon with the tower-footing impedance changing from 5 Ω to 20 Ω. The influence of tower-footing impedance on Donau tower is also studied for comparison (Fig. 1). In section II, the developed Y-shaped pylon model and empirical methods are demonstrated. In section III, the lightning performance of the composite pylon and Donau tower are studied via simulation, and the applicability of the traditional formulas for the Y-shaped pylon is discussed. In section IV, we modify the empirical formulas considering the downlead configuration and the effect of the soil ionization. Finally, we discuss the role of changing footing impedance on lightning performance.

II. Methodology

A. PSCAD Modeling

A double circuit transmission line with seven pylons was modeled as the base of the simulation, assuming lightning hit on the tip of the middle pylon. Bergeron model with a frequency of 1 MHz was used for modeling the downlead system. The pylon adopts a novel unibody cross-arm with an inclination angle of 30°, and the dimensions of the pylon are illustrated in Fig. 2. The length of the cross-arm tube is 12 m. Aluminum Conductor Steel-Reinforced (ACSR) in a duplex bundle is used. According to EN 50341-1 and CIGRE TB. 72 [7], the air clearances between the phase conductor and upper phase conductor to shield wire on the unibody cross-arm should be 3.6 m and 2.8 m, respectively [7]. A bare conductor with radii of 17.5 mm inside each cross-arm is connected with the iron pylon body. The pylon span is 250 m.

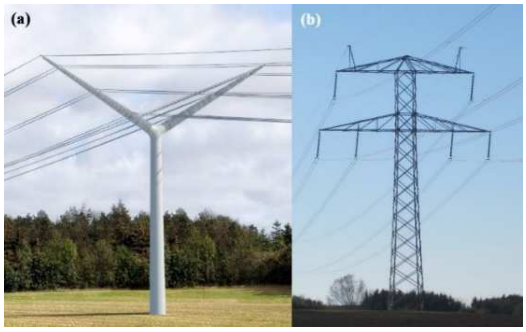

Fig. 1 Concept map of the (a) Y-shaped composite pylon and (b) Donau tower.

(1) Lightning parameters.

Here, the double exponential lightning waveform with front time T_f of 1.2, 2, 4, 8 μs is employed to investigate the transient response of the Y-shaped pylon. The tail time of lightning current has little effect on the transient voltage [8], and a constant tail time T_t of 50 μs is considered in this paper. Only the first strike will be accounted for in the simulation.

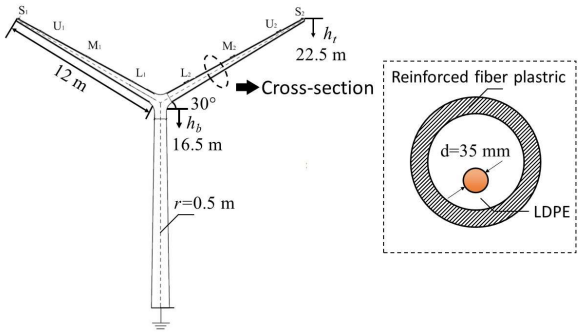

Fig. 2 The parameters of the Y-shaped pylon.

(2) Surge impedance of the down lead.

The surge impedance of the ground system is a key parameter to determining the lightning transient overvoltage. Inspired by a multistory tower model [9], the down lead inside the cross-arm can be divided into a suitable number of parts, as shown in Fig. 3. For calculating the inductance and the capacitance of downlead inside the cross-arm, we treat the segmented FRP circumscribed downlead as a uniform cylinder since its height is much larger than the radius of the cross-arm. The diameter on the geometric center coordinates of the cross-arm is taken as the average diameter. Based on this assumption, formulas to calculate the inductance L and capacitance C are exhibited as (1) and (2). At the high frequencies associated with lightning surges, the surge impedance of each segment is equal to the square root of L/C.

$$L = \frac{\mu_0 l}{8\pi} + \frac{l}{2\pi}\left(\mu_1 \ln\frac{b}{a}\frac{2h-a}{2h-b} + \mu_0 \ln\frac{2h-b}{b}\right) \tag{1}$$

$$C = \frac{2\pi l}{\frac{1}{\varepsilon_1}\ln\frac{b}{a}\frac{2h-a}{2h-b} + \frac{1}{\varepsilon_0}\ln\frac{2h-b}{b}} \tag{2}$$

Where l, h, and b are the length, height, and radius of the cross-arm segments. a is the radius of the down lead. μ_1 and ε_1 are the relative permeability ($\mu_1 = \mu_0$) and permittivity of the LDPE (ε_1=2.2) [10]. The propagation speed is $1/\sqrt{(\varepsilon_1\mu_0\varepsilon_0)}$.

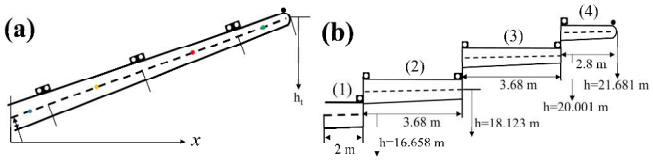

Fig. 3 The sketch of the actual composite cross-arm and the equivalent calculation model.

The surge impedance of the iron pylon cylindrical body can be expressed as (3). The propagation speed is light speed.

$$Z = 60\left[\ln\left(\frac{2\sqrt{2}h}{a}\right) - 1\right] \tag{3}$$

(3) Tower-footing impedance.

A concentrated rod with a radius of 1 m is mounted in the ground as an electrode of this composite pylon as Fig. 4 (a). In order to investigate the effect of the tower-footing impedance on the BFR of the Y-shaped pylon, the tower-footing impedance values R_0 varying from 5 Ω to 20 Ω are adopted. The high magnitude of lightning current flowing through the grounding electrode (i_R) causes soil ionization and discharge, which decreases the tower footing impedance below the measured low-current status (R_0). Thus, the tower-footing impedance depends on the magnitude of the current flowing into the earth. In this paper, the current dependence model is used for tower footing modeling. The critical gradient E-field E_0 for soil ionization is approximately 400 kV/m. The current amplitude I_g required to achieve this gradient can be determined by (4) [11-13].

$$I_g = \frac{\rho E_0}{2\pi R^2} \tag{4}$$

Where ρ is the soil resistivity, and the dynamic tower footing impedance R_i of the concentrated rod electrode can be expressed as a function of I_R [11, 12].

$$R_i = \frac{R_0}{\sqrt{1+(I_R / I_g)}} \tag{5}$$

The dynamic footing impedance when 100 kA lightning strikes on the top of the pylon (Fig. 4 (b)) and then going through the footing electrode is shown in Fig. 4 (b).

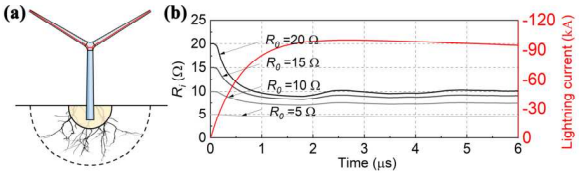

Fig. 4 (a) The schematic of the soil ionization. (b) The R_i changes with different R_0 when the lightning current passes through the pylon footing electrode (black line), and the lightning waveform (red line).

(4) Flashover criterion.

The leader progression method (LPM) is based on the physical process of air gap discharge to characterize the insulation surface flashover. According to the CIGRE WG 33-01, the leader progression time can be calculated as (6).

$$\frac{dx}{dt} = Ku(t)\left(\frac{u(t)}{D-x} - E_0\right) \tag{6}$$

Where x is the length of the leader, $u(t)$ is the voltage at the air gap, D is the length of insulation, E_0 is the threshold electric field of leader progression, and K is the factor of leader progression speed. E_0 and K are related to the type of the insulators and the polarity of the lightning impulse voltage, which are obtained from experiments. Due to similar material composition and insulator length, the flashover characteristics along the composite insulator can be regarded as that of a post insulator [14]. The K and E_0 for negative discharge are recommended by CIGRE to be 1.0×10^{-6} $m^2/V^2/s$ and 670 kV/m [15].

(5) BFR calculation.

The BFR of transmission lines is given by

$$BFR = 0.6 N_L P(I_c) \tag{7}$$

I_c is the striking lightning current that causes flashover. $P(I_c)$ is the probability that the struck current I exceeds the critical current I_c. N_L estimates the number of strikes to the line per year per 100 km, which can be calculated by (8). The highest N_g, in the last twenty years in Denmark was equal to 1.39 flashes/km^2·year [5].

$$N_L = \frac{N_g}{10}(28h_t^{0.6} + D) \tag{8}$$

Where the h_t and D are the height of the pylon and the horizontal distance between the shielding wires.

For 220 kV and above transmission lines, the phase voltage has a considerable impact on the lightning performance [11]. Therefore, the voltage phase and polarity when lightning strikes should be considered. The flashover judgment between upper phase and shielding wire can be expressed as

$$U_L = U_p + U_i \tag{9}$$

Where the U_i is the lightning-caused overvoltage on the cross-arm between the upper conductor and shield wire, and U_p is the phase voltage. Then critical current I_c can be obtained by simulation. The probability of lightning current can be approximately expressed by a lognormal distribution, as (10) shows.

$$f(x) = \frac{1}{\sqrt{2\pi}\beta x} e^{-\frac{1}{2}\left(\frac{\ln(x/M)}{\beta}\right)^2} \tag{10}$$

The two coefficients M and β for lightning current crest are 31.1 and 0.484, respectively [11]. The accumulative probability of the current exceeding a certain value I_c is

$$P(x) = 1 - \int_{I_c}^{\infty} f(x)\mathrm{d}x \tag{11}$$

B. Empirical formulas calculation

The lightning protection level can be evaluated by empirical formulas, which are important in engineering design and application. In general, there are two kinds of empirical methods, including the method based on the lumped-parameter model (LM) and the method based on the distributed-parameter method (DM), to predict I_c. Based on I_c results, BFR can be obtained through formula (7). Here, we studied the applicability of the two methods on the Y composite pylon with different tower-footing impedance. U_L is equal to flashover criteria acquired by LPM in section II A.

(1) Lumped-parameter model formulas.

If the height of the transmission tower is lower than 40 m, the LM can be used to estimate the critical current I_c. This method neglects the effect of the capacitance of the downlead system and calculates the overvoltage level by equivalent inductance. I_c can be calculated by (12) [16].

$$I_c = \frac{U_L}{(1-k)(\gamma R_i + \gamma L / T_f + h_t / T_f)} \tag{12}$$

Where k is the coupling coefficient between shield wire and phase conductor. L_s, L_c, and L_t are the equivalent inductance of the shield wire, the downlead inside the cross-arm, and the steel pylon body. L is the total inductance of downlead and lattice tower. The shunt coefficient γ refers to

the ratio of lightning current going through the tower-footing impedance i_R to the total lightning current I. It is commonly recommended for 400 kV transmission tower to be 0.88 [16].

(2) Distributed-parameter model formulas.

The DM takes the wave traveling process and the effect of adjacent towers into consideration. This method assumes that the surge impedance of the tower body is equal to half of the shield wire; that is, there is no reflection at the conjunction point of the shield wire and tower body. In addition, the wave shape of the voltage is defined as a linear rising front and an infinite tail. The critical current I_c is given by

$$I_c = V_{TT} / K_{TT} K_{SP} \tag{13}$$

V_{TT} is the voltage at the top of the pylon when lightning strikes on the tower, which is equal to U_L+U_c.

$$U_c = kV_{TT} - h_c(1-k)I_c / T_f \tag{14}$$

Where K_{TT} and K_{SP} are

$$K_{TT} = R_e + \frac{Z_g - 2R_i}{Z_g + 2R_i} \frac{L_s + L_c + L_t}{T_f} \tag{15}$$

$$R_e = \frac{R_i Z_g}{Z_g + 2R_i} \tag{16}$$

$$K_{SP} = 1 + \alpha_R(1+\alpha_T)\left[(1-\frac{2T_s}{T_f}) - \alpha_R\alpha_T(1-\frac{4T_s}{T_f}) - \cdots\right] \tag{17}$$

Where α_T is the reflection coefficient at the point of tower footing impedance, and pylon body and α_R is the reflection coefficient at the point of transmission line and adjacent towers. Then, I_c can be calculated accordingly.

III. Simulation and Calculation Results

A. BFR by simulation

BFR for Y-shaped composite and Donau tower with different tower footing impedance are shown in Fig. 5 (a) and (b). In this research, the worst case was for the lightning front time of 1.2 μs and R_0 of 20 Ω, with a BFR of Y-shaped pylon of about 0.07 flashes/100 km-year, which is very similar to that of the Donau tower (0.065 flashes/100 km-year). According to Overhead line Operation Specifications published by China State grid [17], the acceptable BFR for 330 kV and 500 kV transmission lines are 0.2 and 0.12 flashes/100 km-year, respectively. According to the research in [18], the BFR for 400 kV lattice traditional tower is about 0.1 flashes/100 km-year. This kind of Y-shaped composite pylon shows good lightning protection behaviors.

B. I_c Prediction by empirical formulas

The comparison of the I_c obtained by simulation ($I_{c\text{-}S}$) and calculation ($I_{c\text{-}C}$) is shown in Fig. 6. We take the simulation results as the standard, and the calculation error can be defined as $|I_{c\text{-}C}\text{-}I_{c\text{-}S}|/I_{c\text{-}S}$. The calculation errors increase along with the T_f duration increases. Meanwhile, the simulation results in the software show low sensitivity to the change of R_i compared with calculation results.

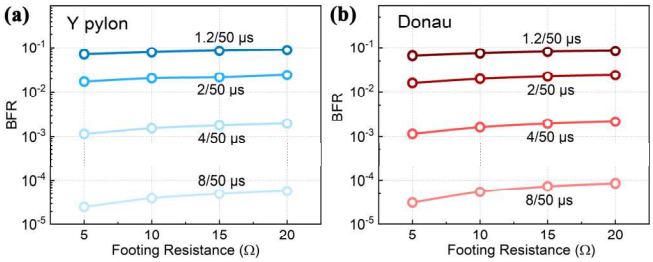

Fig. 5 The BFR (flashes/100 km-year) for (a) Y composite pylon and (b) Donau tower with different tower footing impedance.

To quantify the difference between the calculation and simulation results, the average error, which means the average of the error of all data points, is introduced to indicate the accuracy of the empirical methods. The average calculation errors for both Y-shaped pylon and Donau tower are exhibited in Table I. Compared with the LM, the DM shows a good prediction for composite Y and Donau. However, for T_f of 8 μs, both the two methods have large errors around 40 %. Thus, it is necessary to propose a modified method to improve its accuracy.

TABLE I. Average Calculation Error

Tower	Method	LM	DM
Y	Error (%)	32.26	18.21
Donau		21.33	16.76

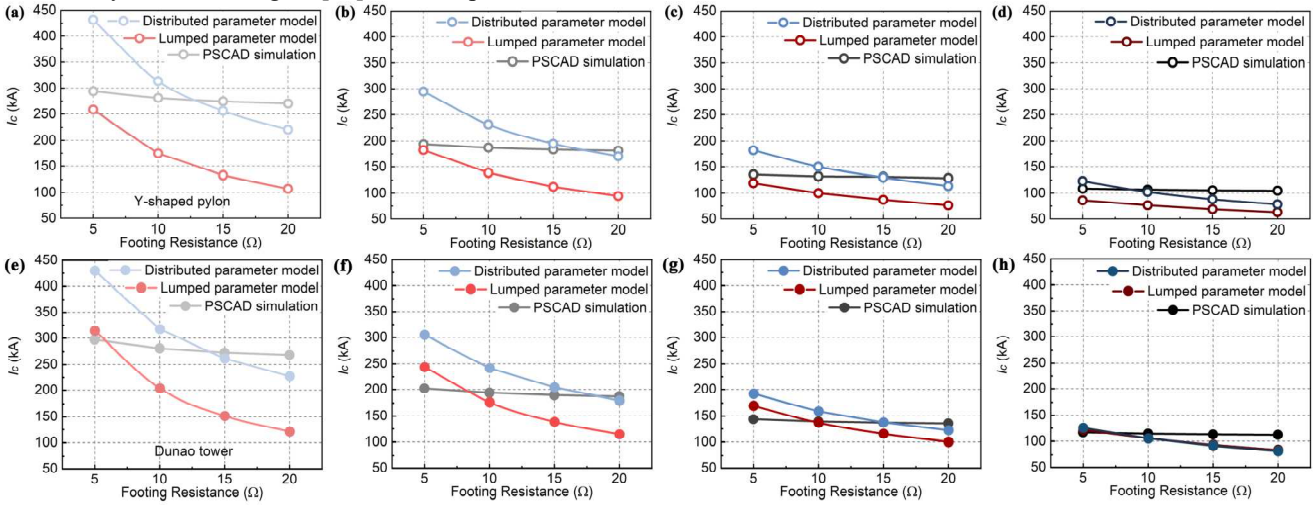

Fig. 6 The comparison of I_c for Y-shaped pylon obtained by PSCAD simulation, LM and DM with T_f of (a) 1.2 μs, (b) 2 μs, (c) 4 μs, (d) 8 μs. I_c for Donau tower obtained by simulation and calculation with T_f of (e) 1.2 μs, (f) 2 μs, (g) 4 μs, (h) 8 μs.

IV. MODIFICATION FOR EMPIRICAL FORMULAS

In order to improve the accuracy of the empirical formulas, the downlead configuration and the effect of soil ionization are considered to modify the existing empirical formulas.

A. Configuration of downlead

For LM, the shunt coefficient γ is the critical factor to determine the calculation accuracy. It depends on the configuration of the tower and the transmission voltage level. Here, we get the precise γ at varied T_f and R_i by the PSCAD simulation, and the results show in Fig. 7. We can find that γ is not a fixed value, and it varies with R_i and T_f. According to the modified γ, the I_c of Y-shaped pylon can be recalculated. By doing this, the average error decreases from 32.26 % to 25.91 %.

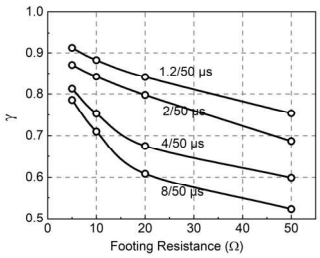

Fig. 7 The γ for Y-shaped pylon with different R_i and T_f.

The DM can be described by lattice diagram, and it fully considers the surge traveling process. The configuration of the downlead is different from traditional towers, and two of the downleads connect with the tower body and form a star-connection structure. Besides, the multi-discontinuities of the surge impedance can lead to a different voltage distribution along the pylon body compared with the Donau tower. Thus, the specific structure and surge impedance discontinuity of Y-shaped pylon are considered in the inference process. Here, the lattice diagram for the surge traveling of Y-shaped pylon is depicted in Fig. 8. there are four points of discontinuity in the equivalent circuit. They produce both reflected and transmitted waves and make the travel process complex. Thus, besides the basic assumptions mentioned in section II B, we suppose Z_g=2×Z_{C1}. Z_{C1} is the surge impedance of the downlead inside the cross-arm. Namely, e=Z_g×I/4, and the surge impedance discontinuities at (1) and (4) are neglected [11].

Subsequently, we define the reflection and refraction coefficient. When lightning current passes point (2) from the cross-arm side to the pylon body side, the reflection coefficient is α_2', and the refraction coefficient is α_2''. While the voltage from tower footing impedance passes through the point (2) from the pylon body side to the cross-arm side, the reflection coefficient is β_2', and the refraction coefficient is β_2''. Wherein, β_2''-α_2'=1, and α_2''-β_2'=1. This case is a multi-outgoing line system. The surge impedance of two outgoing lines should be equivalent in the calculation of traveling coefficients.

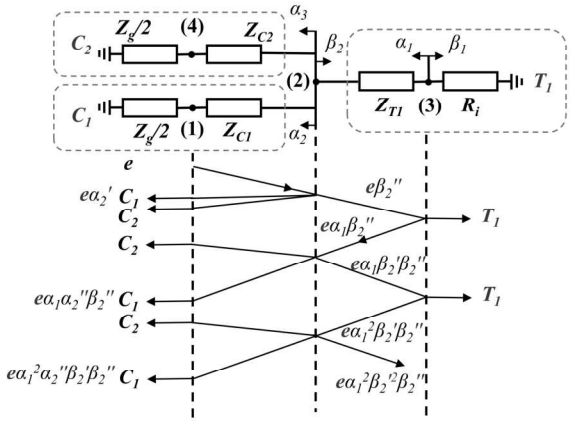

Fig. 8 The lattice diagram for the wave travel of the Y-shaped pylon. (1) and (4) indicate the top of the pylon, (2) is the connection point of the cross-arm and pylon body, and (3) is the bottom of the pylon. C_1 and C_2 are the cross-arms, T_1 is the pylon body.

$$\alpha_2' = \frac{Z_k - Z_{C1}}{Z_k + Z_{C1}} \tag{18}$$

$$\beta_2' = \frac{Z_C - Z_T}{Z_C + Z_T} \tag{19}$$

Where Z_{C2} and Z_T are the surge impedance of the downlead inside the cross-arm and surge impedance of the pylon body. Z_k is Thevenin equivalent surge impedance of Z_{C1} and Z_T. Z_C is the equivalent result of Z_{C1} and Z_{C2}. The V_{TT} is

$$V_{TT} = e\left\{\begin{array}{l} 1+\alpha_2'(1-\frac{2T_C}{T_f})+\alpha_1\alpha_2'\beta_2''(1-\frac{2T_T}{T_f}) \\ +\alpha_1^2\alpha_2''\beta_2'\beta_2''(1-\frac{2T_T+2T_b}{T_f})+\cdots \end{array}\right\} \tag{20}$$

Where T_T, T_C, and T_b are travel time from top to bottom, travel time in the cross-arm, and time in the pylon body, respectively. On the basis of ensuring $2T_T$+nT_b longer than T_f, travel processes where the time exceeds $2T_T$+$2T_b$ are neglected.

The modified MD with the minimum average error of 12.32% delivers an improved match with the simulated results, compared with the unmodified value of 25.91 %.

B. Effect of the soil ionization

The impact of soil ionization when lightning current passes through the footing electrode should be accounted for.

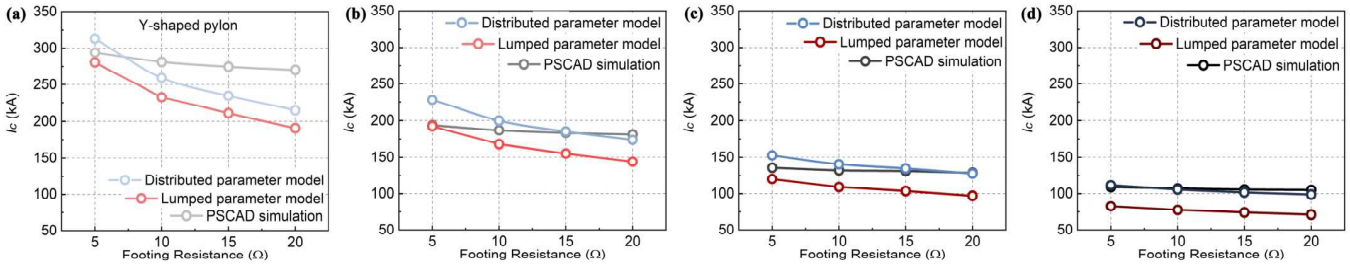

Fig. 9 The comparison of I_c for Y-shaped pylon obtained by PSCAD simulation, LM and DM with T_f of (a) 1.2 μs, (b) 2 μs, (c) 4 μs, (d) 8 μs considering the effect of soil ionization.

The R_i should be calculated through equations (4) and (5) to get the impedance of the soil after ionization. I_c calculated by both the LM and DM is shown in Fig. 9. At this time, the error of the two modified methods further decreases to 19.35 % for modified LM and 7.57 % for modified DM. In addition, the calculated I_c also shows lower sensitivity to R_i. Thus, it seems that the particular configuration of the tower results in a soil ionization effect leading to a relatively flat BFR curve as a function of R_i for Y-shaped pylon.

C. Comparison of two modified methods

After modification, both two methods show improved calculation accuracy. For LM, the formula form does not need to be revised. However, this method's accuracy strongly depends on the shunt coefficient γ, which requires the aid of simulation software. In addition, the neglecting of the capacitance of downlead may cause a relatively high error.

For DM, the calculation accuracy is largely increased even with a broad scope of T_f and R_i, but the disadvantage is that the process of calculation becomes more complex.

V. Effect of Footing Impedance

The traditional empirical calculation for the Y-shaped pylon shows a strong tower-footing impedance dependence, especially for the DM. The dependence of I_c on R_i relies on the proportion of the ground voltage V_g in the overvoltage of the whole tower V_{TT} in the formula. The larger the proportion is, the more sensitive the tower overvoltage is to the change of ground impedance. Here, we introduce a ratio p ($0<p<1$) which is equal to V_g divided by tower top voltage V_{TT} to describe the proportion of the ground voltage on the top voltage. For LM and modified LM, the V_g/V_{TT} is equal to $p=\gamma R_i/(\gamma R_i+\gamma L/T_f+\gamma h_t/T_f)$.

For the original DM, the p is R_e/K_{TT}. While for the modified DM, the p is given by (21).

$$p=\left[\beta_2''+\alpha_1\beta_2''+\alpha_1\beta_2'\beta_2''(1+\alpha_1)(1-\frac{2T_T}{T_f})\right]/V_{TT} \quad (21)$$

The p calculated from the four methods is shown in Fig. 10. We found p is increased with the footing impedance increasing, and p calculated from both modified empirical formulas is lower than that of values from unmodified methods, especially for the DM. The lower the p, the lower the susceptibility to R_i. Thus, the I_c calculated by the modified methods has a weak tower-footing impedance dependence.

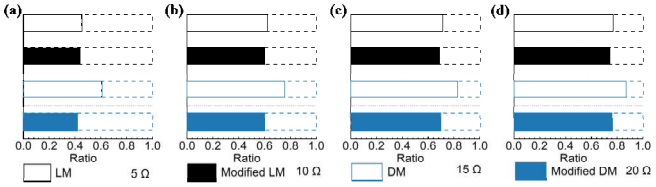

Fig. 10 The ration p of V_g to V_{TT} calculated by four methods as the tower-footing impedance increases when T_f is 8 μs.

VI. Conclusion

This paper reports the effect of tower footing impedance on the lightning performance of a composite Y-shaped pylon. PSCAD/EMTDC is employed to investigate the transient response of lines when a flash of lightning strikes on the top of the pylon. The feasibility of the empirical methods based on the lumped-parameter model and distributed-parameter model for Y-shaped pylon were discussed. The study showed that when empirical methods are applied on the Y-shaped pylon, the calculation error is higher than for a traditional tower, especially for LM. Then, the two methods were modified considering the configuration of the pylon and soil ionization, and their accuracy improved. Finally, through the V_g/V_{TT}, we explain the influence of the tower footing impedance on the lightning performance of the Y-shaped pylon.

References

[1] F. Napolitano, F. Tossani, A. Borghetti and C. A. Nucci, "Lightning Performance Assessment of Power Distribution Lines by Means of Stratified Sampling Monte Carlo Method," IEEE Trans. Power Deliv., vol. 33, no. 5, pp. 2571-2577, Oct. 2018.

[2] Q. Wang, T. Jahangiri, C. L. Bak, F. F. da Silva, and H. Skouboe, "Investigation on Shielding Failure of a Novel 400-kV Double-Circuit Composite Tower," IEEE Trans. Power Deliv., vol. 33, no. 2, pp. 752-760, Apirl 2018.

[3] E. E. D. f. Consultation, "Ten-Year Network Development Plan 2020. At a glance: Power system needs in 2030 and 2040," 2020.

[4] K. Yin, F. F. da Silva, C. L. Bak, H. Zhang, Q. Wang and H. Skouboe, "Electric Field Computation and Optimization for A 400 kV Y-shaped Composite Cross-arm," 2021 International Conference on Electrical Materials and Power Equipment (ICEMPE), 2021, pp. 1-4.

[5] T. Jahangiri, C. L. Bak, F. M. F. da Silva, B. Endahl, and J. Holbøll, "Assessment of lightning shielding performance of a 400 kV double-circuit fully composite transmission line pylon," CIGRE Int. Counc. Large Electri. Syst., 2016.

[6] L. Grcev, "Lightning Surge Efficiency of Grounding Grids," IEEE Trans. Power Deliv., vol. 26, no. 3, pp. 1692-1699, July 2011.

[7] T. Jahangiri, C. L. Bak, F. F. da Silva and B. Endahl, "Determination of minimum air clearances for a 420kV novel unibody composite cross-arm," 2015 50th International Universities Power Engineering Conference (UPEC), Stoke on Trent, UK, pp. 1-6, 2015.

[8] J. Gholinezhad and R. Shariatinasab, "Time-Domain Modeling of Tower-Footing Grounding Systems Based on Impedance Matrix," IEEE Trans. Power Deliv., vol. 34, no. 3, pp. 910-918, June 2019.

[9] M. Ishii *et al.*, "Multistory transmission tower model for lightning surge analysis," IEEE Trans. Power Deliv., vol. 6, no. 3, pp. 1327-1335, July 1991.

[10] Y. Cheng, G. Yu, and Z. Duan, "Effect of Different Size ZnO Particle Doping on Dielectric Properties of Polyethylene Composites," J. Nanomater., vol. 2019, pp. 1–11, 2019.

[11] A. R. Hileman, Insulation coordination for power systems. CRC Press, 2018.

[12] Mohammad Ghomi, et al. "Full-wave modeling of grounding system: Evaluation the effects of multi-layer soil and length of electrode on ground potential rise." International Conference on Power Systems Transients, IPST. Pp. 1-6, June 2019.

[13] Mohammad Ghomi, Claus Leth Bak, Filipe Faria da Silva, "Frequency Dependence of Multilayer Soil Electrical Parameters: Effects on the Input Impedance of Grounding Systems," 16th International conference on AC and DC power transmission, ACDC. 2020.

[14] X. Wang, Z. Yu and J. He, "Breakdown process experiments of 110-to 500-kV insulator strings under short tail lightning impulse," IEEE Trans. Power Deliv., vol. 29, no. 5, pp. 2394-2401, Oct. 2014.

[15] C. W. G. J. C. S. 10, "Guide to procedures for estimating the lightning performance of transmission lines," 1991.

[16] Jia L, Shu L, Zheng S, et al. "Investigation on the lightning withstand level of transmission line considering power frequency voltage," High Voltage Engineering, vol. 32, no. 11, pp. 111-114, 2006.

[17] "110 (66) kV-500 kV overhead transmission line operation specifications (in Chinese)," China State Grid, 2005.

[18] Datsios, Zacharias G., et al. "Estimation of the minimum backflashover current of 150 and 400 kV overhead transmission lines through ATP-EMTP simulations: Effect of the lightning stroke location along line spans." The International Symposium on High Voltage Engineering. Springer, Cham, pp. 1482-1490, 2019.

ISSN (online): 2446-1636
ISBN (online): 978-87-7573-804-5

AALBORG UNIVERSITY PRESS